WEAR OF TUBE MILL LINERS FOR SOUTH AFRICAN POWER INDUSTRY

by

JAN. J. SKORUPA

Submitted to the University of Cape Town in fulfillment of the requirements for the degree of Doctor of Philosophy

March, 1989

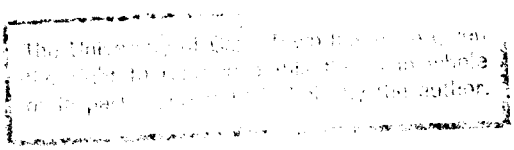

This thesis is dedicated to my Friends from ESKOM
and to Mr. G. Quesnel, my Director

ACKNOWLEDGEMENTS

I would like to thank my supervisor, professor R. K. Dutkiewicz for his guidance, encouragement and friendship over the years.

Also many thanks to staff members of Energy Research Institute in Cape Town for their assistance and friendship through the duration of this work.

I wish to thank Dr. M. Moys from Chemical Engineering at Witwatersrand University for his assistance and helpfulness during the tests, and Dr. T. Dunn from the Department of Mathematical Statistics of University of Cape Town for his assistance in statistical analysis.

I wish to express my sincere appreciation to Dr. J. Csaba from C.S.I.R. for his help in drawing many of the diagrams.

The following people and institutions are also acknowledged:

Management of Stein Industrie France and particularly Mr. G. Quesnel, Industrial Director for encouragement and funding of this research.

Management of Escom for support, assistance and encouragement received through the duration of this work.

SUMMARY

The new Power Stations all over the world are using progressively lower grades of highly abrasive coal. This has brought about a resurgence in the popularity of ball-tube mills as against the vertical-spindle and or ball and race type mills.

Grinding in a tube mill consists of a reduction of lump solid materials to smaller particles by the application of shearing forces, pressure, attrition and impact, so one can say the grinding consists of applying power for rotating the mill shell, thus transmitting energy to some form of media which, in turn, by cascading and cataracting action, fractures material into individual particles.

Mill liners are the agents which transmit this energy and motion through their lifter to grinding medias. The liners therefore really play the part performed in a machine tool, motor vehicle, etc., by the mechanical energy transmission parts (e.g. gear clutch, etc.,).

The efficiency of the whole machine is thus a direct function of the efficiency of the energy transmission part. Therefore, the efficiency of the tube mill can only be maintained when the wear rate of the liners is kept at low level, e.g. the initial profile and height of the lifter is preserved.

This thesis makes a contribution to existing knowledge in the following areas:

(i) A metallurgical evaluation of nine various alloys suitable for liners for tube mills used for power industry has been presented.

(ii) The laboratory wear test procedures simulating impact and attrition are established.

These are supported by industrial experimental evidence.

(iii) The mechanism of wear of liners made from high chrome iron, the most wear resistant alloy has been identified.

(iv) A suitable laboratory test procedure for study of the liner profile on its wear characteristics has been developed.

This procedure is confirmed by results from industrial trials.

(v) Liner Roughness (C_R), a continous variable to be assigned to the liners in such a way, that it would make it possible to interpolate for other liners, not directly tested in the present work has been established.

TABLE OF CONTENTS

LIST OF TABLES

LIST OF FIGURES

NOMENCLATURE

C_R	Liner roughness	
D	Mill diameter	m
G_E	Angle at which the ball impacts the liner	rad
F_f	Frictional force	N
F_r	Total radial force on the ball	N
F_t	Tangential force	N
$F\|\|$	Forces parallel to liner lifter face	N
$F\perp$	Forces perpendicular to liner lifter face	N
H	Hardness of the worn surface	Vickers, Brinell
J	Fractional mill filling	ball vol/mill vol
K	Height of the liner lifter	m
L	Mill length	m
N	Normal force exerted by the liner lifter on the ball	N
N_c	Critical speed	rad/s
N_m	Mill speed	% of N_c
P	Power	Kw
S	Unit vector parallel to the liner lifter face	
S_L	r_L COS β_L	
T	Time	s
ΔW	Volume loss due to wear	$mm^3 (10^{-9} m^3)$
V_L	Linear velocity at the liner lifter tip	m/s
ω	Angular velocity	rad/s
ω_b	Angular velocity of the ball	rad/s
ω_m	Angular velocity of the mill shell	rad/s

a_{cc}	Acceleration	m/s^2
d	Position of intersection of the Davis circle and mill	rad
e	Position of the load shoulder	rad
g	Acceleration due to gravity	m/s^2
j_i	Fractional volume below the equilibrium surface	Ball vol/mill vol
K_m	Spiral constant	
l	Polar length of equilibrium spiral	m
m	Mass	kg
r_o	Radial distance from mill centre to the ball centre	m
r_b	Ball radius	m
r_d	Radius of Davis Circle	m
r_m	Radius of mill	m
s,s'	Position of intersections of equilibrium surface and mill	rad
t	Position of the load toe	rad
u	Fraction of mill circumference covered by the load	
μ	Coefficient of friction	
μ_b	Frictional force between ball and the liner	N
μ_k	Kinetic coefficient of friction between ball and liner	
μ_s	Static coefficient of friction between ball and liner	
V_r	Initial tangential velocity of a parabolic trajectory	m/s
X,Y	General co-ordinates	m
α	Angle of impingement of particle	rad
β	Angle that V_r makes with horizontal	rad

CHAPTER I

I N T R O D U C T I O N

South Africa, in pursuing its policy of making best use of the country's energy reserves, relies on the use of progressively lower grades of coal for combustion in the large boilers at its new power stations. This has brought about a resurgence in the popularity of ball tube mills, as against mills of the vertical-spindle and ball-and-race type.

For soft coals of relatively low ash content and reasonably high volatility, vertical mills were found to be ideal, particularly in view of their large capacities. But, with the subsequent need to allow for the use of coals of lower quality, the ball tube mills have come back into favour as they are better suited to these grades of coals. They are far less sensitive to wear - a vital consideration, and provide for longer running times between maintenance shut-downs.

According to Pitman (40), in a typical case of a vertical-spindle mill, the wear rate is such that the grinding components - comprising rollers and tables - have to be replaced after each period of 5000 to 6000 running hours; while in the case of a ball-and-race type vertical mill, ring changes generally have to be effected after every 15000 to 18000 hours of running time. Grinding ball changes or additions are also necessary two or three times in this period.

By comparison, it is considered possible with ball tube mills to extend the period between successive changes - by using liners of most adequate lifter profile and material between 30000 and 40000 running hours.

Thus, the working life of the wearing parts of a ball tube mill can be twice as long as that of its vertical type equivalent.

Grinding in a ball tube mill consists of a reduction of lump solid materials to smaller particles by the application of shearing actions, compression, attrition and impact. So grinding may be said to consist of the application of power to rotate the mill shell, thus transmitting the energy to some form of media which, in turn, by rolling, sliding and impacting action, fractures materials into smaller, individual particles. Mill liners are the agents which transmit this energy and motion to grinding media. The liners therefore really play the part performed in a machine tool, motor vehicle etc, by the mechanical energy transmission parts (e.g. gear, clutch etc.).

Figure 1.1 Configuration of the ball charge in the tube mill

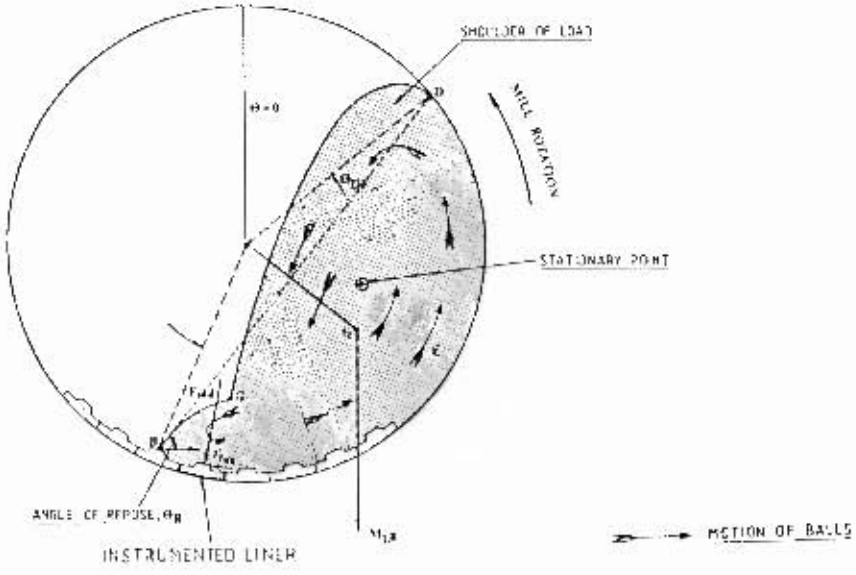

The efficiency of a whole machine is consequently partially dependent on the efficiency of the energy transmission component. Therefore, the efficiency of the ball tube mill can only be maintained when the configuration of the ball charge motion is retained at the designed level. This objective can only be obtained when the initial action of the liner is preserved within permissible profile change, that is the wear rate of the liners is kept at a low level.

Every mechanical process generates friction. Friction influences both the effectiveness of the process and the efficiency of the necessary energy conversion. Besides converting part of the energy input into useless low grade heat, friction also causes wear; ie. it causes a loss of material from surfaces participating in the mechanical process.

Concern about wear is particularly evident to designers of durable equipment such as mills for pulverization of coal. The complex nature of the wear of materials is one of the most frustrating design constraints that engineers have to face. Because of these complexities, adequate solutions, or even good approximations, are scarce.

The replacement cost for "worn out" parts of mills used presently in South African power stations account for twenty million Rands and thousands of tonnes of raw materials annually. The toll for "worn out" mill parts is further increased by the energy costs associated with the manufacturing process and the loss of electricity production due to the time consuming replacement operation. The industrial and economic implications of poor wear behaviour clearly warrants the research necessary to solve these problems.

The focus of the work described in this thesis is the determination of the mechanics of the wear process of ball tube mill liners used for the pulverisation of coal for the power generation in South Africa.

There are two steps in the process of minimizing wear of liners :

1. On the microscopic level the material most resistant to wear must be selected after being exposed to the industrial process under controlled conditions.

2. On the macroscopic level the liner profile which is selected must, when used in conjunction with the best wear resistant material, give the lowest wear and the best operational performance.

From a review of the available literature it is apparent that a very important variable in the study of wear of mill liners is the liner material. Relatively soft manganese steel is used world wide as the material for liners for tube mills grinding coal for the power industry. However considering the highly abrasive nature of South African coals, there is a need to investigate whether better materials can be designed to suit these particular conditions. The first step therefore, will consist of selecting the most wear resistant material for coal grinding application.

Then by using a Scanning Electron Microscope the mechanism of wear particle formation will be investigated and an attempt will be made to separate the relative contribution of the mill ball charge impact (radial component) and sliding abrasion (tangential component).
The ball drop test will then be performed on the most wear resistant liner material in order to reveal the extent of damage under two possible mill operating conditions. The first being direct metal on metal impact in order to simulate the condition when in an

thin layer of a mixture of balls and coal at the tip of the toe of the ball charge (Figure 1.1). In the second condition the balls will impact onto the thin layer of pulverised coal covering the liner. This will be to simulate the condition when the balls end their trajectories on the tip of the toe of the mill charge.

Subsequently a Scanning Electron Microscopy investigation will be performed on the test samples. The extent of damage will be compared with that revealed on the liner subjected to the long term industrial test. The purpose of this is to ascertain the intensity of the impact damage in industrial environment and to investigate if either of the test conditions cause excessive damage of the liner.

This investigation will show the relevance of laboratory scale impact testing to 'real life' conditions.

Measurements of radial and tangential forces that the grinding balls exert on liners will be performed on an instrumented laboratory mill when liner lifter profile, mill filling with balls [J] and mill velocity [N_m] are used as control variables. Simultaneously, cinematographic records of mill ball charge motion, taken by a high velocity camera, will be collected. These will assist in defining the extent of areas at which the grinding balls are in motion relative to the mill shell (liners). The records will also be used to analyse this motion in order to determine under different conditions whether impact or sliding is the dominant mode of contact. Finally, wear tests will be performed over an extensive period of time, on liners of various lifter profiles cast from ceramics.

The purpose of this test is :

1. to verify the scaling down factor used for laboratory experiments, by comparing the worn liner lifter profiles under laboratory wear tests, with those obtained in actual industrial trials.

2. to discover whether any important correlation exists between either of the radial and tangential force measurements and the actual loss of material.

Once this is achieved, data generated under instrumented laboratory mill conditions will be analysed, in order to define the most important parameters influencing the wear of ball tube mill liners. It is hoped that this analysis will contribute to the selection of near best mill operating conditions and liner profiles for this application.

Essentially this study seeks to establish procedures and direction for future studies when liners of various profiles made from ceramics are used in pilot mill experiments. It also seeks to contribute to the optimization of mill operating conditions for the South African coal milling applications.

In the long term, research is needed to maximize the nett production from coal fired power stations, or equivalently to minimize the combined costs namely those of:

- total down-time at liner replacement
- total labour costs of liner replacement
- total power consumed in milling
- capital outlay and maintenance, subject to constraints of :

  - adequate production by mills
  - adequate quality of product
  - available technical expertise and infra-structure

CHAPTER II

REVIEW OF THE LITERATURE

2.1 GENERAL WEAR THEORIES

Wear of materials is so complex that generalized wear theories are inadequate. In order to predict wear behaviour, a wear law would need to include the effects of the interactions of many different parameters. Some of the parameters known to affect wear behaviour are:

1. Impact
2. Attrition
3. Adhesion
4. Deformation resistance
5. Fatigue
6. Fracture properties
7. Shearing of junctions
8. Lubrication
9. Phase changes
10. Frictional heating and thermal stresses
11. Microcutting

Because the interactions of these and other parameters (as they relate to wear) are not well defined, no adequate wear theory has yet been developed. However, several authors have made important contributions to the understanding of the wear process which are discussed hereafter.

2.1.1 The Archard Equation

The adhesion theory was used by Archard (1) to develop the analysis of rubbing surfaces. Adhesion theory predicts that when an asperity contacts an asperity on a mating surface under load, an area of contact is formed (Bowden and Tabor (2)). A simplification assumes the contact area to be a radius, a. A further assumption that the thickness of the particle abraded by this contact is proportional to the radius, leads to the equation

$$\frac{V}{D_i} = KA \qquad (2\text{-}1)$$

where V is the volume removed, D_1 is the distance over which the two surfaces were in contact (equal to the diameter of the contact area), K is a proportionality constant and A is the area of contact. Considering all of the contacting asperities and utilizing the relationship of contact area to load and hardness this equation becomes:

$$\frac{V}{D_1} = \Sigma \frac{V_1}{D_1} = \Sigma K_1 A_1 = K_1 \frac{L_1}{3H} \qquad (2\text{-}2)$$

where K_1 is a proportionality constant, L_1 is the load and H is the material hardness. K_1 accounts for the probablility that a contact event will produce a worn particle. Greenwood and Tabor (3) have shown, using a scaled up model of asperity junctions, that such a mechanism for particle formation is possible and that K_1 must reflect geometric conditions as well as the probability that a wear event may take place. Analytical deficiencies result from the idealized assumptions of particle shape and the incorrect relationship between true contact area, load, and hardness due to neglecting shear stresses. A more serious drawback of the Archard equation, however, appears in the form of the constant of proportionality, K_1. While K_1 can be regarded simplistically as the probability that a wear event will take place, this concept alone offers little insight into the wear behaviour of materials. K_1 is reported to vary between approximately 10^{-2} and 10^{-7} in unlubricated sliding. This wide variation in the wear factor, K_1, renders the equation impractical in all but carefully controlled laboratory experiments, and consequently negates the use of the Archard law as a design criterion.

2.1.2 The Theory of Surface Energy

Another approach to the analysis of the wear particle formation process is offered by Rabinowicz (4). The premise for this analysis is that the stored elastic energy in a potential wear particle must be equal to or greater than the work to create the new surface area required by the particle. Rabinowicz measured average wear particle sizes in adhesive wear situations and concluded that a hemispherical model of an asperity was appropriate. Assuming that the particle (still attached to the substrate) is subjected to simple uniaxial stresses which cause yielding as a result of sliding, the stress and strain states shown in Figure 2.1 result.

The elastic energy stored in the asperity as a result of residual plane strain stresses is given below:

$$\text{Elastic Energy} = \frac{(\nu^2\delta^2)}{2E}\ \frac{(\pi d^3)}{12} \qquad (2\text{-}3)$$

where ν is Poisson's ratio, δ is the flow stress, E is the elastic modulus, and d is the diameter of the hemispherical asperity. The adhesion energy necessary for the fracture of the asperity from the bulk is:

$$\text{Adhesion Energy} = W_{ad}\ \frac{(\pi d^2)}{4} \qquad (2\text{-}4)$$

where W_{ad} is the work of adhesion and $\frac{\pi d^2}{4}$ is the new surface area created. Clearly the stored elastic energy must be greater than the surface energy:

$$\frac{\nu^2\delta^2}{2E}\ \frac{(\pi d^3)}{12} \geq W_{ad}\ \frac{(\pi d^2)}{4} \qquad (2\text{-}5)$$

for the asperity to separate from the bulk. This leads to a minimum size criterion for debris particles:

$$d \geq \frac{6E\ W_{ad}}{\nu^2\delta^2} \qquad (2\text{-}6)$$

Further simplification is suggested by Rabinowicz noting that:

$$\nu^2 \approx \frac{1}{10}$$

$$\frac{\delta}{E} \approx 3 \times 10^{-3}, \text{ and}$$

$$3\delta \approx H$$

where H is the material hardness.

For many materials yielding:

$$d \approx 60\ 000\ \frac{w_{ad}}{H} \qquad (2\text{-}7)$$

which is the minimum diameter of loose debris that can be formed under the above constraints. A plot of wear particle size versus the surface energy to hardness ratio is given in Figure 2.2.This tends to confirm the model for a wide range of materials.

The data were generated in low speed, unlubricated sliding experiments.

Several criticisms of this theory are readily apparent. First, the plane strain assumption is not completely accurate. Furthermore, while the theory predicts the minimum particle diameter it says nothing about the rate of wear or the influence and probability of much larger wear particles. Additionally, the theory has neglected the possibility of the work of attrition acting directly as a driving force for the creation of new surfaces and, consequently, wear debris.

Another shortcoming is obvious in that the data in Figure 2.2 shows considerable deviations among similar materials. For example consider the fact that while lead (point A) has a surface energy to hardness ratio more than ten times that of silver (point B), its wear particles are actually smaller than those of silver sliding on silver. It is clear that the Rabinowicz theory represents a potential wear mechanism in sliding contact situations. However, the extent to which the Rabinowicz mechanism governs any given situation is not clear. Furthermore, the value of knowing this size of wear particles if their quantity is unknown, has not been established.

Figure 2.1
Elastic strain energy model for predicting wear particle size (after Rabinowicz (4). (a) Potential wear particle undergoing compressive stress, (b) wear particle after release of normal stress.

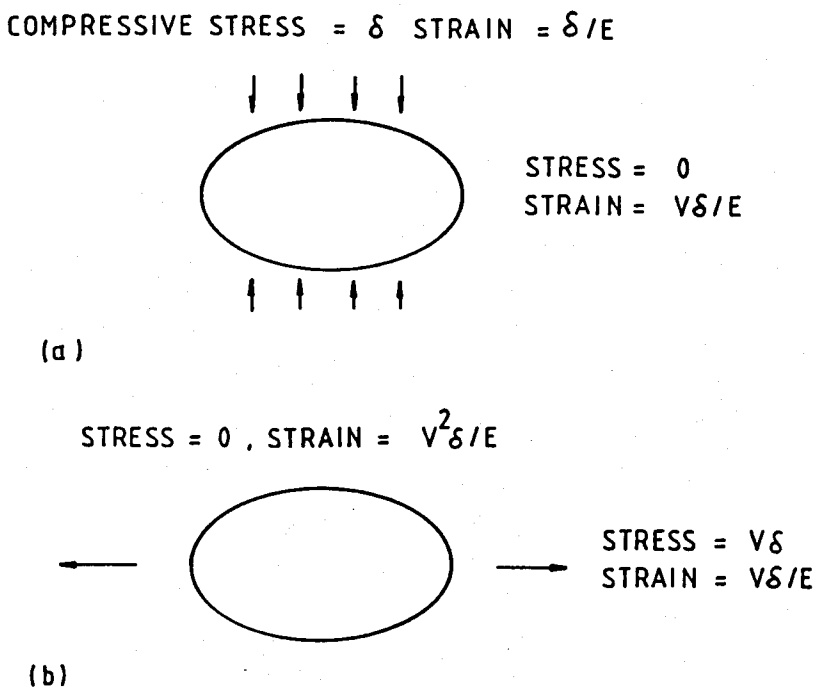

Figure 2.2
Plot of wear particle diameter versus the work of adhesion to hardness ratio for unlubricated sliding for various materials after Rabinowicz (4).

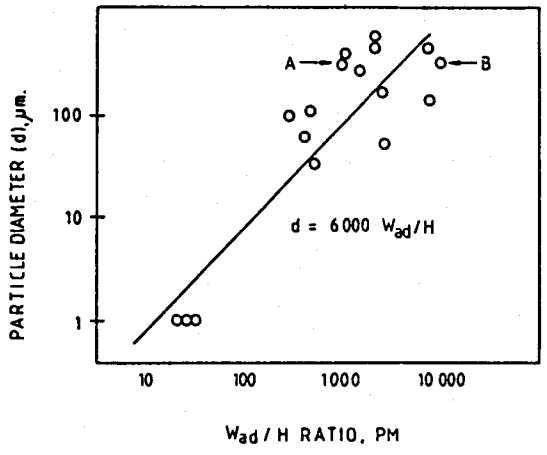

2.1.3 The Theory of Delamination

Suh and co-workers (5) and Jahanmir and co-workers (6) have introduced a theory which relates wear particle shape and size to dislocation behaviour in the near surface regions. This theory suggests a sequence of events which leads to spalling or ejection of a debris particle from the surface. When metal surfaces rub together it is well known that the surface work-hardens and an increase in dislocation density is seen in the near surface region. Suh asserts, however, that there exists a region near the surface which does not exhibit a dislocation density increase, due to the action of the forces from the stress free interface on the dislocations present. The stress acting to move the dislocation to the surface is given by:

$$\delta_i = \frac{Gb}{4\pi(1-\nu)} \cdot \frac{1}{x} \qquad (2\text{-}8)$$

where G is the shear modulus, b is the Burgers vector, ν is Poisson's ratio and x is the distance below the surface. If the image forces (stresses) are larger than the drag stresses, the dislocation will move to the surface, creating an atomic step and reducing the dislocation density. The depth to which this occurs can be approximately calculated by equating the drag stress with image stress and solving for the critical depth X_c.

This is shown below:

$$X_c = \frac{Gb}{4\ \pi\ (1-\nu)\bar{\delta}_d} \qquad (2-9)$$

where δ_d is the drag stress or the friction stress necessary to move a dislocation. If the existence of a dislocation free surface layer is established, Suh (5) postulates that the dislocation density will increase with continued rubbing at depths greater than X_c. X_c is calculated for several materials and varies from 100 microns for 3% silicon-iron to 10 -20 microns for well annealed pure copper.

If dislocations are assumed to pile up below the dislocation free zone, voids will eventually form, especially around hard particle inclusions. Subsequent coalescence is said to lead to the formation of microcracks running parallel to the surface at the critical depth. Once the cracks reach a critical length the stored elastic energy is great enough to give impetus for propagation to the surface, with subsequent removal of the platelet as wear debris. Studies of unlubricated wear of 52100 steel pin on various materials (1020 steel, copper, Fe- 5.8 Mo, Fe-1.3 Mo and Fe-.05 W) confirm the existence of platelike wear debris. Subsequent studies by Pamkies, Teixeira, Saka and Suh (7), of the wear of copper chromium at 0.58 and 0.81 % Cr, copper silicon at 2.3 and 8.6 % Si and copper tin at 1.4, 3.4 and 5.7 % Sn alloys carried out on a lathe using a cylinder-on-cylinder geometry, cite the delamination theory to explain the presence of platelike wear particles in the debris.

A wear rate equation can be derived from the above considerations and is of the form:

$$\text{Wear Rate} = K_o \left(\frac{Gb}{4\ \pi\ (1-\nu)}\right) \left(\frac{L_1 S}{S_o}\right) \qquad (2-10)$$

where L_1 is load, S is the distance slid, S_o is an empirically measured sliding distance necessary to produce one debris particle and K_o is a proportionality constant, related to the geometry.

While the delamination theory offers some insight into the wear process it is deficient in several regards:

1. Its form is not substantially different from the Archard Law.

2. The analytical development is weak considering that the particle thickness argument is predicted from a stress free interface, and it has not been shown that particles do not form while in contact with (and under high stress from) the mating surface.

3. Tsuya (8) has observed microcracks at depths of greater magnitude greater than the depth predicted by the delamintion theory for high purity copper.

However, several significant points are raised by the delamination theory research and are undoubtedly important. These are:

1. Adhesive, fretting, fatigue and abrasive wear may in some cases be caused by the same mechanisms.

2. Metallurgical factors such as inclusions or hard particle carbides can have important effects on wear.

3. Hardness alone does not allow an accurate prediction of resistance to wear.

4. A more detailed study of wear mechanisms is required before individual processes can be understood.

Bitter (9) developed a mathematical model of impact wear that is caused by the impingement of particles. The equation describing the loss of material is given as :

$$W = \frac{M(V\sin\ - Vmax)^2}{2E} \qquad (2-11)$$

where W is the unit volume loss

M is the total mass of impinging particles

V is the particle velocity
is the angle of impact

Vmax is the maximum velocity at which the collision is still purely elastic and is a complex function of the elastic load limit of the material subject to wear

E is the energy required to remove a unit volume of material by impact wear and describes the plastic-elastic behaviour of the material subject to wear

Bitter's (10) work also demonstrated that the most important variable affecting the loss of material during the wear is the E value, which represents the energy required to remove a unit volume of material, and which depends on the plastic and elastic property of material.

Sliding abrasion wear is considered to be as a result of the low-angle impingement of particles. The requirement for this type of wear is that some of the solid particles must have sufficient energy to penetrate and shear a material subject to wear. In practice sliding abrasion wear consists of a cutting action and also incorporates a component of deformation wear. The physical picture of sliding abrasion wear is as shown on Figure 2.4.

Figure 2.4 A physical model of sliding abrasion

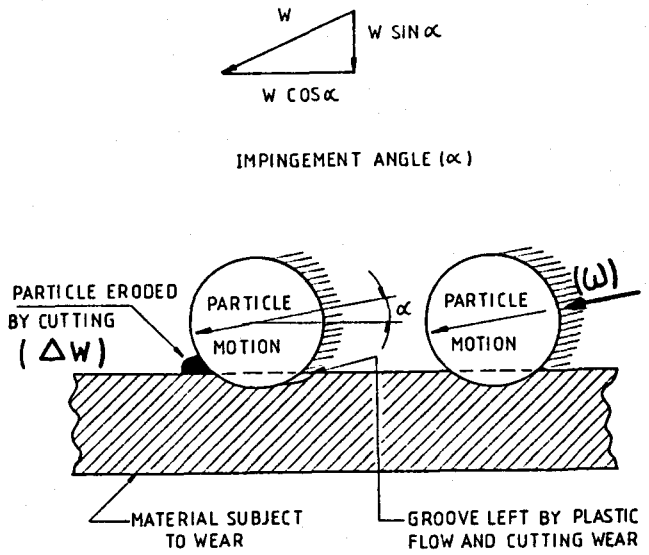

According to Bitter (10) if:

$$W \sin \alpha > W_{max} \qquad (2\text{-}12)$$

where W is the velocity of the particle (ball)
α is the angle of impingement
W_{max} is the velocity of transition between elastic and plastic behaviour of the impacted material

then the particle (ball) will penetrate the material and its sliding action is described by the vector W cos .

Furthermore, according to Bitter (10), the requirement for sliding abrasion wear is that the particle (ball) must have sufficient energy to penetrate and shear material with subsequent gouging of loose fragments.

The analysis of wear, as presented in Paragraph 2.1.1 to 2.1.3. in Chapter II, is relevant to sliding abrasion, as most of the theories developed are related to the wear being a consequence of two moving surfaces.

However, when sliding abrasion is combined with impact, it has a tendency to aggravate the wear, and there is therefore a need to account for this effect in a rational way. Such an account can be attempted from an analysis of the radial (impact) and tangential (sliding) component of the forces generated by grinding balls on the liner, as well as the extent of the agitated area where these forces are active.

The following parameters are expected to have an influence on the wearing process of an air-swept ball-tube mills liners in coal grinding:

a. Liner material.

b. The relative motion (sliding) between the mill charge and the mill shell (liners) depending on:

- mill speed
- liner design and lifter geometry
- composition of the mill charge
- amount of the mill charge
- shape and size of the individual components of the grinding charge.

c. The impact of grinding balls on the mill shell (liners)

- direction of impact
- energy of impact
- size distribution of the product

d. The grindability and abrasive character of the coal.

e. The mill feed rate (percentage of maximum throughput).

In the following pages selected articles from the literature will be examined with regard to points (a), (b) and (c) and their relevance to the wear process of liners will be highlighted.

According to experiments by Rose and Evans (11), if the quantity of the material in the mill is such that it occupies only the voids between the balls, then the kinetics of the ball charge within the rotating mill are largely unaffected by the presence of this material.

In air-swept ball tube mills used in the South African power generation industry, it was observed that the quantity of coal is such that when the mill is stationary only the voids from approximately 50mm below the ball surface down to the bottom of the mill shell, are filled with the coal powder. Assuming that the kinetics of the ball charge as related to (b) and (c) above are unaffected by the presence of coal in the mill, the coal's abrasive character and quantity (points (d) and (e)), although partially influencing the liner wear, will not be considered in the present analysis.

In fact the influence of the above parameters on the wear of liners should be proportional to the quantity of hard minerals contained in the coal such as quartzite and pyrites.

This can be supported by observation of liner wear behaviour in two identical mills grinding two different qualities of coal.

At Arnot Power Station, where highly abrasive coal containing 27% ashes and 4.2% free silica is pulverised, the wear rate of liners is substantial, as revealed after 7500 hours of continuous mill operation as illustrated in Figure 2.5.

This wear is in strong contrast with the less pronounced wear observed on a liner, made from the same material, in Tutuka Power Station on Boiler 1 where less abrasive coal containing 21% ashes and 2.8% free silica, is pulverised. This is illustrated in Figure 2.6 after 10500 hours of continuous mill operation.

Figure 2.5 Arnot Power Station: Liner profiles recorded after 7500 hours of continuous mill operation

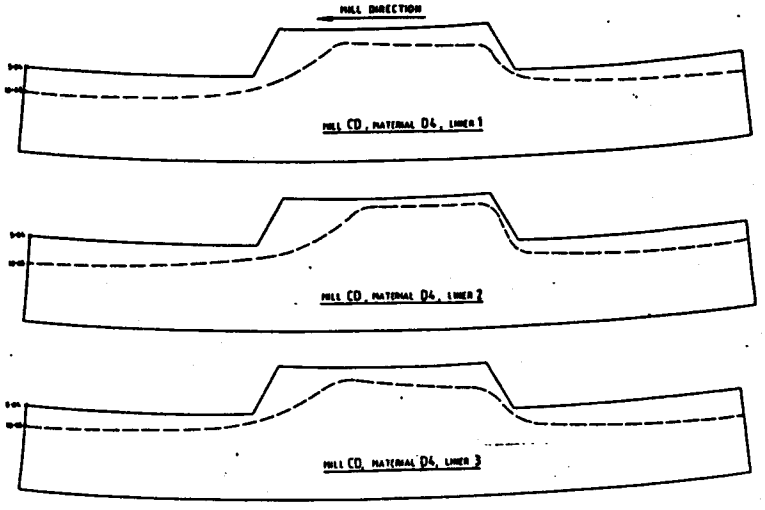

Figure 2.6 Tutuka Power Station: Liner profiles recorded after 10500 hours of continuous mill operation

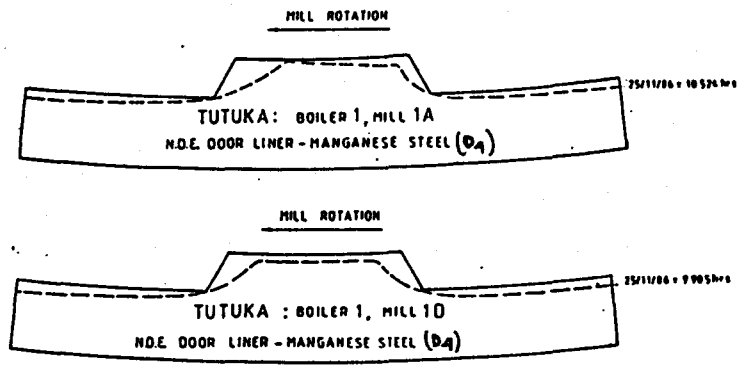

2.2.1 Liner Material

Different materials have different resistances to different types of wear. The wear situation should therefore be analysed carefully before a material is chosen. Experience is often the only guide in choosing the best material to use.

While the literature concerning the wear of tube mill liners is not extensive, several general studies have been conducted which illustrate some important factors.

Bereza (12) reports that martensitic hypoeutectic irons are generally superior to other matrices in impact fatigue ball-dropping test.

Maratray (13) has reported that for liners of grinding mills, ferrous alloys with the highest carbon content have the best abrasion resistance, but because of the severe stresses undergone in service, the material should have sufficient toughness to avoid fracture.
The addition of the alloying elements fixing carbon in the form of carbides which have greater hardness than cementite, as well as simultaneously reducing the content of carbon in the matrix, improves both the toughness and resistance to abrasion.

Norman (14) indicated that in selecting ferrous alloys for mill linings, there are two main considerations : relative abrasion resistance or liner life, and relative toughness. The relative abrasion resistance varies considerably depending on service conditions. For example, in tube mill grinding of silica or other minerals with a Mohs hardness greater than 6.5, the martensitic irons and steels will normally provide only 30 - 60% longer life than the austenitic and pearlitic steels. It should be recognised however, that martensitic iron and steel liners are more susceptible to breakage or spalling in service than the austenitic or pearlitic steels. This is a factor which must be considered in a mill where high impact conditions exist.

Fairhurst and Röhring (15) reported that the high chromium white cast-irons possess a combination of excellent abrasion resistance together with a reasonable degree of toughness. The microstructure of this family of white cast-irons consists of discontinuous eutectic iron-chromium carbides $(Cr, Fe)_7 C_3$ and chromium rich secondary carbides in a matrix of austenite or its transformation products such as martensite, bainite or pearlite. These are obtained by means of heat treatment. Fairhurst and Röhring (15) concluded that optimum abrasion resistance and the best combination of abrasion resistance, strength and toughness, is obtained with irons having a fully martensitic matrix.

In the study of Fulcher, Kosel and Fiore (16) the role of carbide volume fraction (CVF) in developing abrasion resistance was investigated. They measured with dry rubber wheel abrasion test the low stress abrasion resistance against quartz and Al_2O_3 of a series of alloys with varying CVF but with constant matrix and carbide composition. They reported that the abrasion resistance passed through a maximum at an intermediate CVF, near the eutectic composition, for the softer quartz, while the abrasion resistance increased monotonically with the CVF for tests against harder Al_2O_3. They concluded that for quartz abrasive, abrasion resistance decreases with increasing CVF in the hypereutectic composition range because massive M_7C_3 carbides protrude from the worn surface and become vulnerable to cracking. Since Al_2O_3 abrasive particles cut the carbides effectively, the carbides do not suffer cracking, and wear resistance was found to increase monotonically with CVF.

Avery (17) pointed out that although the high hardness of chromium rich $(Cr, Fe)_7 C_3$ carbides in high chromium white cast-irons contributes to wear resistance, the carbides are brittle and the degree to which they are supported by the matrix can play a role in determining whether they crack during abrasion.

Rosenblatt (18) reports that martensitic alloy, white iron such as Ni-hard is the preferred liner material for resisting cutting abrasion, and should be used when impact is not so severe, so as to cause gross impact fracture. When impact is severe martensitic alloy steels should be used to resist abrasion, but they may be subject to gross fatigue failure in the presence of long cycles of heavy impact. Furthermore, Rosenblatt suggests that austenitic steels can be employed should both impact and fatigue accompany highly abrasive ore grinding.

He concludes that although the wear resistance of mill liner materials depends upon the profile of the liners, the operating conditions, and upon the hardness and microstructure of the alloy being employed, suitable liners for today's large diameter mills also call for sufficient impact and sufficient fatigue resistance in the alloy to withstand both surface and gross failure.

Abright and Dunn (19) studied the abrasive wear resistance of a large group of cast-steel and white iron grinding mill liners, using a combination of industrial service and laboratory pin abrasion tests. They found that :

- the hardness of the liner materials appeared to be the most important metallurgical factor relative to weight losses experienced during testing

- martensitic steel liners demonstrated better abrasion resistance than steel liners with other microstructures

- Cr-Mo liners with $(Fe, Cr)_7 C_3$ carbides offered better wear resistance than the Ni-Cr iron liner with M_3C carbides.

A great deal of laboratory abrasion test work has been carried out in support of metallurgical development programmes with various materials, but in many cases it is doubtful whether the wear tests used have simulated the real industrial application precisely enough to produce the same mechanism of wear. This is evident from the fact that the principal studies carried out on high chrome irons have utilised the so-called high stress abrasion pin test and wet sand rubber wheel test to generate data about the influence of compositional or microstructural variables. Neither of these tests can be said to produce loading conditions of repeated impact, although such conditions of loading are a very common feature in actual industrial ball-tube mills.

The mechanism of wear produced in high chrome irons by these two laboratory tests is generally one of micromachining of both the hard eutectic carbide and relatively soft matrix phases, with primary carbide fragmentation occuring in hypereutectic alloys.

For the martensitic matrix with chromium rich carbides, the criterion determining wear resistance of high chrome irons has been obtained. However a complete analysis of all variables influencing such wear has not been made.

Therefore the validity of the proposed criterion is open to criticism as the important variables influencing the wear of air-swept ball-tube mill liners, such as mill rotational velocity, mill filling with grinding balls and (probably the most important) the liner design and lifter geometry, were not considered. In fact the wear resistance of various materials used for ball-tube mill liners grinding coal depends heavily on the ball charge motion inside the mill. This, in turn, is strongly influenced by the above variables and warrants study in order to establish if any correlation exists between the extent and intensity of forces involved, ball charge configuration and wear of liner materials.

Several other authors have contributed "Trade journal" papers concerning the wear behaviour of white irons. Most of these authors agree that martensitic white cast chrome irons provide the highest wear resistance among the alloys used for ball-tube mill liners.

However, it appears in the literature survey that there are no publications on the selection of the most wear resistant material to be used for air-swept coal grinding ball tube mill liners.

2.2.2 Ball Charge Motion

In a ball tube mill, the ball charge is the main working organ, but the liners of the mill play an important part in the milling operation. The part played by the liners is also important for other reasons. Once the mill is started, liner design and lifter geometry will condition the pattern into which the ball charge will settle. The liners will therefore determine all the dynamics of the ball charge in motion, and the way they will agitate this charge determines how the balls will grind and how the liners themselves will wear.

Rose and Sullivan (20) discuss the movement of the ball charge in the mill. Their work is based on the Davis theory which attempts to establish the pattern of the ball charge during mill operation.

It is well known that part of the mass of the ball charge of a mill in operation, remains compact at all times and is driven by the liners at an angular speed which will, in the best of cases, be the same as that of the liner itself. The Davis theory provides a simple means to express the intrinsic force to which any grinding ball is subjected in this mass (independently from the forces exerted upon it by adjacent balls).

The grinding balls in a rotating mill are subjected to the force of gravity and to the centrifugal force. If m is the mass of ball A (Figure 2.7), its gravitational force will be mg, as represented by AB. If ω is the angular speed of rotation of the compact mass, the centrifugal force will be $m\,\omega^2\,r$ as represented by AC, where r is the distance between the centre of gravity of the ball and the axis of the mill. The resultant force is represented by the vector AD. The vector AD will intersect the vertical OV at a point M, and this will be the same for all the balls in the compact mass.

Figure 2.7 Co-ordinate system for the development of the Davis Circle

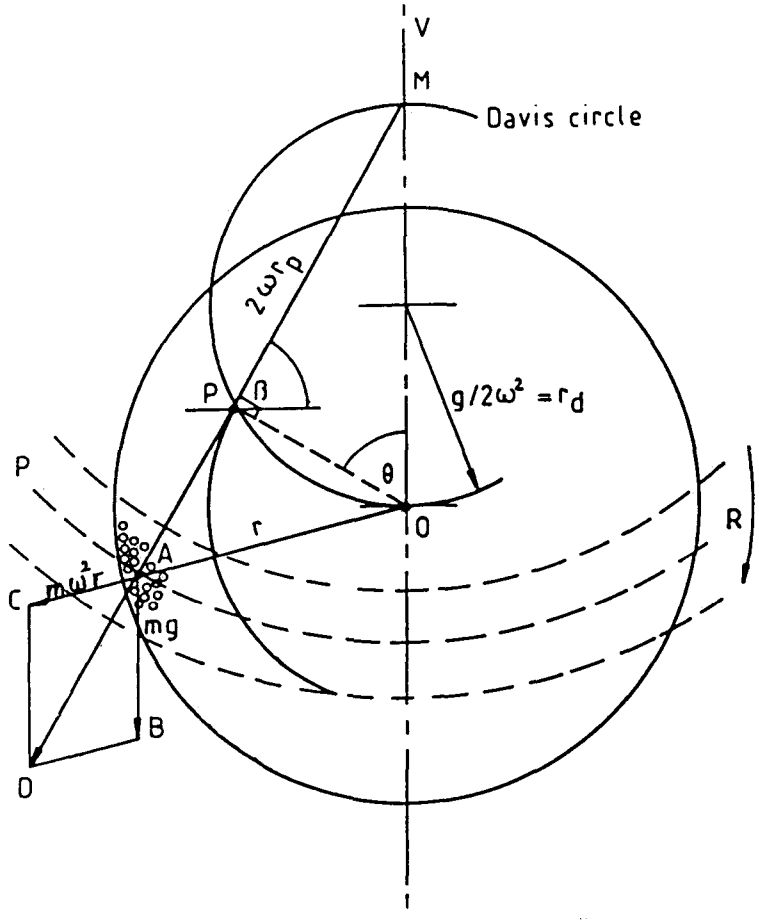

OAM and ABD are congruent triangles and therefore :

$$\frac{OM}{OA} = \frac{AB}{BD} \qquad (2\text{-}13)$$

or $$\frac{OM}{r} = \frac{mg}{m\,\omega^2 r} \qquad (2\text{-}14)$$

or $$OM = \frac{g}{\omega^2} \qquad (2\text{-}15)$$

for any given ball.

On the other hand :

$$\frac{AD}{DB} = \frac{AM}{OA} \qquad (2\text{-}16)$$

$$\frac{AD}{m\omega^2 r} = \frac{AM}{r} \qquad (2\text{-}17)$$

$$AD = m\omega^2\ AM \qquad (2\text{-}18)$$

But AD is a measure of the intrinsic force exerted on the ball (independently from any forces due to contact with adjacent grinding balls).

According to (2-18) above, this force is equal to the centrifugal force which would be exerted if the compact mass revolved around point M, with an angular velocity of ω.

Under this condition, taking M as a centre and drawing a number of circles of different diameters (Figure 2.7), all the balls on each of the circles (e.g. PAR), are subjected to a resultant radial force of constant value. If r_p is the radius MA of the circle PAR, this force will be :

$$f = m\omega^2 r \qquad (2\text{-}19)$$

Circles such as PAR may therefore be considered the contour lines of the compact mass of balls, which form a field, which results from the combination of the force of gravity and the centrifugal force.

Assumption 1:

There is no slip between the particles of the charge and the mill shell (page 35, line 27 and page 45 line 2). This assumption is only realistic for a mill operating far above the critical speed or when unrealistically high value is assumed for the friction factor between the balls and the smooth mill shell. In that case, when the balls leave the surface of the mill shell, they fly across the mill following a parabolic path and impact on the mill shell with considerable energy. At the point of impact, the velocity of the ball is not necessarily equal to the peripheral velocity of the shell lining.

To equalise the speeds of the ball and the lining, the former must accelerate (or decelerate) to reach the speed of the shell lining. While this acceleration lasts, the shell velocity is, by definition, different from the velocity of the balls.

However the equation of motion, when applied to the movement of a ball in a rotating smooth mill shell while using realistic values for the friction factor, predicts that the ball will not follow the rotation of the mill shell, but will be carried along with a velocity smaller than the peripheral velocity of the shell's surface at the point of contact. This will lead to a 'quasi-periodic' movement of the ball. This movement is discussed in the literature under the name of "surging".

Assumption 2:

The authors derive the equation of critical velocity as :

$$W_{CRIT} = \frac{(g)^{\frac{1}{2}}}{(R)} S^{-1} \qquad (2\text{-}20)$$

where $g = 9.81\ m/s^2$

In this formula the angular velocity "W_{CRIT}" refers to the balls and not to the mill shell, though in some cases the angular velocities of the balls and shell liners may be equal.

After this the authors discuss the possiblity of the balls of the charge being projected across the mill shell. They show that the balls can only be projected if they reach a certain height. This depends on:

1. the mill speed and

2. the distance of the ball from the shell centre.

For the ball to be projected from the load, the initial radius of curvature of the parabolic trajectory has to be equal to or less than the radius of the circular path which the ball travels. This condition is satisfied for all points in the mill lying on a circle which passes through the centre of the mill and has its centre $\frac{g}{2w_s}$ above the mill centre.

This circle as shown in Figure 2.7 is named the "Davis Circle", after its formulator.

The radius of the "Davis Circle" is a function of the rotational speed of the mill and can be calculated from the equation

$$r_d = \frac{0.408}{N^2} \qquad (2\text{-}21)$$

After projection from the charge, the balls follow a parabolic trajectory and re-enter the charge to follow a circular path of the same radius.

This implies that the paths of balls do not cross, and that there is no axial mixing of the charge, which is possibly an oversimplification.

Assumption 3:

The authors assume that at the moment of separation from the mill wall, the velocity of the ball is purely tangential. This can only be true if:

1. the balls are not in contact with the shell surface at the moment of separation/projection OR
2. the shell liner is of a smooth type.

In the case of a liner equipped with lifters, the balls in contact with them will:

1. not project from the "Davis Circle" and
2. have a considerable radial velocity component.

The theory as developed by Rose and Sullivan attempts to establish the pattern of the ball charge during mill operation using the following :

Assumption 4:

The internal friction and interference between the balls within the charge at the point of separation is negligible and it follows from this assumption that:

Assumption 5:

All the particles forming the mill charge reach the "Davis Circle" and consequently are projected across the mill.

These two assumptions imply that there is no rolling motion of unprojected balls across the charge body, though it can be shown both experimentally and theoretically that such rolling is the main and sometimes the only mode, depending on the liner lifter profile, of the reverse flow of the charge in the mill.

After this Rose and Sullivan present the theories of Hinsley and Fobelets. Even though they are not entirely satisfactory, they represent an advance on the theories of Davis, mainly through the introduction of the effective friction factor of the charge, as defined by its angle of repose.

Using the effective friction factor, the authors derive a formula that describes the equilibrium surface for the charge, and find that it is an equiangular spiral which has its origin g/w^2 above the mill centre.

This theory states that an equilibrium surface exists within the load, below which balls are subjected to the centrifugal and frictional forces causing them to be locked into the rotation of the mill. Above this surface balls may either follow a parabolic trajectory under the influence of gravity, or they may roll down the load surface. At the equilibrium surface, the balls are at equilibrium with respect to frictional, gravitational and centrifugal forces.

Figure 2.8 Co-ordinate system for a balance on a particle on the equilibrium surface, after Hinsley and Fobelets

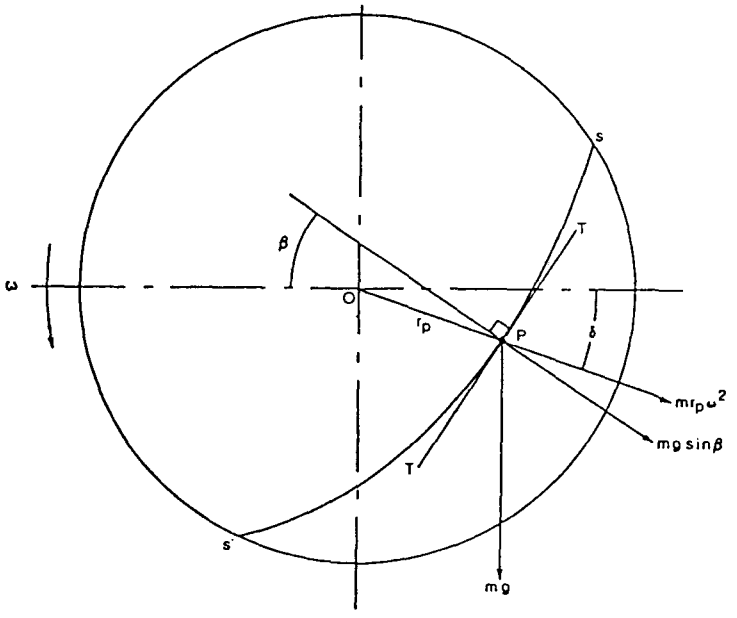

s-s' - Equilibrium surface

T-T - Tangent to s-s' at P

The treatment by Hinsley and Fobelets involves a force balance which includes a coefficient of friction of the mill charge derived from the static angle of repose of the charge (page 55, line 6). A force balance tangential to the equilibrium surface gives :

$$r_p\, um\omega^2 \cos(\beta-\delta) + umg\sin\beta + mr_p\,\omega^2 \sin(\beta-\delta) = mg\cos\beta \qquad (2\text{-}22)$$

Dividing both sides by $m\omega^2$, substituting $x = r_p \cos\delta$ and $y = r_p \sin\delta$, rearranging and integrating gives :

$$\sqrt{x^2 + z^2} = Ce^{\mu\tan^{-1}(z/x)} \qquad (2\text{-}23)$$

where $z = (g/\omega^2 + y)$

This is the equation of a logarithmic spiral expressed in rectangular co-ordinates. To convert this to polar co-ordinates using $x^2 + z^2 = \ell$ and $\tan^{-1}(z/x) = \Psi$, the equation (1 - 23) becomes :

$$\ell = k_{se}{}^{\mu\Psi} \qquad (2\text{-}24)$$

The origin of the spiral can be found when = 0 and is at a point g/ω^2 above the mill centre. According to Rose and Sullivan the constant $k_{\blacksquare}$ relates to the degree at which the ball charge fills the mill. After stating that the factor $k_{\blacksquare}$ depends on the mill filling, Rose and Sullivan do not attempt to find this dependence but present diagrams of different equilibrium surfaces at various mill fillings which shows that the total charge is located below the equilibrium surface at a speed of 70 percent of critical (Figure 2.9). This seems to be incorrect! In fact it could enclose only approximately half of the mill charge as the area under the equilibrium curve represents the part of the charge "going up".

Figure 2.9 Equilibrium surfaces as proposed by Rose and Sullivan

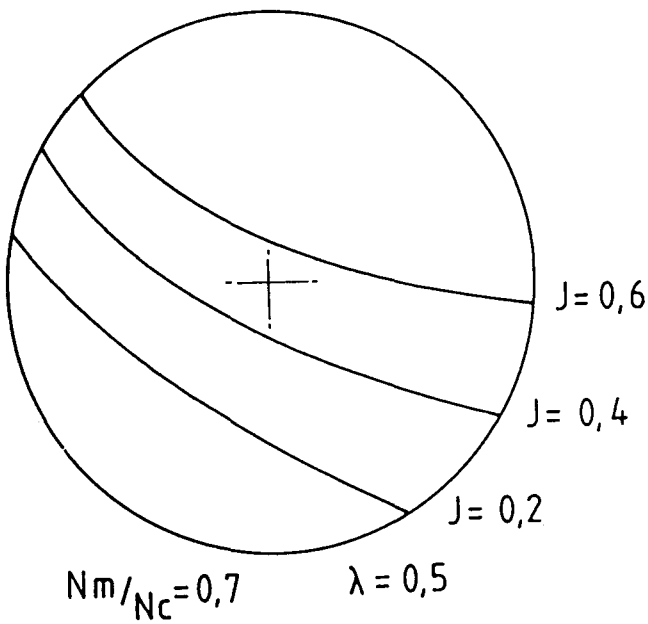

To maintain the constant mass of the charge, an equivalent mass must be "coming down". Some of this returning mass of balls may be projected (only if the equilibrium curve intersects the "Davis Circle"), but most of it will be rolling down on the equilibrium surface. This position will amount to more than just a layer of "a few ball diameters" thickness as suggested by the authors.

While accepting the concept of an equilibrium surface being useful, Rose and Sullivan seem to have misunderstood some of its implications.

1. The highest point of the curve is used as the starting condition for the solution of the differential equation. As such it is freely chosen. In reality it will depend on the lifting capacity of the particular liner chosen and on the mill speed. The dependence on the liner lifter profile does not appear to have been recognised by the authors.

2. The area under the equilibrium line will depend on the highest points reached by the balls, and on the effective friction factor between the ball and liners, but not only, as the authors seem to imply, on the amount of the ball charge present in the mill. In fact, the area "under" the equilibrium curve will be related to the lifting capacity of the mill which is in turn dependent on the liner lifter profile, the mill speed and the amount of the mill charge.

3. The authors' seem to believe that if the "Davis Circle" and the equilibrium surface do not intersect, the mill charge will somehow be built up to reach the "Davis Circle", so that projection of balls can occur (page 58, lines 23-34). The preferred reason forwarded by the authors' is that, "This build-up is clearly possible since, in the mass of balls lying above the main equilibrium surface, but below the "Davis Circle", there exist an infinite number of equilibrium surfaces..." Such a claim is wide open to criticism! It is true that in a mill body there are an infinite number of equilibrium surfaces available, but there is only one which is compatible with the boundary (initial) condition. It is incorrect to choose one equilibrium surface and then abandon it and change to another without any physical reason.

It is obvious from the authors' figures that they seem to labour under three misconceptions:

1. The whole (or almost whole) mill charge is contained "under" the equilibrium surface (page 57, Figure 2.13)

2. The only mechanism the authors' propose for the "return" of the balls is projection after reaching the "Davis Circle" but they do not account for the rolling down of the balls on the equilibrium surface.

3. The authors' assume that projection occurs when the balls reach the "Davis Circle", with an initial velocity purely tangential.

The results of McIvor's (21) work show the important effect of the liner profile on the motion of the mill ball charge. When liner lifters are used, the trajectories of balls depend on the lifter leading angle of the liner. The point at which the balls depart for parabolic flight, and therefore the point where they impact on the mill shell at the end of their parabolic flight, is very sensitive to this angle and an increase in the height of the lifters causes the balls to follow higher trajectories.

According to McIvor, the outer layer of balls in direct contact with the mill shell liners predominantly determine the motion of the entire ball charge, and are therefore responsible for the transfer of energy supplied to rotate the mill to the remainder of the charge.

Furthermore, the portion of the outer layer of balls in relative motion to the mill shell dissipates a significant fraction of the total energy supplied to rotate the mill. This motion of balls relative to the mill shell represents a large loss of energy and according to McIvor can consume up to 10% of the total power delivered to the mill. He concluded that the lifter profile (lifter angle) may have a significant effect on ball mill performance through changes in grinding balls trajectories.

Manz (22) in his study, measured the velocity of the outer layer of grinding balls in the mill. Contrary to Vermeulen (24), he found that the degree of slip of the ball charge depends on the mill speed. Furthermore, the installation of the liner lifters decreases the amount of slip. An increase in the number of rows of lifters also decreases the slip. He demonstrated the beneficial effect of liner lifters by reducing slip by up to 40%.

Fuerstenau and Abouzaid (23) studied the influence of liner lifter geometry on comminution kinetics and energy consumption in a batch grinding ball-tube mill. **They found that the relative specific energy (kwh/t of product) consumed by the mill in the absence of liner lifters, is higher than when lifters are present.** This behaviour is presumably due to the large slip of the mill charge (balls and product) inside of the mill in the absence of liner lifters. Their findings are in agreement with experiments performed by McIvor (21).

Tube milling has for a very long time been a standard procedure for the size reduction of many types of ores and was introduced into the gold-milling plants in South Africa in 1935. However, in view of the large ferrochromium industry in this country and the vast resources of chromite ore, there was a good reason for the Council for Mineral Technology (Mintek) to undertake a fairly extensive research program in order to provide comparative data on the performance of various types of liners for use in the grinding of gold ore. Test work along these lines was initially directed to rod mills, which play an important role in primary grinding. These mills were fitted with liners having lifter bars made from austenitic manganese steel. The bars were rectangular in section, fitting into slots in the backing blocks and bolted through the shell of the mill. One major function of these bars was to provide lift to the charge in the mill. The bars would be expected to have a significant effect on the consumption of electric power used for grinding ore and also to have some protective action in relation to the wear of the total mill lining.

In recent years extensive research work has been performed in South Africa in the field of tube milling of gold ore, most of which was directed to evaluating the influence of liner lifter geometry on mill performance and liner wear.

Measurements made during the test on a 16′ x 30′ mill at East Driefontein mine and on two equal sized 9′ x 12′ rod mills showed that :

1. change in speed of one of two mills with identical lining geometry has a substantial effect on the performance of the mill and on the wear rate of the liners,

2. the data obtained appeared to confirm the selection of the optimum ratio of spacing to height of lifter bars,

3. even simple changes within a given liner design, e.g. the fitting of alternating lines of higher lifter bars can effect a significant improvement in liner life.

4. fitting of lifter bars into large tube mills was shown to be capable of greatly reducing wear of grid liners.

Vermeulen (24) studied the motion of the rods in contact with a smooth liner in a laboratory mill. Since the rods follow almost identical trajectories of motion to those of grinding balls, the conclusions drawn from this work can also apply to a ball mill. The motion of the rods during mill rotation was recorded through a transparent wall by means of a cine camera. The velocities of the rods in motion were calculated from measurements made on successive frames of the relevant film strips. Large fluctuations in the velocities of the rods varying from less than 50% to nearly 100% of mill peripheral velocity, were recorded, in spite of the fact that the mill was rotated at a constant speed. The author stated that these fluctuations with slip of the charge, and a resultant intermittent change in the rods motion from cascading to cataracting and/or from cataracting to cascading, were mainly due to the large fluctuations in local pressure of the charge.

Furthermore, Vermeulen suggested that a minimum pressure of the mill charge is needed to maintain the keying-in action of the charge on the mill shell and at any smaller pressure where the important slip occurs. This slip provokes extensive wear of liners as a result of attrition between the charge and shell as the charge moves across the surface of the lining. This was confirmed by industrial trials where circumferential groovings were observed on smooth liners in the ball mills.

Howat and Vermeulen (25) studied in their experimental work the lifter design as a major influential factor in the mill performance and consumption of liner material. They found that smooth liners were clearly ineffectual, specifically when the speed of the mill was relatively low (see Table 2.1).

Table 2.1 Effect of Liner Lifters on the Performance of the Mill

NUMBER OF LIFTERS	FEED RATE (t/h)	ENERGY CONSUMED PER TON MILLED (Kwh)	WEAR OF LINERS PER TON MILLED (g ie. 10^{-3} Kg)
NONE	51.0	3.25	160.1
12	69.0	3.00	22.2
24	77.4	2.42	12.6

The fitting of lifters improved the mill performances and lengthened the liner life considerably. The tests they performed demonstrated the importance of the prevention of the deleterious slip of the mill charge on the liners by use of an adequately designed liner lifter.

Vermeulen (26) studied the lifting action of liner lifters in tube mills. This study is the most significant work on the behaviour of grinding charge (balls) when liners are equipped with lifters. His method of analysis is to examine the equation of motion of the balls (rods) during the time which they are in contact with the liner lifter.

In the present work the same approach will be adopted, with variation when necessary. Some of the assumptions will be examined and modified.

Assumption 1:

The ball dimensions' relationship to mill shell size are important when the centrifugal force is calculated. In the case of a coal ball-tube mill, when balls are of a much smaller diameter ($\leq$ 1/80 of the mill shell diameter), the use of shell radius in the calculations of the forces balances, will give an error below the experimental inaccuracies expected.

Assumption 2:

Only rectilinear liner lifters are considered. The author recognizes the effect the face angle of the liner lifter has on its performance, but did not give a quantitative analysis. In the present work, such analysis will be attempted.

Assumption 3:

Only sliding interaction is considered between the grinding balls and the liner lifters (rolling action is neglected). The author justifies this assumption in the most convincing manner. Its use will be retained in the present study.

Assumption 4:

The author somewhat over simplifies the behaviour of the grinding balls as they reach the "tip" of the liner lifter. In the present study, a slightly more detailed description will be attempted.

The author's theoretical approach appears correct, and its outlines will be followed in the present work. At this stage, the correctness of his method and conclusions are noted and discussions are reserved until later chapters.

From the above review of literature it appears that:

a. The outer layer of the ball charge in direct contact with liners determine the motion of the entire ball charge.

b. There is a slip of ball charge when smooth liners are used. This slip is reduced by the installation of the lifters which also reduces wear of the liners to a minimum.

c. There is a lack of adequate information on wear resistant materials for the construction of liners for power generation industry.

Furthermore the above literature suggests that the liner lifter profile influences the movement of the mill ball charge, although from the tests performed to date, a firm conclusion can not be made as to the extend of variation of this movement with change in liner lifter profile.

Assuming that the wear of liners is strongly dependent on the mill charge movement, the present work will consist of the study of this movement, using an instrumented laboratory mill, in which various liner lifter profiles, various amounts of mill ball charge [J] and various mill velocities [N_m] are used.

CHAPTER III

PRELIMINARY EXPERIMENTS

3.1 SELECTION OF THE MOST WEAR RESISTANT MATERIAL FOR TUBE MILL LINERS

A wide range of steels and cast irons are used in the mining and mineral processing industries where toughness and abrasion resistance are important. In pulverizing coal for power generation however, mainly steels of soft manganese and harder chrome/molybdenum types are used as materials for mill liners. Over the years, there has been a trend towards the utilization of the harder, more abrasion-resistant materials where good resistance to repeated impact is required.

A great deal of laboratory abrasion test work has been carried out in support of metallurgical development programmes with these materials (References 12, 15, 16, 27, 28, 29, 30, 31, 32 and 33), but it is doubtful in many cases whether the wear tests used have simulated the real industrial environment precisely enough to produce the same mechanism of wear. According to Sare (34), this is evident from the fact that the principal studies carried out on white irons have utilized the so-called high stress abrasion pin test, and the low stress abrasion wet rubber wheel test, to generate data on the influence of compositional or microstructural variables. However, neither of these tests reproduce the loading conditions of repeated heavy impact, common to actual industrial application. There is no information available on any correlation between the wear behaviour of white cast chrome irons tested in laboratory conditions and the wear mechanism which is obtained in an actual industrial ball tube mill pulverizing coal, when repeated impacts are involved.

Nine different materials were selected for metallurgical evaluation prior to laboratory and industrial wear resistance tests. Four South Arican (Scaw, Apex, Mitak and Nordberg) and one European (Magotteaux) foundries were asked to supply liners made from the best materials, according to their experience, for pulverising abrasive coals. The aim of this was to select the most wear resistant material for coal pulverization and to facilitate future development. It is believed that this can be done through a simulation laboratory test using repeated impact abrasion which will have greater validity than the existing high stress abrasion pin test currently used to assess the wear resistance of different materials.

3.2 LABORATORY INVESTIGATION AND RESULTS

3.2.1 Metallurgical Evaluation

3.2.1.1 Chemical Analysis

Determination of chemical composition was undertaken for samples A1, B2, C3, E5, F6, G7(a), G7(b) and H8 by spectographic analysis on a Bausch and Laumb Emission Quantometer, Model No. 3560. The spectrometer was a multi channel instrument operating in a wavelength range of 170 microns to 800 microns in an argon atmosphere with a negative pressure of 7 pascals. Two sparking stages were used, the initial high energy spark for a duration of 25 seconds followed by a secondary spark of lower energy for 8 seconds.

An element percentage was obtained by means of a computerised graphic interpolation. The curves used for the interpolation were obtained using primary standards from Bradley & Foster, Darlston, England (Ref. TI 6241). [For accuracy of the method refer to Appendix A].

The following analysis (Table3.1) was obtained for nine samples.

Table 3.1 : Chemical Analysis

Sample	C %	P %	S %	Si %	Cr %	Mn %	Mo %	Ni %	Cu %
A1	1.28	0.018	0.038	0.375	11.68	0.429	0.969	0.117	0.313
B2	2.58	0.018	0.005	0.445	26.82	0.584	0.061	0.114	0.740
C3	2.93	0.023	0.043	0.804	28.05	0.454	0.081	0.448	0.093
D4	1.35	0.004	0.004	0.890	1.62	11.760	0.020	0.220	-
E5	2.73	0.021	0.120	0.529	27.30	0.727	0.075	0.166	0.093
F6	0.78	0.016	0.014	0.460	2.19	0.917	0.295	0.254	0.098
G7(a)	2.53	0.018	0.035	0.650	23.40	1.050	0.510	0.216	0.168
G7(b)	2.37	0.018	0.014	0.515	14.35	0.727	2.450	0.125	0.180
H8	2.57	0.018	0.022	0.791	28.70	0.442	0.139	0.159	0.112

3.2.1.2 MICROSTRUCTURAL DETAILS

Figures 3.1 - 3.9 show the microstructure of the specimens investigated, as revealed by optical microscopic examination. Magnification of all micrographs approx. 150 X

Figure 3.1
Sample (A1) - grain boundary carbides surrounding a predominently martensitic matrix.

Figure 3.2
Sample (B2) - distribution of chromium carbides in a martensitic matrix.

Figure 3.3
Sample (C3) - distribution of lamella eutectic and hyper-eutectic chromium carbides in a martensitic matrix.

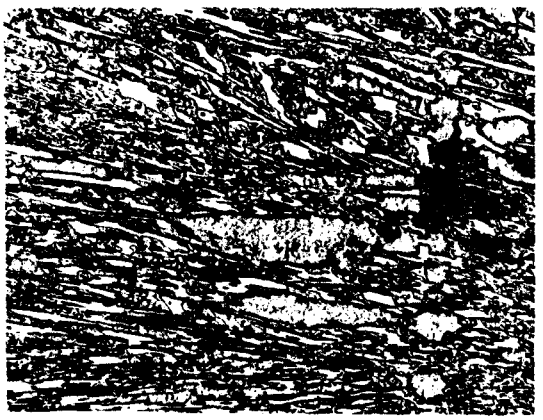

Figure 3.4
Sample (D4) - single phase isotropic microstructure (austenitic), including a sparse and intermittent grain boundry carbide population.

Figure 3.5
Sample (E5) - distribution of lamella eutectic chromium carbides in a martensitic matrix.

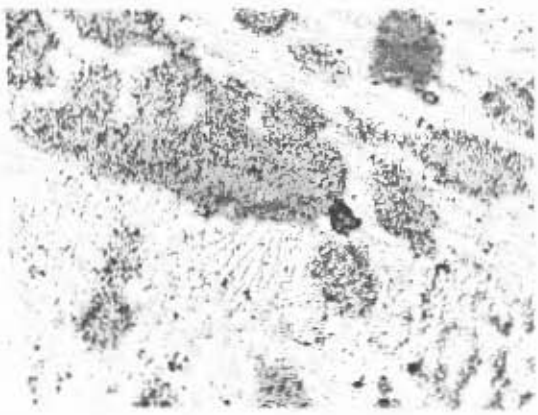

Figure 3.6
Sample (F6) - distribution of fine pearlite and martensite/bainite.

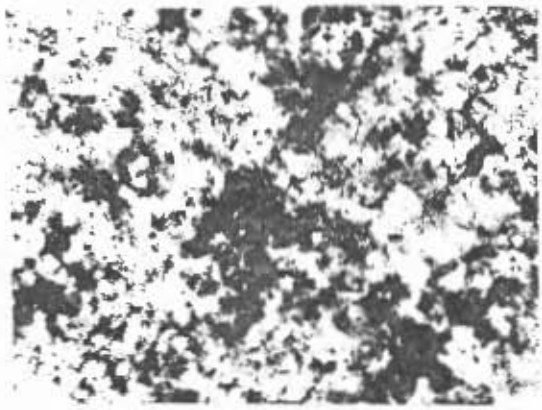

Figure 3.7
Sample (B/a) - distribution of lamella and globular chromium carbides in martensitic/austenitic matrix.

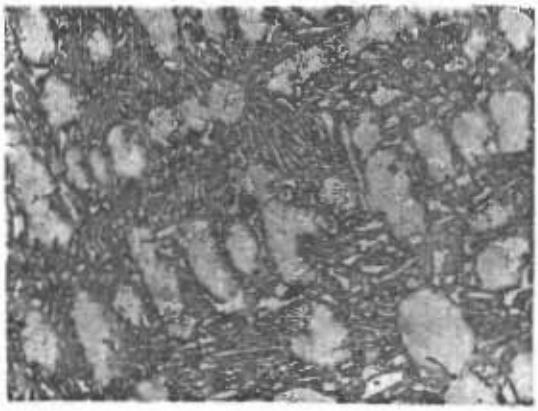

Figure 3.8
Sample (G7b) - distribution of eutectic chromium carbide clusters in martensitic matrix.

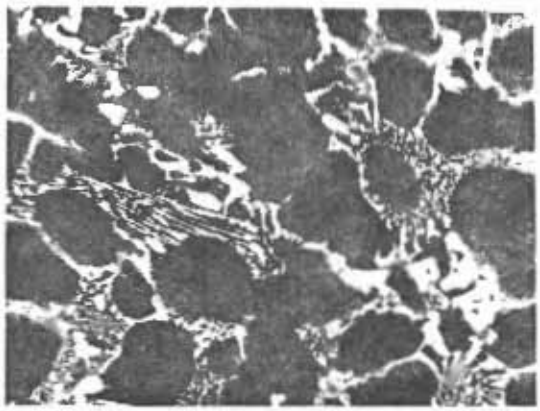

Figure 3.9
Sample (H8) - distribution of lamella and globular chromium carbides in martensitic matrix.

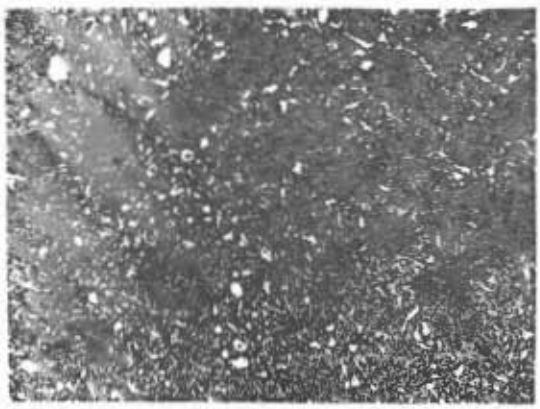

3.2.1.3 Hardness

3.2.1.3.1 Macrohardness

Macrohardness tests were performed on samples before subjecting them to the rubber wheel abrasion tests. The specimen surfaces were assessed using the Vickers tester (30kg load). All values represent an average of at least five indentations.

Table 3.2: Macrohardness of tested specimens (Vickers)

SAMPLE	HARDNESS
A1	590
B2	630
C3	663
D4	249
E5	679
F6	372
G7(a)	532
G7(b)	768
H8	670

3.2.1.3.2 Microhardness (Vickers)

Both the matrix and carbides on the white cast chrome irons were subjected to microhardness testing using the Leitz Miniload 2 tester. The chosen load for testing was 0.25N. The recorded values are given in Table 3.3 below. All values represent an average of at least twenty indentations.

Table 3.3: Microhardness data HV 0.25N from matrix and carbides

SAMPLE	MATRIX	CARBIDES		
		MINI	MAXI	AVERAGE
A1	777	1063	2288	1480
B2	866	1149	2393	1604
C3	705	1377	2896	2243
D4	279	-	-	-
E5	846	1891	2690	2424
F6	361	-	-	-
G7(a)	393	919	2565	1950
G7(b)	844	2143	2690	2343
H8	796	2097	2825	2584

3.2.2 Wear Tests

3.2.2.1 Rubber wheel abrasion test (R.W.A.T.) as per ASTM G-65-80 Procedure A

Abrasion in this test is defined as wear that results in surface metal loss from the localised stresses imposed through the medium of an abrasive. Both deformation and cutting wear are involved.

In the rubber wheel abrasion test, the sample in the form of a rectangular block is pressed against a rotating wheel covered with a chlorobutyl rubber rim of dimensions 0.0127m x 0.0127m. The wheel is rotated at 3.333 rev/s. which corresponds to a linear velocity of 2.38m/s. A 130N load is applied to a lever system to develop a nominal pressure of 0.4 MPa to press the sample against the wheel. The sample is 0.0127m thick x 0.0245m wide x 0.0762m long, a length sufficient to contain the entire wear scar.

The abrasive is gravity-fed between rotating wheel and the sample, through a nozzle with an opening of dimensions 0.0127m x 0.0016m. The flow rate of 5g/s is maintained for 6000 revolutions and wear recorded as sample weight loss.

As an abrasive a ± 50 to ± 70 mesh semi-rounded silica sand (American Foundrymen's Society AFS 50-70, Ottawa Silica, Ottawa, 1161350) was used.

Figure 3.10: Schematic diagram of test apparatus

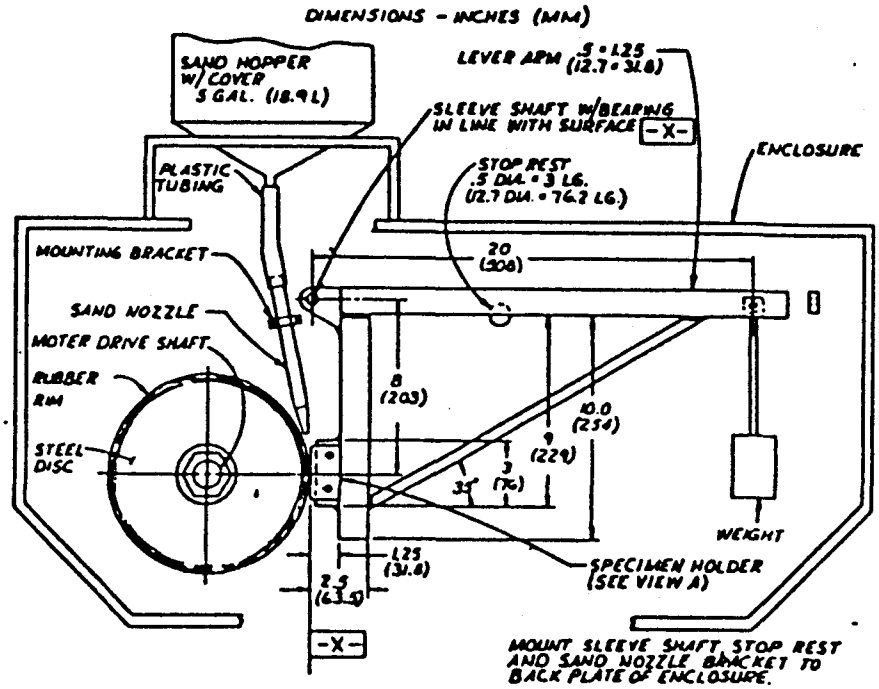

Individual test data from the rubber wheel abrasion test presented in Tables A8 to A16 in Appendix A in the form recommended by ASTM G-65-80.

In Table 3.4 results are presented in the form of volume loss. This table also gives a ranking order of the materials tested under the above conditions.

Mass loss to volume loss was converted according to the following formula:

$$\Delta W = \frac{\text{mass loss (g)}}{\text{density (g/cm}^3\text{)}} \times 1000 \text{ (mm}^3\text{)} \quad (3\text{-}1)$$

Table 3.4 : Summary of the results of the rubber wheel abrasion test

SAMPLE	VOLUME LOSS (mm^3)	RANK
A1	41.9	7
B2	15.5	2
C3	19.7	4
D4	91.6	9
E5	20.9	5
F6	80.9	8
G7(a)	18.6	3
G7(b)	13.8	1
H8	21.8	6

[Refer to Appendix A Table A6 for details of mass loss recorded].

3.2.2.2 Impact abrasion tests

The impact abrasion tests were performed by attaching a specimen of specific dimensions and known mass to a high speed rotating shaft. The specimen was rotated for a specific period of time in a drum containing the abrasive. This test represents a condition in which coarse abrasive materials cut into the wearing surface with considerable force, produce deep gouges and remove relatively large particles of metal from the surface. [Refer to figure 3.11 for schematic representation of the test apparatus].

The interaction between the tested specimen and the abrasive material may be associated with high velocity impact, as generated by grinding balls cataracting onto mill liners.

The abrasive used consisted of 75 percent of 12-25mm Arnot coal, plus 25 percent of 12-25mm quartzite. The quartzite was added later to accelerate the wear rate.

Figure 3.11: Schematic diagram of test apparatus used

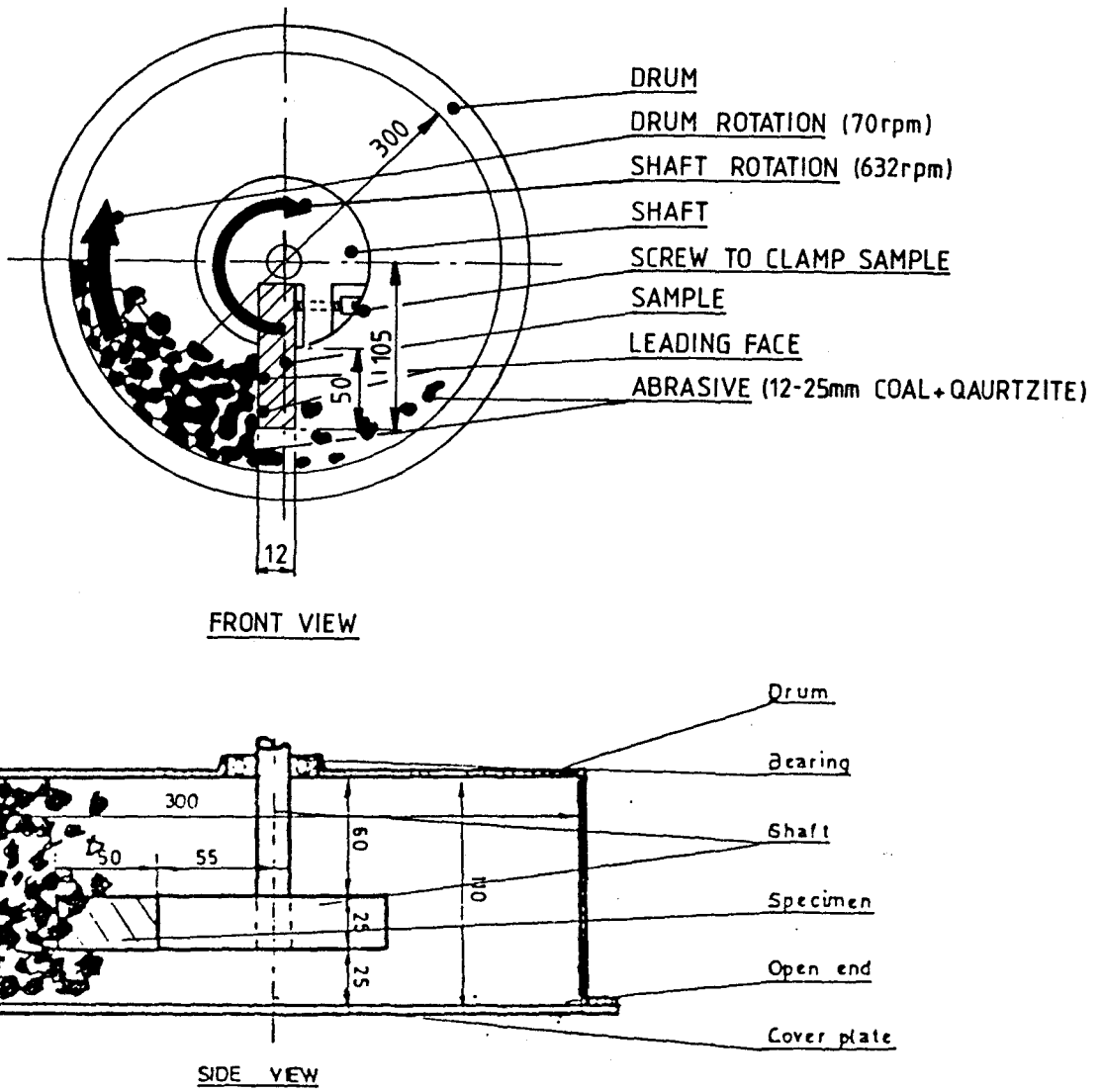

The results are reported as volume loss in cubic millimetres. Mass loss to volume loss was converted according to the formula: (3-1)

Individual test data from the impact abrasion test is presented in Table 3.5.

Table 3.5 : Impact abrasion test

SAMPLE	VOLUME LOSS (mm^3)	RANK
A1	123.5	8
B2	82.5	2
C3	112.4	6
D4	135.8	9
E5	102.8	4
F6	111.4	5
G7(a)	89.7	3
G7(b)	73.0	1
H8	114.1	7

[Refer to Appendix A Table A5 for details of mass loss recorded].

3.2.2.3 Industrial Trials

3.2.2.3.1 Location of Liners in the Mill

Liners conforming to the liner #1 (Figure 5.1) were cast in the nine different materials considered. They were installed in an on-line tube mill pulverising 65 tons of coal per hour in Arnot Power Station. This coal, which was the same as that used in the laboratory impact abrasion test (excluding the quartzitic addition) had the following properties:

* Hardgrove grindability index - 67.
* Coal abrasive index (YGP) - 365 mg Fe.
* Ash content - 27%.
* Free silica content - 4,2%.

It is important to note that these figures were the weekly average obtained over a period of 7500 hours (44 weeks) of continuous mill operation.

Refer to Figure A5 in Appendix A for the positioning of the test liners within the mill.

3.2.2.3.2 Liner Mass Measurement

Prior to the installation in the mill, three liners from each material were weighed. These results were recorded, along with the mass given by the suppliers.

After 7500 hours of continuous mill operation, each liner was removed and weighed on the same balance used for the initial weighing before the test. Table 3.6 is a summary of the liner mass for each of the three liners before the test and after 7500 hours of continuous mill operation.

Table 3.6 : Volume loss of liners after 7500 hours of continuous mill operation

SAMPLE	AVERAGE VOLUME LOSS (mm^3)	RANK
A1	1079220	6
B2	750000	4
C3	1229729	7
D4	2257143	9
E5	572368	3
F6	1673684	8
G7(a)	318421	1
G7(b)	493421	2
H8	820000	5

[Refer to Appendix A Table A7 for details of mass loss recorded].

3.2.2.3.3 Liner Profile Measurement

The profile of each of the 27 liners was recorded using a template with adjustable pins. The profiles were then superimposed on an original liner profile to show the change after 7500 of continuous mill running hours. Figure A6 in Appendix A shows two extreme cases i.e. liner made from alloy D4 with the lowest wear resistance and liner made from alloy G7(a) with the highest wear resistance.

3.3 INVESTIGATION OF MECHANISM OF WEAR PARTICLE FORMATION ON MOST WEAR RESISTANT ALLOY

An investigation was undertaken to evaluate the nature and extent of damage to the industrial liners under normal mill operating conditions and subsequently to define the circumstances under which this damage occurred. In industrial mills there are two possibilities where balls can impact on the liners.

The mill velocity, filling, and liner lifter profile are such, that the trajectories of the grinding balls lead to the impact of balls on the liners, either above the toe of the mill charge or at its tip, where it is cushioned only by a thin layer of the coal.

To determine which of the above conditions the industrial liner was most subjected, tests were performed to simulate the two impact conditions which could have occurred within the mill.

The extent and nature of damage to the liners which were subjected to ball impact tests, was studied using the Scanning Electron Microscopy technique. The results were then compared with those from industrial liners with a view to establishing which laboratory conditions matched with the extent and nature of damage revealed on industrial liners.

3.3.1 Scanning electron microscopy analysis of the industrial liner made from the most wear resistant alloy

Two liner plates manufactured from hard white cast chrome iron and soft chrome malybdenum steel, having a chemical composition and heat treatment similar to Sample E5 and F6 respectively, were installed in an industrial mill. This mill had the same characteristics and operated under the same conditions, as the mill used for industrial evaluation of various alloys.

The position of the liners within the mill was adjacent to the drive end manhole in the direction of the mill rotation i.e. in the third circumferential row from the end of the mill.

After 16000 hours (285 weeks) of continuous mill operation, the liner was removed. The location of Samples A, B, C and D to be extracted from the plate made from the most wear resistant material E5 for scanning electron microscopy investigation, was chosen in order to establish whether or not the wear mechanism was similar over all areas of the liner. It was also an attempt to clarify the metallurgical and physical processes of material removal in actual industrial conditions.

Figure 3.12: Liner (Material E5) After 16000 Hours of Continuous Mill Operation

[Refer to Appendix A Figure A7 for worn profile of liner made from material F6 after 16000 h (285 weeks) of continuous mill operation].

3.3.1.1 Description of Sample Preparation and of Equipment

The samples of 20 x 20 x 25mm were cut out of the liner with a slow speed abrasive cutting wheel, using a tungsten carbide tipped blade. The surfaces of the samples, normal to both the direction of rotation and the surface of the liner subjected to wear, were prepared for scanning electron microscopy examination by successive wet grinding operations to final finish of 1000 grit. The samples were then polished using diamond paste, to a final surface finish of 0.25 microns. In order to reveal the morphology of the carbides in the matrix, the polished faces were etched with a picric/hydrochloric acid solution.

One taper section was also prepared through region of the worn surface in order to permit the sub-surface damage to be examined, and then related to the wear surface.

Figure 3.13 : Sequence of Samples Cutting Operation

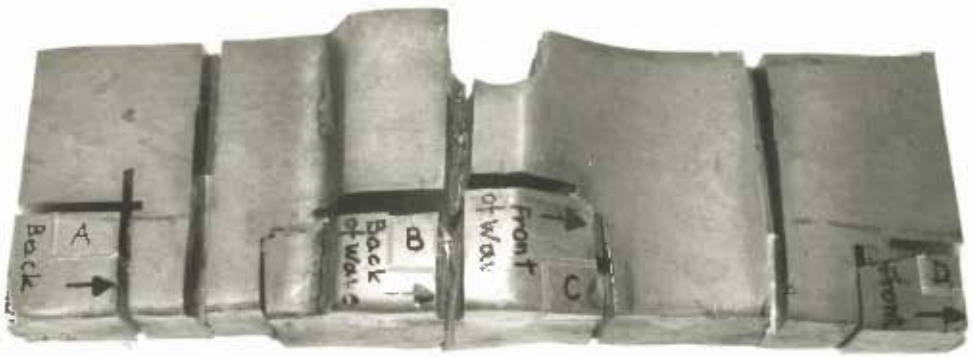

Sample A: Sample of liner removed from rear area of liner plate

Sample B: Sample of liner lifter removed from rear area of the lifter

Sample C: Sample of the leading edge of the liner lifter

Sample D: Sample of liner removed from front area of liner plate

The following four samples were then mounted on aluminium stubs using a conducting graphite-based cement for examination under the Scanning Electron Microscope.
The equipment used was a Phillips Scanning Electron Microscope Model 505 coupled with EDXS (Energy Dispersive X-ray Spectroscopy Unit).

The ease with which a sample may be manipulated in this model allowed the surface of the liner section as well as the adjacent etched face, to be examined without remounting the sample. The motivation behind choosing the Scanning Electron Microscope model was that microstructural phenomena may be positively linked to clearly visible surface features.

3.3.1.2 Scanning Electron Microscopy Photomicrographs

Key to Notation on Scanning Electon Microscopy Micrographs

Example:

Photomicrograph 2 reads:

1mm	30.0KV	7.50E1	0004/00	SAMP. D
A	B	C	D	E

A : These characters correspond to the size of the white marker on the photomicrograph, in order to indicate scale.

B : These characters refer to the accelerating voltage of the S.E.M. in use at the time of taking the photomicrographs.

C : These characters refer to the magnification of the photomicrograph i.e. 7.50E1 = 7.50×10^1 = 75X) (refer also the size of marker).

D : These characters are photomicrograph and user numbers which may be disregarded.

E : These are 7 alpha-numeric characters which may be used for identification purposes on the photomicrograph by reflecting information such as sample numbers etc.

Photomicrograph 1
Detail of Grooving of the Liner Surface showing Wear Scars on the Surface of Carbide Particles
Magnification X 2500

Photomicrograph 2
Magnified View of "Valley" between Carbide Particles
Magnification X 6500

Photomicrograph 3
Disjointing between Chromium Carbides and Matrix. Fracture and cracking of the Carbides Parallel to the Liner Surface can be seen.
Magnification X 2100

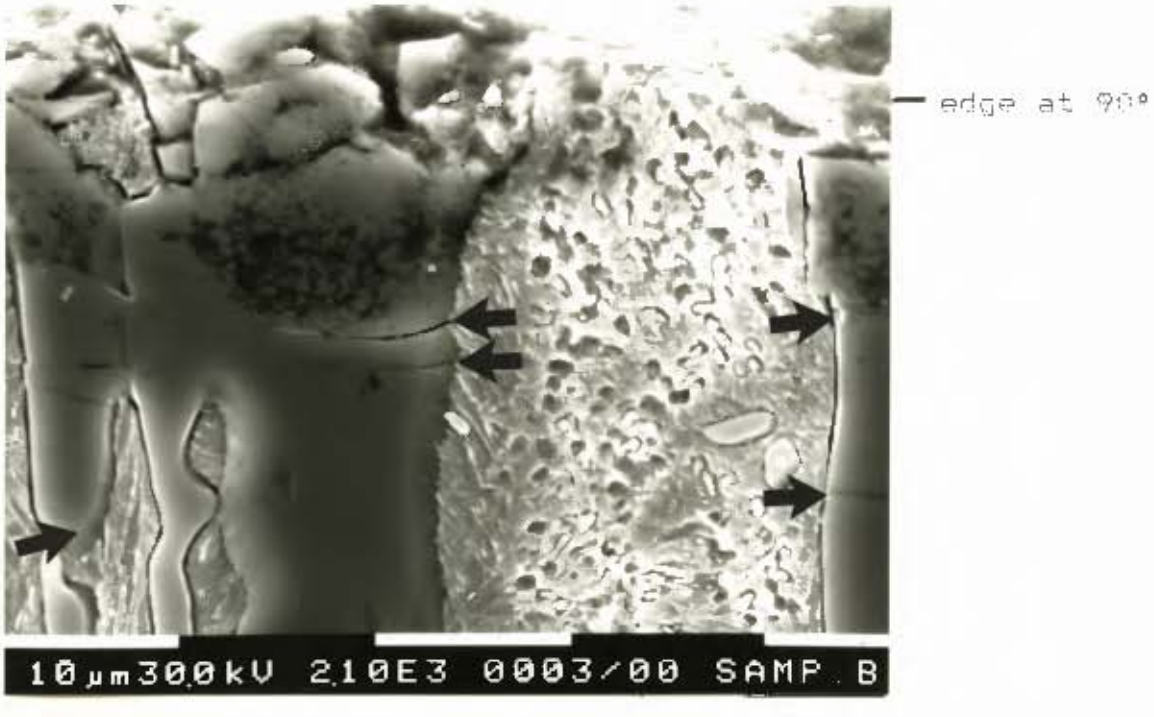

Photomicrograph 3

This photomicrograph shows carbide particles intersecting at the liner surface (angle of intersection of worn and polished surface = 90°). Disjointing between the carbide particles and the martensitic matrix is clearly visible, as well as the cracking of the carbides. This cracking appears to occur roughly parallel to the worn liner surface in most of the cases. Since the cracks do not extend beyond the boundaries of individual carbide particles, this is particularly significant.

Photomicrograph 4

This photomicrograph illustrates the multiple and widespread cracking and microcracking of the carbides that were observed with evidence of material loss having occured by exfoliation of small carbide particles. The orientation of the cracks and microcracks, with respect to the worn liner surface can be seen to be similar in all instances. This was observed to be the case in all sections examined.

The maximum depth below the worn liner surface where damage to the carbide particles was observed on all samples, was measured at approximately 100 microns and is shown in this photomicrograph.

3.4 Investigation Using Ball on Liner Impact Machine

Scanning Electron Microscope investigation on samples removed from the industrial liner made from white cast chrome iron, demonstrated that two events are mainly responsible for wear of liners when grinding coal. They are:

- impact which presumably occurs at the toe of the ball charge initiating and propogating the fatigue cracks of carbides,
- subsequent attrition, producing grooves on the microstructural elements on the liner surface when velocity of the mill shell exceeds the velocity of the mill charge.

However, this investigation did not provide sufficiently reliable information about the circumstances in which the grinding balls impacted the liner. In fact, the damage to the material microstructural elements could be dependent on the liner lifter profile, mill velocity and mill filling, and induced by the direct impact of balls on the liner in the area situated above the toe of the ball charge. Alternatively, this damage could be as a result of grinding balls ending their parabolic flight on a very thin layer of a mixture of balls and coal at the tip of the toe of the ball charge.

The extent of damage when balls impact directly onto the liner is expected to be much more severe than when this impact is generated through a third body, whether it be ball or coal. Therefore, an attempt to establish which of the above conditions the industrial liner was subjected, was undertaken by use of the ball on liner impact machine.

Two tests were performed, one to simulate the motion of balls impacting directly on the liner above the toe of the charge, and the second, to simulate the motion of balls impacting the liner through the layer of coal at the tip of the toe of the ball charge. Subsequently, the extent and depth of damage was evaluated by use of the Scanning Electron Microscopy technique. The results were then compared to those recorded on industrial liners.

3.4.1 Description of the Experimental Machine

The test apparatus provided for the dropping of forged steel balls onto the test liner cast and heat-treated to the same conditions as the liner subjected to the actual industrial test (Sample E5). The machine, as shown in Figures A12 and A13 in Appendix A, consisted of a light weight steel frame, a rubber belt conveyor, together with a ramp system for transporting the balls, and an anvil to support a test liner inside a trough that collected the rebounding balls. [Refer to Appendix A for the detailed description of the experimental machine].

3.4.2 Operation

Two tests were performed. One simulated the impact of balls on an industrial liner above the toe of the mill charge. In this simulation of two body abrasion, a falling ball impacts directly on the liner. The second test consisted of the introduction of a thin layer of coal between impacting ball and tested liner. This was done in order to simulate more closely the expected impact condition in an actual industrial mill, in which coal is usually present at the point of impact between a ball and the liner. This condition occurs when the impact of ball is at, or below the toe of the mill charge. An interruptable light beam on the lower ramp monitored the number of balls that passed.

Before starting up the machine, a test liner was fastened in the holder. Three balls were put into the system in order to generate the impact. Impacts on the test liners occurred at a rate of 500 per hour, not including occasional light impact from rebounding balls.

3.4.3 Test Liners

The alloy composition and heat treatment selected for test liners represented the actual manufacturing conditions as used for the liner subjected to 16000 hours test in industrial conditions (Sample E5). [Refer to Appendix A paragraph 4.1 and 4.2 for chemical composition and hardness].

Test liner blocks were approximately 390mm wide, 400mm long and 45mm thick. The 390 x 400mm surface was the ball impact surface. Before the test the liner blocks were sand blasted and the surface subjected to ball impact was ground with slow speed rotating tungsten-carbide grinder. The test liners were then inspected visually and at a x 10 magnification for cracks and other defects and when none were found, the back (bottom) of the liner block was ground flat, to give good contact with the supporting anvil.

A complete test for a liner entailed a total of 10 000 impacts, after which the liners were removed from the holder and inspected for cracks, spalling and other impact damage. Although each liner in actual industrial conditions could be expected to receive millions of impacts generated by striking grinding balls, it is believed that 10 000 impacts concentrated in one relatively narrow spot (as in the discussed trial) represents a sufficiently severe test in order to generate the damage to the test liner surface and sub-surface similar in its nature to that in an industrial environment.

Figure 3.14 : Liner After 10 000 Impacts Without Coal

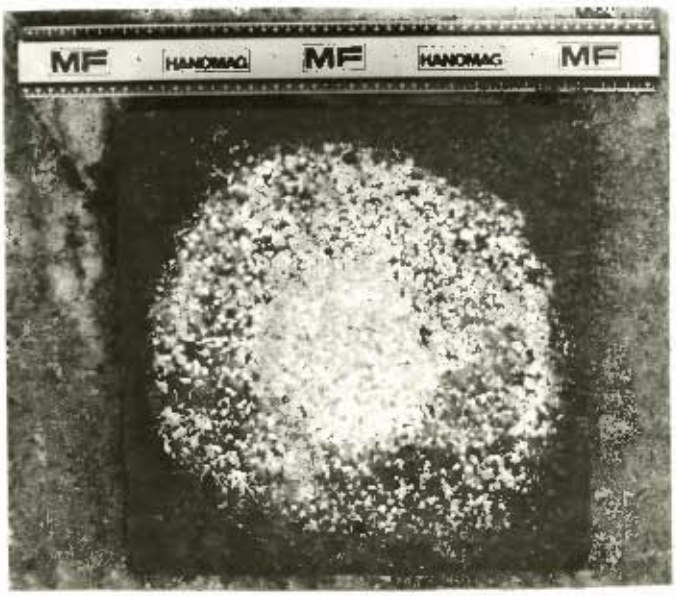

3.4.4 Scanning Electron Microscope Investigation on the Liner Subjected to Ball the Impact Test

3.4.4.1 Sample Preparation

After the ball on liner impact tests were completed, test specimens for Scanning Electron Microscope investigations were cut off from the liners with a slow speed abrasive cutting wheel, using a tungsten-carbide tipped blade. The method of sample removal and preparation for Scanning Electron Microscope investigation was the same as used for samples cut from industrial liner (as per paragraph 3.3.1.1)

3.4.4.2 Photomicrographs of Liner Directly Impacted by Ball Without Coal Present on the Liner Surface

Photomicrograph 5

General View of Damage to the Surface of the Liner Material
Magnification X 300

3.4.4.2 Photomicrographs of Liner Directly Impacted by Ball Without Coal Present on the Liner Surface

Photomicrograph 5

General View of Damage to the Surface of the Liner Material
Magnification X 300

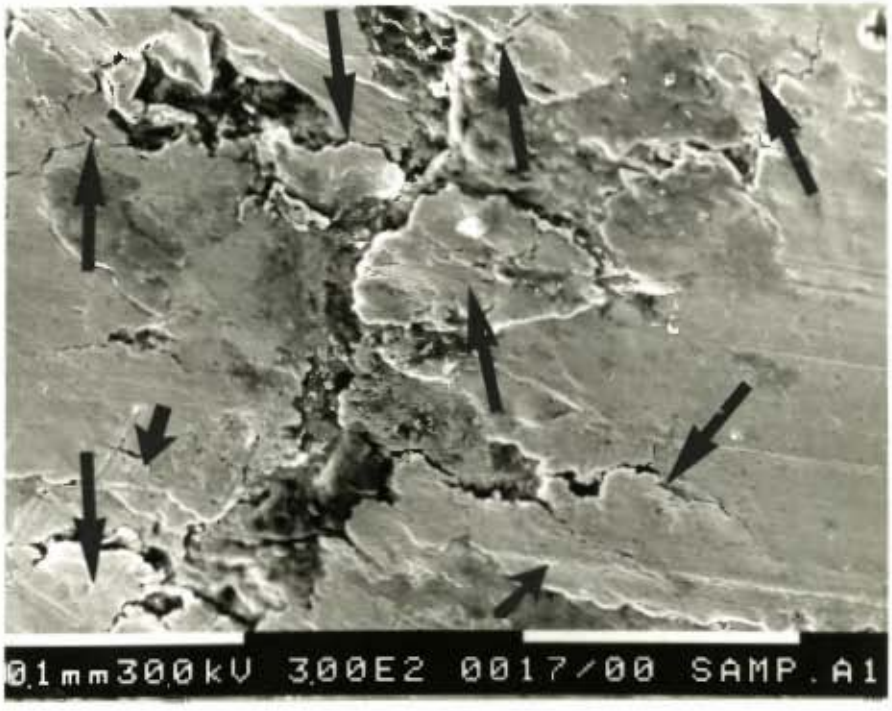

Photomicrograph 6

Intersection of Damaged Surface with Polished Perpendicular Section Showing Crack Propagation
Magnification X 300

Photomicrograph 7

View of the Path Depth, and Morphology of the same crack as shown on Micrograph 6
Magnification X 300

Photomicrograph 8

Magnified View of the End of the Crack Tip as shown on Photomicrographs 6 and 7
Magnification X 1200

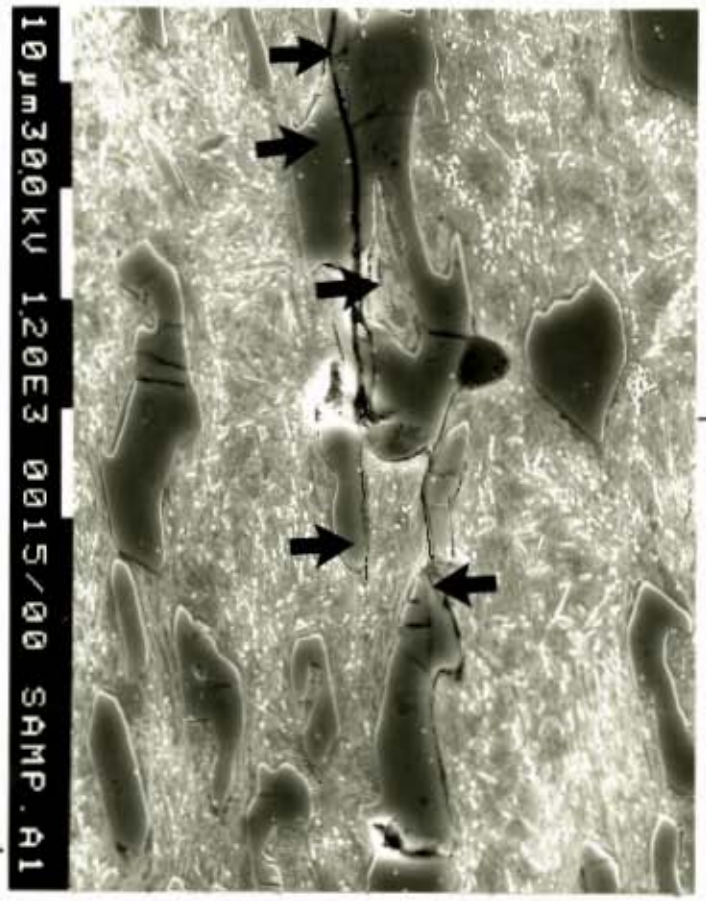

600 microns from the dege at 90°

maxi depth of fractured carbides at 650u

3.4.4.3 Description of Photomicrographs

Photomicrograph 5

This photomicrograph shows very heavy damage induced by balls impacting directly onto the liner surface. Omnidirectional fracturing of the surface can be seen to have occurred. Delamination of a thin layer of the liner material can also be seen.

Photomicrograph 6

A detailed view of the crack on the surface which is propagating into the depth of the liner material. The carbides populating the neighbouring areas are also damaged by multiple omnidirectional fractures.

Photomicrograph 7

The crack on this Photomicrograph is a continuation of the crack as shown on Photomicrograph 5. It propagated through the carbides matrix and along the inter - dendritic carbide network. The direction of the crack is perpendicular to the liner surface, which contrasts to the cracks observed on the liner subjected to industrial test.

Photomicrograph 8

This Photomicrograph represents the liner section approximately 600 microns below the impacted surface where the crack, as shown on Photomicrograph 6 and 7, ended its propagation. Isolated carbides in the immediate vicinity of the main crack are also extensively fractured. The fact that the main crack observed extended beyond the boundaries of individual carbide particles, is significant. The maximum depth at which the fractured carbides were observed was approximately 650 microns below the liner surface.

3.4.4.4 Photomicrographs of the Liner Impacted by Balls, With a Layer of Coal Present on Liner Surface

Photomicrograph 9

General View of Damage to the Surface of the Liner Material
Magnification X 300

Photomicrograph 10
Omni directional Fractures and Cracking of Carbides on the Liner Surface and Sub-surface
Magnification X 1850

Photomicrograph 11
Detailed View of Damage to Carbide Particles Adjacent to the Upper Surface
Magnification X 1200

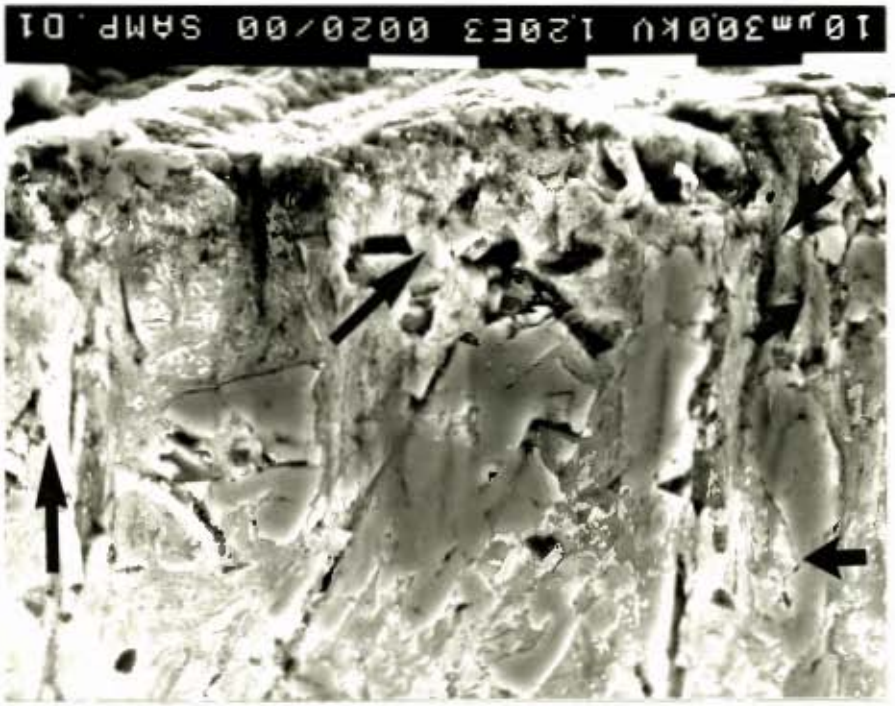

3.4.4.5 Description of Photomicrographs

Photomicrograph 9

This photomicrograph is a representative view of the impacted surface of the liner material. It may be directly compared with Photomicrograph 5. The initial surface condition (i.e. ground) is still discernible. The surface appears to be damaged to a far lesser extent than depicted in Photomicrograph 5. In this instance however, coal was present between impacting ball and liner surface.

Photomicrograph 10

The carbide particles closely adjacent to the impacted surface were found to be cracked and fractured with cracks propagating omnidirectionally. A similar phenomenon had been observed on the samples extracted from the industrial liner.

Photomicrograph 11

The depth of damage to the carbides depicted on this Photomicrograph can be directly compared with Photomicrograph 4. The maximum depth below the impacted liner surface at which damage to the carbide particles was observed, was measured at approximately 60 microns.

3.5 PRELIMINARY DISCUSSION AND CONCLUSIONS

3.5.1 Preliminary discussion

3.5.1.1 Chemical analysis and microstructure

Norman (14) stated that steels and irons used for liners, for mills can be classified into 10 general types. Today from the present investigation, it appears that only 2 types of material are currently used worldwide for liners for tube mill grinding coal. The composition and hardness ranges of each type of these materials are listed below in Table 3.7.

Table 3.7 : Ferrous materials for coal-grinding tube mill liners

MATERIAL	CHEMICAL COMPOSITION RANGE					HARDNESS RANGE VH
	C	Mn	Cr	Mo	Si	
Austenitic 12-14% Mn Steel	1.1-1.4	12.0-14.0	0.5-1.5	0.0-1.0	0.4-1.0	200 - 240
Pearlitic high carbon Cr-Mo steel	0.5-1.0	0.6-0.9	1.5-2.5	0.3-0.5	0.3 0.8	260 - 440

These two compositions represent the principal types of ferrous materials which have survived the test of time and commercial use.

The chemical composition and hardness of materials D4 and F6 incorporated into the present investigation are well within the range of the above Table.

According to the chemical analysis obtained the materials tested can be classified in five groups :

- austenitic manganese steel : Sample D4
- martensitic high carbon chrome/molybdenum steel : Sample A1
- pearlitic high carbon chrome/molybdenum steel : Sample F6
- austenitic white cast chrome iron : Sample G7 (a)
- martensitic white cast chrome irons : Samples B2, C3, E5, G7 (b) and H8

Austenitic manganese steel (Sample D4) is one of the most widely used wear resistant materials available. It provides a combination of high toughness, moderate cost, availability and fairly good abrasion resistance. It also has the rather unique property of work hardening when austenite transforms into martensite, under repeated and heavy impact of grinding balls. The original hardness of 210 to 240 Brinell changes into as much as 400 - 500 Brinell. The yield strength and resistance to plastic flow in service can be improved in this type of steel by additions of chromium and/or molybdenum.

Examination of the microstructure of the sample under investigation revealed the presence of a very small quantity of carbides embedded in the austenitic matrix, as well as some grain boundary carbides which tended to be discontinuous indicating poor austenitization.

[Refer to Appendix A Table A2 for heat treatment details].

Twigg and Volves (35) using a fully quantitative energy dispersive spectrometer, studied samples having similar chemical compositions and subjected to the same heat treatment as Sample D4. They found that the normalised atomic percentage of main alloying elements were as follows :

Table 3.8 : Atomic percentage of main alloying elements of manganese steel

ALLOYING ELEMENT	MATRIX ATOMIC %	CARBIDE ATOMIC %
Chromium	2.6	7.9
Manganese	12.3	16.0
Iron	85.2	76.1

From the above it is suggested that both the manganese and the chromium in manganese steel are taken into the metal carbide at the expense of the iron. However, it cannot be said that this will have any beneficial influence on the wear resisting properties of the material tested because of the very small quantity of these carbides present in the matrix.

Figure 6 represents the well known pearlitic chrome/molybdenum steel (Sample F6) which has been available for cast liners, with only slight modifications since about 1930. This type of steel contains sufficient chromium and molybdenum, and an optional nickel content, so that liners made from this alloy develop a fine pearlitic structure with a hardness of about 350 to 420 Brinell, when they are air cooled or air quenched from the heat- treatment temperature. The alloy content also ensures sufficient ability to harden thoroughly.

[Refer to Appendix A Table A3 for heat treatment details].

When low carbon (up to 2.9% of C) white cast chrome irons solidify (Samples B2, C3, E5, G7(a), F7(b), H8), the first solids to precipitate are austenite dendrites followed by an eutectic mixture of austenite and chromium rich carbides. The eutectic carbides solidify in the spaces between the primary austenite dendrites and take the form of grain boundary or radiating lamellae.

White cast chrome irons must be heat-treated to develop full hardness and maximum wear resistance. The heat treatment process consists of heating to a high temperature (austenitizing), air quenching and finally tempering.

During austenitizing, any product of previous austenite transformation such as pearlite or martensite, changes back into austenite. This applies only to the matrix because the eutectic carbides remained unaffected. This is the first function of austenitizing.

The second function of austenitizing is the precipitation of the secondary carbides. The purpose of it is to destabilise austenite in order to ensure that most of it (if not all) transforms into martensite, which is the ideal structure for the matrix. The mechanism of this destabilisation is that fine, secondary carbides precipitate when the metal is held at the austenitizing temperature for a certain period. The precipitation of these carbides impoverish the austenite of chromium and carbon, with a result that, during cooling after austenitizing, Ms temperature (start of martensite formation) is raised, and thus ensures that a higher percentage of austenite (if not all) is transformed to martensite when the alloys reach room temperature.

[Refer to Appendix A Table A4 for heat treatment details].

The micro constituents clearly observed on white cast chrome irons conform with the above description i.e.

- It is apparent from Figures 3.2, 3.5, 3.7, 3.8 and 3.9 that the alloys under investigation are hypoeutectic, with austenite solidifying as a primary phase. From Figure 3.3 it can be seen that large hypereutectic carbides are also present in the microstructure.

- Transformed austenite surrounds carbides and from the hardness values it is apparent that this phase is martensite (Figures 3.2, 3.3, 3.5, 3.8 and 3.9), except Figures 3.1 and 3.7 where presence of austenite can be seen.

- Secondly carbides are seen as fine, dense precipitates along the martensite grain boundaries.

Therefore it can be said that a general feature of the white cast chrome iron samples subject to present investigation, is the distribution of carbides in a predominantly martensitic matrix, except in Sample 67(a) (Figure 3.7) where the matrix is approximately 50% austenitic and 50% martensitic.

3.5.1.2 Hardness

Generally, the load range adopted in the macrohardness testing was chosen to enable a representative hardness value (for the inhomogeneous microstructure) to be obtained. In the case of microhardness tests, a similar philosophy was adopted. The Leitz Miniload 2 tester, coupled with the Leitz hardness measuring eyepiece digital instrument, was used. The latter is the photoelectric two-co-ordinate linear measuring device, which work in conjunction with the electronic computer-counter-printer. The computer used the following formula for the hardness determination, according to Vickers :

$$HV = \frac{189 \times 10^3 \times F}{d^2}$$

where HV = Vickers hardness
F = test load in N (Newton)
d = mean value of the length of the diagonals of the indentations.

The load used for microhardness was 0.25N. Considering the small size of carbides embedded in the matrix, this load was chosen to ensure that the indentation was representative of the phases investigated, and not unduly influenced by surrounding material. However, it should be noted that there is a dramatic "load" effect associated with small indentation, that results in the measured hardness of a given surface being comparatively higher at lower loads.

According to Buckle (35) this effect is particularly evident at loads below 0.50N or 15 microns, when applied on very hard phase-like chromium carbides. Thus the microhardness data presented in Table 3.3 while representative of the populations of the carbides indented, should not be directly compared to data obtained at different loads.

Care must be taken to assess the data as comparable only with hardness values taken at the same normal loading.

Figure 3.15 : Schematic representation of eutectic reaction in Fe/Cr/C Alloys

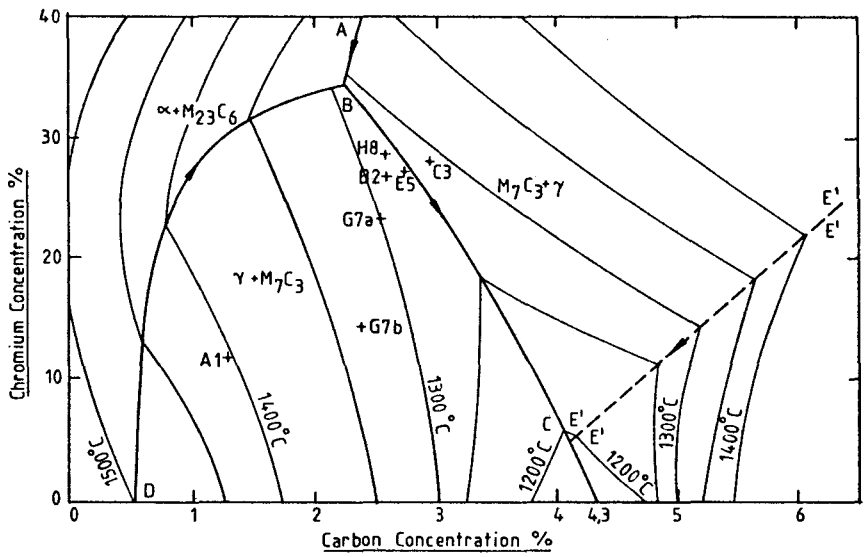

Figure 3.15 is the relevant section of the liquidus surface of the Fe/Cr/C system, i.e. the point at which any alloy within this range begins to solidify. For any given chromium content, a vertical section can be constructed to represent the solidification process. For example, a 10% Cr alloy will be completely eutectic at 3.8%C, whereas a 30% Cr alloy has its eutectic point at 2.7%C.

Description of the phases :

γ	:	austenite
σ	:	sigma (FeCr)
α	:	ferrite
L	:	liquid
M_3C	:	cementite (up to 15 wt% Fe)
M_7C_3	:	trigonal chromium carbide (up to 55 wt% Fe)
M_3C_2	:	orthorhombic chromium carbide (up to 20 wt% Fe)
$M_{23}C_6$	:	cubic chromium carbide (up to 30 wt% Fe)

Table 3.9 : Primary phases formed during solidification

COMPOSITION RANGE	PRIMARY PHASE
Between BC & BD	Primary austenite, followed by M_7C_3 which forms eutectic carbide clusters.
Between BC & E'E'	Primary M_7C_3, followed by austenite eutectic.
Above ABD	$M_{23}C_6$ + ferrite

When hypoeutectic high chromium cast irons solidify, the first solids to precipitate are austenite dendrites followed by an eutectic mixture of austenite and chromium rich carbides of (Cr, Fe)$_7C_3$ type. The eutectic carbides solidify in the spaces between the *primary austenite dendrites, taking the form of grain* boundary or radiating lamellae.

As the Cr and C contents are increased along the tie-line of the band shown in Figure 3.15, carbide volume fraction increases from hypoeutectic to hypereutectic alloys. However the composition of each phase remains essentially the same.

The hypereutectic alloys (those with more than 3% of C) precipitate primary carbides of (Cr, Fe)$_7C_3$ type which are then surrounded by the eutectic reaction product upon solidification, as a mixture of austenite and chromium rich carbides.

The volume of carbides of white cast irons within the microstructure is therefore dependent upon the carbon chromium contents, approximately 10% volume fraction of carbides for each 1% carbon, and 1% chromium. In all cases the microstructure at room temperature consists of eutectic or primary carbides, and austenite or one of its products of decomposition.

Fulcher, Kosel and Fiore (16) studied the role of carbide volume fraction and distribution in developing abrasion resistance of a series of alloys with varying carbide volume fraction, but a constant matrix and carbide (as per paragraph 3.2.2.1.) was used.

In their tests, the examination of the alloys revealed the trend of increasing wear resistance with carbide volume fraction in the hypoeutectic alloys. This can be easily understood in terms of the protection afforded to the matrix by the eutectic carbides. In fact, the carbides are the controlling factor in the wear rate of the hypoeutectic alloys because removal of the matrix (austenitic or martensitic) is prevented by the small spacing between the carbides. Therefore, it is very important that the intercarbide spacing is smaller than the average size of the abrasive. From the microstructural examination of the 9 materials subject to present study, Samples B2, G7(a) & G7(b) seem to comply with the above requirement better than others. In fact, the small intercarbide spacing of the above samples (approximately 25 microns) prevents the effective penetration of the matrix, and its subsequent removal by the abrasives contained in the coal.

These carbides also remain sufficiently supported by the surrounding matrix material to resist a gross fracture generated by the impacting balls. It is expected that they therefore contribute to the wear resistance of these alloys.

In contrast to the above, the wear resistance of the alloy C3 is not as good as the alloys B2, G7(a) and G7(b), because C3 is the alloy of the hypereutectic type containing the massive primary carbides in addition to those of the eutectic type. It can be safely assumed that many of these primary carbides are cracking in service and large pieces of these are spalling off. When this occurs, the matrix is exposed to wear processes of a greater degree, with the result that there is a significant increase in wear rate.

Therefore, in impact condition the large hypereutectic carbides do not contribute to the wear resistance of the alloy. Because of their high hardness they are observed to resist the abrasive better than the softer matrix, but only until the point at which they suffer cracking.

This limitation can be explained by the fact that uncracked large hypereutectic carbides, once the matrix is removed by the abrasive, will protrude from the surface. Consequently they will be less supported by the matrix and therefore more vulnerable to cracking which results from impacts generated by grinding balls.

3.5.1.4 Abrasion tests

The results from rubber wheel abrasion and impact abrasion tests (Tables 3.4 and 3.5) indicate that the materials examined are surprisingly insensitive to the choice of the abrasion test. The ranking orders of the specimens are directly comparable for the first three most abrasion resistant samples. Specimens G7(b), B2 and G7(a) are respectively first, second and third in rank for both rubber wheel abrasion and impact abrasion conditions. The comparability of ranking for the materials of low abrasion resistance is less meaningful in any event, as the differences in volume loss are in general closer as the ranking order descends.

Czichos (38) points out that in order to compare the abrasion behaviour of different materials, the relative wear resistances

$$RW = \frac{W\ (standard)}{W\ (specimen)}$$ have to be defined.

W = Volume loss during the wear test.

Manganese steel (Sample D4) was used as a standard specimen.

Table 3.10 : Relative wear resistance

SAMPLE	RUBBER WHEEL ABRASION TEST	IMPACT ABRASION TEST	INDUSTRIAL TEST
A1	2.1861	1.0995	2.0914
B2	5.9096	1.6460	3.0095
C3	4.6497	1.2081	1.8354
D4	1.0000	1.0000	1.0000
E5	4.3827	1.3210	3.9435
F6	1.1322	1.2190	1.3486
G7(a)	4.9247	1.5139	7.0885
G7(b)	6.6376	1.8602	4.5744
H8	4.2018	1.1901	2.7526

Figure 3.16 : Relative wear resistance : rubber wheel abrasion versus impact abrasion

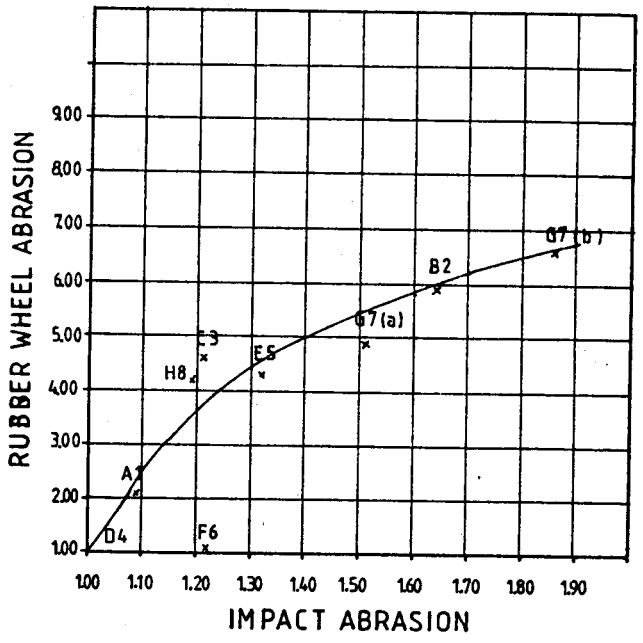

Figure 3.17 : Relative wear resistance : industrial test versus rubber wheel abrasion

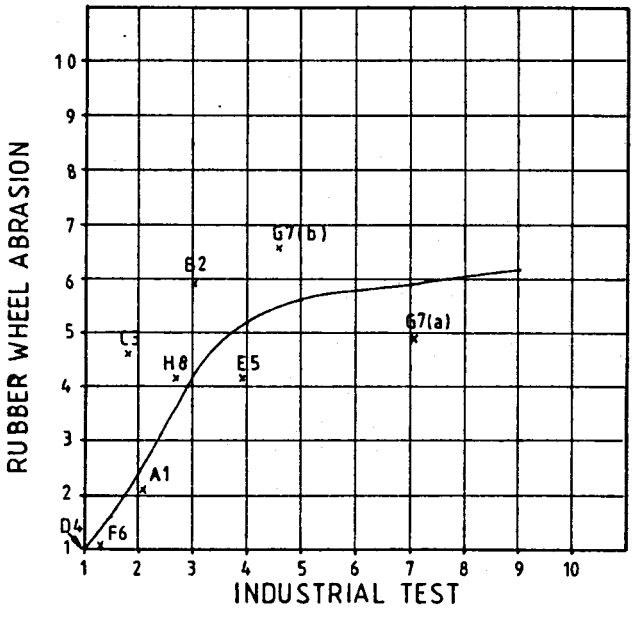

Figure 3.18 : Relative wear resistance : industrial test versus impact abrasion

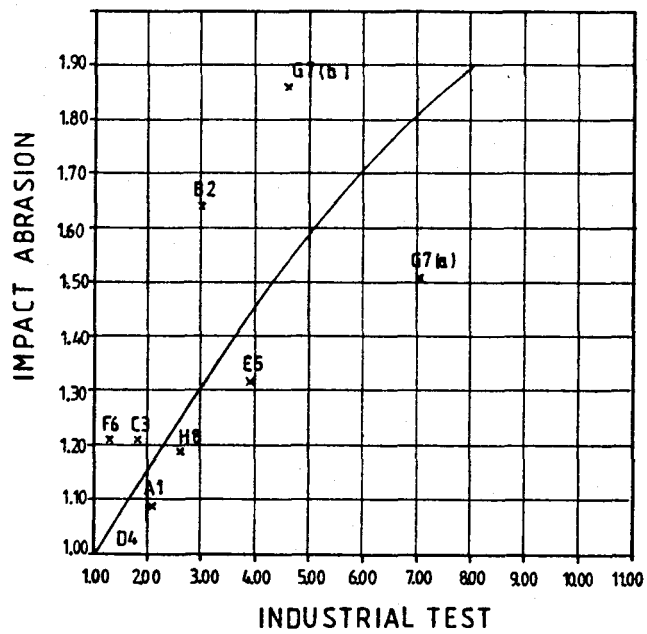

In general, wear tests performed in laboratory conditions are reasonably well supported by wear results obtained during industrial trials after 7500 h of continuous mill operation. There appears to be little real difference in wear resistance under rubber wheel abrasion and impact abrasive technique conditions, for the materials tested. The microstructural features contributing to the satisfactory performance of materials G7(a), G7(b), E5 and B2 in industrial conditions, appear to be high hardness of matrix (with the exception of sample G7(a) delivered in austenitic/martensitic condition), a small carbide size and intercarbide spacing (as a result of good dispersion of the primary carbides produced by optimum heat treatment and judicious choice of alloying elements).

It was interesting to find that the carbide volume fraction does not appear to be an influential factor controlling the abrasion wear resistance of white cast chrome irons tested in laboratory and industrial conditions. The most wear resistant material in laboratory tests and second ranking in industrial trials, G7(b), has a significantly lower carbide volume fraction than other high ranking specimens. This improvement with low volume of carbides can be explained by the vulnerability of hard carbides to the repetitive impact by grinding balls.

3.5.1.5 Scanning Electron Microscopy Investigation

From Scanning Electron Microscopy investigation on liner subjected to the industrial test, it appears that two mechanisms of wear are presumably responsible for material loss on the white cast chrome iron investigated.

Firstly, impact wear occurred at the toe of the ball charge by a process of microspall formation under the impact of grinding balls on the liner surface. The heavily repeated impact of the grinding balls onto the liner surface (protruding eutectic carbide tips) is sufficient to initiate and propagate the fatigue cracks in the carbide particles on the surface and sub-surface of the liner (photomicrograph 5, 6 and 7).

If these cracks propagate sufficiently for a portion of the carbide to fracture, the result will be that the fractured particle is free to be removed from the liner body once the tangential stresses, a consequence of angular displacement of the mill (liners) are applied. Hence this broken carbide debris becomes part of the wearing medium.

The second mechanism of wear took place by the movement of abrasive particles across the liner surface, leading to the dislocation of liner material (broken carbide debris and matrix) by disjointing, deformation and a grooving or cutting mechanism (photomicrograph 1, 2, 3, 4 and 8). Indeed, once cracks have formed they facilitate loss by fragmentation of a portion of individual carbide particles, leaving the matrix standing above the general eutectic carbide level in the surface. The wear resistance offered by the remaining secondary carbide-enriched matrix (photomicrograph 5 and 6) is then partially undermined by impact cracking of the secondary carbides, in a similar manner to that of eutectic carbides. The weakened matrix then deforms plastically under the impact and is removed by movement of harder abrasive particles across the liner surface as thin exfoliations. The cycle will then be repeated.

It is interesting to note the presence of wear grooves on the surface of the hard carbides (photomicrograph 2 and 4). This leads one to deduce that the hardness of the abrasive particles causing these grooves at least approaches that of the carbides. Hardness of chromium rich carbides (1500 Hv) is higher than that of the quartz abrasive (1100 Hv) contained in the coal. Under these circumstances groove formation on the chromium rich carbides is generally not expected. Since the work of Prasad and Kosel (32) demonstrated that quartz abrasive particle, considered the hardest wearing elements contained in the coal, is incapable of causing direct groove formation on the chromium rich carbides, the grooves shown on photomicrograph 2 and 4 must have been formed by a harder substance. The most probable source of groove forming agent is therefore the fragmentation of carbides by the heavy impact of grinding balls.

On the photomicrograph 8, it is clear that when liner is directly impacted by ball without coal present on the liner surface, the maximum depth at which the fractured carbides were observed was approximately 650 microns below the liner surface. This massive damage to the microstructural elements can therefore be expected when the mill operating condition (liner lifter profile, mill velocity (N) and mill filling with balls (J)), are such that the balls are directly impacting on the liner area situated above the toe of the ball charge.

In contrast with this scenario, the photomicrograph 10 illustrates the damage to the liner impacted by balls with a thin layer of coal present on liner surface. The maximum depth the fractured carbides was measured was approximately 100 microns below the liner surface. As the nature of this damage and its maximum depth can be directly compared with photomicrograph 4 from the liner subjected to the test in actual industrial environment, it can be assumed that this test simulated well the mill operating condition to which the industrial liner was subjected, as the grinding balls end their parabolic flights, on a very thin layer of a mixture of balls and coal, at the tip of the toe of the ball charge.

- As the impact wear mechanism is probably much more serious in consequence than the wear by attrition, the mill operating conditions (mill velocity (N_m) and mill filling (J)) and liner lifter profile should be such that the grinding balls do not end their parabolic trajectories on liners situated beyond the thin layer of a mixture of balls and coal at the tip of the toe of the ball charge.

- The direct impact of grinding balls on liners induces and propagates the fatigue cracks in the carbide particles, and promotes the spalling of the liner material with consequent increases of the wear rate.

The small size, fine distribution of chromium rich carbides and small intercarbide spacing will :

* prevent the effective penetration of the soft matrix and its subsequent removal by abrasive particles, such as quartz and broken carbide debris.

* reduce the extent and depth of the carbide fractures, and hence the size of the broken carbide debris.

Sound foundry practice, including optimum combination of alloying elements, melting procedures and heat-treatment should ensure the carbides are given the appropriate distribution and spacing.

CHAPTER IV

THEORETICAL MODEL

4.1 OUTLINE OF THE THEORY OF THE MOVEMENT OF THE BALL CHARGE INSIDE OF THE BALL TUBE MILL

The movement of the ball charge inside of the ball tube mill is governed by the interaction of several forces acting on the balls i.e.

- the force of gravity
- the centrifugal force
- the interaction between the balls (charge material) and the mill inner surface (liners)
- the force of interaction within the ball charge (internal friction).

Rose and Sullivan (17) attempted the first systematic treatment to explain the behaviour of the ball charge in the ball tube mill. In chapter II it is shown that their neglect of the interaction between the ball charge and the mill inner surface (liners) led to results that are inconsistent.

The present work will analyse the theory of movement of a single ball in a rotating mill equipped with smooth and lifter bar liners. It will be demonstrated that liners equipped with different lifter profiles will strongly influence the ball (charge) movement in rotating tube mill, which in turn, will have a bearing on the liner wear pattern.

4.2 MOVEMENT OF A SINGLE BALL IN A ROTATING MILL SHELL

A theoretical study is conducted of the effect that liner lifter-bars of varying face angle will have upon the charge motion within a rotary ball-tube mill. This will demonstrate the important influence that the profile of the lining has upon the ball departure and impact points.

The simplest case of an isolated ball keyed-in to the mill motion is considered. A ball resting on a lifter, against the shell of a rotating tube mill, reaches a point of equilibrium where the sum of the forces acting on it is zero.

Upon referring to Diagrams B-1 and B-2 in APPENDIX B, it can be seen that the forces acting on the ball are :

- gravitational acceleration, acting vertically downwards, mg.
- centrifugal force directed radially outwards towards the mill shell, $m\omega^2 r$.
- normal force of the liner lifter-bar, N.
- frictional force between the ball and liner lifter-bar. This is parallel to the face, and directed towards the base of the liner lifter- bar, μ_f.

For the purposes of this analysis, the forces are resolved into components parallel and perpendicular to the liner lifter-bar leading face, and in the plane of rotation of the mill. The frame of reference is the rotating set of polar co-ordinates following the rotary motion of the mill.

4.2.1 MILL SHELL EQUIPPED WITH A SMOOTH LINER

In a smooth mill shell the movement of a single particle (ball) can be discussed in terms of the following concepts:

ω_b The angular velocity of the ball (S^{-1}), which, due to the possibility of a 'slip' between the mill shell and the ball, is not necessarily the same as the angular velocity of the shell. The angular velocity of the mill shell, which is constant, is denoted by ω_s.

θ_b The angular (polar) coordinate of the ball's position vector. By differentiating this, the angular velocity of the ball is obtained.

Thus the angular velocity of the ball is :

$$\omega b = \frac{d}{dt}\theta_b = \dot{\theta}_b \qquad (4\text{-}1)$$

The angular velocity of the ball can differ from that of the mill shell not only with respect to size, but also with respect to direction.

By definition the frictional force will point in the direction opposite that of the velocity of the ball relative to the lining. For this reason the expression giving the size of the friction force must be accompanied by the function $Sgn(\dot{\theta}_b - \omega_s)$ (the 'Sign' function).

The radial component of the force acting on the ball will be :

$$F_r = m[r_s\dot{\theta}_b^2 - g\sin(\theta_b)] \qquad (4\text{-}2)$$

The frictional force, acting in the tangential plane, will be :

$$F_f = -\mu_b Sgn(\dot{\theta}_b - \omega_m) Fr = -\mu_b Sgn(\dot{\theta}_b - \omega_m) m[(r_m \dot{\theta}_b^2 - gsin(\theta_b)] \quad (4-3)$$

Substituting this into the equation of the tangential force, and equating this force with the product of the mass and the acceleration yields the differential equation describing the angular motion of the ball while it is in contact with the liner.

$$F_t = mr_m\ddot{\theta}_b = F_f - mgcos(\theta_b) = m[\mu_b Sgn(\dot{\theta}_b - \omega_m)(gsin(\theta_b) - r_m\dot{\theta}_b^2 - gcos(\theta_b)] \quad (4-4)$$

This nonlinear ordinary differential equation of the second order was implemented on a personal computer (100% IBM compatible), using a "MICROSOFT" Quick Basic 4.5 compiler (refer to Appendix G for listing). The program gives a primitive graphical output, showing how a single ball moves inside a rotating mill shell. The output shows that the ball slides up and down the mill shell surface, finally arriving at the 'steady' pattern of movement. The interesting thing about this 'steady' pattern is that it depends not only on the physical conditions prevailing in the mill (as one would expect), but also on the initial conditions (the initial angle of position and the initial angular velocity). This gives a theoretical foundation to the wellknown fact that in a tube-ball mill with a smooth liner the ball charge is liable to move in an unsteady pattern, referred to as 'surging'.

4.2.2 MILL SHELL EQUIPPED WITH A LINER OF THE LIFTER BAR TYPE

The interaction of the balls with a liner lifter bar is slightly more complicated than the interaction of a ball with a smooth mill shell lining. The history of the ball during its cyclic (tumbling) motion inside the mill shell embraces the following stages :

a) rest relative to the liner, while the radial component of the acting forces remains positive.

b) the point of equilibrium is reached where all the forces balance out.

c) when the radial component of the active forces is negative, the ball will slide on the face of the liner towards the centre of the mill shell.

d) when the ball reaches the tip of the liner lifter-bar face it will separate from the liner and be projected into flight.

e) after separation from the liner lifter bar, the velocity at the point of separation can have a substantial radial component, as opposed to the case of smooth type liners.

At the point of equilibrium the following equations have to be satisfied.

Forces parallel to liner lifter face,

$$F_{||} = m\omega^2 r_o.\cos\beta_o + \mu_m N - mg.\sin\gamma_o = 0 \qquad (4\text{-}7)$$

Forces perpendicular to lifter face.

$$F_{\perp} = N - mg.\cos\gamma_o - m\omega^2 r_o.\sin\beta_o = 0 \qquad (4\text{-}8)$$

Substituting for N (from equation (4-8)) into equation (4-7), and dividing by m :

$$\rightarrow \sin\gamma_o - \mu_m.\cos\gamma_o = \frac{1}{g}.\omega^2 r_o(\cos\beta_o - \mu_m.\sin\beta_o) \qquad (4\text{-}9)$$

From Diagram B-1 in APPENDIX B, it can be seen that :

$$\text{Sin}\beta_o = \frac{\delta}{r_o}$$

where $\delta = [R-(L + K)].\sin\alpha - r_b \equiv$ constant. (4-10)

Now $\cos^2\beta_o + \sin^2\beta_o = 1$

$$\rightarrow \cos\beta_o = \sqrt{1 - \left(\frac{\delta}{r_o}\right)^2}$$

So :

$$\sin\gamma_o - \mu_m.\cos\gamma_o = \frac{\omega^2}{g}\ (r_o \sqrt{1 - \left(\frac{\delta}{r_o}\right)^2} - \mu_m\ \delta) \qquad (4\text{-}11)$$

$\rightarrow$

For s the unit vector parallel to the liner lifter face and directed outwards, we have at the point of equilibrium:

$s = s_o$ and $\beta = \beta_o$ where :

$$s_o = r_o.\cos\beta_o \qquad (4\text{-}12)$$

$$\beta_o = \arcsin\left(\frac{\delta}{r_o}\right) \qquad (4\text{-}13)$$

Using equations (4-11), (4-12) and (4-13) the ball's location at the point of equilibrium can be fully determined. Equation (4-11) can be solved by numerical methods with the aid of a computer.

The distance S_L and angle β_L when the ball is at the tip of the liner lifter bar can be calculated, as seen in Diagram B-3 in APPENDIX B.

From Δ OLO', we get

$$S_L = \left[R-(L+K)\right].\cos\alpha \qquad (4-14)$$

$$\beta_L = \arctan\left(\frac{\delta}{S_L}\right) \qquad (4-15)$$

Between the point of equilibrium and the tip of the liner lifter, the ball rolls and slides down the face of the lifter. It is not projected into free flight from the point of equilibrium because its tangential velocity is reduced, due to the retarding force of gravity, whereas the liner lifter maintains a constant tangential velocity. Thus the lifter continues to exert a normal force on the ball as it travels down the face of the lifter.

If the static coefficient of friction is greater than zero, the ball will start by undergoing pure rolling due to the torque applied by μ_f (Diagram B-2 in APPENDIX B), where :

$$\mu_f \leq \mu_s N$$

According to Vermeulen, sliding is the primary form of motion along the face of the liner lifter. One must also consider that the natural vibrations in a mill tend to promote sliding rather than pure rolling along a surface. Therefore only the sliding motion of a ball along a liner lifter is considered.

As there is a torque about the centre of mass, there must be an angular acceleration of the ball, but this does not contribute to or affect the linear motion. Some of the energy loss due to friction is converted to rotational motion. A combination of rolling and sliding yields a linear motion that is equivalent to pure sliding. The equation of motion is given by :

$$m\omega^2 r.\cos\beta - mg.\sin\gamma + \mu_k N = \frac{md^2s}{dt^2} \qquad (4-16)$$

Using Force = mass x acceleration, referring to Diagram B-2 in APPENDIX B, and considering the forces resolved parallel to and perpendicular to the face of the liner lifter, we have:

parallel to liner lifter face :

$$m\omega^2 r.\cos\beta + \mu_k N - mg.\sin\gamma = m.\frac{d^2 s}{dt^2} \qquad (4\text{-}17)$$

perpendicular to liner lifter face :

$$N - mg.\cos\gamma - m\omega^2 r.\sin\beta = 0 \qquad (4\text{-}18)$$

Substituting for N from equation (4-18) into equation (4-17) yields the linear acceleration.

$$\omega^2 r(\cos\beta + \mu_k.\sin\beta) + g(\mu_k.\cos\gamma - \sin\gamma) = \frac{d^2 s}{dt^2}$$

Now : $s = r.\cos\beta$
and $\delta = r.\sin\beta \equiv$ constant

$$\frac{d^2 s}{dt^2} - \omega^2 s = g\left[\mu_k.\cos(\gamma_o + \omega t) - \sin(\gamma_o + \omega t)\right] + \omega^2 \mu_k \delta \qquad (4\text{-}19)$$

The boundary conditions at t = 0 are :

$$s(o) = s_o \text{ and } \left(\frac{ds}{dt}\right)_{t\,=\,o} = o$$

Equation (4-19) is a linear non-homogeneous second order differential equation. It is found that the solution consistent with these boundary conditions is :

$$\begin{aligned} s(t) = &\left[s_o + \mu_k\delta + \frac{g}{2\omega^2}(\mu_k.\cos\gamma_o - \sin\gamma_o)\right]\cosh\omega t \\ &-\left[\frac{g}{2\omega^2}(\mu_k.\sin\gamma_o + \cos\gamma_o)\right]\sinh\omega t \\ &-\frac{g}{2\omega^2}\left[\mu_k.\cos(\gamma_o + \omega t) - \sin(\gamma_o + \omega t)\right] - \mu_k\delta \end{aligned} \qquad (4\text{-}20)$$

$$\begin{aligned} \frac{ds}{dt} = \omega &\left[s_o + \mu_k\delta + \frac{g}{2\omega^2}(\mu_k.\cos\gamma_o - \sin\gamma_o)\right]\sinh\omega t \\ &-\left[\frac{g}{2\omega}(\mu_k.\sin\gamma_o + \cos\gamma_o)\right]\cosh\omega t \\ &-\frac{g}{2\omega}\left[-\mu_k.\sin(\gamma_o + \omega t) - \cos(\gamma_o + \omega t)\right] \end{aligned} \qquad (4\text{-}21)$$

Equation (4-20) is solved numerically for $s(t) = s_L$ to yield t, which in turn yields the velocity and position for the ball at the tip of the liner lifter-bar.

At the tip of the liner lifter, the ball is immediately projected into free flight. There is no further significant interaction with the tip of the lifter, due to the radial velocity of the ball, and the curve of its surface.

Here a sharp edge is assumed, but if the lifter is worn or rounded at the tip, this may not be the case.

The free flight trajectory of the ball is illustrated in Figure 4.1

Figure 4.1 Free-flight trajectory of the ball from its point of departure from the liner lifter-bar.

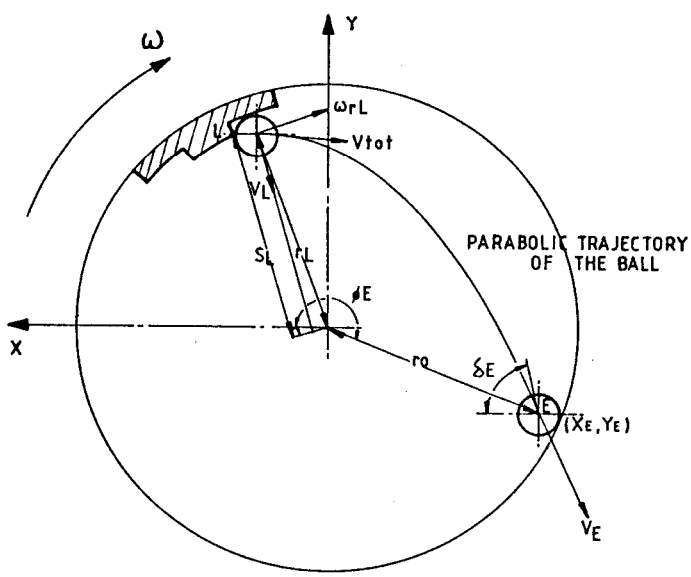

At the tip of the lifter the following are known :

V_L, S_L, θ_L, β_L, γ_L

$$r_L = \frac{S_L}{\cos\beta_L} \qquad (4\text{-}22)$$

$$\phi_L = \gamma_L - \beta_L \qquad (4\text{-}23)$$

This gives the radial co-ordinates of the ball; $(r_L;\phi_L)$

For determining the free-flight trajectory it is convenient to change the reference frame to static cartesian coordinates,

$$(X_L, Y_L) = (r_L.\cos\phi_L,\ r_L.\sin\phi_L) \qquad (4\text{-}24)$$

V_L is the velocity of the ball along the face of the liner lifter, to this must be added the velocity due to the rotation of the mill, arising from the change of reference frames. This velocity component is tangential and equals $r_L w$.

$$(V_{xL}\ ;\ V_{yL}) = (V_L.\cos\gamma_L - \omega r_L.\sin\phi_L\ ;\ V_L.\sin\gamma_L + \omega r_L.\cos\phi_L) \qquad (4\text{-}25)$$

Once in free flight the ball follows a parabolic path given by:

$$(x, y) = (x_L + V_{xL}t\ ,\ Y_L + V_{yL}t - \tfrac{1}{2}gt^2) \qquad (4\text{-}26)$$

The point at which the ball strikes the mill shell (liner), assuming no interaction with the charge mass en route, is satisfied by the condition :

$$X_E^2 + Y_E^2 = r_o^2 \qquad (4\text{-}27)$$

The velocity components are given by :

$$(V_{xE}, V_{yE}) = (V_{xL}\ ,\ V_{yL} - gt) \qquad (4\text{-}28)$$

So the velocity of impact with the mill shell is :

$$V_E = \sqrt{V^2_{yE} + V^2_{xE}} \qquad (4\text{-}29)$$

at an angle δ_E to the horizontal.

$$\delta_E = \arctan\left(\frac{V_{yE}}{V_{xE}}\right) \qquad (4\text{-}30)$$

The full path of the ball in flight, and its conditions of impact with the shell have thus been derived.

4.3 CALCULATED MOVEMENT OF A SINGLE BALL IN A ROTATING MILL EQUIPPED WITH DIFFERENT LINER PROFILES

Using the above equations of motion the point of departure, trajectory, and point of impact on the mill shell (liner) of a ball was calculated for a range of lifter-bar face angles (liner #1, Figure 5.1 in Chapter V) of 60°, 65° and 80°. This was to illustrate the effect of changing this parameter upon the charge (ball) motion.

It was found that the departure angle for ball parabolic flight as well as the angle at which the ball impacts on the mill shell (liner) differs for different lifter-bar face angles i.e.

Angle of lifter-bar	Angle of departure	Angle of impact	Impact radial velocity	Impact tangential velocity
60°	44.37°	237.45°	2.51	0.71
65°	49.31°	228.72°	2.38	1.01
80°	61.80°	208.09°	1.91	1.58

These parabolic flights are illustrated in the following Figures 4.2, 4.3 and 4.4.

Figure 4.2 Trajectory of a single ball when 60° liner lifter-bar is used.

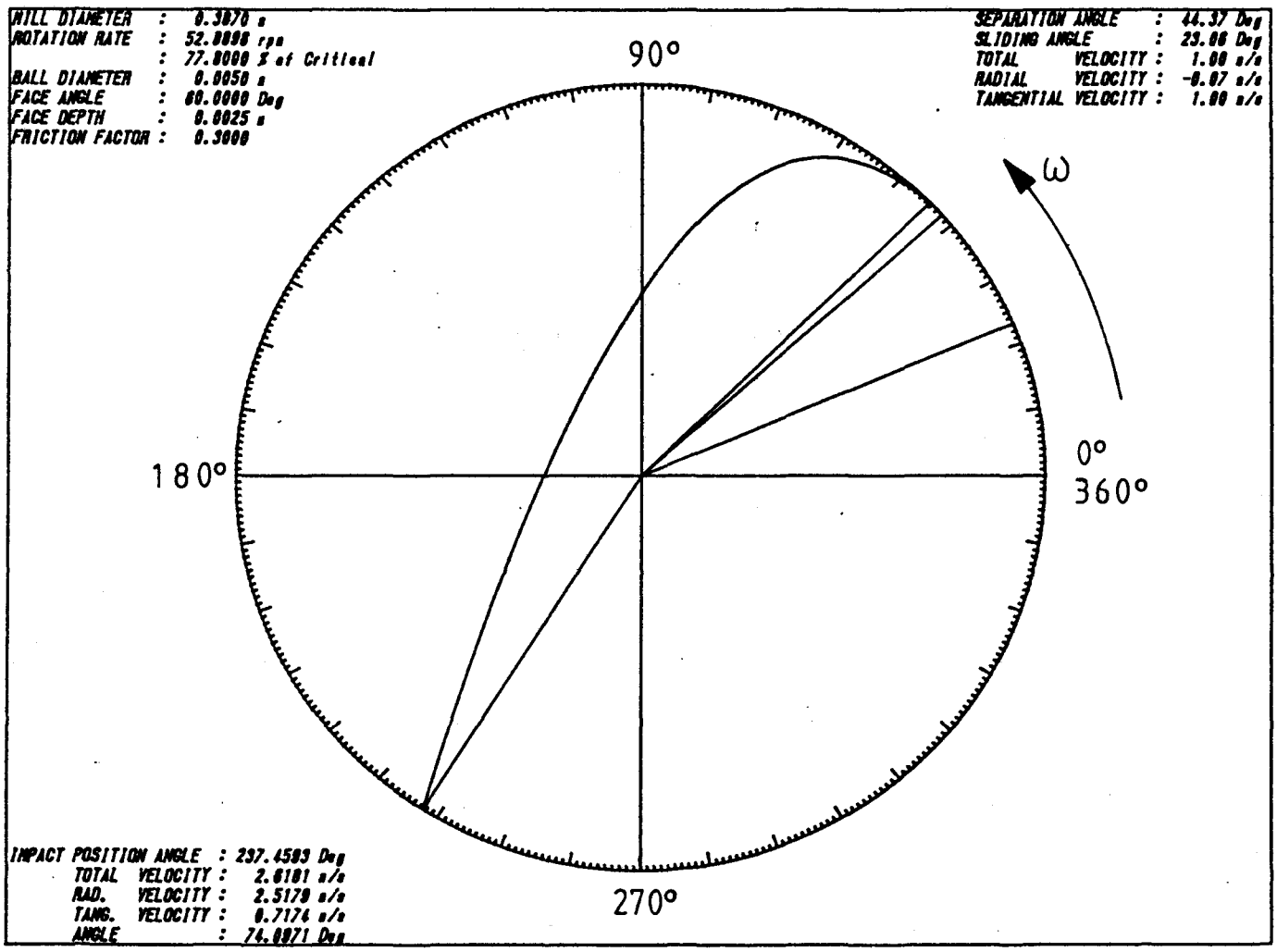

Figure 4.3 Trajectory of a single ball when 65° liner lifter-bar is used.

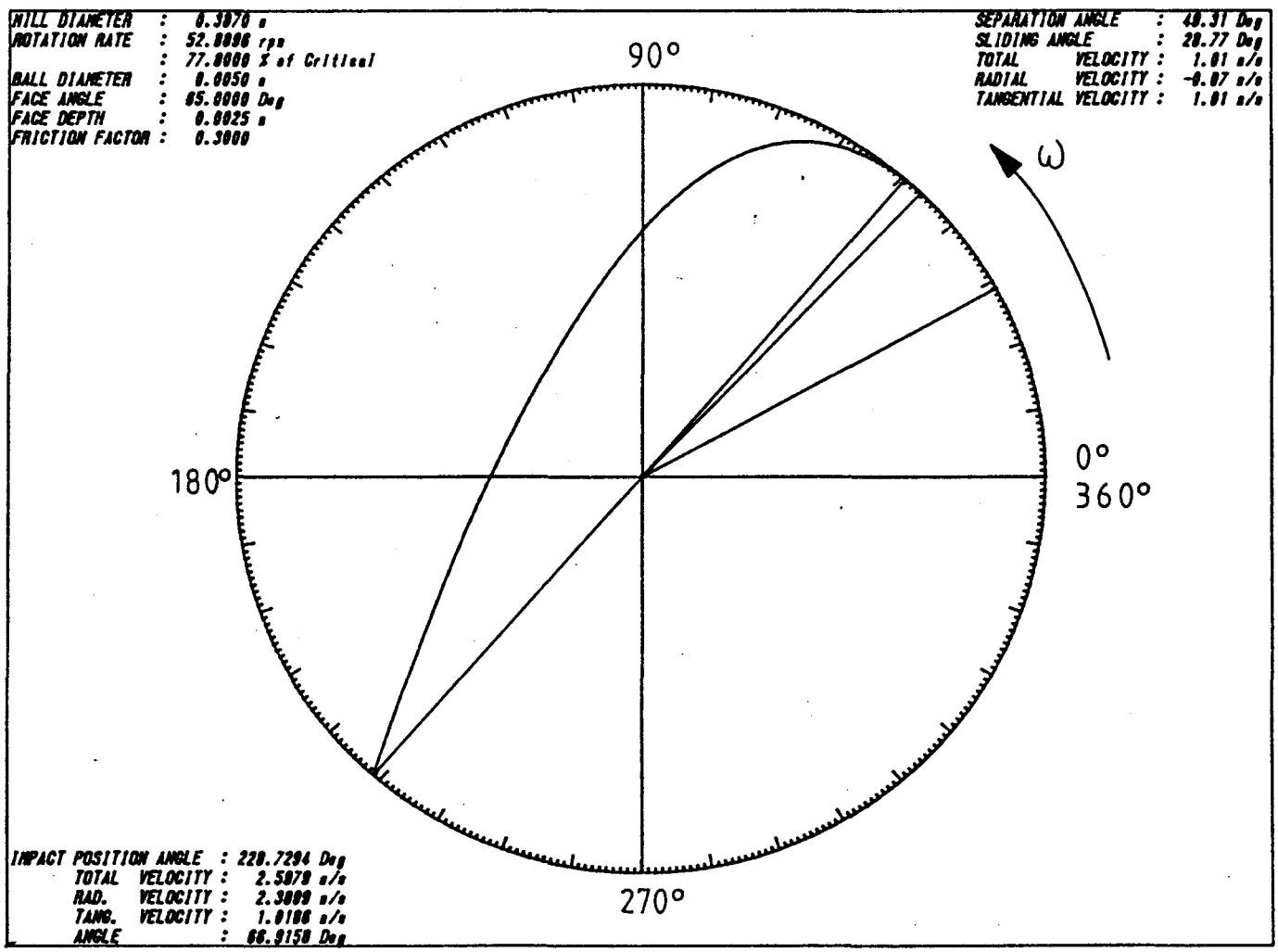

Figure 4.4 Trajectory of a single ball when 80° liner lifter-bar is used.

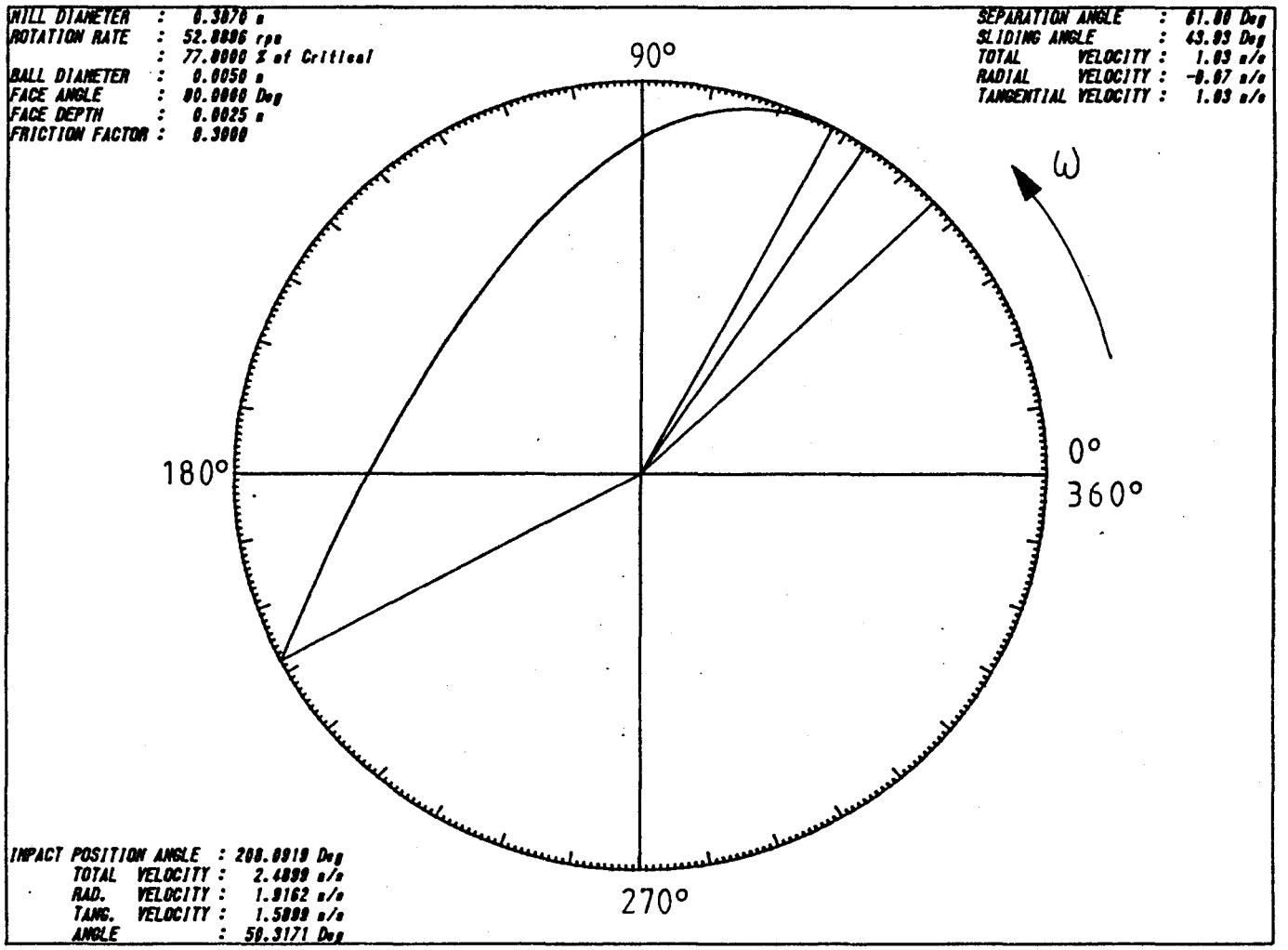

From the above diagrams it can be clearly seen that when varying the liner lifter-bar angle (profile), the pattern of the charge (ball) motion also changes. This has an influence on the radial and tangential components of the impact velocity of the ball on the liner, as well as on the extent of the agitated areas between the balls in motion and mill liners.

It is expected that all the above mentioned elements will have a bearing on the mill liner wear pattern.

CHAPTER V

5.1 EXPERIMENTS USING THE LABORATORY MILL

From the preliminary experiments, it appears that the direct impact of grinding balls on liners situated above a thin layered mixture of balls and coal at the tip of the toe of the ball charge, induces and propagates the fatigue cracks in the carbide particles of white cast chrome irons which were revealed as the most wear resistant material for tube mill liners for coal pulverization. Furthermore, the consequence of this direct impact is that the spalling and grooving of liner material is promoted, once the tangential stresses, as a result of angular displacement of the mill (liners), are applied.

From the survey of literature, it is assumed that the extent and point at which grinding balls impact the liners depends on the mills operating conditions, namely mill velocity, mill filling with balls and liner lifter profile.

The purpose of this investigation was therefore to examine the position and action of the ball charge within the mill and to measure the forces that are exerted by the ball charge on the liner, under different conditions of mill liner lifter profile, mill velocity and mill filling with balls.

The position and action of the ball charge was measured by:

- sensitive load beams, the instrumented liner of each profile was mounted on for measurement of radial (impact) and tangential (attrition) forces exerted by the ball charge on the mill liners.

- cinematographic records, using a high velocity camera.

The wear of liners of different lifter profiles cast from hard and soft ceramics was also measured, while the operating conditions of the mill were close to those at which the industrial mills are presently operating ie.

N_m = 65.0%, 78.0% and 91.0% of critical velocity and
J = 15%, 24% and 36.7% of the total useful mill volume.

From industrial observations it is clear that liners of the same lifter profile (liner #1 Figure 5.1) made from hard high chrome iron and soft chrome-molybdenum material (E5 and F6 Table 3.1 respectively) present different patterns of wear (Figure 3.12 and A7 respectively) as viewed after 16000h of continuous mill operation.

During preliminary laboratory experiments the wear of liners of six different lifter profiles (Figure 5.1) made from both hard and soft ceramics was measured. The operating conditions of the mill were close to those under which industrial mills for power generation industry are presently operating (N_m = 78.0% and J = 24%). Visual comparison of the hard (material 05) and soft (material 08) ceramics version of these liners suggested that the major difference observed was accelerated wear of liners made from soft ceramic (Figure C-3 to C-7) and that the liner #1 mimicked the industrial observations (Figure 3.12 and A7). Thus for subsequent laboratory experiments the hard ceramic was chosen.

The use of hard ceramics for liners for this research was to simulate the wear behaviour of hard high chrome irons which, in industrial and laboratory environments, exhibited better wear resistance than the soft materials tested, like manganese and chrome molybdenum steels.

5.2 DESCRIPTION OF THE EXPERIMENTAL MILL

The experiments were performed using a laboratory mill mounted on a milling rig to permit precise experimentation into various aspects of mill design and control.

The mill is illustrated in Figure 5.2 It has an internal diameter of 0.387m ($\pm$ 0.005m, depending which liner was inserted), which is one tenth of the diameter of the mills used for coal pulverising at Tutuka Power Station, and an internal length of 0.3m. It was precision engineered to produce equipment with negligible (< 0.1mm) out-of-roundness and variation in length. The mill shell thickness was 10mm and 0.5m diameter flanges 15mm thick were welded to each end. One end wall was made of highly wear resistant transparent glass 20mm thick, to allow for cinematographic records, while the other was made of 10mm perspex, fastened to the mill with a metal flange and four 10mm bolts and wingnuts for easy removal. The mill was mounted on a conical flange attached to the drive axle of the milling rig, described in details in Appendix C. Maximum deviation of the surface of the mill from average position was 0.1mm during a full rotation of the mill.

5.2.1 Mill liner profiles

Six mill liner profiles were investigated, as illustrated in Figure 5.1 and listed in Table 5.1

Figure 5.1: Mill Liners Profiles Tested

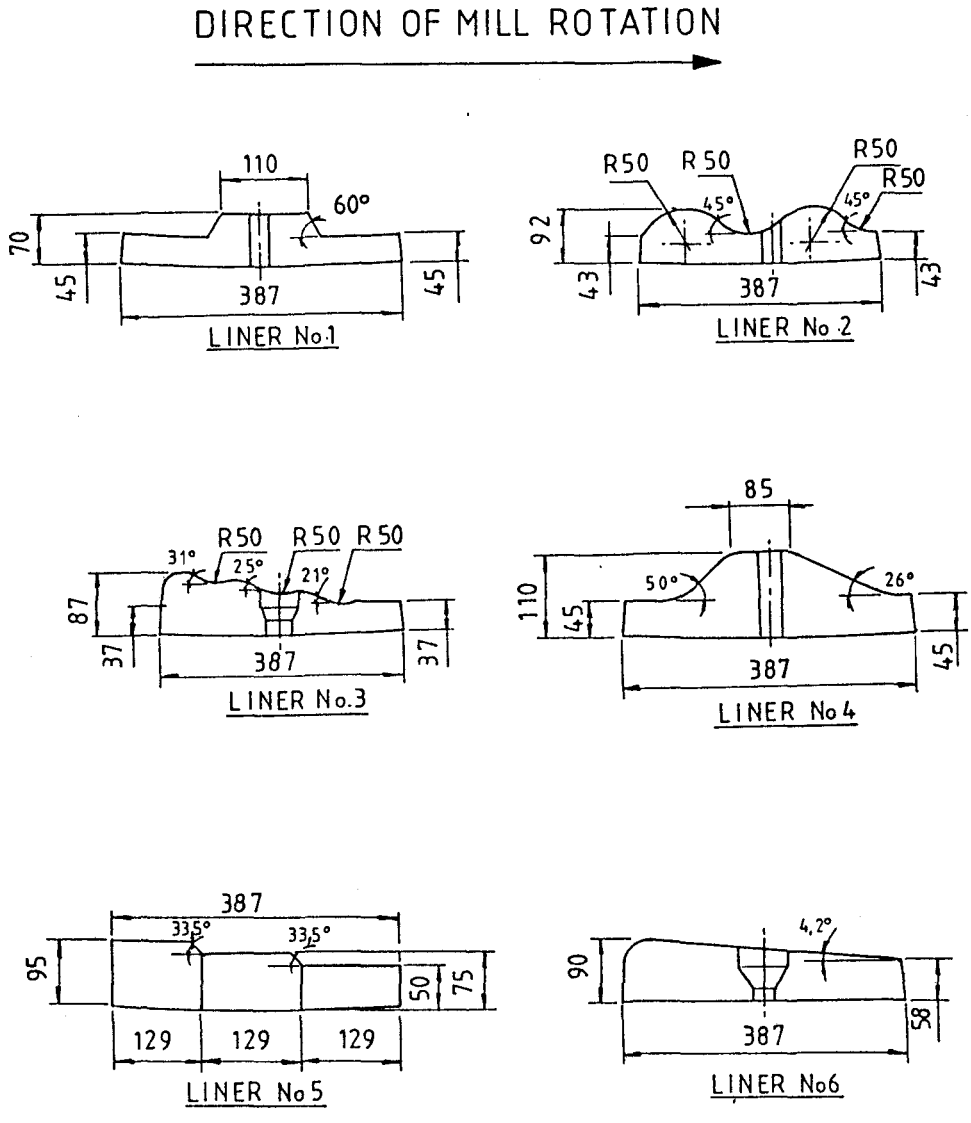

These liners were scaled down from the engineering drawings used for their industrial-scale manufacture.

Table 5.1 : Liners Specification

Liner Number	Description	Mill Types	Application
1	Lifter Bar	Tube Mill Double Conical Mill	Coal, Phosphate Gypsum
2	Double Wave	Tube Mill	Cement
3	Triple Wave	Tube Mill	Cement
4	Asymmetrical	Tube Mill	Gold, Platinum, Copper
5	Triple Wave	Experimental	Not Yet Used
6	Wedge Type	Tube Mill	Cement

5.2.2 Ball charge

The ball charge consisted of equally distributed 3, 4 and 5mm diameter steel balls having a density of 4.48 $kg/10^{6}mm^{3}$ which corresponds to the density of the ball charge used in industrial mills.

The same principle as successfully used by Vermeulen (24), for his test, was adopted for the choice of the size of the balls:

$$\frac{A}{B} = \frac{C}{D}$$

where A = diameter of industrial mill
B = diameter of industrial balls
C = diameter of laboratory mill
D = diameter of laboratory balls

Therefore the size of the balls was scaled down by a factor of ten from the 30, 40 and 50mm balls used in industrial conditions. It was only possible to obtain a sufficient quantity of balls to fill 36.7% of the mill volume. Since industrial mills used for coal pulverizing are operating at 20-25% of mill volume, this was sufficient for the purpose of this research.

5.2.3 Ceramic for liners

The liner material used for the scaled down laboratory mill had to satisfy the following requirements:

- wear rate had to be relatively high so that wear effects could be observed after a reasonable time period,
- the relative wear rate of the liner being a function of liner profile, mill speed, amount of ball charge and grinded material had to be observable.

With the above in mind the relatively soft ceramics were chosen ie.

- material 05 to simulate hard high chrome irons made from clay casting, fired at 1030°C during 6.5h,
- material 06 to simulate softer manganese and chrome molybdenum steels made from clay casting, fired at 945°C during 6.0h.

These ceramics have a similar microstructure to cast liner alloys subject to this research. Both consist of hard crystalline phase cemented by a softer matrix to form the whole, as it is depicted in photomicrograph 1 in Chapter III and photomicrograph 1 in Chapter V. These show the similarity of the microstructure for high chrome iron and ceramics (material 05) respectively.

Photomicrograph 1
Detail of the liner surface made from ceramic (material 05)
Magnification x1999

Assumption was also made that the relative wear pattern of the liner profile is reasonably insensitive to the type of material from which it is constructed. This is supported by a very similar wear pattern obtained from ceramic liners for liner #1 (Figure C-3 in Appendix C) when compared to the metal liners (Figure 3.12 in Chapter III for hard high chrome iron, and A-7 in Appendix A for softer chrome molybdenum steel) in the industrial mill.

It was therefore concluded that the choice of ceramic material was sufficient for the required purpose, namely to observe the relative wear rates of the liners as a function of the lifter profile and the operating conditions.

5.2.4 Description of the test rig (See Appendix C for specification of equipment used)

The rig was designed to drive any mill which draws a power less than 3 kW. It allows the dynamic determination of the mass of the load in the mill within an error of less than 1 Kg, but the only features relevant to this research were its ability to provide:

(a) any desired mill speed and

(b) the continuous measurement of properties on and in the rotating mill itself, together with the transmission of these measurements to the "outside world".

Figure 5.2: General View of the Mill Rig

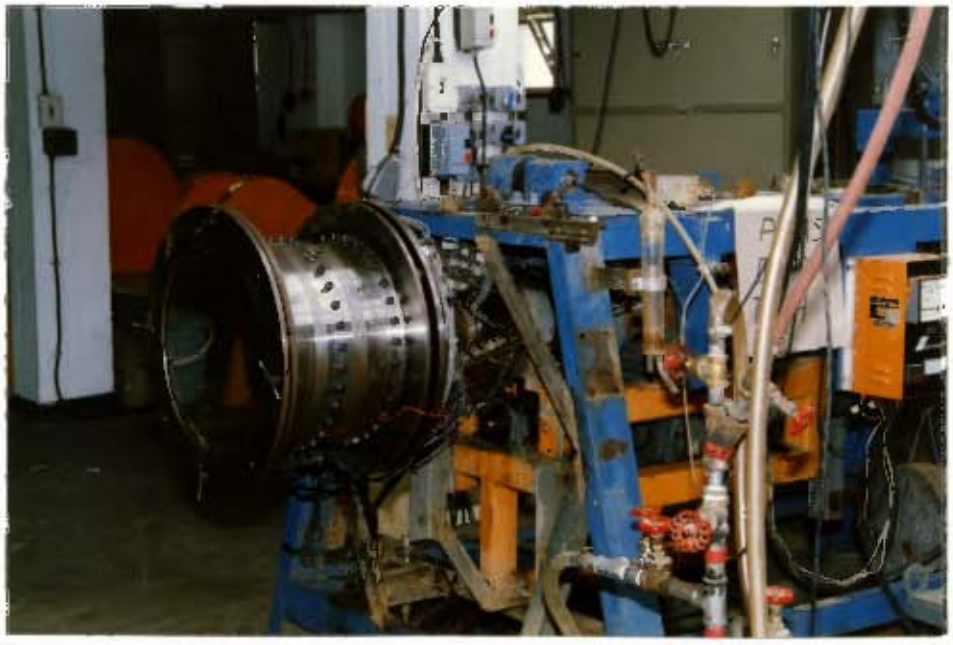

[Refer to Annexure C Figure C-1 for schematic representation of the mill rig].

Figure 5.3: Arrangement for Mill Speed Control and Dynamic Orientation of the Ball Charge in Mill

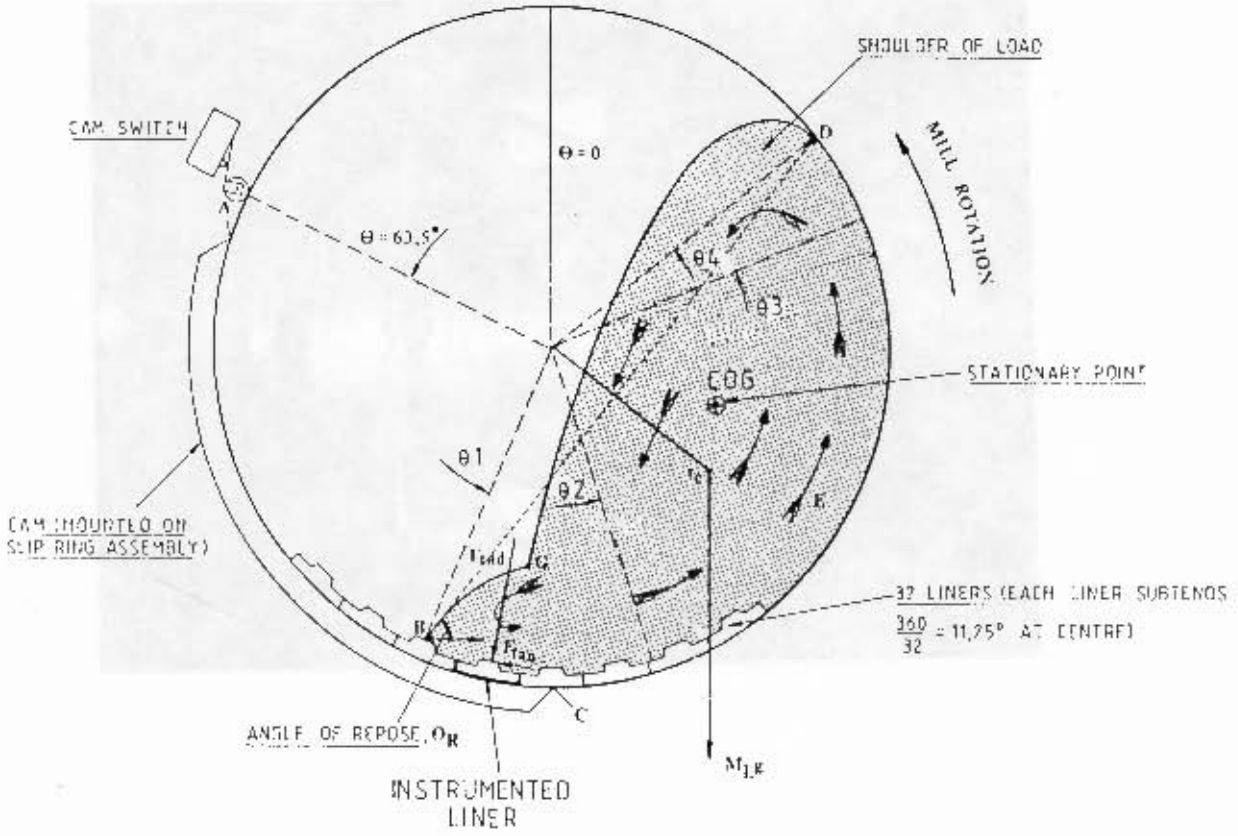

5.2.6 Measurement of Forces Exerted by Ball Charge on Instrumented Liner

The ball charge exerts a force on the liner which can be resolved into radial (F_{rad}) and tangential (F_{tan}) components as shown in Figure 5.5. These forces were measured using the apparatus illustrated in Figure 5.4 and Figure C-2 in Appendix C.

[Refer to Appendix C for detailed description of the apparatus used for measurement of forces exerted by ball charge on liner].

Figure 5.4: Liner Load Beams Assembly

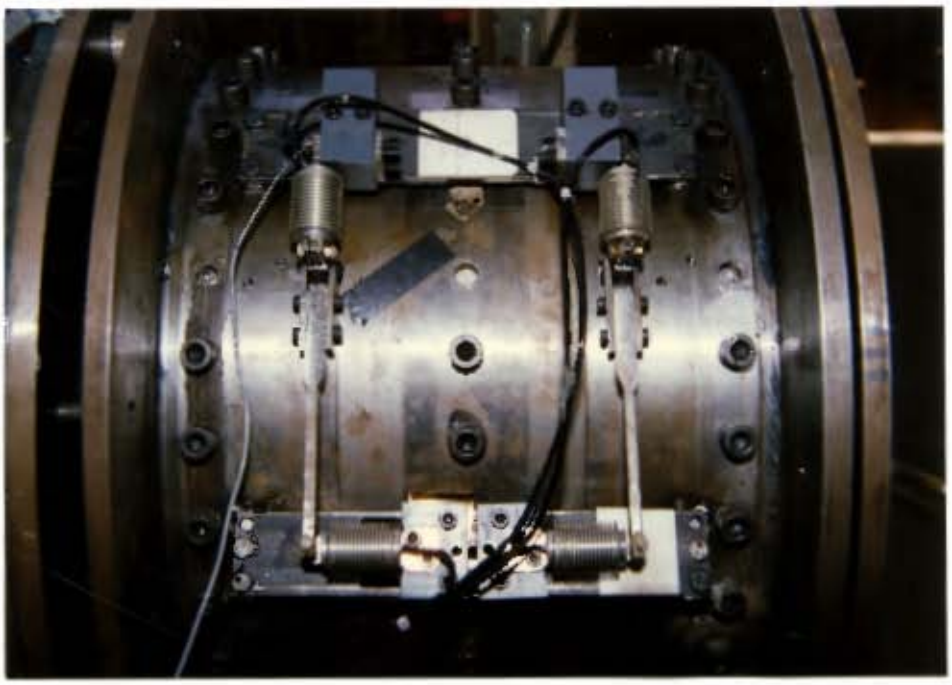

F_{tan} and F_{rad} can be related to the measurements obtained from the load beams by considering a static force balance on the liner. Consider the simplified diagram of the measurement apparatus in Figure 5.5
A radial force balance yields:

$$F_{rad} = F_{rad,m}$$

while taking moments around point A yields

$$F_{tan} = F_{tan,m} (x_p/x_w)$$

where x_p and x_w are distances to the pivot point and the inner liner surface.

Figure 5.5: Schematic Representation of the Measurement of Radial and Tangential Forces

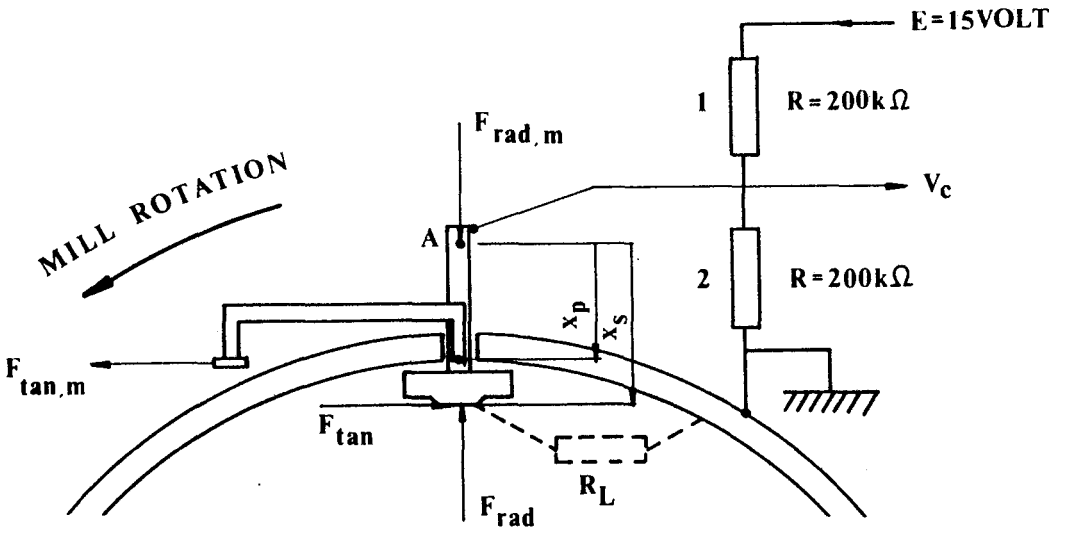

5.2.7 Slip Rings for Transfer of Data From the Mill

Various electrical measurements were made using electronic equipment mounted on the mill. Electrical power and signal measurements were transferred to and from the rotating mill via 10 slip rings mounted on the rear end of the axle, as shown in Figure C-1 in Appendix C. Five brass rings of progressively larger diameter were recessed into each side of a PVC disc mounted on the axle. Each ring was connected to a cable which was threaded through the axle and was available for connection to transducers on the mill. Three rings were used for transmission of DC power supplies at +20V -20V (ground), leaving seven available for signal transmission.

5.3 EXPERIMENTAL METHOD

The experimental programme had as its objective, the measurement of the behaviour of the ball charge on the instrumented liner as a function of:

- ball load volume J (expressed as a percentage of the total mill volume) i.e. 0, 10, 15, 18, 21, 24, 27, 30 and 36.7%.

- mill speed N_m (expressed as a percentage of mill critical speed) i.e. 10, 25, 50, 60, 65, 70.5, 73.3, 77.6, 82.0, 86.3, 90.6, 100, 110, 120 and 135%.

- liner profile (illustrated in Figure 5.1).

The computer was programmed to ensure that the sequence of experiments to be performed in terms of values of liner profile J and N_M, as discussed above, was carried out. The programme paused at appropriate points to allow the changing of liners or the addition of balls to the mill and gave instructions (via the computer screen) re: the mass of balls to add, etc. Once the correct mass of balls has been added, the button "continue" was pushed and the computer then performed a suite of measurements of the ball load behaviour as a function of mill speed. All data measured for each mill speed was printed out and relevant data items were stored on disc. Data was also plotted on-line providing the experiments with valuable graphical (as against numerical) feed back on the quality of data collected.

5.3.1 Measurement of Forces Exerted by the Ball Charge on the Liners

The computer programmer executed the following steps:

i) it continuously monitored V_{comm} until the test liner passed θ_A = 63.5 degrees.

ii) it instructed the HP2240A computer to measure 30 readings of V_R and V_t (where V_R and V_t are the voltages obtained from the radial and tangential load beams respectively) at time intervals spaced uniformly over the next period. This ensured that the 30 readings spanned the period of time that the test liner was underneath the ball load.

iii) it repeated the above for 5 consecutive revolutions of the mill.

iv) it applied calibrations to the voltages to get radial and tangential forces in Newtons and calculate θ corresponding to the times at which the measurements were made.

v) it calculated the average of this data (this was done for all speeds and values of ball load volume J, including J = 0).

vi) If J = 0 it read the data corresponding to J = 0 for the liner and speed corresponding to the current experiment and calculated the net forces (radial and tangential) exerted on the liner by the load from:

$$F_{net\ (\theta,J,N)} = F_{(\theta,J,N)} - F_{(\theta,J=0,N)}$$

This removed the effect of the inertia and the weight of the liners of the forces measurements.

vii) it printed all average data for experiment.

viii) it plotted the data obtained for this experiment as discussed in 5.3.8 below.

5.3.2 Measurement of Mass of the Mill

The relevant sub-routine measured 200 readings of the voltages from the load beams (used for measuring the mass of the mill + liner + load), calculated average and relative standard deviations and applied calibrations to yield estimates of the mass. The mass of the load was obtained by subtracting the mass of the mill + liners. These readings took 14 seconds to obtain and thus, in general spanned several revolutions of the mill. This ensured that periodic oscillations in the readings resulting from the rotation of the mill, were averaged out.

5.3.3 Control and Calibration of Mill Speed

The relevant sub-routine calculated the voltage corresponding to a required N_{mst}, and used the analogue output card to supply this voltage setpoint to the mill speed controller. After the speed setpoint was changed, the computer waited five seconds before taking any measurement. This ensured that the mill speed, and the behaviour of the ball charge in the mill, had reached a steady state.

5.3.4 Recording "Current Status"

At the end of each experiment (i.e. when measurements at a particular speed were completed) the relevant sub-routine was called up. It stored all indicators of the current status of the programme ensuring that, in the event of any unforeseen interruption, or if the computer was switched off overnight, it would be easy to re-start the programme at the point corresponding to the completion of the last experiment.

5.3.5 Insertion of New Liner

The computer was paused while the new liner was inserted. Once this operation was completed, the mill was run at 77.6% of critical speed, while the new mass offset was measured. This offset was then stored in the status file, and used in all future measurements of the mass of the load:

Mass of the load = Total mass - mass offset

5.3.6 Calibration of Analogue Inputs

The relevant sub-routine allowed the user to select any two analogue input channels, measured the voltages on these channels every 0,2 seconds, and displayed these voltages together with a smoothed value obtained from:

$$V_{smooth,i} = aV_i + (1 - a)\, V_{smooth,i} - 1$$

where a = 0,10

5.3.7 Description of Output

A continuous record of all information was printed, plotted and stored on magnetic disk for later processing. The online use of the plotter was particularly helpful during the experiments, and was the main source of information about the quality of the data being accumulated.

5.3.8 Printed Output

An example of the printed output for one experiment is given in Appendix C, Table C-1

a) The first line gives the time at which the experiment was performed (HHMMSS), the J set point (% of mill volume) and corresponding mass setpoint (kg) the measured mass (kg), the N setpoint and measured value (% of critical speed). M-RNOC, P-RNO, P-RNOC (the record numbers of data stored in the MONITOR and PROFILES files).

b) Fractional standard deviations defined by:

$$\delta_1 = \left[\left(\sum_{i=1}^{n} (X_i - \bar{X})^2 \right) / (n - 1) \right]^{\frac{0.5}{\bar{x}}}$$

are printed below the relevant measurements. n = 200 for MMEAS, while N = N_{accept} for other measurements (see (c) below).

c) THET (30) is the angle at which the last measurement of F_{rad} and F_{tan} was made. Line (c) thus shows how accurately (in terms of θ) the measurement of those variables for this experiment (i.e. in this case J = 24%) was matched to their measurement at J = 0. It is essential to obtain a good match, otherwise it is difficult to calculate the net forces as discussed in section 5.3.2.

d) The four lines in the PROFILE DATA tables are, respectively, θ, V_c (mv), F_{rmd} and F_{tmn} (the last two terms are to be divided by 100 to obtain the measurement in Newtons). The data for each revolution is provided, together with the average of the data in table (f). Generally, only the average data was reported; however, for industrial values of N_m and J more detailed results are provided.

5.3.9 Graphical Output

A graph, illustrated in Figure C-8 in Appendix C was produced on line during experiments.

a) Figure C-8 represents a record of the data collected during a suite of mill speed experiments at a selected J for the current liner profile. Torque $\pm$ standard deviation is plotted as a function of N_m (not considered in this research). F_{rmd} and F_{tmn} are plotted as functions ofθ being angular position of the instrumented liner for each mill speed.

5.3.10 Detailed Record of Profile Data

At selected values of N_m and J, a graph of all the F_{rmd} and F_{tmn} data points, together with a line passing through the average values, was plotted, an example of which is given in Figure C-9 in Appendix C. This graph reveals the scatter inherent in the measurement and also records more clearly the average profile for important mill speeds.

6.2 Research Outline

Six liners, of different profile geometry, made from high chrome iron material were selected for experimental investigation. The object of the study was to ascertain which liner profiles, if any, are superior to the current established choice (liner #1), under current mill conditions. It was also to explore controllable aspects of the milling process which enhance the durability of liners. The study consists of two separate experiments. The first involves the industrial use of six liner profiles in mills at a particular ESKOM Power Station. Periodically, when the opportunity will be available, data relating to liner wear will be collected. The data will technically constitute the material of a longitudinal observational study rather than a statistically designed and replicated experiment. The advantage of this approach, is that appropriate data are obtained inexpensively, and that the costly industrial processes involved are subject to only a minimal and acceptable level of disruption. The disadvantages involve problems associated with the relative smallness of the data sets, possible confounding factors and difficulties associated with effective experimentation being precluded by prohibitive cost.

In the second experiment, a suitably scaled version of the liner wearing process of interest was implemented. A preliminary test suggested that wear in high chromium irons may be emulated by wear in ceramic liners, although at appreciably different rates. In consequence, there is a possibility of studying liner profiles under accelerated wear conditions in suitably scaled-down ball-tube mill processes, providing that extrapolation to the industrial setting can be acceptably motivated.

It is a matter for further research to explore to what extent conclusions from the small-scale ceramic liner profile studies can be extrapolated to the industrial context. Results from the two experiments will be compared in as much as the differences in design will allow. If it proves possible to extrapolate reliably, there is a prospect of an extended small-scale ceramic study with industrial optimization in mind. The second part of the investigation is aimed at studying the effect of the following independent variables :

- the geometry of the liner profile
- the mill speed.
- the amount of material contained in the mill (mill charge).

The liner wear rate was chosen as the dependent, or primary response variable. Other variables were also studied as secondary variables (covariates). These were :

- the "lift" (as a percentage of the mill diameter) achieved by the mill under different operating conditions
- the forces (radial and tangential acting on the mill liners at the points of impact and separation from the liner)
- the areas of disturbance associated with the points of separation and of impact

The acting forces were measured electronically, using instruments designed specially for this purpose, which recorded both the radial and the tangential components of the force. The "lift" was measured using high velocity cinematographic records, together with the areas of disturbance at the points of separation and impact. From the directly measured secondary variables were constructed the tertiary or derived variables :

- the total force acting on the liner
- the acting pressure at the points of impact and separation
- the total area of disturbance

Independent variables used in a regression model are called regressor variables. The dependent variable is called a response. In the analyses that follow, secondary and tertiary variables will generally be regressors when they are involved, but they will be treated as responses in some contexts.

6.3 THE DESIGN OF THE EXPERIMENTS

6.3.1 Assumptions and the outline of the tests.

The experiment was designed as a 5x3x3 factorial of one dependent and three independent variables (factors). The independent variable was in the first instance the liner wear rate (g/6h), the independent variables; the liner profile, the mill speed and the mill ball charge, respectively. These variables are called control variables.

The values or levels of independent variables can be arbitrarily chosen and implemented, without any interaction between themselves. These levels affect the dependent variable (response) either directly (main effects) or indirectly (interaction effects). Over and above the effects of the factor levels, one can presume that the response is additionally subject to individual independent error (noise) variations.

Testing all possible combinations of the independent variables implies the examination of fifty four different cases or trials for every replication. The number of replications was determined by the practical constraints on time and effort, to be one. This single replication complicates the analysis but is a valid experimental design.

As the purpose of the trials was to study the effect of the chosen independent variable on the liner wear, independently from the liner material (the study of which forms the subject of a different study), it was decided to use ceramic materials for these trials. This was done as they are capable of showing a measurable degree of wear in a much shorter time than that of the liners made of metal. It was found that in the scaled down experimental mill, six hours was enough to give interpretable results.

To eliminate the effect of material differences, that is to make sure that all the observed effects are attributable to the chosen and defined independent variables, it was essential to ensure the greatest uniformity of the ceramic material. This made it necessary to ensure that all the material obtained was of the same raw material and of the same firing. This requirement placed a limitation on the amount of ceramic material which could be used for the tests. More complex experimental designs could have been used for non-uniform experimental material, but a simple design was preferred.

Constraints of time and the availability of the material, together with the fact that only one experimental mill equipped with the necessary instruments was available, effectively ruled out a full repetition of the experiment.

In order to get some indication of the ability to repeat the trials, the acceptability of some assumptions and the predictive power of the conclusions, a few additional trials were carried out. For each liner profile either one or two additional trials were conducted. A few were performed using the independent variables corresponding to the conditions most interesting to the users of the mills, these were points in the experimental design.

The purpose of these trials was to test the ability to repeat the experimental procedure, to give some sense of the reliability of the wear rate measuring process and to allow for comparison of pure and assumed random error.

A few more additional tests were performed using combinations of the independent variables different from any combination used in the primary series of tests. This was necessary in order to test the predictive power of the analysis (ie how well the data would allow for forecasts or predictions of responses at points not in the experimental design).

There was no 'a priori' information available concerning the linearity of the expected relations. As nonlinearity could not be ruled out, it was necessary to use at least three values (levels) for each independent variable. Using this structure is a well known technique and rests upon the assumption that the non-linearity can be approximated by a quadratic over the studied range of the controlled variables.

This structure made it possible to fit both a linear (first order) and a quadratic (second order) polynomial to the experimentally determined responses. A significant difference between the two indicates a non-linear relation between the dependent variable and the control variables.

In this kind of experimental design, it is important that the values of the independent variables forming the "frame" of the test should be reasonably spaced. The most interesting combination of mill speed and volume of ball charge for the coal pulverisation for power industry is :

Mill Speed : 77.6 % of critical mill speed

Ball Charge Volume : 24 % of mill volume

To make the results as relevant as possible, it was initially decided to use this combination as a pivot of the experiment, and place the other eight combinations around it, to obtain the following equally spaced fram of design points ie.

Mill Speed : 73.2 % - 77.6 % - 82.0 %
Ball Charge Volume : 18.0 % - 24.0 % - 30.0 %

However, other mills in the mining industry, handling different minerals and ores, work under slightly different conditions. To make the applicability of the present work more general, it was decided to extend the frame of the design to include the conditions of such other processes. Thus the final frame for the experimental work became :

Mill Speed : 65.0 % - 77.6 % - 90.6 %
Ball Charge Volume : 15.0 % - 24.0 % - 36.7 %

The third factor in the design is the liner lifter profile. There were six liners tested, including a smooth (flat) one without lifter bars.

Liner No. 6. was expected to be qualitatively different from the other profiles, in that it would exert appreciably less lifting force on the ball charge.

On first consideration it would seem natural to use it as the basis of comparison against which all the other liners would be evaluated. Unfortunately this is not feasible as theoretical studies have shown that a smooth liner does not yield a stable pattern of movement inside the mill. Consequently it is of no practical use or interest. The theoretically predicted instability was confirmed by experiment in the small scale experimental mill.

In the analysis the liner wear (dependent variable) and the secondary variables were plotted against the independent (regressor) variables. The resulting plots have shown that the points corresponding to the smooth liner could not be regarded as a member of the set comprising of the other liners (refer to Figure D-1, D-2 and D-3 in APPENDIX D). However the data clearly confirmed that this profile experienced minimal wear when made from hard ceramic.

Due to the obvious nature of this misfit, it was decided to leave the smooth liner out of the analysis of the design, and concentrate on the other five.

As a result of the above considerations, the final experimental design was decided to consist of five liner profiles, three mill speeds and three ball charge volumes, defining the number of trials for analysis as 45. The analysis therefore focussed in the first place on the 45 multivariate observations from the 5x3x3 factorial design.

Eight additional trials were performed on the five liners in order to gain at least some idea of the repeatability of the trials and the predictive power of the analysis. These trials were incomplete in the sense that only the wear rate (dependent variable) was recorded, while the secondary variables were not observed.

According to the theory of experimental design, 45 trials should have been performed in a random order, so as to prevent the introduction of any serial effects into the results.

One of the earliest precautions decided was to keep the handling of the ceramic liner elements to a minimum and to carry out all the trials on a one liner profile before refitting the experimental mill with another.

It was felt that to fit and refit the same set of liners would have certainly introduced an error into the results at least comparable with possible serial effects caused by the non-random sequence of the trials. The subsequent analysis of the data indicates that even if serial effects occur, there are apparently very strong effects associated with the factors.

The trials were conducted in sequence, one profile at a time. Within this mill velocity levels were cycled and ball volume levels were most rapidly cycled.

6.4 THE OUTLINE OF THE ANALYSIS

6.4.1 The scope of the analysis.

The basis of the analysis is the previously described factorial design, consisting of five liner profiles, three mill speeds and three ball charge volumes. The liner wear rate was chosen as the primary dependent variable. Secondary variables were the lifting height of balls achieved by the mill, the forces acting on the mill liners at the high and low ends of the trajectories of the balls, the areas of relative motion between balls and mill shell liners associated with the points of separation and impact and the pressures measured at the design points.

The dependence of the primary and the secondary variables on the experimental factors was studied. In addition, the relationship of the primary and secondary variables to each other was also examined in the hope that it might improve an understanding of the physics of the liner wear during the grinding process.

The primary and secondary dependent variables were all analysed individually. The decision not to treat the data as a multi-variate sample was based on two considerations:

- there were doubts concerning the appropriateness of assuming a multivariate Gaussian (normal) distribution for any of the variables.

- there appeared a possibility of reducing the number of the degrees of freedom of the system below an acceptable level.

For these reasons, it was decided to treat each of the primary and secondary variables alone, as if each were the only response of interest.

The choice of model on which to base the regression was influenced by the knowledge of the physics of the system. For example; it seems safe to assume that the "lift" of balls achieved by the mill will depend on the centrifugal force acting on them. The centrifugal force in turn depends on the square of the mill speed. For this reason it is reasonable to expect the relationship between the "lift" and the mill speed to have a significant non-linear component. In the light of these, and similar considerations, it was felt that to limit the analysis to a search for linear relationships would be too restrictive.

In searching for a credible model there was another difficulty which had to be overcome - assigning appropriate quantitative units to the variables (that would allow later extrapolation to industrial context). In the case of the mill speed and the ball charge volume, the assignment is self evident.

The ball charge volume is expressed as the percentage of the useful mill volume occupied by the charge (steel balls and coal in an industrial mill, balls only in the laboratory mill).

The similarity criteria for ball-tube mills are well established. It is known that if the diameter of a ball-tube mill is reduced by a factor, and if similarity of movement of the ball charge in the mill interior is to be preserved, the mill speed must be increased by the square of the same factor. If, as in the present case, this scaling law is observed, one of the consequences of similarity is that the mill speed can be expressed in terms of the mill's critical speed. This rule will be followed in this study, and the mill speed will be quoted as a percentage of the critical speed.

In the case of the liner lifter profiles there is no such self-evident way of assigning numerical values. The most obvious quantity appears to be the Surface Factor - that is the ratio of the upper face length of the liner profile and its base. Analysis has shown this to be inadequate, so a compound quantity was introduced, formed as a product of the above defined surface factor and the sum of tangent of the liner's face-angle, and denoted as the liner's Roughness Coefficient (C_R).

For the present analysis this Roughness Coefficient will serve as the quantitative description of the liner profile and consequently as the corresponding independent variable (the derivation of these quantities is explained in detail elsewhere).

A regression model with the control variables or functions of those variables as regressors that adequatly summarized the data, would be sought for the response, and some of the covariates, to inform further research.

Further linear regressions with the covariates as possible additional regressors, would be investigated for each variate that was treated as a response. After initial analysis, it was clear that particular attention was warranted for the liner profiles #3, #4 and #5. The entire analysis was repeated on this reduced 3 x 3 x 3 experiment, with similar assumptions being made 'mutatis mutandi' for each model. Clearly 27 cases were available for this updated analysis.

6.4.2 The method of analysis.

The analysis of the experimental data was carried out using two different methods namely:

1. A ranking (non parametric) method.
   These analysis were performed with a calculator.
2. A regression (parametric) method.
   These analysis were conducted on the Sperry main frame at the University of Cape Town, using the BMDP programs P1R, PR2, P9R and PV2.

This approach may at first appear wasteful, as most of the findings of the non-parametric approach would be confirmed in the results of the parametric approach. The reason for this was the initial state of ignorance concerning the model. Non-parametric methods make only minimal model assumptions. It was anticipated that the mill speed and the charge volume would be independent (regressor) variables that can be handled with relative ease in a parametric approach. The same could not be assumed of the third variable, that is the liner profile geometry. At the beginning of the analysis it could not be forseen with certainty that a continuous measure which could be used as a quantitative description, would be found. Using such a measure renders the whole of the wearing process accessible to the more rigorous quantitative (parametric) approach. It was found only after experimental data became available, that a Roughness Coefficient, (an artificial description of the geometry of the liner's profiles), was identified as a suitable basis for a fully parametric evaluation of the experimental data.

To explore if fully parametric evaluation was possible, the wear rate response (and that of other important covariates) was plotted against the values of mill speed and charge volume (Figure D-4, D-5, D-6, D-7 and D-8 in Appendix D). When this was done for all liners on the same chart, it could be seen that the surfaces representing the different liners did not intersect, and behaved in a reasonable manner. A similar plot was produced showing the interpolated (linear) surfaces corresponding to the different liners. The outcome was much the same, that is the various surfaces still did not intersect. This consistency of pattern indicated that a Roughness Coefficient might indeed be a suitable basis for a fully parametric analysis.

Consequently, the evaluation was carried out in three steps:

1. An exploratory analysis, was conducted to establish the independence of the variables of mill speed and charge volume, by showing that it is reasonable to assume that there is no significant interaction between them and the liner profile geometry. This analysis also suggests that the trend surfaces representing the wear on different liners do not intersect, and are roughly parallel.

2. The second step was to treat each response separately, and to subject its data to both types of analysis. This approach allows one to show that the five liners have different effects, but it was still impossible to use the results to draw conclusions for liners not included in the experimental design.

3. The third step was to incorporate a Roughness Coefficient of the liners into the analysis, as a continuous variable representing the different liner profile geometry. This extended the extrapolatory power of the model.

6.4.2.1 The Non-parametric Approach.

Non-parametric (ranking) methods are useful in the analysis of data whose statistical behaviour is not known, as the method depends only on the ordinal aspects of the data and not on their distribution.

These methods make fewer assumptions than parametric ones, as they are not concerned with questions such as how close the data cases are to each other, but only with the order in which the cases are ranked. Consequently the methods have far wider application than their parametric counterparts.

The Statistic consistently used here is Friedman's Chi-square, which is calculated from the formula:

$$\left[\{SUM\ (\ T(i)\ \ **\ 2\ )\} * 12\ /\ \{m * k * (k-1)\}\right] - \left[3 * m * (k-1)\right]$$

where m is the number of groups (blocks), k is the number of elements (treatments) ranked within each group and T(i) is the sum of the m ranks associated with the set of elements (treatments), for i running from 1 to k. The maximal value occurs when the ranks are constant for each element, and is m * (k - 1). The minimum is zero. The statistic is *approximately Chi-square in distribution under a null* hypothesis that there is no correlation across the ranks of the k elements through the m groups. In all comparisons of liner profiles R=5, m=9 and the maximum possible value is 36. In all comparisons of the velocity x volume settings R=9, m=5 and the maximum possible value is 40.

6.4.2.2 The Parametric Approach.

6.4.2.2.1 Model Choice

Using a parametric approach is equivalent to constructing a mathematical or statistical model of the process that is to be analysed.

This usually consists of fitting a regression function to the available data, and optimizing the fit of the resulting curve.

If not enough is known of the process, then the usual first step is to fit a linear model to the data, and to analyse the resulting correlations between the different sets of data. In the present case this involves (for example) fitting a straight line to the Wear rate of each liner, using the mill speed as independent variable, while keeping the ball charge volume constant.

The curve-fitting (regression) is usually accomplished using some method to minimise the errors.

The Error is defined as the difference between the value of the regression function calculated using a value of the independent variable and the measured (observed) value associated with the same value of the independent variable. An accepted method of optimizing a regression function is the Method of Lest Squares. This is the method to be used in the present analysis. The regression can be extended to more regressor variables than one.

There are many regression models available. In fact it is valid to say that any investigator is justified in setting up his own new model, based on his own understanding of the process involved, if the new model can improve on the explanatory and predictive power of previous models. In the present case there is not yet enough known to allow a choice of a more realistic model than a Polynomial Regression. On the other hand enough is known to indicate the presence of non-linear components in the process. For this reason it was decided to go further than linear curve-fitting, and allow second order terms in the regression.

The results of a regression analysis can be presented as a curve (one regressor and one dependent variable) or a surface (two regressor variables and one dependent variable). Beyond this, visual presentation becomes impossible, as to present the results geometrically, recourse to a multi-dimensional hyper-surface would have to be made. The comparison of the value of this regression curve (or surface) and the corresponding value of the measured variable gives rise to the concept, already introduced, of the Error.

The study of the Errors forms the greater part of Regression Analysis. In formulating a mathematical or statistical model the study of the Errors allows one to:

- Minimize the errors, thus ensuring that the regression curve gives the best possible fit compatible with the restrictions imposed, such as the choice of the model, the order of fit (in case of a polynomial regression), the range and spread of the independent variables, etc.

- Promote parsimony or economy in the formulation of the model. This means that one of the most important guiding principles in building a model is that the model must be as simple as possible. The study of the Errors helps in this task by showing up the relative importance of each of the independent variables, thus indicating whether or not it is in fact necessary to include each of them in the analysis. Only the independent variables with a strong explanatory power will be retained in the final regression model formula. The study of the errors promotes parsimony through showing (in case of polynomial regression), the highest necessary order of the polynomial.

6.4.2.2.2 Estimation

When one is about to embark on the construction of a mathematical model, one of the most important requirements affecting the choice of the model is "parsimony". To satisfy this requirement it is recommended that the effect of all the variables is studied. A strong contribution from the regression formula is indicated by the correlation coefficient (r) of the particular independent variable and the dependent variable. Negative r-values indicate an inverse relationship between the variables, while a positive r-value indicates a direct relationship.

If the correlation of all the independent variables and the dependent variable is calculated, it is usually found that some of the independent variables effect the final outcome more than some of the others. Having decided upon a particular initial model, one estimates parameters associated with each of its variables. These estimates are examined with a view to finding variables which can be deleted from the model and incorporating those which have a good explanatory role for the data at hand. The process is essentially repetitive until an acceptable model is decided. Then for that model one may find the fitted values and the residuals (the estimated responses and errors).

All parameter estimates and fitted values should be understood as having an associated standard error that reflects the precision with which they are estimated in a given model for data.

The strength of the relationship between the observed and fitted response values is described by the single or multiple correlation coefficient (R). One measure of how much of the variation in the data is explained by a particular fitted model is the squared multiple correlation coefficient (R-sq).

Generally one seeks models where the R-sq values are high (as close as possible to the theoretical maximum, namely one). Because every variable added increases the observed R and R-sq values one also attempts to identify variables whose omission would radically reduce the values of R and R-sq, such variables are kept in the model. In this way it is possible to discard those variables from the analysis whose contribution is shown to be negligible, or of lesser importance.

For example, if the multiple correlation coefficient between three independent variables and the dependent variable is (say) 95 percent, and the introduction of a fourth variable increases it to 96 percent, then in the interest of economy the fourth independent variable might be safely left out of the regression model formula.

In deciding which variables are to be left out and which ones are to be kept it is usually self evident. However it can be placed on a quantitative (objective) basis by using a method such as Mallow's C-p statistic. The basis of this criterion is that every new variable introduced into the model will cause an improvement (however small) in the correlation coefficient. Mallow introduces a penalty for the introduction of each new variable.

This penalty is then compared with the improvement caused in the correlation, and the decision of whether to retain or to discard the variable can be made on the basis of this comparison. One therefore may choose to use that subset of regressor variables for a model which minimises C-p.

Two more concepts play an important role in the analysis of the Errors :

- the Standard Deviation of the errors.

- the Standard Errors of the Estimates.

The Standard Deviation is associated with the accuracy of the measurements that provide the response data base for the analysis. If the experimental work achieved good control over the experimental conditions, then the Standard Deviation of the errors is expected to be small. The Standard Deviation is the measure of the scatter of the experimental (measured) points around the regression curve. It is expected to find about 95 percent of the experimental points within a band of approximately two Standard Deviations around the regression curve (or surface). A narrow band indicates precise measurements.

The Standard Errors of the Estimates reflect the predictive properties of the Regression Function, and is closely associated with the Standard Deviation and the number of trials generating the data of the analysis. It is possible that a regression based on a small number of observations produces the same Regression Function as one based on a great number of observations. In this case one instinctively associates better performance with the one based on the greater number of points, and a preferance for its parameter estimates.

The Standard Error of the Estimate puts this instinct on a quantitative basis, by introducing an adjustment in the precision for the number of points participating in the analysis.

The last concept to introduce in the context of the Parametric Analysis is the concept of the diagnostic analysis.

This involves examining the contribution of the individual data cases to the Regression Function. It is possible that some of the cases forming the database may exert an undue influence on the results, usually due to their position. The detection of points with an undue influence of their existence can be accomplished by using Cook's distance measure (D-i).

An alternative approach examines the successive elimination of each data point in turn, and comments on the average effects of that type of reflexive or internal prediction, and of each response datum from the rest of the data, i.e. on the average deleted residual (ADR). To use this method it is necessary to compare each response value with its fitted value. This is obtained by fitting a model to the reduced data set by removing the entire case from the data, and applying that model to the omitted case. The average differences between these fitted values and responses of points should be zero. If the average of these differences ADR is different from zero, this indicates that the model misrepresents the relationship between the dependent and independent variables, possibly because some data points have undue influence. An ADR markedly different from zero is an indicator of consistent bias in the model, or equivalently that the fitted model is consistently mispredicting the signal.

It is noted that predictions are always affected by the noise or random error in the data, and that they are usually presented with an associated standard error of prediction : se(pred)

6.4.2.2.3 Noise.

The noise component is attributed to random variations alone, and is called (statistical) error. Distributional assumptions are made about the individual error or residual terms.

Often we assume a Gaussian or normal distribution with zero mean and constant variance for these terms. The Guassian assumption requires checking, but if no clear evidence against a normal distribution emerges from the estimated error terms (residuals), one may assume that little is lost by proceeding as if it were correct. The purpose of this assumption is to provide a theoretical basis for accepted statistical tests applied in the subsequent analysis.

In this connection one examines the histograms and normal probability plots of residuals in the BMDP output. These plots alert one to both non-normal distribution patterns, and to possible single anomalies in the response variable, called outliers.

Two further common assumptions are; statistical independence of the true residual terms, and constant variance of the true residuals at all observations. Evidence against the independence can arise from the calculation of serial correlation coefficients (R/s) that are too large to be attributable to change variations in the estimated residuals, or by using the Durbin-Watson statistic (D-W).

Bivariate plots of residuals against predicted values of the response, or against functions of the regressor variables, are standard techniques for exploring violations of the constant variance assumption. They also assist in suggesting possible transformations of the variables that can be usefully applied in the liner regression model for the data.

6.4.2.2.4 Computer analyses

In addition to the plots previously described, BMDP programs provide many summary statistics which allow one to make decisions on model selection issues. These statistics include:

sample means

sample variances

parameter estimates

fitted values	estimates for average response at regression points (predicted from the signal model as estimated)
residuals	estimates of response data noise or random error (observed response minus fitted value)

MSE	mean square error (variance estimate)
df	degrees of freedom
se(est)	standard error of estimation (square root MSE)
se(pred)	standard error for a predicted value
t-statistics	for individual signal parameter estimates
F-statistics	for sets of signal parameter estimates
p-value	observed level of significance
r	correlation coefficient for two variables
R	multiple correlation coefficient
R-sq	fraction of variation explained by a model
R/s	serial correlation coefficient
C-p	Mallow's C-p
deleted residuals	deleted response minus reduced-data fitted value
D-W	Durbin- Watson statistic
D-i	Cook's distance for the case influence - measure)

These summary statistics are presented in organised tables in the printed output of the programs. Only the major features of interest for each analysis are extracted and presented here.

Many analyses are well summarised by an Analysis Of Variance (ANOVA) table. Extensive use is made here of this method of presentation.

The use of a factorial experimental design leads naturally to an ANOVA table, because the various parameters of the model can be separated into subsets, each being associated with a fixed portion of the variation, whatever sub-model is choosen. Furthermore, these portions of the variation are statistically independent, which simplifies the model selections that focus on the partitioned parameter subsets.

The output of P2V programs gives the unique ANOVA, and the elimination of some subsets of the dummy regressors in the underlying model as is sometimes indicated. It is possible that these ANOVA's can be further reduced by setting up explicit artificial regression models.

The ANOVA does not in itself allow extrapolation of the patterns in these data to other contexts. Linear regressions which use an assumption of the continuous extension of the data patterns between the design points were also investigated. The simplest of these employ only the control variables (liners , velocity and volume), but models using one or more of the five covariates, as possible regressors, are also examined.

Regression models do not offer the advantage of unique partitions of variation. Each ANOVA table is particular to the order in which the regressors and their parameters have been included in the model the ANOVA seeks to depict. In other words any regression ANOVA table for a model can be replaced by any other representing a different ordering of the same parameter and regressors. Regression ANOVA's will therefore be used in context where a particular ordering is implicit or desirable for some explanatory purpose.

The purpose of using the covariates is two-fold. It is possible that covariates are strongly related to a response of interest, in which case it is important to know about, and use them. But it is also possible that such analysis suggest alternative variables to be controlled, with a view to better predictions of the primary response of interest (wear-rate). Thus the regression analysis may suggest efficient directions, to explore in later studies, for optimizing the response.

There p-values are presented alongside statistics, they generally represent the probability of obtaining a value as extreme or more extreme than the observed value of the statistic, if chance alone were the sole source of variation in the data. The p-values therefore lie between zero and one. Large p-values suggest that chance alone can be an adequate explanation for the observed statistic in question. Small p-values (close to zero) represent evidence that something other than chance alone is required to explain the value of the statistic.

It is preferable to make decisions about the statistic and report the p-values rather than adopt a single strict criterion (eg.p-values below 0.05) as a standard comparison. The preferred approach tends to yield similar conclusions, but to better report the strength of the evidence on which the conclusion is based.

6.4.2.3 Ordering of the Data

Individual data cases are occasionally referenced in the discussions. The table below presents the original numbering of the data cases, and their general order of presentation in the report. The order of presentation best reflects the patterns that the data sets exemplify. The levels of velocity and volume respectively are indicated.

It has been noted that the original ordering was non-random, with the profiles being handled sequentially, and within each profile the velocities were set and used in ascending order. Within each velocity, the volumes were set and used in ascending order.

TABLE 6.1 CASE NUMBERS

	Liner Profiles				
LEVELS	#2	#1	#3	#5	#4
3-1	16	7	25	43	34
3-2	17	8	26	44	35
3-3	18	9	27	45	36
2-1	13	4	22	40	31
2-2	14	5	23	41	32
2-3	15	6	24	42	33
1-1	10	1	19	37	28
1-2	11	2	20	38	29
1-3	12	3	21	39	30

6.5 EXPLORATORY ANALYSIS OF THE DATA

6.5.1 Wear rate responses

Initial analysis focussed on the wear-rate data as a response from the 5x3x3 factorial design. The covariates were ignored. The current industrial application is liner #1 at the second levels of both velocity (78%) and volume (24%) evidence is sought for improved (reduced) response.

6.5.1.1 Non-parametric analysis

Viewed from a non-parametric perspective, the data proved to be very consistent in pattern. At each point in the 3x3 design subspace, the Wear rate observations on the five liners satisfied indentical rankings: #2 #1 #3 #5 #4 (max-min). The rankings of the nine velocity x volume combinations were almost identical across the five profiles, and may be styled 3-1, 3-2, 3-3 and 2-1, 2-2, 1-1,2-3, 1-2, 1-3 (max-min), where the digit pairs give the levels of velocity and of volume respectively.

TABLE 6.2 NON-PARAMERTRIC STATISTICS FOR LINER WEAR RATE (g/6hr).

levels	#2	#1	#3	#5	#4	velxvol	profiles
3-1	4.221	4.041	3.788	3.601	3.042	1 1 1 1 1	1 2 3 4 5
3-2	3.631	3.444	3.354	3.223	2.753	2 2 2 2 2	1 2 3 4 5
3-3	3.551	3.213	3.041	2.831	2.112	3 4 3 3 4	1 2 3 4 5
2-1	3.333	3.240	2.793	2.564	2.281	4 3 4 4 3	1 2 3 4 5
2-2	2.662	2.281	2.112	1.973	1.723	5 5 5 5 5	1 2 3 4 5
2-3	2.220	1.764	1.738	1.564	1.393	7 7 7 7 7	1 2 3 4 5
1-1	2.251	2.123	1.952	1.801	1.721	6 6 6 6 6	1 2 3 4 5
1-2	1.823	1.681	1.586	1.442	1.211	8 8 8 8 8	1 2 3 4 5
1-3	1.629	1.437	1.126	1.042	0.941	9 9 9 9 9	1 2 3 4 5

Friedman's Chi-square =	39.68	36.00
df =	8	4
Observed significance :	p< 10e-6	p< 10e-6

This analysis suggests that the response surfaces for the profiles do not intersect, and that the original assumption of, no three factor interaction, is unlikely to be seriously violated. Using the Friedman's non-parametric analysis of ranks procedure, we may conclude from the data that the described orderings of five profiles and of nine design settings arose from overwhelming evidence of differences within those two groups. We may suspect that some velocity x volume interaction occurs because of the similarity in ranks between 3-3 and 2-1, and because of the consistent transposition of ranks 6 and 7 between 1-1 and 2-3.

The data of Table 6.2 are presented in Appendix D. Figure D-8 Surfaces were fitted through these observed values by means of an appropriate computer program. The relevant graphs are presented in Appendix D Figure D-9 to D-13. These graphs are intended to convey how the continuous response surfaces move as the liner profiles change.

6.5.1.2 Experimental design analysis

The projected experimental design was examined using the technique of the Analysis of Variance (ANOVA). The results of the analysis are shown in Table 6.3. The results of the analysis suggest that the mathematical model of the wear process should be based on a choice of:

- liner (discrete)
- ball charge volume (continuous)
- mill speed (continuous)

as independent variables. The interactions of liner and speed mill, mill speed and ball charge volume should also be considered. The relatively low value of the F-statistic and the relatively high value of the p-value associated with the liner and ball charge volume interaction indicate that this particular interaction can be left out of the model without impairing its accuracy.

TABLE 6.3 ANOVA: WEAR-RATE ON FACTORIAL DESIGN

SOURCE	SS	df	MS	F-stat	p-value
liner	4.3237	4	1.0809	137.62	.0000
velocity	23.0801	2	11.5401	1469.27	.0000
volume	5.6830	2	2.8415	361.27	.0000
lnr x vel	.3290	8	.0411	5.24	.0024
lnr x vol	.0746	8	.0093	1.19	.3636 n.s.
vel x vol	.1794	4	.0448	5.71	.0047
residuals	.1257	16	.00785	-	-
TOTAL	33.7955	44	-	-	-

se(est) = 0.089 F = 153.08 df = 28,16
R-sq = 0.9962 R = 0.9981 (full model)

se(est) = 0.091 F = 201.21 df = 20,24
R-sq = 0.9941 R = 0.9970 (omit lnr x vol)

As the experiments were not fully replicated, and because the liners could not be represented by a continuous variable, it was not feasible to use a Multiple Comparison Approach. In the absence of such an approach, the interest must be concentrated on the wear pattern of the individual liners. Table 6.2, with the fitted values as Table 6.4, shows that the lowest wear rate is associated with liner #4, at 65% mill speed and 37% charge volume. A Bonferroni Approximation applied to the present case indicates a range, calculated as (root 2) * 6 * se = 0.7552, which is the

longest distance between the minimum of the data set and any point still regarded as being of interest. Looking at the problem exclusively from the point of view of wear, and neglecting any other factors affecting mill performance, the range of interest to the data cases shown in the enclosed area of the Table 6.4 is limited.

TABLE 6.4 FITTED VALUES FOR WEAR-RATE (g/6hr)

	liner profiles				
Levels	#2	#1	#3	#5	#4
3-1	4.209	4.051	3.802	3.596	3.035
3-2	3.715	3.454	3.383	3.222	2.661
3-3	3.479	3.193	2.998	2.819	2.241
2-1	3.316	3.150	2.799	2.587	2.358
2-2	2.586	2.316	2.144	1.977	1.748
2-3	2.313	2.018	1.721	1.537	1.290
1-1	2.280	2.203	1.933	1.783	1.651
1-2	1.816	1.636	1.545	1.439	1.308
1-3	1.608	1.403	1.187	1.063	0.915

To eliminate the possibilty that an unrecognized main effect or an unforseen interaction may dominate the results, two "reduced" models were examined, both using three liners (#1, #2, #4). Liners #3 and #5 were left out because they are too similar for the model to differentiate between them.

- In the first model the liner and volume interaction was omitted (Table 6.5)
- In the second model all possible terms were allowed (Table 6.6)

TABLE 6.5 ANOVA: WEAR-RATE for REDUCED FACTORIAL DESIGN MODEL

SOURCE	SS	df	MS	F-stat	p-value
regression	33.5529	11	3.0503	414.99	.0000
residuals	.2426	33	0.00735	-	-

se(est) = 0.0895 F = 414.99 df = 11,13
R-sq = 0.9919 R = 0.9960

y(wear): 3 lnr, 2 vel, 2 vol, 3 lnr x vel, and 1 vel x vol terms + error

TABLE 6.6 ANOVA: WEAR-RATE for REDUCED FACTORIAL DESIGN MODEL

SOURCE	SS	df	MS	F-stat	p-value
regression	33.6129	13	2.5856	439.01	.0000
residuals	.1826	31	.00589	-	-

se(est) = 0.0767 F = 439.01 df = 13,31
R-sq = 0.9946 R = 0.9973

y(wear): 3 lnr, 2 vel, 2 vol, 3 lnr x vel, 2 lnr x vol,
and 1 vel x vol terms + error

Examination of Tables 6.5 and 6.6 shows no violation of the model's assumptions, indicating that:

- The data acquired during the tests does not suggest faulty test procedures.
- The model is adequate for the description of the wear process

Eight additional points during the tests introduced to the reduced models, has shown that the residuals they generate fall within the range of the estimated random error, which allows these points to be used in analysis with reasonable confidence.

These points do not give clear evidence against the assumption that three factor interactions are effectively random error.

6.5.1.3 Control Variables Regression Analysis

The actual values for the three levels of velocity and volume in a regression analysis were now used in order to be able to extrapolate to other values of those variables. The regression analysis present some fitted models and their ANOVA's, but make no judgement about the industrial applications of the models.

Since the control variables were of essential interest, a model with a common constant and common slope parameters for velocity and volume was fitted (Table 6.7). It attained a multiple correlation coefficient of 0.9135. This model ignores possible liner profile differences.

Table 6.7 ANOVA: WEAR-RATE on VELOCITY and VOLUME (alone)

SOURCE	SS	df	MS	F-stat	p-value
velocity	22.7443	1	22.7433	169.781	.0000
volume	5.4242	1	5.4242	40.480	.0000
residuals	5.6265	42	.1340	-	-
total	33.7955	44	-	-	-

se(est) = 0.3660 F = 105.135 df = 2, 42
R-sq = 0.8335 R = 0.9135 R/s = 0.7285 (full model)
R-sq = 0.6730 R = 0.8204 (vel alone)
R-sq = 0.1605 R = -0.4006 (vol alone)

y(wear) = -1.91491 + 0.06802 vel - 0.03900 vol + error

The subsequent inclusion of liner profile differences as LINER dummy (indicator) effects in the model led to a significantly better fit, with multiple correlation 0.9805 (Table 6.8). This improvement was to be expected in view of the significant liner profile differences that had already emerged in the non-parametric analysis. It will be noted that, even in this model, the factors have orthogonal and hence independent SS's, because of the original design. Consequently we have evidence that the control variables have a dominating effect on the responses.

Table 6.8 ANOVA: WEAR-RATE on LINERS, VELOCITY and VOLUME

SOURCE	SS	df	MS	F-stat	p-value
liners	4.3224	4	1.0806	31.487	.0000
vel & vol	28.1689	2	14.0845	410.627	.0000
residuals	1.3041	38	.0343	-	-
total	33.7955	44	-	-	-

se(est) = 0.1852 F = 157.878 df = 6, 38
R-sq = 0.9614 R = 0.9805 R/s = 0.7285 (full model)
R-sq = 0.6730 R = 0.8204 (vel alone)
R-sq = 0.1605 r = -0.4006 (vol alone)
R-sq = 0.1279 R = 0.3577 (liners alone)

y(wear) = -2.07869 + lnr(i) + 0.06802 vel - 0.03900 vol + error

where lnr(1) = 0.37789 lnr(3) = 0.16522 lnr(5) = 0
lnr(2) = 0.58867 lnr(4) = -0.31289

However as non-linearity of the response over VELOCITY, and over VOLUME, seemed possible from ANOVA decompositions and data plot inspection, the squares of these variables were incorporated in the model. The model fit was significantly improved, but despite being quadratic it had no component for the indicated interactions. A velocity x volume product term for interaction did not significantly improve the fit of the quadratic model.

Table 6.9 ANOVA: WEAR-RATE on VELOCITY and VOLUME QUADRATICS and LINERS

SOURCE	SS	df	MS	F-stat	p-value
liners	4.3224	4	1.0806	84.026	.0000
vol and vel quadratics	28.7644	4	7.1911	365.284	.0000
residuals	0.7087	36	.0197	-	-
al	33.7955	44	-	-	-

se(est) = 0.1403 F = 210.09 df = 8, 36
R-sq = 0.9790 R = 0.9895 R/s = 0.1345 (full model)
ADR = 0.0246 PMS = 0.0246 D-W = 1.7042

y(wear) = 6.01480 + lnr(i) - 0.106027 vel - 0.112952 vol
+ 0.00111809 velsq + 0.00141415 volsq + error

where lnr(1) = -0.210778 lnr(2) = 0 lnr(3) = - 0.423444
lnr(4) = -0.901556 lnr(5) = - 0.588667

The models reflected in Tables 6.7 to 6.9 can be fitted to the complete data set of 53 observations. Using the reported fitted models, predicted values for the eight additional cases were obtained, and each of these differed from the observed values by an amount that was easily explicable in terms of the observed random error (se(est)). It may be inferred that the assumptions of the models are not contradicted by the data, and thus expect good prediction from the observed data, particularly under the model of table 6.9, for each liner profile at new design points within or close to the velocity x volume subspace.

A model similar to that of Table 6.9 was fitted by P2R, which dropped the velocity term when the F-to-enter value was set at 4.00. The resulting fitted values are presented in Table 6.9a.

Table 6.9a Fitted values for WEAR RATE (g/6hr)

	Liner Profiles				
Levels	#2	#1	#3	#5	#4
1-1	2.430	2.219	2.007	1.842	1.529
1-2	1.910	1.699	1.487	1.321	1.008
1-3	1.566	1.355	1.142	0.977	0.664
2-1	3.218	3.007	2.795	2.629	2.317
2-2	2.698	2.487	2.274	2.110	1.796
2-3	2.354	2.143	1.930	1.765	1.452
3-1	4.177	3.966	3.753	3.588	3.275
3-2	3.657	3.450	3.233	3.068	2.755
3-3	3.312	3.102	2.889	2.724	2.411

It is therefore appropriate to refit the models using all 53 data values in the complete data set. Within the limitations of this family of models (no simple interaction term appears available), the refitted models use all the information available from the data set to estimate the parameters, the data and the predicted values for new design points. There are difficulties associated with predictions for liner profiles other than the five studied here, because without a quantitative description of the profiles, we have no formal basis for prediction and extrapolation. One possible method of overcoming this limitation is to assume that there will not be marked changes between a current profile and one which is very similar to it, and to plan future designs which explore moderate variations in shape around the current five profiles.

However a problem arises in deciding which values of the covariates to ascribe to intended future observations in the same way that one does for the control variates. We may therefore choose to adopt the model of this section as optimal for our purposes, and leave the analysis of covariates to a descriptive section (6.5.1.5).

6.5.1.4 Exploring Interactions

The ANOVA of the experimental design suggested various interactions were operating. A multiplicative interaction using VEL x VOL, as a single additional regressor, failed to improve the fit. Neither did transformations of variables to natural log scale, and subsequent model fitting, appear to give any explanation of interactions.

In consequence, interaction was incorporated by fitting the model with linear effects for VELOCITY and VOLUME separately to each LINER profile, but with an additional assumption of a common variance across profiles. No evidence was found to contradict this assumption, and the consequent model fitted almost as well as the preceding approximations to the complete experimental design model. It was therefore fitted (Table 6.11) to the complete set of 53 cases to explore its possible usefulness.

Providing that one is fitting constants for the liner profiles, there is little benefit in fitting separate coefficients of VEL and VOL in each group (R-sq moves from 0.9614 in Table 6.8 to 0.9642 here). A common pair of coefficients may suffice.

Despite the significant F-statistic, one may conclude that another method to model the liner x vel and the vel x vol interactions would be preferable. Moreover the quadratic model discussed in the preceding section (Table 6.10) yields a higher multiple correlation coefficient (R = 0.9884) with fewer parameters than the model of Table 6.11 and is therefore clearly superior.

There remains one further option, namely that one fits a separate quadratic model for each liner profile. Such a model implies the use of a total of 25 parameters, and therefore lacks parsimony. We do not consider it as an alternative to the model of Table 6.11 for describing interactions.

Table 6.11 ANOVA: WEAR-RATE on VELOCITY and VOLUME (1 model per liner)

SOURCE	SS	df	MS	F-stat	p-value
vel & vol	33.1326	2	16.5663	125.487	.0000
residuals	6.6008	50	.1320	-	-
lnr x model	5.177	12	.431	11.513	.0000
res in lnrs	1.424	38	.037	-	-
total	39.7334	52	-	-	-

se(est) = 0.3633
R-sq = 0.8339 R = 0.9132 R/s = 0.6612 (single model)
R-sq = 0.9642 R = 0.9819 (model x liner)

y(wear) = -1.94221 + 0.06923 vel - 0.04206 vol+ error (single)

y(wear) = -1.88010 + 0.07267 vel - 0.04663 vol + error (lnr1)
y(wear) = -2.12374 + 0.07478 vel - 0.03618 vol + error (lnr2)
y(wear) = -2.26178 + 0.07288 vel - 0.04101 vol + error (lnr3)
y(wear) = -1.16988 + 0.05201 vel - 0.03836 vol + error (lnr4)
y(wear) = -2.29944 + 0.07092 vel - 0.04021 vol + error (lnr5)

One additional effect of fitting interaction by grouping (into five submodels) is to significantly reduce the serial correlation in the estimated residuals to values acceptably close to zero.
Presumably serial correlations were partially confounded with lack of fit to a common coefficient model, within each LINER profile, and that lack of fit emerged as an apparent serial correlation because of the non-random ordering of the treatments.

No individual cases appeared to be anomalous or influential, so that there is little likelihood of interactions being masked by outliers. It is therefore necessary to concede that there is no easy way to handle interaction in the models envisaged here.

6.5.1.5 Covariate Regression Analyses

When all the liner dummy variables, the control variables and covariates were fitted in a multiple linear regression, a multiple correlation coefficient R = 0.9887 was obtained for the data set of size 45 (Table 6.12).

This figure was largely the consequence of several individual variables which each had a high individual correlation with the response (eg. height of LIFT).

Table 6.12 ANOVA: WEAR-RATE on ALL VARIABLES

SOURCE	SS	df	MS	F-stat	p-value
12 variates	33.0368	10	3.3037	148.053	.0000
residuals	0.7587	34	.0223	-	-
total	33.7955	44	-	-	-

se(est) = 0.1494
R-sq = 0.9776 R = 0.9887 R/s = 0.2603 (full model)
R-sq = 0.9187 R = -0.9585 (lift alone)

y(wear) = int + lnr(i) + b1 VEL + b2 VOL + b3 LIFT + b4 AW1 + b5 AW2 + b6 FA1 + b7 FA2 + error

where lnr(1) = 0.0 int = 1.91051 b4 = .14070e-2
lnr(2) = .04077 b5 = .46940
lnr(3) = -.12907 b1 = .04538 b6 = -.11832
lnr(4) = -.35417 b2 = -.02531
lnr(5) = -.25191 b3 = -.05784

The variable LIFT was most highly correlated with the response, and was singled out for special further analysis, as is evident from the accompanying ANOVA for the regression (Table 6.13), the two control variables (Table 6.7) did not together achieve a better fit than LIFT.

Table 6.13 ANOVA: WEAR-RATE on LIFT

SOURCE	SS	df	MS	F-stat	p-value
lift	31.0479	1	31.0479	485.900	.0000
residuals	2.7476	43	.0639	-	-
total	33.7955	44	-	-	-

se(est) = 0.2528
R-sq = 0.9187 r = -0.9585 (lift alone)
R-sq = 0.9242 R = +0.9614 (lift and liners)
R-sq = 0.9741 R = +0.9870 (lnrs,vel,vol,lift)

y(wear) = 12.8482 - 0.1986 lift + error

This suggests that lift may be a useful variable to adopt as a control variable in subsequent studies, even though it is practically more difficult to achieve nominated values of lift as opposed to nominated values of velocity and volume. Nonetheless a linear model in liners, velocity, volume and lift is slightly inferior in multiple correlation to the quadratic model of Table 6.9.

In none of these analyses did it appear that any cases in the data were unduly influential.

Artificial regression models can be fitted to this response, but it appears preferable to examine the covariates separately, since it is not evident that anything useful will be forthcoming from artificial selection of subsets. Plots of residuals from the foregoing models against the omitted variables did not suggest any crucial relationships beyond those specified above. Moreover the variables that were strongly related to wear-rate individually, tend also to be strongly related individually to each other. The models selected above are parsimonious in covariates and close to an optimum in multiple correlation.

6.5.2 COVARIATES as RESPONSES.

There are six covariates; lift, average forces (1) and (2), radial force, and areas of wear (1) and (2) analysed as responses. They are presented graphically in Appendix D, Figure D-14 to D-18. These analyses for the covariates of most interest, were suggested and motivated in section 6.2.

6.5.2.1 Lift Height Analysis

The height of lift is firstly examined under the non-parametric approach and it is evident that the same preference for liner #4 and vel-vol level 1-3 as from the wear data is indicated. The rankings are perfectly preserved within the liner and control variable groups, but some interaction is to be expected because of the apparent switching of ranks between the 1-1, 2-2 and 2-3 vel-vol control settings.

Table 6.14 Non-parametric statistics for HEIGHT of LIFT (% diam)

Levels	Liner Profiles #2	#1	#3	#5	#4	Ranks of Vel x Vol	profiles
3-1	43.3	44.0	47.7	48.7	50.7	9 9 9 9 9	1 2 3 4 5
3-2	44.4	47.5	49.7	50.1	51.2	8 8 8 8 8	1 2 3 4 5
3-3	45.0	48.4	50.2	50.8	52.0	7 7 7 7 7	1 2 3 4 5
2-1	49.2	51.4	51.4	52.2	53.0	6 6 6 6 6	1 2 3 4 5
2-2	52.2	53.9	54.1	55.5	55.9	4 4 4 4 4	1 2 3 4 5
2-3	54.0	54.9	55.1	55.7	56.4	3 3 3 3 3	1 2 3 4 5
1-1	50.7	51.4	53.1	53.7	54.3	5 5 5 5 5	1 2 3 4 5
1-2	55.8	57.3	58.0	58.2	59.4	2 2 2 2 2	1 2 3 4 5
1-3	56.5	57.5	58.4	58.7	59.7	1 1 1 1 1	1 2 3 4 5
			Friedman's Chi-square =			40.00	36.00
			df		=	8	4
			Observed significance :			p < 10e-6	p < 10e-6

The data of Table 6.14 are presented graphically in Appendix D Figure D-4. The experimental design analysis (Table 6.15) confirms the interaction, and again there a very good fit (R = 0.9986) of the design model.

Table 6.15 ANOVA: LIFT on FACTORIAL DESIGN

SOURCE	SS	df	MS	F-stat	p-value
liner	117.4689	4	29.3672	219.48	.0000
velocity	490.5293	2	245.2647	1832.99	.0000
volume	136.6253	2	68.3127	510.54	.0000
lnr x vel	18.8085	8	2.3511	17.57	.0000
lnr x vol	3.6058	8	.4507	3.37	.0185
vel x vol	18.0213	4	4.5053	33.67	.0000
residuals	2.1409	16	.1338	-	-
total	787.1999	44	-	-	-

se(est) = 0.3658 F = 209.55 df = 28, 16
R-sq = 0.9973 R = 0.9986 R/s = -0.2226 (full model)

se(est) = 0.4433 F = 201.21 df = 20, 24
R-sq = 0.9941 R = 0.9970 (omit lnr x vol)

In order to facilitate extrapolation of LIFT values for possible use as a control, a multiple regression model (Table 6.16) was fitted, using P9R to select from the parameters for a quadratic in velocity and volume with liner profile additive constants. The selection criterion was Mallow's C-p.

The model seems likely to estimate lift very well for the design points and the liners specified. It is also clear that if lift is to be made a control variable in later studies, more design points in the region around the 1-3 vel-vol combination should be used, if high lift is desirable. We observe that LIFT responds quadratically to changes in the control variables.

We may infer from these analyses that LIFT may be a surrogate for the quadratic terms in velocity and volume. If height of LIFT is amenable to control, it may allow simpler linear models in similar studies to the current ceramic experiments, but it will involve more complicated and tenuous links to industrial applications, where control is indirect at best, and difficult to verify.

One way to apply the information of Table 6.16 is to obtain prediction intervals for lift values (using the estimated model) at or near the best current design points that will be industrially acceptable. From these intervals one may infer whether or not an acceptable lift is achieved sufficiently often at the proposed design points, and proceed to select new design points on that basis.

Table 6.16 ANOVA: LIFT on VELOCITY and VOLUME QUADRATICS and LINERS

SOURCE	SS	df	MS	F-stat	p-value
liners	117.4689	4	29.3672	32.04	.0000
vel & vol linear	583.0201	2	291.5100	318.07	.0000
velsq & volsq	44.1344	2	22.0672	24.08	.0000
vel x vol	10.4973	1	10.4973	11.47	.0000
residuals	32.0791	35	0.9165	-	-
total	787.1999	44	-	-	-

se(est) = 0.9574 F = 91.54 df = 9, 35
R-sq = 0.9593 R = 0.9794 R/s = 0.0471
ADR = -0.0011 PMS = 1.1928 D-W = 1.8760

y(lift) = 3.75483 + lnr(i) + 1.05414 vel + 1.33804 vol
- 0.00792442 velsq - 0.0145221 volsq
-0.00519126 vel x vol + error

where lnr(1) = 1.54444 lnr(2) = 0 lnr(3) = 2.95556
lnr(4) = 4.61111 lnr(5) = 3.61111

No cases appeared to be outlying or influential.

6.5.2.2 Areas of Wear Analysis

There is a great deal of variability in the area of wear observations that does not seem easily reconciliable with a smooth underlying model. Possibly the method of establishing the areas from film is somewhat less precise than is desirable. In the data table below some anomalies, which appear to break patterns in the corresponding data on other variables, have been indicated.

Table 6.17 Non-parametric statistics for AREA of WEAR (1).

	Liner Profiles					Ranks of	
Levels	#2	#1	#3	#5	#4	Vel x Vol	Profiles
3-1	1240	1039	752	790*	654	1 1 1 1 2	1 2 4 3 5
3-2	1004	875	677	660	665	2 2 2 2 1	1 2 3 5 4
3-3	780	765	591	606	525	3 3 4 4 3	1 2 4 3 5
2-1	756	667	602	617*	504	4 4 3 3 4	1 2 4 3 5
2-2	744	656	559	455*	472	5 5 5 7 5	1 2 3 5 4
2-3	555	547	516	422	418	7 7 6 8 7	1 2 3 4 5
1-1	661	558	473	465*	472*	6 6 6 5 6	1 2 3 5 4
1-2	543	547	451	462	343	8 8 8 6 8	1 2 3 4 5
1-3	461	459	408	336	311	9 9 9 9 9	1 2 3 4 5
	Friedman's Chi-square =					36.51	32.00
	df =					8	4
	Observed significance :					p < 10e-6	p < 10e-6

The data of Table 6.17 is presented graphically in Appendix D, Figure D-5.

Once more evidence exists to suggest that the optimal design point involves liner #4 at the 1-3 levels of velocity and volume. It is not unexpected since there is strong bivariate correlation between the first area-of-wear measure and either of lift and wear.

No explanations for the indicated apparent anomalies were found from the residual plots. If changes in variance occur at different velocity or volume levels, one would expect more violation of pattern. If variance changes between liners, and is appreciably more at liner #5, then it is possible that liner #5 was less precisely measured than other data.

Table 6.18 ANOVA: AREA of WEAR (1) on FACTORIAL DESIGN

SOURCE	SS	df	MS	F-stat	p-value
liners	429935.2444	4	107483.8111	49.15	.0000
velocity	756093.7333	2	378046.8667	172.87	.0000
volume	217596.4000	2	108798.2000	49.75	.0000
lnr x vel	69151.1556	8	8643.8944	3.95	.0093
lnr x vol	31751.8222	8	3968.9778	1.81	.1477 ns
vel x vol	19648.2667	4	4912.0667	2.25	.1097 ns
residuals	34990.1778	16	2186.8861	-	-
total	1559166.7251	44	-	-	-

se(est) = 46.76 F = 24.89 df = 28, 16
R-sq = 0.9776 R = 0.9887 R/s = -0.4177 (full model)

Analysis by the experimental design model indicates that quadratic models with some interaction component for liner x velocity will be a good fit. That interaction may be required for the model to fit well at the anomalous values.

Table 6.19 ANOVA: AREA of WEAR (1) on VELOCITY and VOLUME QUADRATICS and LINERS

SOURCE	SS	df	MS	F-stat	p-value
liners	429935.2444	4	107483.8111	27.57	.0000
extra terms	984961.7839	3	328320.5946	84.20	.0000
residual	144269.6971	37	3899.1810	-	-
total	1559166.7251	44	-	-	-

se(est) = 62.443 F = 51.84 df = 7, 37
R-sq = 0.9075 R = 0.9526 R/s = 0.0063
ADR = +0.0649 PMS = 4831.2 D-W = 1.9694

y(area) = 1641.83 + lnr(i) - 33.383 vel + 0.30932 velsq
-0.10215 vel x vol + error

where lnr(1) = -70.111 lnr(2) = 0 lnr(3) = -190.555
lnr(4) = -264.444 lnr(5) = -214.555

Table 6.19 summarises the features of area of wear (1) as a response to the control variables. A quadratic model approximates the experimental design moderately well but no further insight is obtained. A model incorporating VOL would increase the R-sq value to 0.9098, and does not give an improvement of fit (MSE increases).

Case 16 (y = 1240 at 3-1) has a large estimated absolute standardised residual of 3.97 and a Cook's distance of 0.48. The corresponding area of wear (1) value is outlying, and may be the result of an imprecise measurement. It is a candidate for exclusion from the data set, or for a repeated measurement.

The second area of wear measure at the point of the projection of balls into parabolic flights does not appear to conform to any obvious pattern. In the non-parametric analysis the repeated values gave rise to a large number of tied ranks. No half-ranks for equal-value pairs are shown in the table, and ranks in the table were allocated for visual simplicity. The first of each of these pairs is indicated by a star (*) for convenience. The statistics were calculated using the half-ranks wherever necessary.

Table 6.20 Non-parametric statistics for AREA of WEAR (2).

	Liner Profiles					Ranks of									
Levels	#2	#1	#3	#5	#4	Vel x Vol					Profiles				
3-1	295	306	408	465	300	8	7	9	2	8	5	3	2	1	4
3-2	248	295	419	379	386	9	8	8	8	1	5	4	1	3	2
3-3	402	328	441	498	322	5	6	4	1	5*	3	4	2	1	5
2-1	449	459	441	444	289	3	1	3*	3	9	2	1	4	3	5
2-2	343	284	430	401	364	6	9	6	6	2	4	5	1	2	3
2-3	390	383	462	368	322	7	3	2	9	6	2	3	1	4	5
1-1	472	415	419	422	311	1*	2	7*	4	7	1	4	3	2	5
1-2	413	372	430	390	343	4	5	5*	7	4	2	4	1	3	5
1-3	472	372	462	401	354	2	4*	1*	5*	3	1	4	2	3	5

Friedman's Chi-square	=	7.987	13.24
df	=	8	4
Observed significance :		p > 0.20	p < 0.025

The data of Table 6.20 is presented graphically in Appendix D Figure D-19.

From the ANOVA we may infer that all the main effects of the factors, and all the liner interactions strongly influenced the data. Liner profiles are clearly the over-riding determinant of area of wear at the point of projection, and this accords with the 'a priori' expectations.

Table 6.21 ANOVA: AREA of WEAR (2) on FACTORIAL DESIGN

SOURCE	SS	df	MS	F-stat	p-value
liners	64363.2000	4	16090.8000	15.12	.0000
velocity	10459.2444	2	5229.6222	4.91	.0217
volume	8789.5111	2	4394.7556	4.13	.0358
lnr x vel	33024.5333	8	4128.0667	3.88	.0101
lnr x vol	25249.6000	8	3156.2000	2.96	.0306
vel x vol	7436.6667	4	1859.0556	1.75	.1891 ns
residuals	17032.6667	16	1064.5417	-	-
total	166354.9653	44	-	-	-

se(est) = 32.62 F = 5.010 df = 28, 16
R-sq = 0.8976 R = 0.9474 R/s = -0.5223 (full model)

In Table 6.22 we present an analysis of a quadratic model. It appears that there is only evidence for a relationship between area of wear(2) and vel sq. Liners 1 and 2 do not differ significantly, and in the presence of a constant term in the model, parameters for these liners are redundant.

There is no evidence to suggest that the analysis was unduly influenced by particular cases in the data. It is unlikely that this model will provide good extrapolation, due to the moderate value of R-sq. There may be anomalies of liner effects in the data, in that the areas of wear (2) do not follow a preferred ordering 2-1-3-5-4, as other variables do.

Table 6.22 ANOVA: AREA of WEAR (2) on VELOCITY and VOLUME QUADRATICS andLINERS

SOURCE	SS	df	MS	F-stat	p-value
liners	60313.1220	3	20104.3740	8.41	.0000
liner 1 (dropped)	4050.0780	1	4050.0780	1.65	ns
velsq	10414.5214	1	10414.5214	4.91	.0430
residuals	95627.3144	40	2390.6829	-	-
total	166354.9653	44	-	-	-

se(est) = 48.89 F = 7.40 df = 4, 44
R-sq = 0.4252 R = 0.6520 R/s = -0.1155
ADR = -0.0094 PMS = 2631.07 D-W = 2.1103

y(area2) = 429.568 + lnr(i) - 0.00933988 velsq + error

where lnr(1) = 0 lnr(2) = 0 lnr(3) = 62.5556
lnr(4) = -39.7778 lnr(5) = 46.5556

6.5.2.3 Radial Force Analyses

Strong patterns re-emerged in the radial force observations. The profile ranks were interesting in that, within profile pairs #1 and #2, and #3 and #5, rank differences were barely distinguishable, though it is clear that the pairs jointly differ from one another and from profile #4. This feature may have implications for further experimental designs, as it reflects shape comparisons amongst the profiles.

The pattern of rankings of the velocity x volume design points is similar to the consistent 1-2-3-4-5-7-6-8-9 rankings of most other covariates, but with the 1-2 and 2-3 levels almost indistinguishable. Again it seems reasonable to presume the pattern arises from the strong correlations already noted between most pairs of co-variates.

Table 6.23 Non-parametric statistics for RADIAL FORCE.

	Liner profiles					Ranks of															
Levels	#2	#1	#3	#5	#4	vel	x	vol			profiles										
3-1	1.2205	1.0288	0.6531	0.6984	0.5541	1	1	1	1	1	1	2	4	3	5						
3-2	0.9782	0.9073	0.5587	0.5435	0.5329	2	2	2	2	2	1	2	3	4	5						
3-3	0.8278	0.7136	0.4886	0.5239	0.4478	3	3	4	3	3	1	2	4	3	5						
2-1	0.6916	0.6218	0.4941	0.4980	0.4088	4	4	3	4	4	1	2	4	3	5						
2-2	0.6358	0.5845	0.4517	0.3492	0.3558	5	5	5	5	6	1	2	3	5	4						
2-3	0.4420	0.4431	0.3871	0.3303	0.3161	8	8	8	6	7	2	1	3	4	5						
1-1	0.5909	0.5257	0.3787	0.3625	0.3869	6	6	6	7	5	1	2	4	5	3						
1-2	0.4345	0.4672	0.3698	0.4394	0.2373	7	7	7	8	8	3	1	4	2	5						
1-3	0.3582	0.3747	0.2973	0.2498	0.2087	9	9	9	9	9	2	1	3	4	5						
Friedman's Chi-square =						38.82					27.82										
df =						8					4										
Observed significance :						p < 10e-6					p < 10e-6										

The data of Table 6.23 is presented graphically in Appendix D Figure D-7.

The parametric analysis confirms the 'a priori' expectation that the velocity is the major contributor to the radial forces (in the velocity ranges under study here). The volume was also expected to contribute in the model, since it is in fact a surrogate for mass. Liner profiles are presumably making a significant indirect contribution through the configuration of balls determined by the profile at each studied setting. The velocity interactions dominate the subsidiary effects.

Table 6.24 ANOVA: RADIAL FORCE on FACTORIAL DESIGN

SOURCE	SS	df	MS	F-stat	p-value
liner	.5977	5	.1494	63.25	.0000
velocity	.8546	2	.4273	180.88	.0000
volume	.2439	2	.1220	51.62	.0000
lnr x vel	.1447	8	.0181	7.66	.0003
lnr x vol	.0326	8	.0041	1.72	.1688
vel x vol	.0143	4	.0036	1.51	.2469
residuals	.0378	16	.0024	-	-
total	1.9255	44	-	-	-

se(est) = 0.0486 F = 28.53 df = 28, 16
R-sq = 0.9843 R = 0.9901 R/s = -0.2226 (full model)

Radial forces have been of interest as it seemed reasonable 'a priori' to expect this variable to be a contributor to wear. In this study the design may have been too broad for the contribution of the radial forces to become distinguishable from that of the co-variates to which it is strongly related. There is no reason to suggest that future designs should not again envisage data collection on this variable.

From an analysis (Table 6.25) that allows extrapolation, we find that a quadratic model in velocity and liner effects requires an additional term VEL x VOL for interactions. If we use volume in place of the interaction the R-sq value is slightly reduced to 0.879536 and includes volume as an additional covariate increases R-sq to 0.883087. There appears to be no clear choice amongst these models, but we report that arising from the C-p criterion. It opts for the VEL x VOL product interaction.

Table 6.25 ANOVA: RADIAL FORCE on VELOCITY and VOLUME QUADRATICS and LINERS

SOURCE	SS	df	MS	F-stat	p-value
model	1.7001	7	0.242871	39.87	.0000
residuals	0.2254	37	0.006092	-	-
total	1.9255	44	-	-	-

se(est) = 0.07805 F = 39.87 df = 7, 37
R-sq = 0.8829 R = 0.9397 R/s = 0.1172
ADR = 0.0002 PMS = 0.00748 D-W = 1.7631

y(radf) = 2.31192 + lnr(i) - 0.0530632 vel + 0.0010440193 velsq
-0.000106280 vel x vol + error

where lnr(1) = -0.0680889 lnr(3) = -0.233378
lnr(2) = 0 lnr(4) = -0.303489
lnr(5) = -0.242722

From the diagnostics we find case 16 as a possible outlier, and that it exerts a moderate influence on the parameter estimates. It has an estimated absolute standardised residual of 3.53, but is not so anomalous as to warrant exclusion. It is highly likely that an interaction effect is generating this case.

6.5.2.4 Averaged Force Analyses

Averaged forces (total force averaged over area of wear), were calculated by the appropriate transformations of measured values. These forces denoted AVE.FORCE (1) are operating at the regions of impact and AVE.FORCE (2) are operating at the regions of departure of balls from the mill lining. The formula applied is given by:

F(ave) = sqroot [{ F(rad) ** 2 } + { F(tang) ** 2 }]

The non-parametric analysis of values for the first area-of-wear confirmed the established rankings of the profiles and the rankings of the velocity x volume design points. These results probably have the same explanation as for previous patterns: there is a strong correlation between the variables over the set of observations.

Table 6.26 Non-parametric statistics for AVE.FORCE (1).

Levels	#2	Liner profiles #1	#3	#5	#4	Ranks of vel x vol	profiles
3-1	1.3876	1.1198	0.7872	0.7839	0.5892	1 1 1 1 1	1 2 3 4 5
3-2	1.1124	0.8798	0.6511	0.6068	0.5668	2 2 2 2 2	1 2 3 4 5
3-3	0.8533	0.7490	0.5641	0.5446	0.4648	3 3 3 4 3	1 2 3 4 5
2-1	0.7996	0.6682	0.5924	0.5672	0.4422	4 4 4 3 4	1 2 3 4 5
2-2	0.7797	0.6559	0.5354	0.4075	0.3834	5 5 5 6 6	1 2 3 4 5
2-3	0.5416	0.4846	0.4755	0.3720	0.3375	7 8 6 7 7	1 2 3 4 5
1-1	0.6881	0.5715	0.4498	0.4226	0.4105	6 6 7 5 5	1 2 3 4 5
1-2	0.5408	0.5273	0.4198	0.3647	0.2538	8 7 8 8 8	1 2 3 4 5
1-3	0.4770	0.4160	0.3616	0.2881	0.2233	9 9 9 9 9	1 2 3 4 5

Friedman's Chi-square	= 38.88	40.00
df	= 8	4
Observed significance :	p < 10e-6	p < 10e-6

The data in Table 6.26 is presented graphically in Appendix D-6.

In the experimental design model the main effects again dominate the analysis. All the factors contribute to significant differences but velocity takes precedence in the main effects and in the interactions. The overall pattern of the analysis is not unlike that for the radial forces, from which, 'inter alia', the average force is calculated.

Table 6.27 ANOVA: AVE.FORCE (1) on FACTORIAL DESIGN

SOURCE	SS	df	MS	F-stat	p-value
liner	.8660	4	.2150	92.00	.0000
velocity	.9704	2	.4852	207.62	.0000
volume	.3322	2	.1661	71.08	.0000
lnr x vel	.1294	8	.0162	6.92	.0005
lnr x vol	.0481	8	.0061	2.57	.0513 ns
vel x vol	.0327	4	.0082	3.50	.0311
residuals	.0374	16	.0023	-	-
total	2.4101	44	-	-	-

se(est) = 0.0483 F = 36.262 df = 28, 16
R-sq = 0.9845 R = 0.9922 R/s = -0.3688 (full mode

A regression model (Table 6.28) indicates that the average force at the impact point is largely dependent upon the liner profile and the velocity, with volume intruding mainly as an interaction term. It would be preferable for simplicity and parsimony to have a model that used VOL in place of VEL x VOL. The corresponding value: R-sq = 0.895812 could then be obtained. The only parameter estimates to change would be those for the intercept and the MSE. From the diagnostics it can be found that case 16 is moderately influential on this analysis, and is a likely outlier with an absolute standardised residual value of 3.91.

Table 6.28 ANOVA: AVE.FORCE (1) on VELOCITY and VOLUME QUADRATICS and LINERS

SOURCE	SS	df	MS	F-stat	p-value
liners	.8660	4	.2150	34.05	.0000
velocity terms	1.3105	3	.4368	69.19	.0000
residuals	.2336	37	.0063	-	-
total	2.4101	44	-	-	-

se(est) = 0.07946 F = 49.24 df = 7, 37
R-sq = 0.9031 R = 0.9503 R/s = 0.0569
ADR = 0.0002 PMS = 0.007807 D-W = 1.8817

y(force1) = 1.99738 + lnr(i) - 0.0425416 vel + 0.000382066 velsq
-0.000125607 vel x vol + error

where lnr(1) = -0.119738 lnr(3) = -0.257022
lnr(2) = 0 lnr(4) = -0.386511
lnr(5) = -0.310300

The same lack of pattern as occurred in the area-of-wear (2) analysis, is to be found in the average force(2) values. Because of the strong relationship between area-of-wear (2) and average force (2) the rankings appear to be somewhat similar, but this may be noticeable only because of their differences from the other ranking patterns.

Table 6.29 Non-parametric statistics for AVE.FORCE (2).

	Liner profiles					Ranks of	
Levels	#2	#1	#3	#5	#4	vel x vol	profiles
3-1	0.3016	0.2459	0.5465	0.4213	0.1913	7 3 9 1 6	3 4 1 2 5
3-2	0.2152	0.2001	0.5732	0.1954	0.3248	8 5 7 6 1	3 4 1 5 2
3-3	0.1599	0.1226	0.7647*0.1606		0.2093	9 9 1 9 5	4 5 1 3 2
2-1	0.4366	0.4085	0.6789	0.3837	0.1901	4 2 3 2 8	2 3 1 4 5
2-2	0.3122	0.1654	0.5772	0.2032	0.2256	6 6 6 5 4	2 5 1 4 3
2-3	0.5220	0.1369	0.5885	0.1843	0.1909	2 8 5 7 7	2 5 1 4 3
1-1	0.4959	0.4182	0.6914	0.3519	0.1830	3 1 2 3 9	2 3 1 4 5
1-2	0.4198	0.2070	0.5646	0.1769	0.2347	5 4 8 8 2	2 4 1 5 3
1-3	0.5337	0.1413	0.6107	0.2431	0.2319	1 7 4 4 3	2 5 1 3 4

Friedman's Chi-square = 5.707 24.18
df = 8 4
Observed significance : p > 0.20 p < 10e-5

Liner profile dominates the strong performance of the experimental design model (Table 6.30), through the main effects but with appreciable interaction. Velocity effects are minor and generally depend on the liner profile involved. Fitting a quadratic model (Table 6.31) we again observe liner effects as dominant. As it is preferable not to introduce product interaction terms in regression if it involves an omitted regressor variable, we note that an almost equal R-sq value of 0.7943 is obtained for an alternative regression.

Table 6.30 ANOVA: AVE.FORCE (2) on FACTORIAL DESIGN

SOURCE	SS	df	MS	F-stat	p-value
liner	1.0313	4	.2578	61.83	.0000
velocity	.0262	2	.0131	3.14	.0710 ns
volume	.0705	2	.0353	8.45	.0031
lnr x vel	.0926	8	.0116	2.78	.0392
lnr x vol	.1216	8	.0152	3.65	.0133
vel x vol	.0103	4	.0026	.62	.6578 ns
residuals	.0667	16	.0042	-	-
total	1.4191	44	-	-	-

se(est) = 0.0646 F = 11.583 df = 28, 16
R-sq = 0.9530 R = 0.9762 R/s = -0.0899 (full mode

It can be reported that the alternative model relating to Table 6.31 for completeness, though it is unlikely that average force at the point of projection will inform any future experimental designs. Because of the separability and independence (orthogonality) of the design, the common parameters have the same estimates and the model diagnostics have virtually identical values. None of the data cases exhibit anomalous features, and we may conclude that either of the models is adequate for describing these average force responses.

Table 6.31 ANOVA: AVE.FORCE (2) on VELOCITY and VOLUME QUADRATICS and LINERS

SOURCE	SS	df	MS	F-stat	p-value
liners	1.0313	4	.2508	32.72	.0000
velocity terms	.0964	3	.0321	4.08	.0250
residuals	.2916	37	.0079	-	-
total	1.4193	44	-	-	-

se(est) = 0.08877 F = 20.44 df = 7, 37
R-sq = 0.7946 R = 0.8914 R/s = -0.1268
ADR = -0.0001 PMS = 0.007807 D-W = 2.2009

y(force2) = 0.856867 + lnr(i) - 0.029897 vol - 0.000014690 velsq
+ 0.000510274 volsq + error

where lnr(1) = -0.150111 lnr(3) = 0.244311
lnr(2) = 0 lnr(4) = -0.157256
lnr(5) = -0.119611

Alternative model:

y(force2) = 0.943227 + lnr(i) - 0.029897 vol - 0.00227355 vel
+ 0.000510274 volsq + error

where lnr(1) = -0.150111 lnr(3) = 0.244311
lnr(2) = 0 lnr(4) = -0.157256
lnr(5) = -0.119611

6.5.3 FINDINGS

These analyses indicate that there are significant differences between the effects of the profiles, between those of the velocity x volume settings for the wear-rate response, and some of the covariates. Minimal wear is associated with profile #4, lower velocities and higher volumes. Here is a prospect of substantially reducing wear-rate in the current industrial setting with minimal disruption of the processes.

Generally the data confirm the expectation that the current liner profile can be replaced by a more durable profile that exhibits appreciably less wear and promises comparable work by reason of having an acceptable configuration of balls when the tube-mill is operational. Although the velocity and volume controls may dominate the responses examined in this report, it is not unreasonable to focus on the three best performing liner profiles in more analysis on a reduced data set of 27 cases. The idea of the reduced analysis is to find any interesting features which may inform a subsequent experimental design. This is pursued in the next section.

Only case 16 in the data gives rise to large estimated residuals for the covariates examined as responses. It does so on the three related measurements: area of wear (1), average force (1), and radial force. These large residuals may arise from one imprecise measurement compounding itself through the transformations by which they are derived. However it is likely that some interactions are operating at this point. It is unecessary to examine this case further as it is not in the reduced region of interest suggested by the complete experiment (profiles #3 to #5).

If one keeps in mind the industrial applications to dry-milling of coal and hard ores, it will not be helpful to use the whole experimental region in further work. From other evidence in the film records, it is clear that adequate lift does not in itself ensure sufficient impact force creation, and that the lowest velocity level does not generate the impact forces required for efficient pulverization of the above materials. Furthermore it is apparent that the highest volume level demands additional power consumption by the mill, mainly through the rotation of larger volumes of charge that are stationary, relative to the mill.

6.6 ANALYSES of REDUCED DATA

Parallel analyses to most of those preceding are now presented for the 27 cases in the reduced 3 x 3 x 3 design obtained by eliminating profiles #1 and #2. Such a focus can be important when the two additional levels of the profile factor have been influential in the data analysis. In other words, their inclusion can hide underlying relationships in the variables and responses for the restricted subset of profiles. On most variables of interest, these three profiles appear to be substantially better than profiles #1 and #2. Further analysis may therefore indicate elements of future designs for optimizing wear rate by means of profile modifications, and adjustments to velocity and volume.

6.6.1 Wear-Rate Analysis

The same overall features of the relationships between the response and the experimental design are repeated in the 3 x 3 x 3 subset of data.

Table 6.32 ANOVA: WEAR-RATE on FACTORIAL DESIGN

SOURCE	SS	df	MS	F-stat	p-value
liner	1.0614	2	.5307	81.97	.0000
velocity	12.7275	2	6.3638	982.91	.0000
volume	3.3605	2	1.6803	259.53	.0000
lnr x vel	.2260	4	.0565	8.73	.0051
lnr x vol	.0023	4	.0057	.09	.9835ns
vel x vol	.0598	4	.0149	2.31	.1460
residuals	.0518	8	.00647	-	-
total	17.4893	26	-	-	-

se(est) = 0.0804 F = 153.08 df = 18, 8
R-sq = 0.9970 R = 0.9985 (full model)

The reduced part of the factorial design model appropriate here again indicates slight overfitting by the full 3 x 3 x 3 design. The multiple correlation is almost the same, while the se(est) is smaller.

Table 6.33 ANOVA: WEAR-RATE on REDUCED FACTORIAL

SOURCE	SS	df	MS	F-stat	p-value
regression	17.4239	9	1.9360	504.14	.0000
residuals	.0653	17	.00384	-	-

se(est) = 0.0620 F = 504.14 df = 9, 17
R-sq = 0.9963 R = 0.9981 (part model)

The significant interaction terms fitted in the reduced model involve an improvement for liner #4 across velocity levels, and an increase in wear component for the 2-1 vel*vol combination.

For extrapolation quantitative models must again be fitted. Allowing for selection from possible quadratic terms and multiplicative interaction in the control variables, a best subset regression model from the P2R program was obtained. There were four additional cases available for this sub-design from the original eight additional cases. Since these gave no evidence which differed from the fitted values by values, inexplicable in terms of random error, they were incorporated into the data for the calculation of the fitted equation.

Table 6.34 ANOVA: WEAR-RATE on QUADRATIC MODEL

SOURCE	SS	df	MS	F-stat	p-value
regression	19.9011	6	3.3168	203.07	.0000
residuals	.3921	24	.01633	-	-
Total	20.2932	30			

se(est) = 0.1278 F = 203.07 df = 6, 24
R-sq = 0.9807 R = 0.9903 R/s = 0.2152
ADR = 0.0003 PMS = 0.0215 D-W = 1.5159

y(wear) = 7.89233 + lnr(i) - 0.168423 vel - 0.0943108 vol
+ 0.0014957 velsq + 0.00106408 volsq + error

where lnr(3) = 0 lnr(4) = -0.451489 lnr(5) = -0.168600

Again case #36 is associated with the maximal diagnostic statistics, with a largest standardised residual of -2.45 and 0.37 for the Cook's distance. This corresponds with moving the parameter estimates to the edge of a 11.09% confidence ellipsoid, and does not constitute inordinate influence. If the inclusion of lift, and the product interaction term is deemed unacceptable, then a model replacing them with volume and volume-square, attains an R-sq = 0.9806. Compared with R-sq = 0.9772 for volume alone, one can infer that a quadratic model fits the data fairly well, even though it forces parallel quadratic graphs to the three liner responses.

These analyses are comparable with those of Tables 6.3, 6.5 and 6.6, 6.7 and 6.8 respectively. There do not appear to be anomalies in the wear rate analyses including or excluding liner profiles #1 and #2. Over the ranges of the control variables studied here, there is a clear non-linear relationship between the response and the controls, which is suitably characterised by a quadratic approximation. The model appears to have good predictive power, though it is possible that a replicated experiment would have produced more comparable MSE and PMS values.

The signal to noise ratio for profile #4 is almost -3.0, and suggests that profile #4 is likely to be superior, despite the tenuousness of all the assumptions and approximations underpinning this analysis.

6.6.2 Covariates as Responses

Analyses that parallel section 6.5.2 now follow. These involve the application of the reduced experimental design to each of the covariate responses.

6.6.2.1 Height of Lift analysis

Routine analysis again confirms that the experimental design model fits the response VERTICAL HEIGHT of LIFT very well. To extrapolate for future designs we examine the quadratic model.

Table 6.36 ANOVA: LIFT on FACTORIAL DESIGN

SOURCE	SS	df	MS	F-stat	p-value
liner	12.5119	2	6.2560	68.18	.0000
velocity	219.9496	2	109.9748	1198.51	.0000
volume	66.8941	2	33.4470	364.51	.0000
lnr x vel	.8193	4	.2048	2.23	.1551
lnr x vol	.1948	4	.0487	.53	.7172ns
vel x vol	11.6237	4	2.9059	31.67	.0001
residuals	.7341	8	.09176	-	-
total	312.7273	26	-	-	-

se(est) = 0.3029 F = 378.00 df = 18, 8
R-sq = 0.9977 R = 0.9988 (full model)
se(est) = 0.2684 F = 480.43 df = 9, 17
R-sq = 0.9661 R = 0.9980 (omitting terms)

y(lift): intercept, 3x2 main effects, 3 interactions + error

If an artificial experimental design is fitted, forward selection of model parameters will fit the main effects for all three factors, and three interaction terms that adjust lift downward for all profiles at any velocity and minimal volume, and upward for profile #4 with any volume at the largest velocity.

A somewhat improved prediction is possible for liner profiles of this subset of the data. One explanation would be that having less aggressive lift profiles, they achieve similar lift at the chosen velocity and volume levels of this study. The effect of including the other profiles in the analysis introduces more aggressive lift and violation of the similarity, and hence a fit which had a larger se(est) than is obtained here.

Table 6.37 ANOVA: LIFT on QUADRATIC MODEL

SOURCE	SS	df	MS	F-stat	p-value
regression	306.2664	7	43.7523	128.64	.0000
residuals	6.4622	19	.34011	-	-
total	312.7273	26	-	-	-

se(est) = 0.5832 F = 128.64 df = 7, 19
R-sq = 0.9793 R = 0.9896 R/s = -0.5679
ADR = -0.0001 PMS = 0.4840 D-W = 3.1059

y(lift) = 25.0692 + lnr(i) + 0.553755 vel
+ 1.28839 vol -0.00543735 vel*vol
- 0.00441765 velsq - 0.01355610 volsq + error

where lnr(3) = 0 lnr(4) = 1.65556 lnr(5) = 0.655556

None of the cases appear to be inordinately influential. Case #34 has the largest standardized residual (2.48) and Cook's distance (0.38). The signal to noise ratio associated with liner profile #4 is almost 3.0, again suggesting that the conclusion of its superiority is fairly robust.

6.6.2.2 Areas of wear analyses

The area of wear (1) factorial design analysis showed only the main effects of the factors as statistically significant. We may therefore envisage attributing the interaction SS's to error, along with the three-factor interactions. If we do so, we find that the se(est) decreases and the F-stat increases. We may conclude that the main effects of the factors describe the important elements of the response.

By fitting the quadratic model we find that the relationship of the response to the factors can be well summarised by a quadratic and an interaction term. The reported model is optimal on the C-p criterion, but is only one of several models that show high R-sq values.

Table 6.38 ANOVA: AREA of WEAR (1) on FACTORIAL DESIGN

SOURCE	SS	df	MS	F-stat	p-value
liners	25573.407	2	12786.703	7.48	.0147
velocity	273480.074	2	136740.037	80.00	.0000
volume	79480.074	2	39740.037	23.25	.0005
lnr x vel	4066.593	4	1016.648	0.59	.6766ns
lnr x vol	4068.593	4	1017.148	0.60	.6764ns
vel x vol	2587.926	4	646.982	0.38	.8182
residuals	13674.741	8	1709.343	-	-
main effects	378533.54	6	63088.92	51.72	.0000
error	24397.840	20	1219.892	-	-
total	402931.378	26	-	-	-

se(est) = 41.344 F = 12.72 df = 18, 8
R-sq = 0.9661 R = 0.9829 (full model)
se(est) = 34.927 F = 51.72 df = 6, 20
R-sq = 0.9394 R = 0.9693 (omitting terms)

y(force1): intercept, 3x2 main effects, + error

In the quadratic model we can again examine diagnostics of the model fit, and check for possible anomalies.

Table 6.39 ANOVA: AREA of WEAR (1) on QUADRATIC MODEL

SOURCE	SS	df	MS	F-stat	p-value
regression	377946.528	4	43.7523	83.16	.0000
residuals	24994.427	22	1136.110	-	-
total	402940.955	26	-	-	-

se(est) = 33.7062 F = 83.16 df = 7, 19
R-sq = 0.9380 R = 0.9685 R/s = -0.3413
ADR = 0.4132 PMS = 1365.6 D-W = 2.6276

y(area1) = 255.366 + lnr(i) - 0.0781927 vel*vol +
+ 0.0742532 velsq + error

where lnr(3) = 0 lnr(4) = -73.8889 lnr(5) = -24.0000

None of the cases appears to be inordinately influential. Case #41 has the largest standardized residual (-2.45) and Cook's distance (0.22).

A similar procedure follows for area of wear (2) responses. Only liner profile differences appear to be statistically significant, but some liner x volume interaction may occur.

Table 6.40 ANOVA: AREA of WEAR (2) on FACTORIAL DESIGN

SOURCE	SS	df	MS	F-stat	p-value
liners	54544.667	2	27272.333	32.26	.0001
velocity	626.889	2	313.444	0.37	.7014 ns
volume	990.889	2	495.778	0.59	.5787 ns
lnr x vel	4041.778	4	1010.444	1.20	.3831 ns
lnr x vol	11479.111	4	2869.778	3.39	.0664
vel x vol	1656.889	4	414.222	0.49	.7438 ns
residuals	6762.444	8	845.306	-	-
total	80102.655	26	-	-	-

se(est) = 41.344 F = 12.72 df = 18, 8
R-sq = 0.9661 R = 0.9829 (full model)
se(est) = 34.927 F = 51.72 df = 6, 20
R-sq = 0.9394 R = 0.9693 (omitting terms)

y(area1): intercept, 3x2 main effects, + error

In order to extrapolate we examine possible quadratic models. Under the C-p criterion the optimal quadratic involves only a constant for liner profile #4.

Table 6.41 ANOVA: AREA of WEAR (2) on QUADRATIC MODEL

SOURCE	SS	df	MS	F-stat	p-value
regression	53392.667	1	53392.667	49.97	.0000
residuals	26710.000	25	1068.400	-	-
total	80102.667	26	-	-	-

se(est) = 32.6864 F = 49.97 df = 1, 25
R-sq = 0.6666 R = 0.8164 R/s = -0.4357
ADR = 0.0000 PMS = 1152.2 D-W = 2.5904

y(area2) = 426.667 + lnr(i) + error

where lnr(3) = 0 lnr(4) = -94.3333 lnr(5) = 0

If one insists on a model distinguishing between all three liners, the value of R-sq increases to 0.6809, and the increase is not significant.

It thus follows that the controls and covariates do not have a strong association with the area of wear through attrition. In this model none of the cases appear to be inordinately influential. Case #45 has the largest standardized residual (2.25) and case #35 has the largest Cook's distance (0.19).

The signal to noise ratio for profile #4 is again almost 3.0 and suggests a smaller area of wear by attrition for this liner.

6.6.2.3 Radial force analyses

The standard analysis suggests velocity and volume effects on the response radial force, with the possibility of one or more liner profile parameters.

Table 6.42 ANOVA: RADIAL FORCE on FACTORIAL DESIGN

SOURCE	SS	df	MS	F-stat	p-value
liner	.02609	2	.01304	4.77	.0434
velocity	.24860	2	.12430	45.42	.0000
volume	.07801	2	.03901	14.25	.0023
lnr x vel	.00454	4	.00113	0.41	.7940 ns
lnr x vol	.00144	4	.00036	0.13	.9666 ns
vel x vol	.00439	4	.00110	0.40	.8029 ns
residuals	.02190	8	.00274	-	-
total	.38496	26	-	-	-

se(est) = 0.0523 F = 7.37 df = 18, 8
R-sq = 0.9431 R = 0.9711 (full model)
se(est) = 0.0402 F = 36.44 df = 6, 20
R-sq = 0.9162 R = 0.9572 (main effects)

y(lift): intercept, 3x2 main effects, + error

The reduced artificial experimental design models fit the main effects of velocity and volume, but only one profile parameter (for profile #4). No interaction terms are significant.

Table 6.43 ANOVA: RADIAL FORCE on QUADRATIC MODEL

SOURCE	SS	df	MS	F-stat	p-value
regression	0.35151	4	0.08788	57.77	.0000
residuals	0.03347	22	0.00152	-	-
total	0.38498	26	-	-	-

se(est) = 0.0390 F = 57.77 df = 4, 22
R-sq = 0.9131 R = 0.9555 R/s = -0.3930
ADR = 0.0002 PMS = 0.001777 D-W = 2.7383

y(frad) = 1.34783 + lnr(i) - 0.0288758 vel
- 0.0060070 vol + 0.000243334 velsq + error

where lnr(3) = 0 lnr(4) = -0.0654389 lnr(5) = 0

The quadratic model apparently allows a further model simplification by virtually discarding the quadratic effect of volume.

None of the cases appear to be inordinately influential. Case #38 has the largest standardized residual (2.33) and Cook's distance (0.16).

6.6.2.4 Average force analyses

Standard analysis shows the main effects of all factors in the experimental design to be significant for the average force (1) response.

Table 6.44 ANOVA: AVERAGE FORCE (1) on FACTORIAL DESIGN

SOURCE	SS	df	MS	F-stat	p-value
liner	.07624	2	.03812	24.56	.0004
velocity	.31568	2	.15784	101.70	.0000
volume	.11264	2	.05632	36.29	.0001
lnr x vel	.00375	4	.00094	0.60	.6704ns
lnr x vol	.00367	4	.00092	0.59	.6784ns
vel x vol	.00345	4	.00086	0.56	.7013ns
residuals	.01242	8	.00155	-	-
total	.52786	26	-	-	-

se(est) = 0.0394 F = 18.45 df = 18, 8
R-sq = 0.9765 R = 0.9882 (full model)
se(est) = 0.0341 F = 72.20 df = 6, 20
R-sq = 0.9559 R = 0.9777 (main effects)

y(lift): intercept, 3x2 main effects, + error

No interaction terms appear important. It is necessary to seek evidence for extrapolation by examining the quadratic model, and find that it approximates the design surface very well.

Table 6.45 ANOVA: AVERAGE FORCE (1) on QUADRATIC MODEL

SOURCE	SS	df	MS	F-stat	p-value
regression	0.50609	6	0.084349	77.46	.0000
residuals	0.02178	20	0.001089	-	-
total	0.52787	26	-	-	-

se(est) = 0.03300 F = 77.46 df = 6, 20
R-sq = 0.9587 R = 0.9792 R/s = -0.2799
ADR = 0.0004 PMS = 0.001535 D-W = 2.4955

y(force1) = 0.352923 + lnr(i) - 0.0118757 vol -0.000114547 vel*vol
+ 0.000084743 velsq + 0.000261938 + error

where lnr(3) = 0 lnr(4) = -0.129489 lnr(5) = -0.0532778

None of the cases appears to be inordinately influential. Case #43 has the largest standardized residual(2.34) and Cook's distance (0.38). Its removal would shift the parameters to the edge of a 11.71% confidence ellipsoid.

The signal to noise ratio for profile #4 is almost 4.0, and suggests that the profile has appreciably less average force at the region of impact than the other profiles.

The average force (2) response, seems to have dominating liner profile effects, with some possible interaction effects.

Table 6.46 ANOVA: AVERAGE FORCE (2) on FACTORIAL DESIGN

SOURCE	SS	df	MS	F-stat	p-value
liner	.88534	2	.44267	103.15	.0000
velocity	.00153	2	.00076	0.18	.8402ns
volume	.01979	2	.00990	2.31	.1619ns
lnr x vel	.00116	4	.00029	0.07	.9900ns
lnr x vol	.07392	4	.01848	4.31	.0377
vel x vol	.00766	4	.00192	0.45	.7727ns
residuals	.03433	8	.00429	-	-
total	1.02373	26	-	-	-

se(est) = 0.0655	F = 12.81	df = 18, 8	
R-sq = 0.9665	R = 0.9831	(full model)	
se(est) = 0.0457	F = 117.09	df = 4, 22	
R-sq = 0.9551	R = 0.9773	(omit terms)	

y(lift): intercept, liner #3, 3 interaction terms
+ error

An artificial experimental design suggests that one liner profile effect and three interactions dominate the response.

To extrapolate a good quadratic model is needed. However it appears that fitting constants for two liners is almost as good as the artificial design, and it suffices to say there are only liner profile effects.

Table 6.47 ANOVA: AVERAGE FORCE (2) on QUADRATIC MODEL

SOURCE	SS	df	MS	F-stat	p-value
regression	0.88524	2	0.44262	76.87	.0000
residuals	0.13838	24	0.005766	-	-
total	1.02363	26	-	-	-

se(est) = 0.07594	F = 76.77	df = 2, 24	
R sq = 0.8648	R = 0.9300	R/s = -0.3339	
ADR = 0.0000	PMS = 0.006487	D-W = 2.5299	

y(force1) = 0.621744 + lnr(i) + error

where lnr(3) = 0 lnr(4) = -0.401567 lnr(5) = -0.363922

None of the cases appears to be inordinately influential. Case #43 has the largest standardized residual (2.28) and Cook's distance (0.22). Its removal would shift the parameters to the edge of a 19.37% confidence ellipsoid.

The signal to noise ratios for profiles #4 and #5 are close 5.0, suggesting marked differences attributable to profiles. It appears that the average force (2) values depend mainly on the liner profile, and that as far as the subset of three liner profiles is concerned, none of the control variables appears to have any effect on the second average force.

6.7 FINDINGS

The response of major interest is wear-rate. These analyses establish that there are important effects associated with each of the control variables, but that there is interaction of liner type and velocity,and between velocity and volume for wear-rate responses. The models developed here do not seem to explain the liner x velocity interaction, so alternatives will be sought in a later chapter. There is however clear evidence that the wear-rate response surface is adequately approximated (for this design) by a quadratic function.

Covariate responses were well explained by similar model families, but interactions generally seemed to be absent, although quadratic effects were observed in almost all the covariate responses.

Given that there were replicates for only a handful of design points, it was found that the postulated models based on the control variates seem to perform fairly well in exhibiting the effects of those variates and predictively. However, it is possible that additional replicates could suggest substantial improvements to these models, and provide checks on model assumptions.

Normality assumptions for the residuals in the foregoing analyses were examined by means of normal probability plots. Some evidence of non-normality was found for some of the variables, but in the absence of any clear alternative the analyses are presented in the conventional form.

Marked serial correlations appear to hold for the estimated residuals of these analyses. These correlations are negative for all responses except wear-rate. An examination of residuals plots suggests that the negative correlations may be the result of circumstantial features in the data, such as a large positive standardized residual being preceded and followed by negative residuals.

There does not seem to be any obvious mechanism by which compensatory variations could be induced in successive data measured, though such a feature cannot be ruled out as the ordering of the trials was non-random.

If refuge is taken in the assumptions that the uncontrolled conditions were fairly uniform, and that the trials were independent, it may be inferred that profile #4 is superior and that the factorial levels 1-3 for velocity and volume give rise to less wear under the conditions of this experiment.

CHAPTER VII

LINER PROFILE ROUGHNESS

7.1 THE ROUGHNESS MEASURE

The main purpose of the experiments was to study the influence of the liner profile on its wear characteristics. Despite uncertainty it was hoped that a continuous variable could be assigned to the liners in such a way as to make it possible to interpolate for other liners not directly tested in the present series.

To find such a variable is a primary aim of this study. Another primary aim is to confirm that the liners showed significant differences during the trials,and that these differences were consistent over the ranges of the experimental control variables.

If in the study of any effect, the independent variables can be regarded as continuous, than the use of 'parametric' statistical methods is recommended. One of the main strengths of the 'parametric' methods is that they allow the determination of the expected value of the dependent variable at values of the independent variables that were not part of the measured data set. The control variables are on such a continuous scale, but the five liner profiles admitted no such natural scale.

Fortunately, a continuous variable was found capable of describing the liner profile in the form of the liner's roughness coefficient (C_R). This variable appeared to sucessfully summarise the relevant geometrical properties of the individual liner profiles.

Liner profile dummy variables in the data models were therefore replaced by a single variable which was intended to be a measure of profile roughness (C_R). It was assumed that wear resulted from liners having surfaces which deviated from smoothness, and that the wear-rate would be directly related to an appropriate measure of the deviation from smoothness.

Clearly there are many possible measures. Attention was devoted to selecting one which was intuitively simple and apparently acceptable.

The choice was:

$$C_R = \left[\{\text{sum(tan angles)}\} * \text{upper surface length}\right] / \text{lower surface length.}$$

The values obtained were:

- liner #2 : 2.2894
- liner #1 : 1.8293
- liner #3 : 1.5147
- liner #5 : 1.3767
- liner #4 : 0.5040

The first step in the evaluation of the test results after incorporating this C_R variable is to present the data graphically. This presentation includes plotting the values of the wear rate against:

a. The mill speed and the charge volume for each liner (Figure D-8 in Appendix D)
b. The roughness coefficient and the mill speed for each charge volume (Figure E-1, E-2 and E-3 in Appendix E)
c. The roughness coefficient and the charge volume for each mill speed (Figure E-4, E-5 and E-6 in Appendix E)

These plots show that the response-surfaces behave reasonably and that they do not intersect. These findings were confirmed by the statistical analysis, using the non-parametric method (Chapter VI Table 6.2). It was also shown, using a Bonferroni-Approximation, that liner #1 and liner #2 can be left out of consideration, because of their poor performance as compared to the other three liners (Chapter VI Table 6.4).

Since it has been established that liner profiles #3, #4 and #5 were of primary interest for the coal-milling application, the analysis of the data was conducted on those profiles only, and thus only used their values of the roughness variable. The reduced 3 x 3 x 3 design was modelled with wear-rate with each of the covariates in turn being viewed as the response.

The analysis proceeded as in the previous Chapter VI, with each response in turn being modelled by some quadratic in the variables roughness, velocity and volume. Some of the benefits of the original experimental design carry over into these analyses, because of the orthogonality of the factors.

As a result when some alternative models are presented, there may be several parameter estimates which are unchanged. However liner roughness appears as an additional possible regressor variable, and contributes to possible interaction regressors rough*vel and rough*vol.

To facilitate comparison in the analysis of each response variable, diagnostics for different models are presented alongside one another. The Tables now show the signed maximum absolute standardized deviation (max $|e(i)|$), and the maximal Cook's distance, with associated case numbers, and the percentage of the associated confidence ellipsoid shift. As before some elements of the design structure balance the design in such a way that influential observations are unlikely to be found, or that they have to be extraordinary outliers before they are categorised as influential. On the other hand, outliers are still possible, and where present, are explicitly noted.

7.2 ANALYSIS USING ROUGHNESS MEASURE

7.2.1 Wear Rate Analysis

The analysis of the liner wear begins with the fitting of a 'trend-surface' model to the experimental points, using three models with different contents.

Model I contains (beside a constant) only first order terms of the roughness coefficient, the mill and speed and the charge volume.

Model II contains (beside a constant) the first and second order terms of the roughness coefficient, mill speed and the charge volume.

Model III contains all the terms included in model II, with the addition of a product term (rough * vel) of the mill speed and the roughness coefficient, to handle interactions of profile and velocity.

The analysis of these models is summarized in Table 7.1. The table shows that all three models fit the data very well, yielding correlation coefficients Ø.978, Ø.988 and Ø.995, with high values of F-statistics, indicating a convincing fit. This is supported by graphical presentation (Figure E-7 in Appendix E) of liner wear rate (measured) vs liner wear rate (fitted as per model III). In this and the subsequent tables the results of the corresponding parametric analysis in Chapter VI is included to make comparison easier.

After this, Model III was fitted again, this time including the available additional three observations (table 7.2). This table shows no evidence of any 'lack of fit', and model III is shown to be superior both to the linear model (model I) and to the quadratic model, without the roughness*mill speed interaction (model II). The Table shows no evidence of any serial correlation.

For the sake of completeness a 'full' model was also constructed, containing the three independent variables (roughness coefficient, mill speed and charge volume), their squares, the six covariates and the interaction terms involving the charge volume. This model is presented in Table 7.3. The outcome was, as expected, that this model was found superior to any of the models previously presented, including the model chosen for the same observations, but containing only the control variables. However it is not useful for future experimentation.

Generally, wear decreases with the roughness coefficient across all the velocities studied here, but there is a trade-off in respect of changes in other responses (eg. the covariates), and any experimentation seeking an industrially optimal liner profile will have to examine those responses too.

It can be observed, in passing that no data cases appear to be outlying or influential. There is no evidence of non-normality in the residuals and the serial correlation is mild, and is not cause for concern.

7.2.2 Covariates as Responses

A regression analysis, similar to the one done on the liner wear rate, was performed on all the 'covariates'. The analysis included the linear and the quadratic terms of the independent variables and some of their products. The results of the 'non-parametric' analysis performed on the same variable is shown in Chapter VI. The results of the parametric (regression) analysis show, that the introduction of the liner roughness coefficient has improved the performance of the models. This is reflected in a higher F-statistics, higher correlation or smaller error of estimate, than found in the corresponding models without the roughness coefficient as a control variable (Table 6.32, 6.34, 6.35, 6.37 and 6.43). As far as the 'fit' of the formulae is concerned, the improvements are only moderate, but as the results of the parametric study with roughness coefficients included have the power to predict the behaviour of different liners, not included in the data set, they are to be preferred to the results of the analysis without roughness as discussed in Chapter VI.

The regression formulae produced for the different covariates involves the following independent (regressor) variables:

Lift	:	speed, volume, roughness coefficient (model I)
	:	speed, square of speed, volume, square of volume, roughness, speed*volume (model II)
	:	speed, square of speed, volume, square of volume, speed*volume, roughness*speed (model III) (Table 7.4)
Impact Area	:	speed, volume, roughness coefficient (model I)
	:	square of speed, speed*volume, roughness coefficient (model II) (Table 7.5)
Separation Area	:	roughness coefficient (model I) (Table 7.6)
Radial Impact Force:		speed, volume, roughness coefficient (model I)
	:	speed, square of speed, volume, roughness coefficient (model II) (Table 7.7)
Total Impact Force	:	speed, volume, roughness coefficient (model I)
	:	roughness coefficient, square of speed, square of volume, speed*volume (model II)
	:	square of speed, square of volume, speed*roughness coefficient, speed*volume (model III) (Table 7.8)
Separation force	:	roughness coefficient (model I) (Table 7.9)

7.2.2.1 Height or Lift Analysis

From previous evidence in this study, it appears that only lift, among the covariates measured, contributes substantially to an understanding of the process involved. It cannot be used as an explicit control variable, but acceptable lift is an industrial constraint.

7.2.2.4 Average Force Analysis

A linear model in Table 7.8 for average force (1) fits well but can be improved by either of two somewhat artificial models. There are two likely outliers in cases #41 and #43, but low serial correlations, and the remaining residuals plot are well against normal probabilities. Roughness seems to give little new insight to the average force (1) response.

On the other hand, using roughness in Table 7.9 sacrifices a great deal of model fit for average force (2), since it is thus known from Table 6.47 that there are significant differences between liners. The method of Table 6.47 is thus preferable.

Table 7.1 ANOVA: WEAR-RATE on QUADRATIC MODEL

SOURCE	SS	df	MS	F-stats seq	F-stats simul	p-value simul
speed	12.4278			61.31	11.63	0.003
volume	3.3021			45.02	20.88	0.000
rough	1.1659			31.02	22.74	0.000
vel*vel	0.1443			14.69	33.52	0.000
vol*vol	0.0584			3.13	6.55	0.019
rough*vel	0.2121			23.72	23.72	0.000
regression	17.3106	6	2.8851	-	322.93	0.000
residuals	0.1787	20	.008934	-	-	-
total	17.4893	26				

MODEL	I	II	III	Table 4.1
se(est)	0.1805	0.1364	0.0945	0.0804
MSE	0.0326	0.0186	0.0089	0.0065
F	171.35	183.75	322.93	153.08
df	3, 23	5, 21	6, 20	18,8
R-sq	0.9572	0.9777	0.9898	0.9970
R	0.9784	0.9888	0.9950	0.9985
R/s	0.4500	0.4456	0.1651	-
D-W	1.0833	1.0970	1.6680	-
ADR	0.0058	0.0007	0.0006	-
PMS	0.0384	0.0247	0.0125	-
max |e(i)|	-1.98	-2.36	2.03	-
case#	41	36	22	-
max D-i	.29	.32	.29	-
case#	30	36	35	-
% ellipse	16.51	10.66	6.59	-

y(wear) = -2.36832 + 0.0649130 vel - 0.0392860 vol
+ 0.432325 rough + error(I)

y(wear) = 6.27336 - 0.147523 vel - 0.0846389 vol + 0.432325 rough + 0.00136469 velsq + 0.000867284 volsq + error(II)

y(wear) = 7.94084 - 0.168974 vel - 0.0846389 vol - 1.04102 rough + 0.00136469 velsq + 0.000867284 volsq + 0.0189538 rough*vel + error(III)

Table 7.2 ANOVA: WEAR-RATE on QUADRATIC MODEL (n = 31)

SOURCE	SS	df	MS	F-stats seq	F-stats simul	p-value simul
velocity	14.5794			73.96	29.48	0.001
volume	3.7268			52.56	32.04	0.000
rough	0.9563			25.10	15.84	0.000
vel*vel	0.4722			22.00	45.02	0.000
vol*vol	0.1016			5.57	10.56	0.003
rough*vel	0.2535			29.92	29.92	0.000
regression	20.0899	6	3.3481	-	395.02	0.000
residuals	0.2033	24	.008472	-	-	-
total	20.2932	30				

MODEL	I	II	III	Table 4.3
se(est)	0.1954	0.1352	0.0921	0.1278
MSE	0.0382	0.0183	0.0085	0.0163
F	168.20	217.06	395.04	203.07
df	3, 27	5, 25	6, 24	6, 24
R-sq	0.9492	0.9775	0.9898	0.9807
R	0.9743	0.9887	0.9950	0.9903
R/s	0.2525	0.3690	0.1497	0.2152
D-W	1.4151	1.2290	1.6285	1.5159
ADR	0.0059	0.0007	0.0010	0.0003
PMS	0.0438	0.0235	0.0116	0.0215
max |e(i)|	1.95	-2.36	2.03	-2.85
case#	27	36	22	36
max D-i	.20	.32	.29	.36
case#	27	36	35	36
% ellipse	10.55	10.66	6.59	10.10

y(wear) = -2.316596 + 0.064651 vel - 0.039076 vol
+ 0.388027 rough + error(I)

y(wear) = 7.248181 - 0.168828 vel - 0.0944556 vol
+ 0.402437 rough + 0.00149812 velsq
+ 0.00106753 volsq + error(II)

y(wear) = 8.63031 - 0.183737 vel - 0.0917953 vol
- 1.11121 rough + 0.00145356 velsq
+ 0.00100419 volsq + 0.0197550 rough*vel
+ error(III)

y(wear) = 7.89233 + lnr(i) - 0.168423 vel - 0.0943108 vol
+ 0.0014957 velsq + 0.00106408 volsq + error(IV)

where lnr(3) = 0 lnr(4) = -0.451489 lnr(5) = -0.168600

Table 7.3 ANOVA: WEAR-RATE on ALL VARIABLES

SOURCE	SS	df	MS	F-stat	p-value
regression	17.3106	6	2.8851	395.04	0.000
ave f(2) changes	0.0587	1	0.0587	9.31	0.024
residuals	0.1138	19	0.0060	-	-
total	17.4893	26			

MODEL	Table 7.1	Model II	Table 4.4
se(est)	0.0945	0.0774	0.1278
MSE	0.0089	0.0060	0.0163
F	322.93	414.36	193.01
df	6, 20	7, 19	6, 20
R-sq	0.9898	0.9935	0.9830
R	0.9950	0.9967	0.9915
R/s	0.1651	-0.1774	0.3187
D-W	1.6880	2.2281	1.2814
ADR	0.0006	0.0000	-0.0008
PMS	0.1249	0.0088	0.0215
max |e(i)|	-1.98	1.77	-2.45
case#	41	22	36
max D-i	.29	.26	.37
case#	30	36	36
% ellipse	16.51	3.95	11.09

y(wear) = 8.81575 - 0.133005 vel - 0.0521232 lift
+ 0.251867 ave force(2) - 1.08906 rough
+ 0.00111487 velsq - 0.000392977 vel*vol
+ 0.0177118 rough*vel + error (II)

y(wear) = 7.72748 - 0.165647 vel - 0.0780521 vol
+ 0.311733 ave force(2) - 1.14654 rough
+ 0.00134048 velsq + 0.000753899 volsq
+ 0.0192233 rough*vel + error

Table 7.4 ANOVA: LIFT on QUADRATIC MODEL

SOURCE	SS	df	MS	F-stats seq	p-value simul	simul
velocity	216.8082			56.55	6.15	0.022
volume	52.6273			29.16	77.09	0.000
rough	11.5700			8.41	31.25	0.000
vel*vel					9.00	0.007
vol*vol					40.83	0.000
vel*vol	24.3180	3	8.1060	21.90	19.80	0.000
rough => rough*vel	0.4144				34.34	0.000
regression	305.7378	6	50.9567	-	145.81	0.000
residuals	6.9896	20	.3495	-	-	-
total	312.7273	26				

MODEL	I	III	Table 4.6
se(est)	1.1744	0.5912	0.5832
MSE	1.3792	0.3495	0.3401
F	67.92	145.81	128.64
df	3, 23	6, 20	7, 19
R-sq	0.8986	0.9777	0.9793
R	0.9479	0.9888	0.9896
R/s	-0.1379	-0.4062	-0.5679
D-W	2.0909	2.6908	3.1059
ADR	-0.0391	-0.0017	-0.0001
PMS	1.6355	0.4818	0.4840
max |e(i)|	-2.22	2.08	2.48
case#	28	34	34
max D-i	.34	.34	.38
case#	28	34	34
% ellipse	20.05	9.39	

y(lift) = 22.622079 - 0.2271128 vel - 0.156836 vol
- 1.462987 rough + error(I)

y(lift) = 27.495286 + 0.553755 vel + 1.288388 vol
- 1.462987 rough - 0.00441765 velsq
- 0.0135561 volsq - 0.00543735 vel*vol
+ error(II)

y(lift) = 25.839527 + 0.575240 vel + 1.288388 vol
- 0.00441765 velsq - 0.0135561 volsq
- 0.00543735 vel*vol - 0.0189837 rough*vel
+ error(III)

Table 7.5 ANOVA: AREA of WEAR (1) on QUADRATIC MODEL

SOURCE	SS	df	MS	F-stats seq	F-stats simul	p-value simul
velocity	269290.0442			50.41	205.35	0.000
volume	78904.0791			34.57	60.22	0.000
rough	24586.7807			18.75	18.75	0.000
residuals	30173.3666	23	1311.89	-	-	-
vel*vel	271881.8590			51.87	305.90	0.000
vol*vol	80503.4126			38.21	71.23	0.000
rough*vel	24586.7807			21.81	21.81	0.000
residuals	25984.2331	23	1129.67			
total	402956.2855	26				

MODEL	I	II	Table 4.8
se(est)	36.2200	33.6106	33.7062
MSE	1311.8855	1129.6740	1136.1079
F	94.71	111.2375	83.16
df	3, 23	3, 23	7,19
R-sq	0.9251	0.9355	0.9380
R	0.9618	0.9672	0.9685
R/s	-0.1789	-0.2618	-0.3413
D-W	2.3391	2.5010	2.6276
ADR	0.6551	0.4349	0.4132
PMS	1479.4197	1276.3542	1365.6
max |e(i)|	-2.66	-2.62	-2.45
case#	41	41	41
max D-i	.16	.20	.22
case#	43	28	41
% ellipse	7.64	10.27	

y(area1) = -139.689 + 9.555045 vel - 6.072629 vol
+ 67.4385 rough + error(I)

y(area1) = 146.412 + 0.0742532 velsq - 0.0781927 vel*vol
+ 67.4835 rough + error(II)

Table 7.6 ANOVA: AREA of WEAR (2) on QUADRATIC MODEL

SOURCE	SS	df	MS	F-stats seq	F-stats simul	p-value simul
rough	54523.4099			53.29	53.29	0.000
residuals	25579.0534	25	1023.1660	-	-	-
total	80102.5606	26				

MODEL	I	Table 4.10
se(est)	31.9870	32.6864
MSE	1023.1550	1068.4007
F	53.29	49.97
df	1, 25	1, 25
R-sq	0.6807	0.6666
R	0.8250	0.8164
R/s	-0.5405	-0.4357
D-W	2.6917	2.5904
ADR	0.0098	0.0000
PMS	1096.9395	1152.2
max |e(i)|	2.51	2.25
case#	45	45
max D-i	.20	.19
case#	35	35
% ellipse	33.86	

y(area2) = 281.5593 + 100.429627 rough + error(I)

Table 7.7 ANOVA: RADIAL FORCE on QUADRATIC MODEL

SOURCE	SS	df	MS	F-stats seq	F-stats simul	p-value simul
velocity	0.23902			40.97	3.68	0.068
volume	0.07719			26.93	51.41	0.000
rough	0.02608			14.06	17.39	0.000
vel*vel	0.00953			6.31	6.31	0.020
residuals	0.04260	22	0.001503	-	-	-
total	0.38489	26				

MODEL	I	II	Table 4.12
se(est)	0.04304	0.03877	0.0390
MSE	0.001852	0.001503	0.001521
F	61.61	58.82	57.77
df	3, 23	4, 22	4, 22
R-sq	0.8893	0.9141	0.9131
R	0.9430	0.9561	0.9555
R/s	-0.1895	-0.4228	-0.3930
D-W	2.3355	2.7756	2.7383
ADR	0.0008	0.0002	0.0002
PMS	0.002052	0.001740	0.001777
max |e(i)|	2.52	2.46	2.33
case#	38	38	38
max D-i	.18	.17	.16
case#	38	38	38
% ellipse	9.42	4.85	

y(rad) = -0.200144 + 0.0090032 vel - 0.0060070 vol
+ 0.0694664 rough + error(I)

y(rad) = 1.24740 - 0.0288758 vel - 0.0060070 vol
+ 0.0694664 rough + 0.000243334 velsq
+ error(II)

Table 7.8 ANOVA: AVERAGE FORCE (1) on QUADRATIC MODEL

SOURCE	SS	df	MS	F-stats seq	p-value simul	simul
velocity	0.31133			35.87	181.17	0.000
volume	0.10734			23.52	62.41	0.000
rough	0.06979			40.58	40.58	0.000
residuals	0.03954	23	0.001719	-	-	-
vel*vel	0.31416			36.72	83.17	0.000
vel*vol	0.11034			25.58	9.30	0.006
rough	0.06979			47.61	50.27	0.000
vol*vol	0.00315			2.27	2.27	0.147
residuals	0.03056	22	0.001389	-	-	-
rough => rough*vel				50.69	50.69	0.000
residuals	0.03038	22	0.001381	-	-	-
total	0.52800	26				

MODEL	I	II	III	Table 4.14
se(est)	0.04146	0.03727	0.03717	0.0330
MSE	0.001719	0.001389	0.001381	0.001089
F	94.72	89.51	90.08	77.4693
df	3, 23	4, 22	4, 22	6, 20
R-sq	0.9251	0.9421	0.9425	0.9587
R	0.9618	0.9706	0.9708	0.9792
R/s	-0.0231	0.0478	0.0888	-0.2799
D-W	2.0396	1.9035	1.8196	2.4955
ADR	0.0011	0.0004	0.0005	0.0004
PMS	0.001960	0.001731	0.001693	0.001535
max |e(i)|	-2.58	-2.36	-2.39	2.34
case#	41	41	41	43
max D-i	.20	.30	.22	.38
case#	28	34	34	43
% ellipse	10.74	12.52	7.44	11.71

y(force1) = - 0.271898 + 0.010622 vel - 0.007082 vol
+ 0.113610 rough + error(I)

y(force1) = 0.018900 + 0.000095015 velsq
- 0.00017806 vel*vol + 0.113610 rough
+ 0.000130989 volsq + error(II)

y(force1) = 0.084556 + 0.000084605 velsq
- 0.000178734 vel*vol + 0.00145021 rough*vel
+ 0.000131978 volsq + error(III)

Table 7.9 ANOVA: AVERAGE FORCE (2) on QUADRATIC MODEL

SOURCE	SS	df	MS	F-stats seq	p-value simul	simul
rough	0.39788			15.89	15.89	0.0005
residuals	0.62585	25	1023.1660	-	-	-
total	1.02373	26				

MODEL	I	Table 4.16
se(est)	0.1582	0.07594
MSE	0.0250	0.0057669
F	15.89	76.77
df	1, 25	2, 24
R-sq	0.3887	0.8648
R	0.6234	0.9300
R/s	0.6368	-0.3339
D-W	0.6553	2.5299
ADR	0.0015	0.0000
PMS	0.0261	0.006487
max |e(i)|	1.92	2.28
case#	27	43
max D-i	.13	.22
case#	27	43
% ellipse	27.51	19.37

y(force2) = 0.059536 + 0.271298 rough + error(I)

CHAPTER VIII

SUMMARY AND RECOMMENDATIONS

8.1 INTERIM INDUSTRIAL FINDINGS

The five newest coal fired Eskom power stations once completed will use boilers serviced by 162 tube mills. Liner wear, liner replacement cost and the resulting unavailability of the mills for power generation results in huge expenditure. Consequently there is a scope for considerable cost-cutting if the industrial life of the liners can be extended at the current mill operating conditions.

The early findings regarding materials for the liners (as per Chapter III) induced Eskom Management to change the specification for liner material from manganese steel (sample D-4) to high chrome iron (sample B2 and G7(b)). Management of Eskom was also willing to explore the suitability of alternative liner profile to that originally specified (liner #1). Accordingly each of the set of five mills of Boiler 4 at Tutuka power station was completely lined with one of the five liner profiles used in the present laboratory study.

In each of the five mills three liners in indentical positions were chosen for continuous monitoring through their industrial life until their destruction.
The mills working conditions were:

- mill speed (77.6% of critical)
- ball charge (24% of mill volume)
- mill output (53000 kg/h)
- mill power (950 kW)

The liner material (high chrome iron of a hardness of 600 Brinell) was identical in the five mills. The only known difference between the mills was the liner lifter profile.

It was originaly expected that access to these mills to make the first reading of mass loss and profile change would be available in June 1989. However due to maintenance requirements at Boiler 4 this access became already available in January 1989.

The coal had the following properties on an average basis as measured over the test period :

* Hardgrove grindability index - 55.7
* Coal abrasive index (YGP) - 397
* Ash content - 25.6%
* Free silica content - 5.33%

The three liners in each mill were dismantled and the mass loss was recorded. Table 8.1 presents these interim results.

TABLE 8.1 Interim Results Tutuka Boiler 4

Liner Profile as per Table 5.1	Mill Working Hours	Initial Average Mass [Kg]	Total loss of Mass [Kg]	Loss of Volume per 1000 h of Mill Working Hours [mm^3]	Ranking
4	8868	118.05	3.72	55194	1
5	9500	119.61	4.60	63712	2
1	9684	90.03	5.03	68343	3
3	5870	103.48	3.81	85626	4
2	5371	98.94	4.61	112935	5

These results coincide substantially with those obtained during laboratory investigation of equivalent ceramic liners and the corresponding working conditions as evidenced in Table 8.2

TABLE 8.2 Ranking of Industrial and Laboratory Results

Liner Profile as per Table 5.1	Industrial Trials	Laboratory Trials	
4	1	1	best
5	2	2	↓
3	4	3	
1	3	4	
2	5	5	worst

It was noted that there was an interchange in the wear ranks of liner #1 and #3. This interchange could be due to differences between laboratory and industrial wear, but it is possible that temporal aspects may be operative here. Further research may discover an appropriate explanation.

8.2 CONCLUSIONS

After evaluating the results of the tests both statistically and in the light of the classical grinding theory, the following conclusions have emerged:

a. After a critical assessment of the current milling theory, the work of Rose and Sullivan can be seen to contain important mathematical discrepancies rendering it unsuitable as a basis for the interpretation of the present research.

b. The design and implementation of the experimental method of this study were found to have been appropriate and consistant. Statistical analysis has shown no evidence of any unreliability.

c. Laboratory tests involving high speed photography have shown that the principle of scaling the mill speed was valid.

This principle is further supported by evidence obtained during industrial tests, which show that the first wear measurements after approximately 8000 h of continuous mills operation are in reasonably good agreement with the results of the laboratory experiments.

d. The use of ceramics as liner material for laboratory experiments reduced the time needed for the wear tests, and yet appear to present the differences of wear between liners consistently, and in agreement with the initial industrial evidence.

e. Liner #4 showed performance and wear characteristics superior to the other liners tested. This finding suggests that, after some corroborative studies, liner #4 could replace the present liner #1 as the standard liner for industrial mills.

f. It was found that the 'Roughness Coefficient' (C_R) associated with each liner is a continuous variable suitable to serve in the characterisation of the liner profiles.

g. Some of the secondary variables (covariates) showed very good correlation with the wear rate. The height of lift was particularly good in this respect. (Refer to Figure F-1 to F-5 in Appendix F for an illustration of the height of lift for liner #1 to #5 as depicted on films when mill velocity was at 78% of critical and ball charge at 24% of mill volume). This correlation suggests that lift may be used as a surrogate variable for the wear rate. Use of this surrogate could simplify the design and implementation of further tests, by allowing the research to focus on achieving some optimal configuration of balls in a working mill.

8.3 FURTHER RESEARCH

8.3.1 Improvements To Methodology

a. Improve, if possible the uniformity of the ceramic materials used in the tests. It may be possible that differences in the resilience of the different materials may partially distort the true relations. Otherwise employ suitable experiments that compensate for variability in the materials.

b. Experimental trials should be performed in a random order, so that the standard statistical methods may be used with more confidence. If complete randomization is impossible, then restricted randomization schemes can be used.

c. The experiments should be performed with repeated observations. Replication would provide a higher degree of freedom, so that a study of a three-way interaction could be attempted.

d. In this study an apparently good continuous variable was found in the form of the 'Roughness Coefficient' (C_R). This opens the road towards the study of various liner profiles, characterized by their roughness coefficients.

e. An alternative, independent continuous variable to C_R can be sought to describe the profile of the liners. If such a continuous variable can be found, then it can be incorporated into the future statistical analysis as an additional variable.

8.3.2 Temporal Patterns

a. A study should be initiated into the temporal aspects of the wearing process. This study should aim at establishing the wear rate's time dependence, so that the deterioration of performance due to wear can be understood.

CHAPTER IX

R E F E R E N C E

1. J F Archard — "Contact and Rubbing of Flat Surfaces" Journal Applied Physics 24, 1953.

2. F P Bowden and D Tabor — "The Friction and Lubrication of Solids" Clarendon Press, Oxford, 1964.

3. J A Greenwood and D Tabor — "The Properties of Model Friction Junctions". Proceedings of the Conference on Lubrication and Wear. London: The Institution of Mechanical Engineers 1958.

4. E Rabinowicz — "Friction and Wear of Materials". New York: J Wiley and Sons, Inc. 1958.

5. N P Suh — "The Delamination Theory of Wear". Wear 25, pp. 111-124, 1973.

6. S Janamir, N P Suh and E P Abrahamson — "Mircroscopic Observations of Wear Sheet Formation by Delamination", Wear 28, pp. 235-249, 1974.

7. J J Pamies-Teixeira, N Saka N P Suh — "Wear of Copper Based Solid Solutions", Wear 44, pp. 65-75, 1977.

8. Y Tsuya — "The Behaviour of the Layer Damaged by Friction". Japan Society Precision Engineering 2, 1967.

9. J G A Bitter — "A Study of Erosion Phenomena". Part II, Wear, Vol 6.1963. pp. 169-190.

10. J G A Bitter — "A Study of Erosion Phenomena". Part I, Wear, Vol 6. 1963. pp. 5-21.

11. H E Rose and D E Evans — "The Dynamics of the Ball Mill".Part II, Proceedings of the Institution of Mechanical Engineers 1956, Volume 1970, Number 23, pp. 783-813.

12. J M Bereza — "Wear and Impact Resistant White Cast Irons". Proceeding of The Institute of British Foundrymen National Conference in Edinburgh 1981, FWP Journal, pp. 33-48, 1981.

13. F Maratray — "L'amelioration et la Recherche de Nouveaux Materiaux Resistant a l'abrasion", Materiaux et Technique, pp. 289-295, 1979.

14. T E Norman — "A Review of Materials for Grinding Mill Liners". Climax Molybdenum Company of Michigan, Research Report, pp. 207-218, 1974.

15. W Fairhurst and K Róhrig — "Abrasion Resistant High Chromium White Cast Irons, Foundry Trade Journal, pp. 685-698, 1974.

16. J K Fulcher, T H Kosel, N F Fiore — "The Effect of Carbide Volume Fraction on the Low Stress Abrasion Resistance of High Cr-Mo White Cast Irons", Wear 84, pp. 313-325, 1983.

17. H S Avery and H J Chapin — "Selection of Grinding Mill Liner Alloys for Optimum Wear Resistance", Society of Mining Engineers of AIME, Print Number pp. 69-86, 1969.

18. D N Rosenblatt — "Factors Involved in Liner Wear". Proceedings American Institute of Mining and Metallurgical Engineers, National Metal Congress in Chicago, 1977.

19. D L Albright and D J Dunn — "Wear behaviour of Iron and Steel Castings for the Mining Industry". Journal of Metals, pp. 23-27, 1983.

20. H E Rose and R M Sullivan — "A Treatise on the Internal Mechanics of Ball Tube and Rod Mills". Chemical Publishing Co. Inc, New York, pp. 86-87, pp. 196-197, 1975.

21. R E McIvor — "Effects of Mill Speed and Liner Configuration on Ball Mill Performance". Mining Engineering, pp. 617-622, 1983.

22. R Manz — "Experimental Investigation Into the Slip of the Charge of Grinding Medium in Ball Mills". Dechema - Monographien, Vol 69, pp. 721-749, 1972.

23. D W Fuerstenau and A Z M Abouzeid — "Scale Up of Lifters in Ball Mills". International Journal of Mineral Processing, 15, pp. 183-192, 1985.

24. L A Vermeulen — "Fluctuation inthe Slip of the Grinding Charge in Rotary Mills with Smooth Liners". Journal of Mineral Process, pp. 153-168, 1986.

25. D D Howat and L A Vermeulen — "The Design of Linings for Rotary Mills. A Major Factor in the Throughput and Consumption of Energy and Metal". Journal of South African Institute of Minerals and Metallurgy, Vol 86, pp. 251-259, 1986.

26. L A Vermeulen — "The Lifting Action of Lifter Bars in Rotary Mills". Journal of South African Institute of Mineral and Metallurgy. Vol 85, N2 February 1985, pp. 41-49.

27. K H Zum Gahr and D V Doane — "Optimising Fracture Toughness and Abrasion Resistance in White Cast Irons". American Society for Metals, Volume 11A, April 1980 pp. 613-620.

28. S F Scieszka — "A Technique to Study Abrasive Wear in Contacts with Particulate Materials". Wear 119, pp. 237-249, 1987.

29. F Borik — "Using Tests to Define the Influence of Metallurgical Variables on Abrasion" Metals Engineering, May 1972.

30. W Fairhurst — "The Use of Abrasion Resistance High Chromium Molybdenum Cast Irons in Minerals Processing" Mine and Quarry October and December 1976.

31. K H Zum Gahr and G T Eldis — "Abrasion Wear of White Cast Irons". Wear 64, pp. 175-194, 1980.

32. S V Prosad and T H Kosel — "A Study of Carbide Removal Mechanisms During Quartz Abrasion". Wear 95, pp. 87-102, 1984.

33. N F Fiore, J P Coyle S P Udvardy, T H Kosel and W A Konkel — "A Abrasive Wear - Microstructure Interactions in a Ni-Gr White Irons". Wear 62, pp. 387-404, 1980.

34. I R Sare — "Abrasion Testing and Fracture Toughness of White Cast Irons". CSIRO Tribophysics Tech, Rep. 77/ME, September 1977.

35. H Búckle — "Progress in Micro-indentation Hardness Testing". Metallurgical Reviews, Vol 4, No 13,1959

36. F Maratray and R Usseglio-Nanot — "Factors Affecting the Structure of Chromium and Chromium - Molybdenum White Irons". Publication of Climax Molybdenum S.A. 1970.

37. R W Durman — "Basic Metallurgical Concepts and the Mechanical Testing of Some Abrasion-Resistant Alloys". Publication of Bradley and Foster, Limited (UK), 1970.

38. H Czichos — "Tribology" Elsevier Scientific Publishing Company, New York 1978.

39. A S Sarkar — "Friction and Wear". Academic Press, New York, 1980.

40. B Pitman — "Power Generation", supplement to Engineering News, pp.35, 28 June 1985.

CHAPTER X

B I B L I O G R A P H Y

1. A D Sarkar — "Scanning Electron Microscopy Observations of Worn Surfaces of Metals in Tribological Contact with Loose Solid Particles". Wear 73, pp. 311-323, 1981.

2. A W Ruff — "Deformation Studies at Sliding Wear Tracks in Irons". Wear 40, pp. 59-74, 1976.

3. K H Zum Gahr — "How Microstructure Affects Abrasive Wear Resistance". Metals Progress, Vol 116, pp. 46-52, 1979.

4. D J Dunn — "Optimising Ball Mill Liners for Production and Economy". Mining Engineering pp. 32-34, Dec 1976.

5. R T Hukki — "The Principles of Communition : an Analytical Summary". Engineering and Mining Journal, pp. 106-110, May 1975.

6. G Nilson — "Rubber Lining Design for Grinding Mills Influence on Economy and Capacity", The Canadian Mining and Metallurgical Bulletin, pp. 59-64, November 1979.

7. L A Vermeulen, M H Ohlson de Finet and F Schakowski — "Physical Information from Inside of a Rotary Mill". Journal South African Institute Mineral and Metallurgy, Vol 84, No 8, pp. 247-3253, August 1984.

8. P Slegton — "La broyage a boulets a l'echelle pilote". Industrie Minerale Août - Sept 1980.

9. P A Korpi and G W Dopson — "Angular Spiral Lining Systems in Wet Grinding Grate Discharge Ball Mills". Mineral Engineering 43, pp. 57-60, 1982.

10. R Hogg and D W Fuerestenau — "Power relationship for Tumbling Mills" Society of Mining Engineers, Vol 252, December 1972.

11. P Bernutat — "Wear of Grinding Media and Liner Plates". Lement-Kalk-Gips, No 9, pp. 397-409 1964.

12. S G Malghan — "Methods to Reduce Steel Wear in Grinding Mills". Mining Engineering, pp. 684-690, June 1982.

13. D N Rosenblatt — "Factors Involved in Wear". SME-AIME, pp. 158, 1978.

14. L G Austin — "Ball Wear and Ball Size Distributions in Tumbling Ball Mills". Power Technology 41, pp. 279-286, 1985.

15. F C Bond — "Metal Wear in Crushing and Grinding" AICHER Annual Meeting, Huston, pp 53, 1963.

16. P I Nickelson — "Applied Designs of Rubber Mill Liners for Different Conditions and Maximum Efficiency". North West Queensland Branch Mill Operators Conference, Sept 1982.

17. A K Ganopadhyay and J J Moore — "Assessment of Wear Mechanisms in Grinding Media". Minerals and Metallurgical Processing, pp. 145-151, August 1985.

18. W H Zieman — "Forum on Ball Rod Mill Liners". Transactions, Volume LXII, pp. 273-290 April 1959.

19. J M Menacho and F Concha — "Phenonomenlogical Model of Ball Wear in a Tumbling Mill". XVth Institute Mineral Processing Congress, Cannes, 2-9 June 1985.

20. L G Austin R R Klimpel and P T Luckie — "Process Engineering in Size Reduction : Ball Milling". Society of Mineral Engineering, New York Chapter 16, 1984.

21. F W Bowdish — "Theoretical and Experimental Studies on Kinetics of Grinding in Ball Mill". Trans. AIME, Vol 217, pp. 194-202, 1960.

22. J S Grisi — "Selecting Balls and Liners for Grinding Mills". Chemical Engineering, pp. 127-129, Sept 1981.

23. I Iwasaki, S C Riemer and J N Orlich — "Effect of Percent SOLIDS and Mill Loading on Ball Wear in Laboratory Raconite Grinding. Mineral and Metallurgical Processing, pp. 185-192, August 1985.

24. T K Bentice — "Ball Wear in Cylindrical MILLS" Trans, AIME Vol 169, pp. 147-154, 1946.

25. E W Rozenkrantz and D M Skeen — "Internal Components of Grinding Mills". The South African Mechanical Engineer, pp. 88-96, March 1972.

26. J E Worsdale — "Grinding Techniques in the Portland Cement Industry". The South African Mechanical Engineer, pp. 107-113, Sept 1967.

27. A Joisel — "Mechanique interne du broyeur a boulets". Revue des Materiaux de Construction. Travaux Publiques, Eolit C, 1952.

28. E W Davis — "Fine Crushing IN BALL Mills". AIME Trans, Vol 61, pp. 250-297, 1919.

29. D J Dunn and R G Martin — "Measurement of Impact Forces IN BALL Mills". Trans Society Mineral Engineering AIME Vol 264, pp. 384-388, 1978.

30. J D Wray and K W Daykin — "The Design of Coal Preparation Plant To Combat Wear". Tribology in Mineral Extraction, International Conference in Nottingham, UK. 17-19 Sept 1984.

31. A M Gow, A B Campbell and W H Coghill — "A Laboratory Investigation of Ball Milling". Trans AIME, pp. 51-81, 1930.

32. A F Taggart — "Handbook of Mineral Dressing". New York, John Wiley and Sons, pp. 5-27 1954.

33. I V Kragelsky, M N Dobrychin and V S Kombalow — "Friction and Wear". Permagon Press, New York, pp. 1-44.

34. Hinsley and Fobelets — Work discussed by Rose and Sullivan in 20.

35. G Quesnel — "Les theories du Professeur Hukki". Extrait de la Revue de l'Industrie Minerale, Volume 42, Septembre 1960.

APPENDIX A

1. ACCURACY OF THE METHOD USED FOR DETERMINATION OF CHEMICAL COMPOSITION OF TESTED SAMPLES.

The primary standards were established in the laboratories of Bradley and Foster (U.K.) using the following methods.

All elements were checked chemically except for sulphur, phosphorus and copper whose concentration were obtained spectrographically.

Carbon - Strohlein method : combustion followed by absorption into potassium hydroxide and direct burette reading

Accuracy - ± 0.5%

Silicon - Gravimetric
Accuracy - ± 0.3%

Manganese - Colorimetric titration with sodium arsenite
Accuracy - ± .01% at .1, .1% at 14

Nickel - Gravimetric : Dimethyl glyoxime complex
Accuracy - ± 0.3%

Chromium - Colorimetric titration : Ferrous ammonium sulphate and potassium dichromate
Accuracy - ± 0.3%

Molybdenum - Gravimetric : 8 hydroxyl quinoline complex
Accuracy - ± 0.3%

2. CARBIDES

2.1 Carbide volume fraction

The carbide volume fraction of white cast chrome irons was

- the cut-out carbide images were weighed from optical micrographs. In this way the total area (which is proportional to volume) was determined.

- computerised image analysis

100 areas on each specimen were examined at a microscopic magnification of 500x. A statistical analysis of the volume of massive carbides used the values of 100 areas counted for each white cast chrome iron. The samples were etched using picric/hydrochloric acid solution.

Table A1 : Carbide Volume Fraction

SAMPLE	PHOTOM CUT OUTS	IMAGE ANALYSIS	MEAN
A1	-	-	-
B2	32%	30.05%	31.02%
C3	35%	34.04%	34.52%
D4	-	-	-
E5	26%	24.50%	25.25%
F6	-	-	-
G7(a)	27%	27.10%	27.05%
G7(b)	17%	15.66%	16.33%
H8	23%	23.40%	23.20%

2.2 Carbide size and distribution

Carbide size and distribution in white cast chrome iron samples were determined by quantitative image analysis. The samples were etched with a picric/hydrochloric solution, and the line intercept method (Figure A1) was adopted.

Figure A1 : Carbide size - principle of image analysis

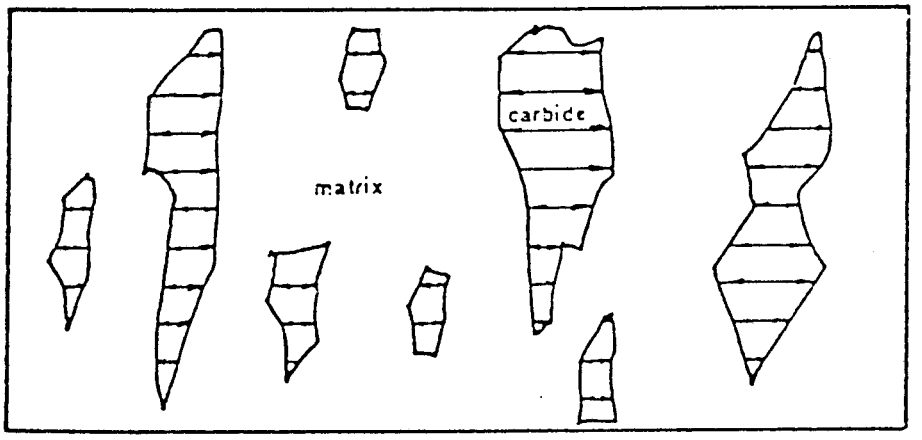

Figure A2 : Summary of results obtained for carbide size and distribution

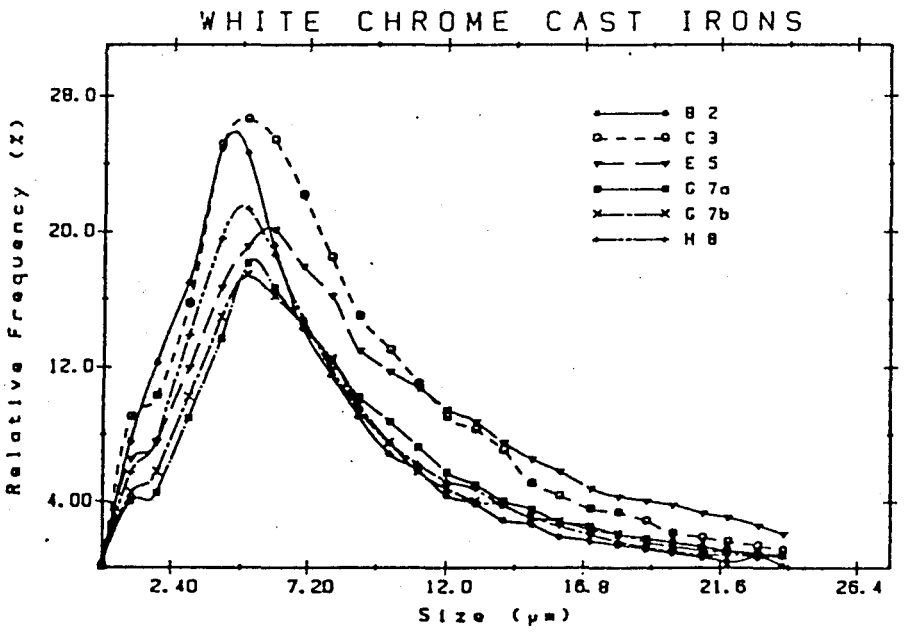

2.3 Intercarbide spacing

Intercarbide spacing on white cast chrome iron samples was determined by quantitative image analysis. The samples were etched with a picric/hydrochloric acid solution. The line intercept method (Figure A3) was adopted.

Figure A3 : Intercarbide spacing - principle of image analysis

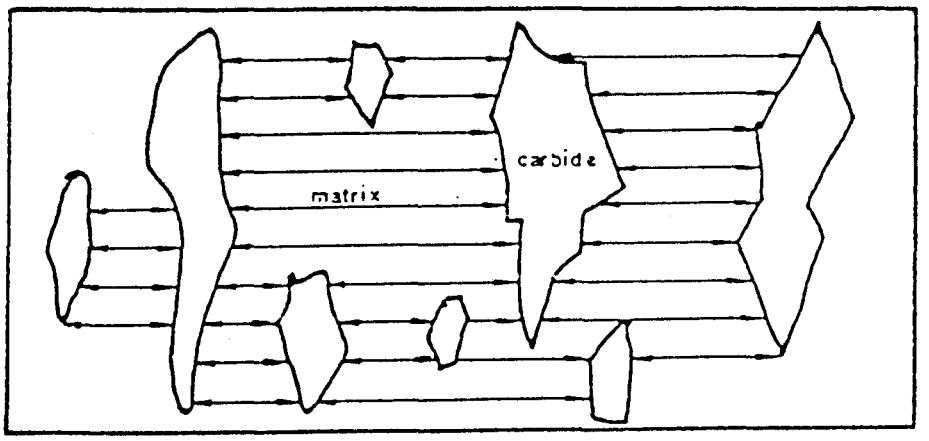

Figure A4 : Summary of results obtained for intercarbide spacing

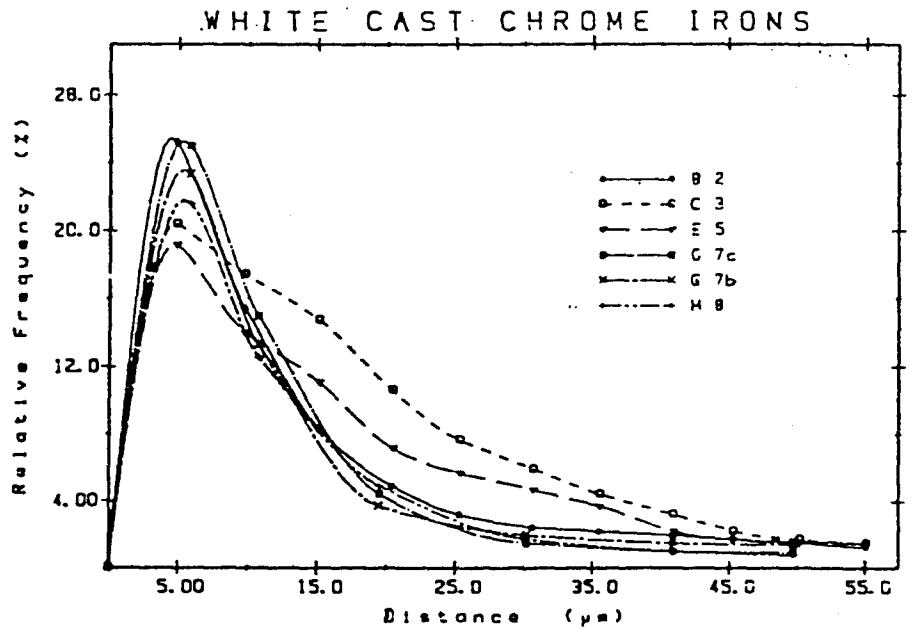

3. INDUSTRIAL TRIALS

3.1 Location of liners in the mill

Figure A5 : Position of Liners

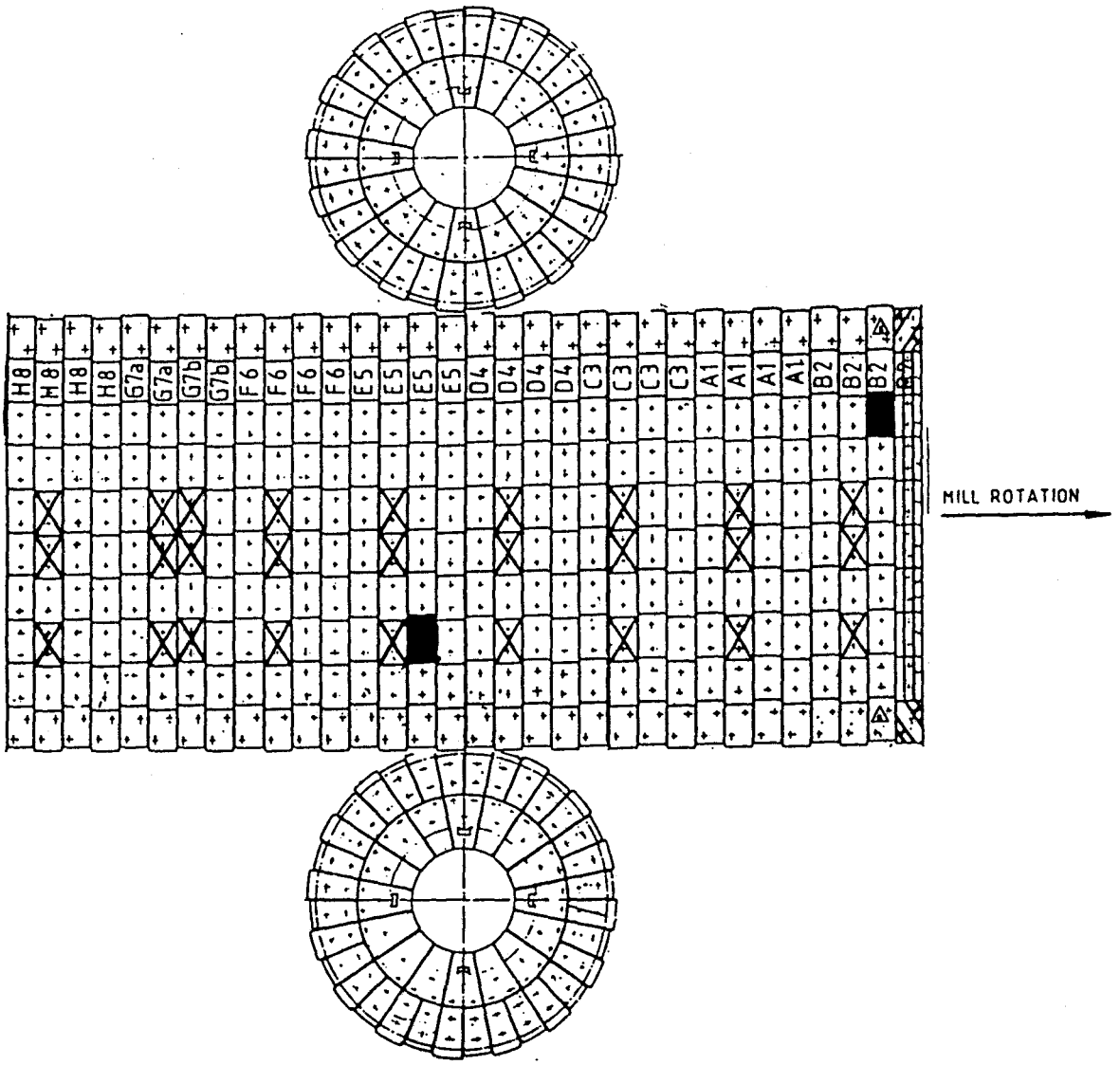

The positioning of the test liners within the mill was determined to ensure that the measurement of the resulting wear was representative of actual operating conditions.

The three shell liners were therefore positioned in the third row back from the direction of mill rotation, in each set of four rows.

3.2 Liner profile measurement

Figure A6 : Liner profiles recorded after 7500 hours of mill operation

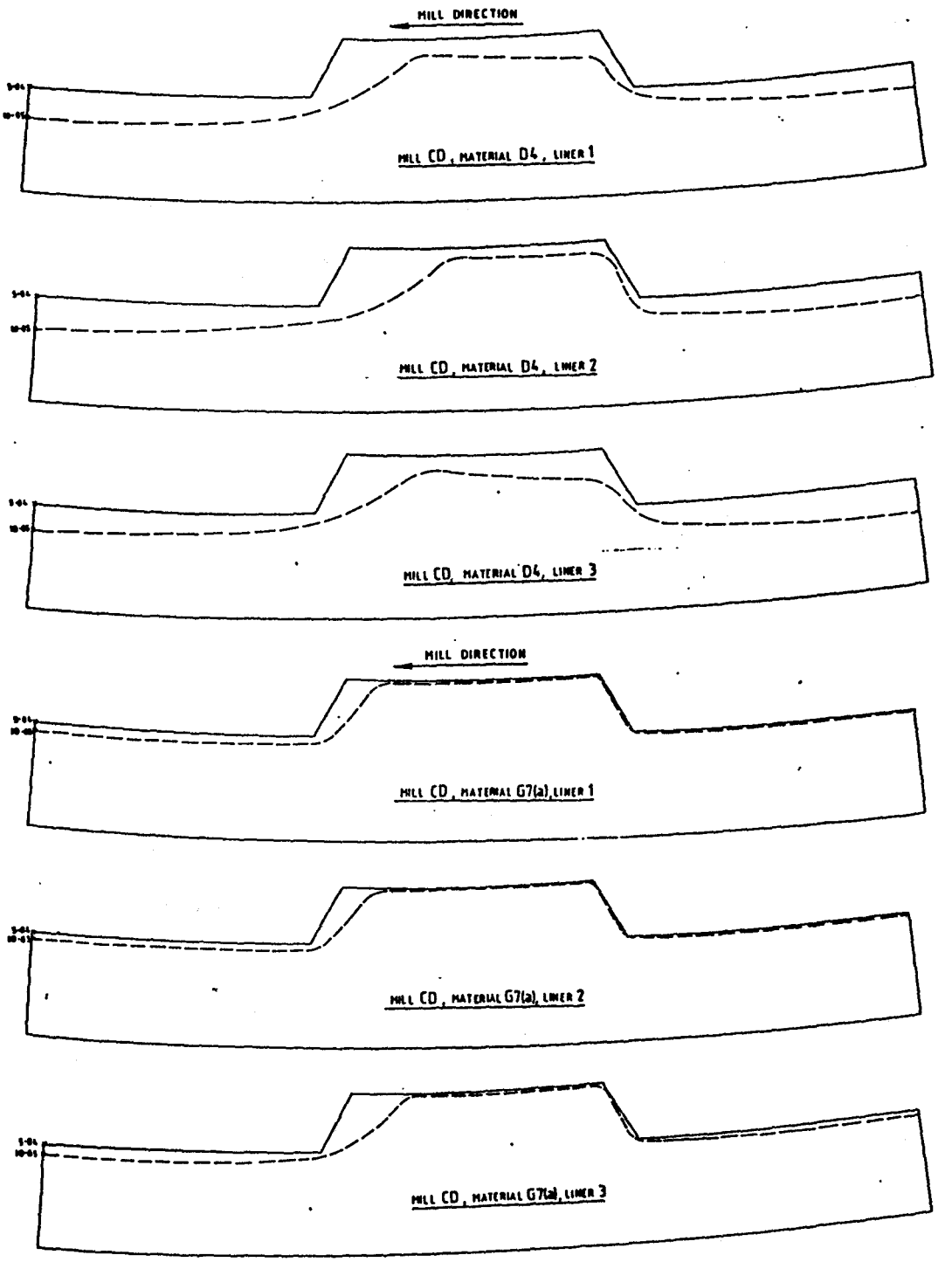

Figure A9 : View of carbide/matrix disjunction. Centre of field of view corresponds to approximately 10 micron below the worn surface of the liner (taper section 11°
Magnification x 1200

Figure A10 : General view of microstructure 600 microns below the worn surface of the liner
Magnification x 1200

Figure A11 : View of intersection between cut and polished surfaces at 90°
Magnification x 526

4.1 Description of Photomicrographs

Figure A8 :

This photomicrograph shows a particle, identified via an Energy Dispersive X-Ray Spectroscopy Unit as a rounded quartz particle, presumably embedded by impacting balls in the liner surface. The size of the quartz particle may be measured as 25 microns.

Figure A9 :

This view of a taper section (11°) shows carbide/matrix disjunction, and is 50 microns from the edge of the taper section and the worn surface of the liner. It is approximately 10 microns perpendicularly below the worn surface of the liner.

Figure A10 :

A view of general microstructure 600 microns below the worn liner surface. No cracking of the carbide particles is apparent, and no disjunction between the carbides and the martensitic matrix appears to have occurred as a result of abrasive cutting, grinding and polishing operations during sample preparation.

Figure A11 :

This photomicrograph shows that no damage was caused to carbides and martensitic matrix by abrasive cutting, grinding and polishing operations during sample preparation.

Figure A12 : Experimental machine for ball on liner impact test

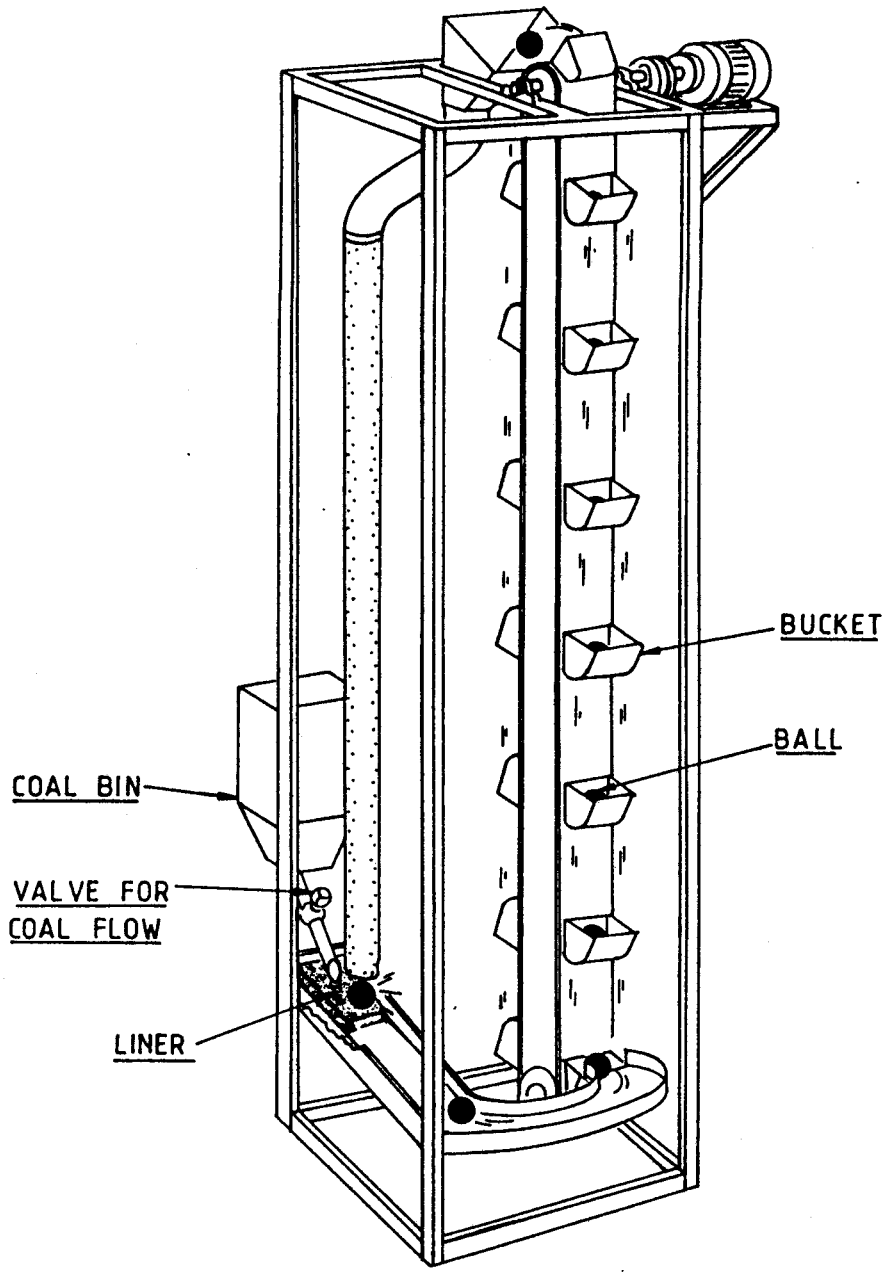

BALL DROPPING MACHINE

BALL FREE FALL = 3.8m
BALL MATERIAL = FORGED STEEL OF SF55 TYPE
LINER MATERIAL = WHITE CAST CHROME IRON IN MARTENSITIC CONDITION
NO OF IMPACTS = 10000
COAL TYPE = ARNOT COAL (100% THROUGH 1000 MICRONS)

5. DETAILED DESCRIPTION OF THE EXPERIMENTAL MACHINE FOR BALL ON LINER IMPACT TEST

The rubber belt conveyor, with steel buckets driven by a gear head motor and chain reduction drive mounted on top of the steel frame, lifted the balls onto the test liner cast. The balls were then heat treated to the same conditions as the liner, subjected to the actual industrial test (Sample E5). The conveyor travelled at 0.5m/sec. On the top of the frame a ball catching ramp was mounted to direct the balls to the vertical drop tube. The drop tube with a 0.1m diameter and a length of 3.5m guided the balls to the test liner. The lower end of the tube was 0.3m above the test liner, to allow space for rebounding balls. Under the opening, an inclined ramp caught and directed the balls into the conveyor pick-up point.

The test liner was tilted about 15 degrees (0.262rad), relative to the axis of falling balls, in order to simulate the position of the liner in an industrial mill, where balls first impact at the region of the ball charge toe. It also served to ensure that a rebounding ball was directed into the conveyor pick-up point. The impacted balls were of the same quality as those used in the industrial test. They had a nominal 0.05m diameter, and were commercial grinding balls made of forged steel of SF55 type and heat-treated by the supplier to a Brinell hardness of HB630.

Mounted on the frame was a coal hopper with a steel tube that carried coal to a side port located 0.1m from the lower end of the drop tube. The coal trickled onto the test liner in the region of ball impact. The coal eventually found its way to the lower part of the inclined ramp to be discharged through small holes into the collecting box.

Figure A13 : Side view of the experimental machine for ball on liner impact test

5.1 Chemical Composition

The chemical composition of two tested liners was determined by the same spectrometer, and in the same conditions, as used for determination of the chemical composition of the nine samples in preliminary experiments for selecting the most wear resistant alloy, for coal tube mill liners (as per paragraph 1.1.1 Chapter II)

C	P	S	Si	Cr	Mn	Mo	Ni	Cu
2.71%	0.032%	0.14%	0.62%	27.22%	0.86%	0.04%	0.20%	0.12%

5.2 Hardness

Macrohardness tests were performed on liners before the ball impact tests. The specimen surfaces were assessed using the Vickers test (30Kg load) machine. The average of 10 indentations performed was 672Hv. Therefore, the liner blocks subjected to a ball on liner impact test, were expected to provide the same modes of failure as industrial liners, depending on the conditions of the test.

6. MICROSTRUCTURE OF ALLOYS TESTED

Table A2 : Heat treatment details of manganese steel

SAMPLE	HEAT TREATMENT
D4	Austenitizing at 1030° C for 4h Water quenching.

Table A3 : Heat treatment details of chrome molybdenum steels

SAMPLE	HEAT TREATMENT
A1	Tempering at 240° C for 6h
F6	Heating at 920° C for 4h Cooling down in furnace to 830°C Forced air cooling Tempering at 250°C for 6h

Table A4 : Heat treatment details of white cast chrome irons

SAMPLE	HEAT TREATMENT
B2	Unknown
C3	Austenitizing at 950°C for 4h Forced air cooling Tempering at 250°C for 6h
E5	Austenitizing at 1020°C for 4h Cooling down in furnace to 830°C Forced air cooling Tempering at 250°C for 6h
G7(a)	Tempering at 220°C for 10h
G7(b)	Austenitizing at 1020°C for 4 h Still air cooling Tempering at 220°C for 10h
H8	Austenitizing at 1000°C for 5h Forced air cooling Tempering at 240°C for 6 h

6. MICROSTRUCTURE OF ALLOYS TESTED

Table A2 : Heat treatment details of manganese steel

SAMPLE	HEAT TREATMENT
D4	Austenitizing at 1030° C for 4h Water quenching.

Table A3 : Heat treatment details of chrome molybdenum steels

SAMPLE	HEAT TREATMENT
A1	Tempering at 240° C for 6h
F6	Heating at 920° C for 4h Cooling down in furnace to 830°C Forced air cooling Tempering at 250°C for 6h

Table A4 : Heat treatment details of white cast chrome irons

SAMPLE	HEAT TREATMENT
B2	Unknown
C3	Austenitizing at 950°C for 4h Forced air cooling Tempering at 250°C for 6h
E5	Austenitizing at 1020°C for 4h Cooling down in furnace to 830°C Forced air cooling Tempering at 250°C for 6h
G7(a)	Tempering at 220°C for 10h
G7(b)	Austenitizing at 1020°C for 4 h Still air cooling Tempering at 220°C for 10h
H8	Austenitizing at 1000°C for 5h Forced air cooling Tempering at 240°C for 6 h

7. ABRASION TESTS

Table A5 : Impact abrasion test

SAMPLE	RECORDED MASS LOSS (g ie 10^{-3}kg)			AVERAGE (g ie 10^{-3}kg)
A1	0.988	0.846	0.999	0.951
B2	0.582	0.642	0.657	0.627
C3	0.849	0.782	0.864	0.832
D4	0.968	1.153	1.018	1.046
E5	0.809	0.795	0.737	0.781
F6	0.859	0.796	0.872	0.847
G7 (a)	0.731	0.679	0.635	0.682
G7 (b)	0.547	0.561	0.551	0.555
H8	0.856	0.828	0.888	0.856

Table A6 : Rubber wheel abrasion test

SAMPLE	RECORDED MASS LOSS (g ie 10^{-3}kg)					AVERAGE (g ie 10^{-3}kg)
A1	0.328	0.324	0.296	0.321	0.319	0.317
B2	0.100	0.133	0.120	0.111	0.118	0.116
C3	0.144	0.147	0.141	0.141	0.143	0.143
D4	0.698	0.715	0.703	0.698	0.702	0.703
E5	0.141	0.142	0.220	0.141	0.140	0.156
F6	0.644	0.582	0.563	0.624	0.615	0.606
G7(a)	0.142	0.138	0.140	0.139	0.137	0.139
G7(b)	0.122	0.101	0.096	0.098	0.101	0.104
H8	0.172	0.151	0.163	0.161	0.159	0.161

Table A7 : Industrial test

SAMPLE	AVERAGE MASS PRIOR TO INSTALLATION [kg]	AVERAGE MASS AFTER 7500H OF MILL OPERATION [kg]	AVERAGE MASS LOSS AFTER 7500H OF MILL OPERATION [kg]
A1	95.02	86.71	8.31
B2	91.37	85.67	5.70
C3	90.78	81.68	9.10
D4	92.77	75.39	17.38
E5	92.18	87.83	4.35
F6	94.20	81.48	12.72
G7(a)	89.88	87.46	2.42
G7(b)	91.65	87.90	3.75
H8	93.55	87.40	6.15

TABLE A8 : RUBBER WHEEL ABRASION TEST - SAMPLE A1

ASTM G-65-80 Procedure A

Material:	A 1				
Surface preparation:	Ground				
Wheel diameter:	225 mm				
Wheel width:	12,7 mm				
Wheel hardness:	A - 60				
Test No.	1	2	3	4	5
Test load: N	130	130	130	130	130
Wheel revolutions	6 000	6000	6000	6000	6 000
Sand flow g/min	300	300	300	300	300
Initial mass, g	185,874	185,546	180,134	179,838	161,112
Final mass, g	185,546	185,222	179,838	179,517	160,793
Mass loss, g	0,328	0,324	0,296	0,321	0,319
Average mass loss:	0,317				
Density, g/cc	7,70				
Volume loss, mm^3	41,91				

TABLE A9 : RUBBER WHEEL ABRASION TEST - SAMPLE B2

ASTM G-65-80 Procedure A

Material:	B 2				
Surface preparation:	Ground				
Wheel diameter:	225 mm				
Wheel width:	12,7 mm				
Wheel hardness:	A - 60				
Test No.	1	2	3	4	5
Test load: N	130	130	130	130	130
Wheel revolutions	6000	6 000	6 000	6000	6000
Sand flow g/min	300	300	300	300	300
Initial mass, g	176,060	175,960	171,694	171,574	160,239
Final mass, g	175,960	175,827	171,574	171,463	160,121
Mass loss, g	0,100	0,133	0,120	0,111	0,118
Average mass loss:	0,116				
Density, g/cc	7,60				
Volume loss, mm^3	15,50				

TABLE A10 : RUBBER WHEEL ABRASION TEST - SAMPLE C3

ASTM G-65-80 Procedure A

Material:	C 3				
Surface preparation:	Ground				
Wheel diameter:	225 mm				
Wheel width:	12,7 mm				
Wheel hardness:	A - 60				
Test No.	1	2	3	4	5
Test load: N	130	130	130	130	130
Wheel revolutions	6 000	6000	6000	6000	6 000
Sand flow g/min	300	300	300	300	300
Initial mass, g	135,351	135,207	121,890	121,759	142,441
Final mass, g	135,207	135,060	121,759	121,618	142,298
Mass loss, g	0,144	0,147	0,141	0,141	0,143
Average mass loss:	0,143				
Density, g/cc	7,40				
Volume loss, mm^3	19,66				

TABLE A11 : RUBBER WHEEL ABRASION TEST - SAMPLE D4

ASTM G-65-80 Procedure A

Material:	D 4				
Surface preparation:	Ground				
Wheel diameter:	225 mm				
Wheel width:	12,7 mm				
Wheel hardness:	A - 60				
Test No.	1	2	3	4	5
Test load: N	130	130	130	130	130
Wheel revolutions	6000	6 000	6 000	6000	6000
Sand flow g/min	300	300	300	300	300
Initial mass, g	152,250	151,498	172,669	171,985	182,112
Final mass, g	151,498	150,785	171,985	171,359	181,416
Mass loss, g	0,694	0,659	0,632	0,578	0,643
Average mass loss:	0,641				
Density, g/cc	7,70				
Volume loss, mm^3	91,60				

TABLE A12 : RUBBER WHEEL ABRASION TEST - SAMPLES E5

ASTM G-65-80 Procedure A

Material:	E 5				
Surface preparation:	Ground				
Wheel diameter:	225 mm				
Wheel width:	12,7 mm				
Wheel hardness:	A - 60				
Test No.	1	2	3	4	5
Test load: N	130	130	130	130	130
Wheel revolutions	6 000	6000	6000	6000	6 000
Sand flow g/min	300	300	300	300	300
Initial mass, g	160,127	159,986	172,207	171,987	164,123
Final mass, g	159,986	159,844	171,987	171,848	163,983
Mass loss, g	0,141	0,142	0,220	0,141	0,140
Average mass loss:	0,156				
Density, g/cc	7,60				
Volume loss, mm^3	20,90				

TABLE A13 : RUBBER WHEEL ABRASION TEST - SAMPLE F6

ASTM G-65-80 Procedure A

Material:	F 6				
Surface preparation:	Ground				
Wheel diameter:	225 mm				
Wheel width:	12,7 mm				
Wheel hardness:	A - 60				
Test No.	1	2	3	4	5
Test load: N	130	130	130	130	130
Wheel revolutions	6000	6 000	6 000	6000	6000
Sand flow g/min	300	300	300	300	300
Initial mass, g	184,788	184,114	187,779	188,403	179,114
Final mass, g	184,114	183,562	187,216	187,779	178,499
Mass loss, g	0,644	0,582	0,563	0,624	0,615
Average mass loss:	0,606				
Density, g/cc	7,60				
Volume loss, mm^3	80,96				

TABLE A14 : RUBBER WHEEL ABRASION TEST - SAMPLE G7a

ASTM G-65-80 Procedure A

Material:	G 7a				
Surface preparation:	Ground				
Wheel diameter:	225 mm				
Wheel width:	12,7 mm				
Wheel hardness:	A - 60				
Test No.	1	2	3	4	5
Test load: N	130	130	130	130	130
Wheel revolutions	6 000	6000	6000	6000	6 000
Sand flow g/min	300	300	300	300	300
Initial mass, g	165,889	189,007	188,869	175,226	175,087
Final mass, g	165,747	188,869	188,729	175,087	174, 50
Mass loss, g	0,142	0,138	0,140	0,139	0,137
Average mass loss:	0,139				
Density, g/cc	7,60				
Volume loss, mm^3	18,61				

TABLE A15 : RUBBER WHEEL ABRASION TEST - SAMPLE G7b

ASTM G-65-80 Procedure A

Material:	G 7b				
Surface preparation:	Ground				
Wheel diameter:	225 mm				
Wheel width:	12,7 mm				
Wheel hardness:	A - 60				
Test No.	1	2	3	4	5
Test load: N	130	130	130	130	130
Wheel revolutions	6000	6 000	6 000	6000	6 000
Sand flow g/min	300	300	300	300	300
Initial mass, g	179,847	179,725	164,737	164,641	169,881
Final mass, g	179,725	179,623	164,641	164,543	169,780
Mass loss, g	0,122	0,102	0,096	0,098	0,101
Average mass loss:	0,104				
Density, g/cc	7,60				
Volume loss, mm^3	13,64				

TABLE A16 : RUBBER WHEEL ABRASION TEST - SAMPLE H8

ASTM G-65-80 Procedure A

Material:	H 8				
Surface preparation:	Ground				
Wheel diameter:	225 mm				
Wheel width:	12,7 mm				
Wheel hardness:	A - 60				
Test No.	1	2	3	4	5
Test load: N	130	130	130	130	130
Wheel revolutions	6 000	6000	6000	6000	6 000
Sand flow g/min	300	300	300	300	300
Initial mass, g	192,161	191,989	185,834	185,671	182,224
Final mass, g	191,989	191,838	185,671	185,510	182,065
Mass loss, g	0,172	0,151	0,163	0,161	0,159
Average mass loss:	0,161				
Density, g/cc	7,50				
Volume loss, mm^3	21,81				

FIGURE B-1 : BALL SET-UP ON A LINER LIFTER-BAR IN A TUBE MILL.

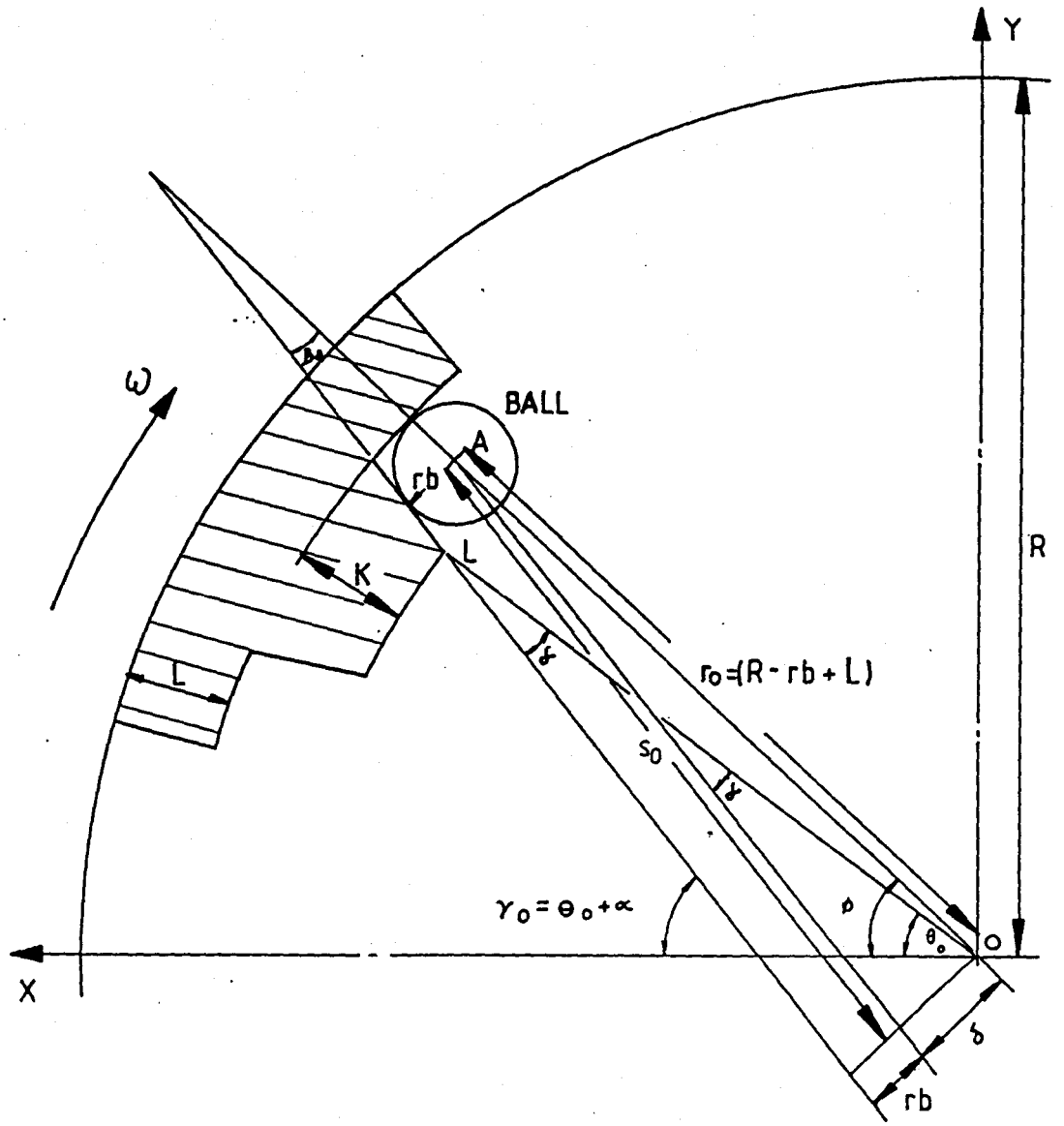

FIGURE B-2 : FORCES ACTING ON A BALL IN CONTACT WITH A LINER LIFTER-BAR.

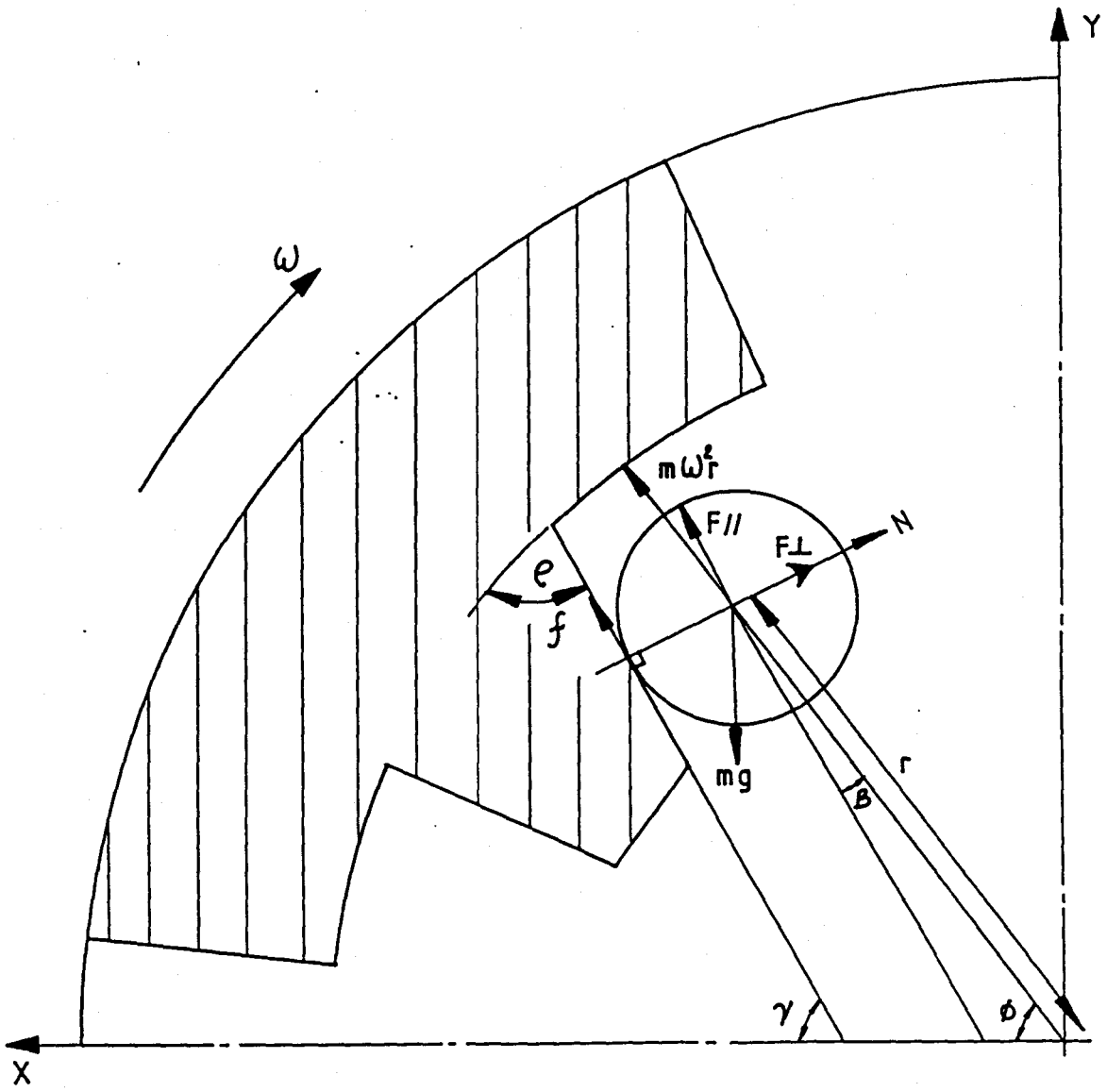

FIGURE B-3 : BALL AT THE POINT OF DEPARTURE INTO ITS PARABOLIC FLIGHT FROM THE LINER LIFTER-BAR.

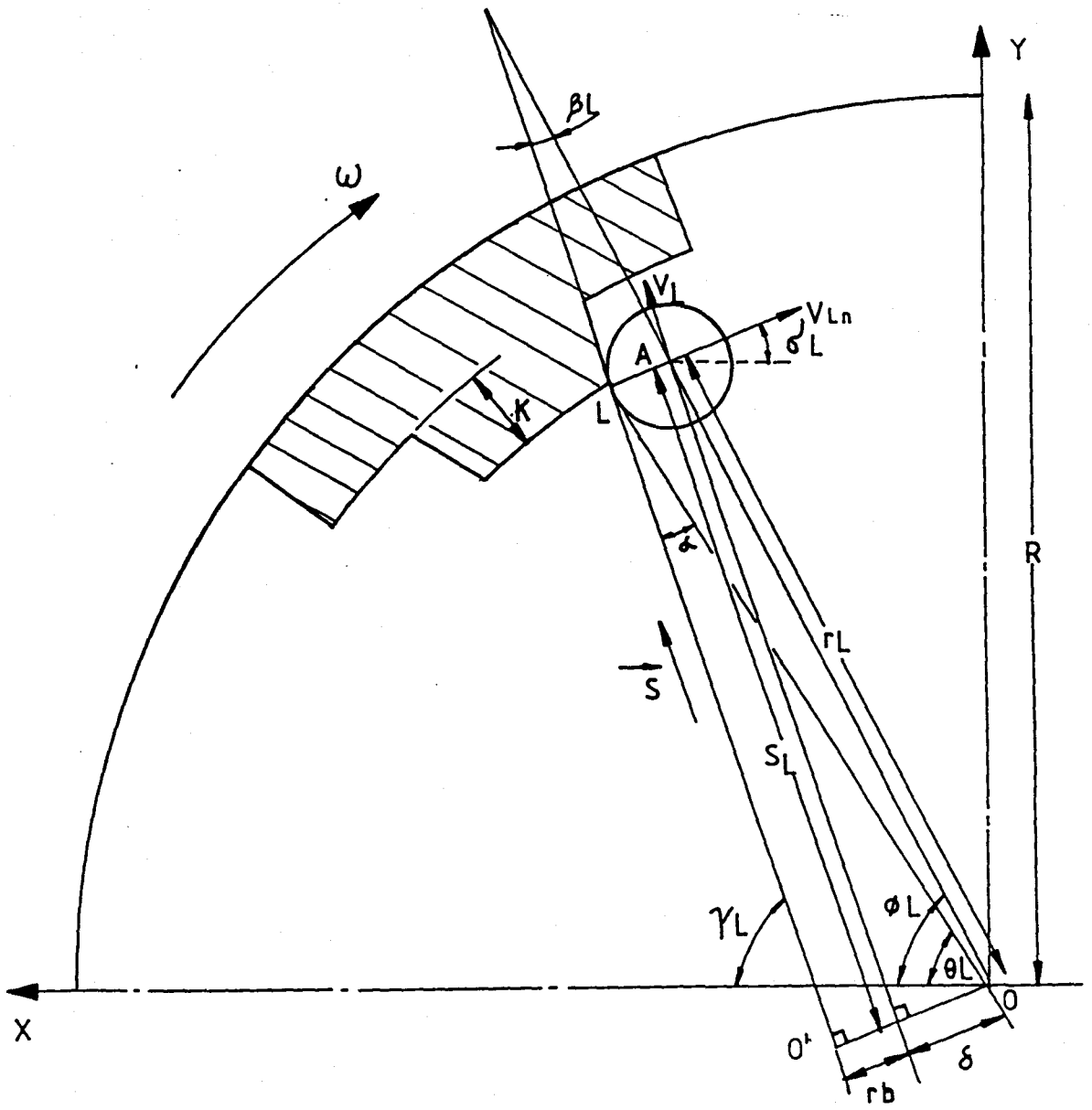

APPENDIX C

1. DETAILED DESCRIPTION OF THE EXPERIMENTAL MILL

Figure C-1 : Schematic representation of the mill rig.

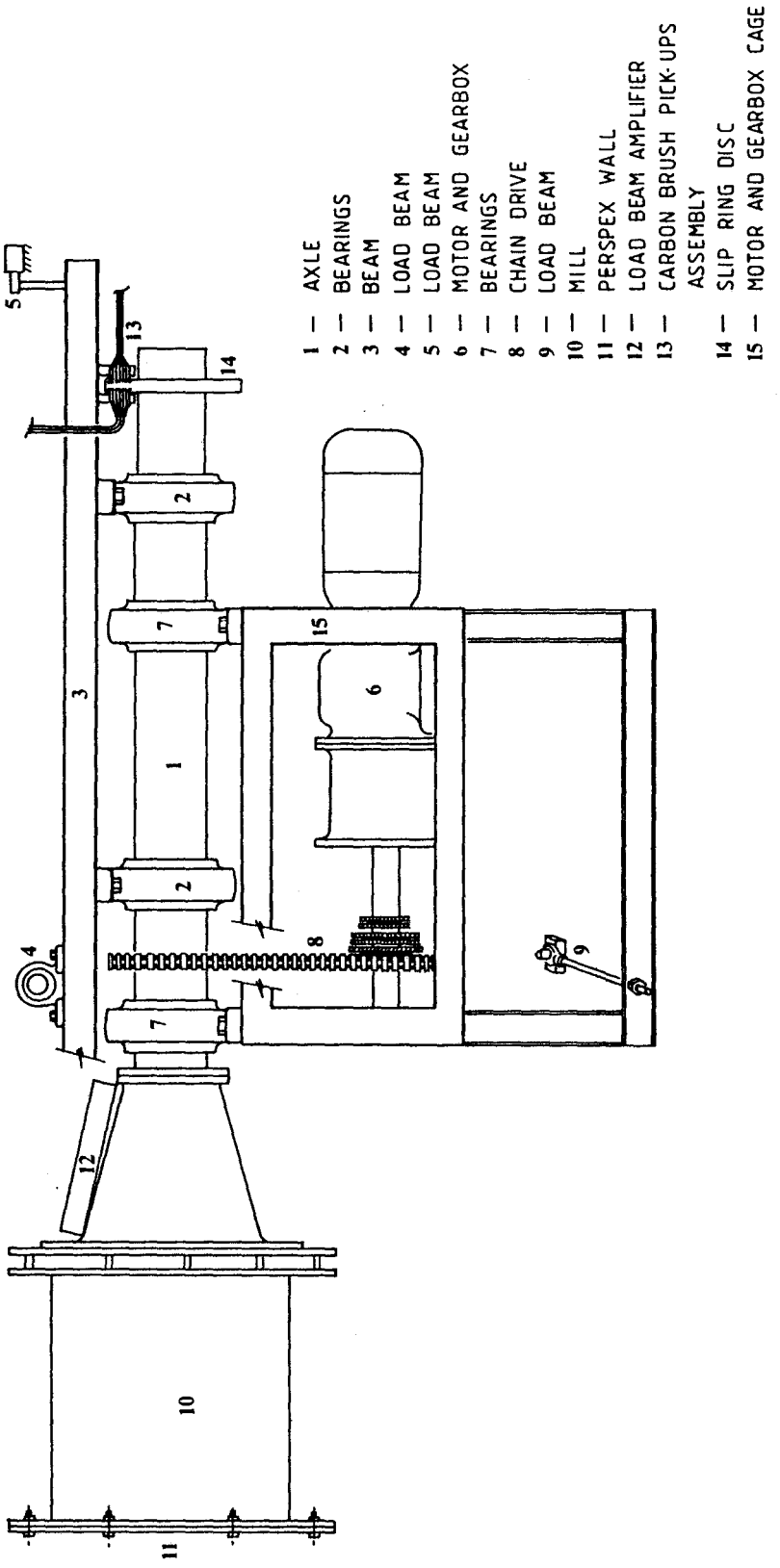

Figure C-2 : Schematic representation of load beams arrangement.

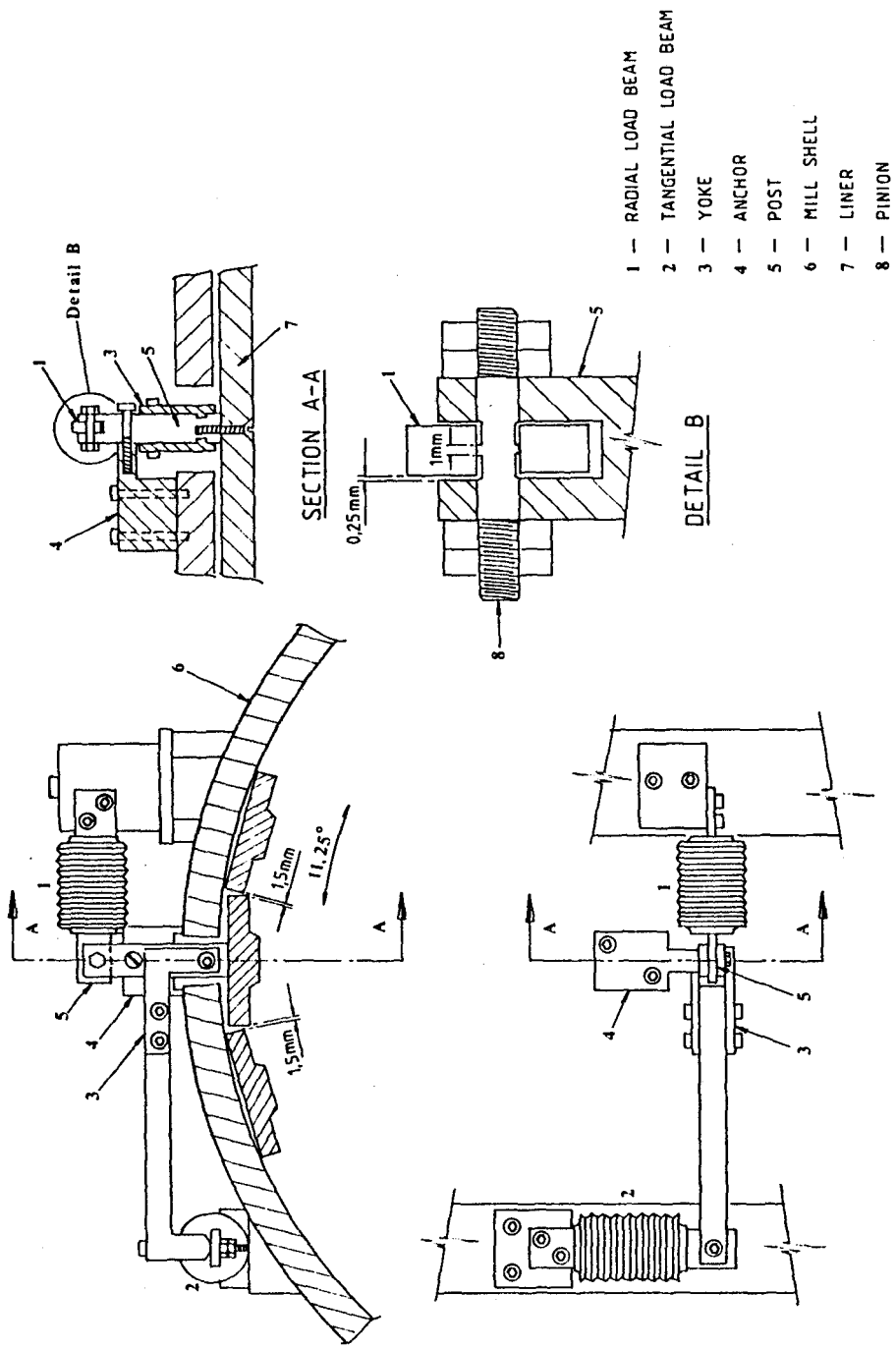

1.1. DESCRIPTION OF APPARATUS USED FOR MEASUREMENT OF FORCES EXERTED BY BALL CHARGE ON LINER

The liners in the mill were bolted to the shell using 10mm Allen screws. One of these liners was removed and 2,0mm was machine off its edges. Two holes were drilled in the mill shell at centers 75mm from each end of the mill. Two radial posts were attached rigidly to the liner using counter-sunk Allen screws such that the posts passed through the center of the holes in the mill shell. The other end of each post was bolted to the radial load beam which was attached to a platform on the mill shell shown. The position of these load beams could be adjusted to ensure that the surface of the liner was the same distance away from the center of the mill as the other liners. The connection between the post and the load beam was carefully machined to allow a minimum of friction between the components, as shown on Figure B2 detail B. Clearances of approximately 0,25mm were maintained between the contact surfaces, and the pinion was machined to ensure minimal contact area between itself and the load beams. This meant that the liner and post assembly was free to rotate around the point of connection with the load beams. This freedom was removed by the use of yokes connected to tangential load beams as shown. The pivot point between the yoke and the post was placed as close to the surface of the liner as possible, to ensure that the point of measurement of F_{tan} was as close to the point of application of F_{tan} i.e. the inner surface of the liner. The tangential load beam was attached to a platform so that its measurement axis coincided with a tangent through the pivot point. The position of the tangential load beams was adjusted to ensure uniform gaps between the liner and its neighbours. Finally fine adjustments were made after a new test liner was mounted in the position of one of the tangential load beams to ensure that no net forces were transmitted through the whole assembly (a problem inherent in any 4-point stabilisation of a rigid body).

Each pair of load beams was connected in parallel to load beam amplifiers mounted on the mill as shown in Figure B1.

The 0-2 volt output of the amplifiers was fed to the HP2240 interface via the sliprings on the mill axle. The linearity of the measurement, obtained by the computer of the forces exerted on the load beams was tested, by weighing seven accurately know masses in the range 0-6,854 kg. The correlation coefficient between the masses and the corresponding voltages was 0,9999, indicating exceptionally good linearity of the measurement.

Signals were picked up off the rings via carbon brushes which were mounted on a yoke which straddled the disc, as shown in Figure C-1. Contact resistance was less than 1,5 ohm on all rings. Signals were transmitted via individually shielded signal lines as voltages (nominally 0-10V) to the high impedence HP2240 measurement and control processor, rather than as milliamp signals, to avoid voltage variations caused by high frequency fluctuations in its contact resistance.

1.2 SPECIFICATION OF EQUIPMENT USED

1.2.1 Variable speed power transmission

Motor type :

Speed range : 300 - 3000 r.p.m.
Power at maximum speed : 3,0 kw.
Controlled by : SAFTRONICS DCI Series Thyrister Drive Type.

A225 Connected via 40 : 1 gearbox to drive shaft.
Four sprockets with 23, 25, 30 and 40 teeth respectively mounted on drive shaft.
Slave sprocket on mill axle has 38 teeth, providing the capabilities listed below :

No. of teeth on drive sprocket	23	25	30	40
Drive : slave ratio	0.605	0.658	0.789	1.053
Mill speed as maximum motor speed Nmax	45.4	49.4	59.2	79.0

1.2.2 Load beams for measurement of mill mass

Manufactured by : Bofors Elektronik (Sweden)
Type : Cylindrical shear beam K1S-3
Rated accuracy : 0,02% of rated output
Temperature effect : 0,001% of rated output per °C

1.2.3 Load beams used for measurement of balls feed rate circulating density and forces on liners

Manufactured by : BLH Electronics (USA)
Type : Alpha Load Beam
Measurement range : 0-15 kN (0-15 kg)
Rated Accuracy : 0,02% of rated output
Temperature effect : 0,0015% of rated output °C

1.2.4 Load Beam Amplifiers for all off-mill load beams

Manufactured by : Bofors Elektronik (Sweden)
Type : Bodil B-1-RF (Rack mounted)
Output : ± 10 volts
Temperature effect : ± 0,005% of rated output per °C

1.2.5 Load Beam Amplifiers for measuring forces on the liners

Manufactured by : BHL Electric (USA)
Type : 'Alpha', 2 S/N 1471
Output : -0 + 10 volts or 3,0 mV/V
Rating : 100 Newtons
Temperature effect : ± 0,005% of rated output per °C
± 0,008% of rated output per °F

1.2.6 Power Supplies

Types : KEPCO ATE-25-20M (0-20 Amps DC)
WEIR MINOREG PS325 (0-0,5 Amps DC)

Both capable of providing stable power supply voltages 0-25V; and with current or voltage limitation features.

1.2.7 Computer Equipment

All manufactured by Hewlett-Packard.
All communications via HPIB interface.

1.2.8 Computer

Type : HP9816 Series 200
Storage capacity 7
Programmed in HP Basic 2.1

1.2.9 Real-time Interface

Type : HP2240A Measurement and Control Processor
Facilities :

(i) Analog Input Card HP22900A
16 differential analog input channels
12 bit accuracy (± 0,05% accuracy)
50 kHz sampling rate on one channel

(ii) Analog output card HP22901B
4 analog output channels
12 bit accuracy (± 0,05% accuracy)

(iii) Digital Output card HP22904A

32 channels
response time approximately 15 ms

(iv) Counter-stepper card HP22905A
Used for :

(a) measuring frequency or period of input signals (3-1000 00 Hz)

(b) totalising no. of pulses in an input signal

(c) outputting pulses to a stepper motor.

(v) Low Level Analog Input Card HP22915A
Provides interfaces for amplifying and filtering 16 differential input voltages; gain varies from 1 to 500. Input impedence 10 megohms.

1.2.10 Plotter

Type : HP7470A Graphics Plotter

1.2.11 Printer

Type : Mannesmann Tally MT160
Number of columns per 8 inch line : 80-160 programmable
Print speed : 160 CPS & 10 CPI
Buffer size : 2000 characters (large buffer essential to ensure rapid transfer of data to printer in real time)
Communication via Rs232 Interface.

FIGURE C-3: LINER #1

MILL ROTATION →

LINER BEFORE TEST

MILL ROTATION →

HARD CERAMICS

MILL ROTATION →

SOFT CERAMICS

FIGURE C-4: LINER #2

MILL ROTATION

LINER BEFORE TEST

MILL ROTATION

HARD CERAMICS

MILL ROTATION

SOFT CERAMICS

FIGURE C-5: LINER #3

MILL ROTATION

LINER BEFORE TEST

MILL ROTATION

HARD CERAMICS

MILL ROTATION

SOFT CERAMICS

FIGURE C-6 LINER #4

MILL ROTATION →

LINER BEFORE TEST

MILL ROTATION →

HARD CERAMICS

MILL ROTATION →

SOFT CERAMICS

FIGURE C-7: LINER #5

MILL ROTATION

LINER BEFORE TEST

MILL ROTATION

HARD CERAMICS

MILL ROTATION

SOFT CERAMICS

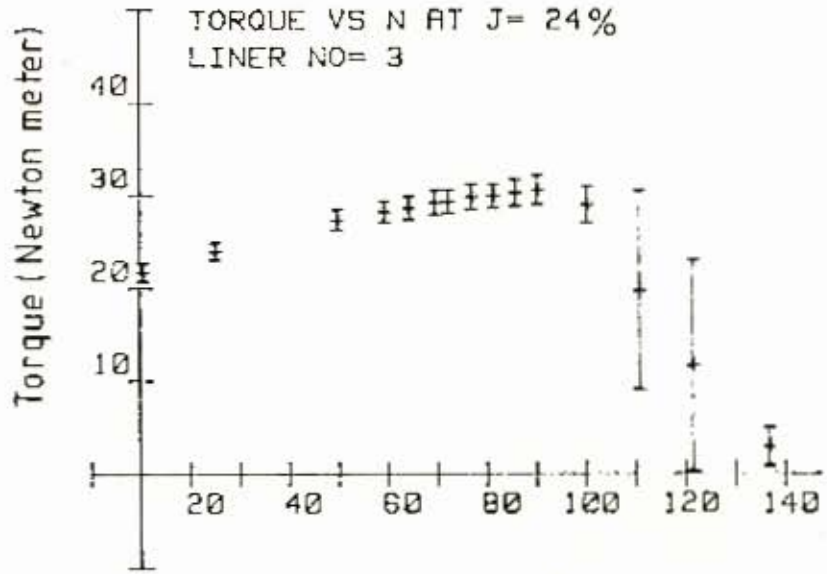

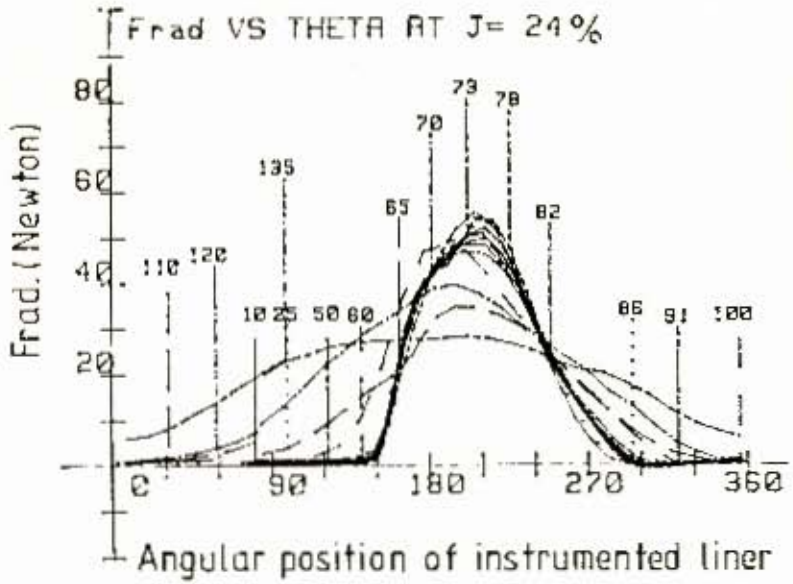

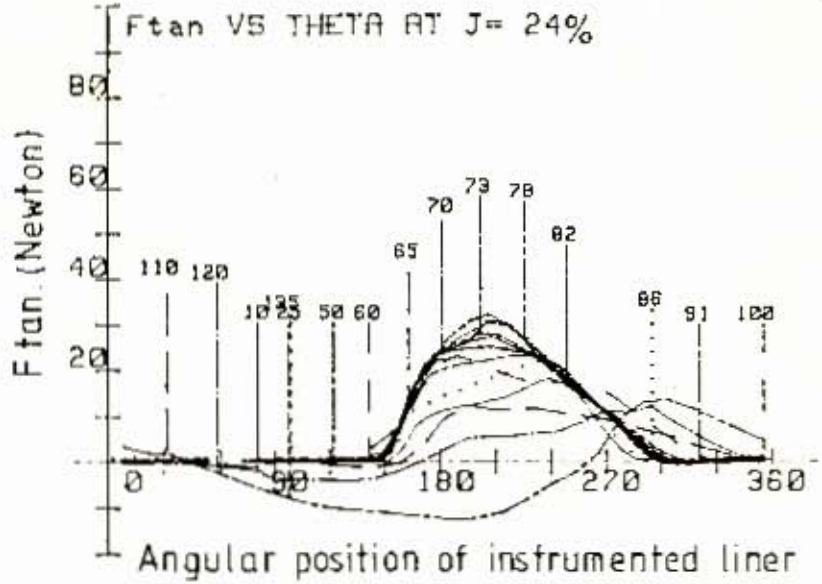

FIGURE C - 8 : GRAPHICAL OUTPUT OF DATA MEASURED AT J=24%, Nm=10% to 135% FOR/LINER No. 3

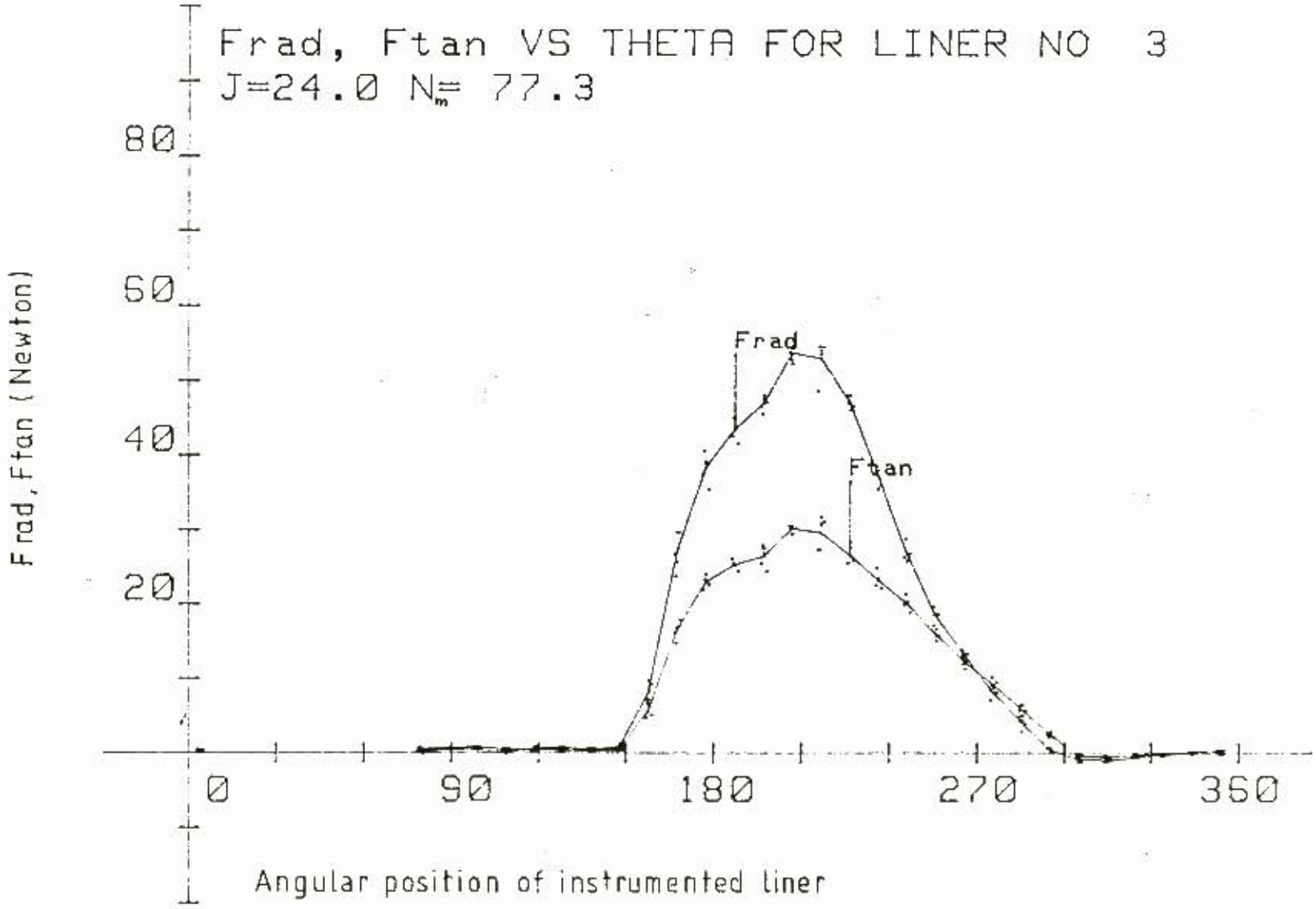

FIGURE C-9 : GRAPHICAL OUTPUT OF DETAILED DATA MEASURED AT J=24%,Nm=77.6% FOR LINER No.3

TABLE C-1 : PRINT OF OUTPUT MEASURED AT J=24%, N_m=77.6% FOR LINER No.3

```
   #PASS     JSET    MSET    AMEAS   HSET    HMEAS    TDR     TH_B    TH_D   THETA   PERIOD  TBD_AV  N_RMD  N_RMDC  P_RMD   P_RMDC
*****************************************************************************************************************************
(a) 2 44  4  24.0    35.6    35.5    77.6    77.3    29.6    193.4   256.6   44.0   1126.5    0.0     445    445     400     400
(b) FRACTIONAL STD DEVIATIONS: 0.0000                    .0456   .0392   .0478   .1518   .0031   .2129
    J    TA      TB      TD      TH_B    TH_D    TBD     PER     THETA   CBD/TBD  ACCEPT
    1 -32121 -31780 -31499    178     257     201     1124     37.7    .594     1
    2 -30997 -30605 -30423    184     241     182     1127     37.8    .559     1
    3 -29879 -29607 -29284    192     246     203     1123     38.8    .818     1
    4 -28747 -28344 -28160    198     256     246     1129     50.9    .762     1
    5 -27618 -27224 -26996    195     256     228     1130     45.3    .575     1
    6 -26488 -26092 -25926    196     244     186     1124     40.1    .892     1
    7 -25364 -24999 -24721    185     263     276     1131     43.9    .658     1
    8 -24233 -23802 -23638    267     249     164     1123     48.0    .707     1
    9 -23110 -22714 -22410    195     281     304     1131     57.9    .510     1
   10 -21979 -21591 -21395    193     245     196     1123     39.3    .956     1
(c) THET(30)NOW AND AT J=0 ARE    364.9   362.2
(d) PROFILE DATA:LINES ARE THET,COND,TDR,Frad,Flan:
   80   90  100  110  120  129  139  149  159  169  179  188  198  208  218  228  237  247  257  267  277  286  296  306  316  326  335  345  355  365
    3    3    3    3    0    3    3    3    3    3 1173    3-1173    0-1173-1173-1173-1173-1173    0    3    3    3    3    3    3    3    3    3
 2906 2681 3625 3044 2634 3082 3266 3093 2861 2851 2958 2873 3121 3072 3056 2977 2900 2938 2671 3121 3187 3482 2966 2996 3095 3015 2149 3121 3111 3041
   19   59   77   57   89   73   64   71  919 2988 3548 4154 4737 5526 5453 4657 3651 2674 1855 1326  806  385    9 -121  -66  -61  -19   10   36   43
   -7   43   43   24   62   56   32   37  507 1784 2259 2444 2439 3018 3109 2586 2208 1882 1565 1227  943  567  213  -28  -75  -50  -12    2  -14    8
 THET(30)NOW AND AT J=0 ARE    363.9   362.2
 PROFILE DATA:LINES ARE THET,COND,TDR,Frad,Flan:
   79   89   99  109  119  128  138  148  158  168  177  187  197  207  217  227  238  248  258  268  278  285  295  305  315  325  334  344  354  364
    0    3    3    3    3    0    3    3    3    3    3-1173-1173-1173-1173-1173-1173-1173    0    0    0    3    3    3    3    3    3    3    3
 2986 3625 3122 3141 3602 3082 3025 2900 2861 2947 3131 3169 3121 2947 2900 3025 3044 3082 3176 3121 2996 2958 2966 2948 2995 3169 3237 3625 2917 3044
   69   58   77   57   40   73   64   71  820 2572 3894 4352 4757 5427 5354 4608 3798 2674 1851 1326  806  435   58  -71 -115  -61  -15   10   36   43
   27   43   43   24   62   21   32   37  646 1680 2294 2514 2752 3053 3179 2760 2347 1996 1565 1227  874  637  281  -28  -41  -15  -47  -33   20    8
 THET(30)NOW AND AT J=0 ARE    363.3   362.2
 PROFILE DATA:LINES ARE THET,COND,TDR,Frad,Flan:
   79   89   99  108  118  129  138  148  157  167  177  187  197  206  216  226  236  246  255  265  275  285  295  304  314  324  334  344  353  363
    3    3    3    0    3    3    3    3    3-1173    3-1173-1173-1173    0-1173-1173    0    0    3    5    3    3    3    3    3    3    3    3
 3034 3074 3170 3141 2938 2914 3122 3093 2861 2941 3227 2926 2932 2896 2112 2937 2996 3257 3121 2929 2944 3082 3130 3117 3102 3015 2948 2929 2967 3044
   69   58   77   57   40   73   14   71  671 2375 4062 4500 4553 5279 5453 4707 3846 2872 1851 1277  935  435   58  -71 -115  -61   19   10   36   43
   27   43   43   24   27   21   32   37  562 1472 2329 2548 2786 3018 2728 2551 2485 2125 1600 1192 1013  637  213  -28  -75  -50  -12    2  -14    8
 THET(30)NOW AND AT J=0 ARE    362.9   362.2
 PROFILE DATA:LINES ARE THET,COND,TDR,Frad,Flan:
   78   88   98  108  118  127  137  147  157  167  177  186  196  206  216  226  235  245  255  265  275  284  294  304  314  324  334  343  353  363
    3    3    3    3    3    3    3    3    3    3    0    0-1173-1173-1173-1173-1173    3    0    3    3    0    3    3    3    3    3    3    3
 3093 3074 3095 2966 2938 3082 3176 3093 2995 2899 3035 2976 2926 2996 3206 3218 2948 2773 3035 3073 3044 3032 3179 3092 2919 2949 3044 2977 3015 2952
   19   58   77   57   40   73   64   71  721 2671 3746 4253 4658 5378 4860 4805 3848 2825 1950 1376  768  484   58  -71 -115  -61  -19   10   36   43
   27   43   43   24   27   21   32   37  472 1610 2190 2618 2542 3053 2728 2551 2242 1986 1704 1296  839  567  248  -63  -41  -50  -47    2   20   43
 THET(30)NOW AND AT J=0 ARE    363.9   362.2
 PROFILE DATA:LINES ARE THET,COND,TDR,Frad,Flan:
   79   89   99  109  119  128  138  148  158  168  177  187  197  207  217  227  236  246  256  266  276  285  295  305  315  325  334  344  354  364
    3    3    0    3    0    3    0    3    0    0-1173    0-1173-1173-1173-1173-1173-1173    0    3    3    3    3    3    3    3    3    3    3
 2890 2937 3074 3544 2938 3131 3114 3044 2912 2953 3083 3073 3025 3106 3160 2886 2851 2906 3073 3025 3092 2986 2698 2851 2958 3463 3149 3216 3269 2965
   69   58   77   57   89   73   64  121  986 2968 3914 4500 4806 5353 5464 4835 3851 2576 1654 1226  806  367    9 -121 -115  -61  -19   10   36   43
   27   43   43  -10   27   55   32   71  715 1680 2378 2514 2682 2948 3075 2829 2312 2021 1496 1123  908  498  248  -63  -75  -15  -42    2  -14    8
 TH_B_AV,TH_B_FAR,TH_D_AV,TH_D_FAR= 193.4  152.5  254.6  302.2
(f) AVERAGE PROFILE DATA:(LINES ARE THET,COND,TDR,Frad,Flan)
   79   89   99  109  119  128  138  148  158  168  177  187  197  207  217  226  236  246  256  266  275  285  295  305  315  325  334  344  354  364
    2    3    2    2    2    2    2    3    2    2 -763 -234 -938 -538 1173 -959-1173-1173 -234    1    2    3    2    3    3    3    3    2    3    3
 2992 2977 3083 3073 2986 3082 3179 3044 2990 2997 3093 3044 3055 3044 3152 3015 2940 3005 3092 3054 3073 3034 2834 3065 2978 3034 3149 3054 3044 3044
   49   58   77   57   59   73   54   88  820 2711 3833 4352 4698 5388 5395 4717 3729 2684 1831 1307  806  405   58  -91 -105  -61  -19   10   36   43
   20   43   43   17   41   35   12   44  577 1645 2294 2527 2648 3016 2964 2656 2319 2000 1596 1213  915  581  242  -42  -62  -35  -28   -5   -4   15
 STORED PROFILE AT P_RMD= 400
 ***** SETPOINT CHANGE: X CRIT SPD,= 82.0 RPM= 56.5
```

SPEED : 65 % CHARGE VOLUME : 15 %

HEIGHT OF LIFT (%) - LINER WEAR RATE (g/6h)

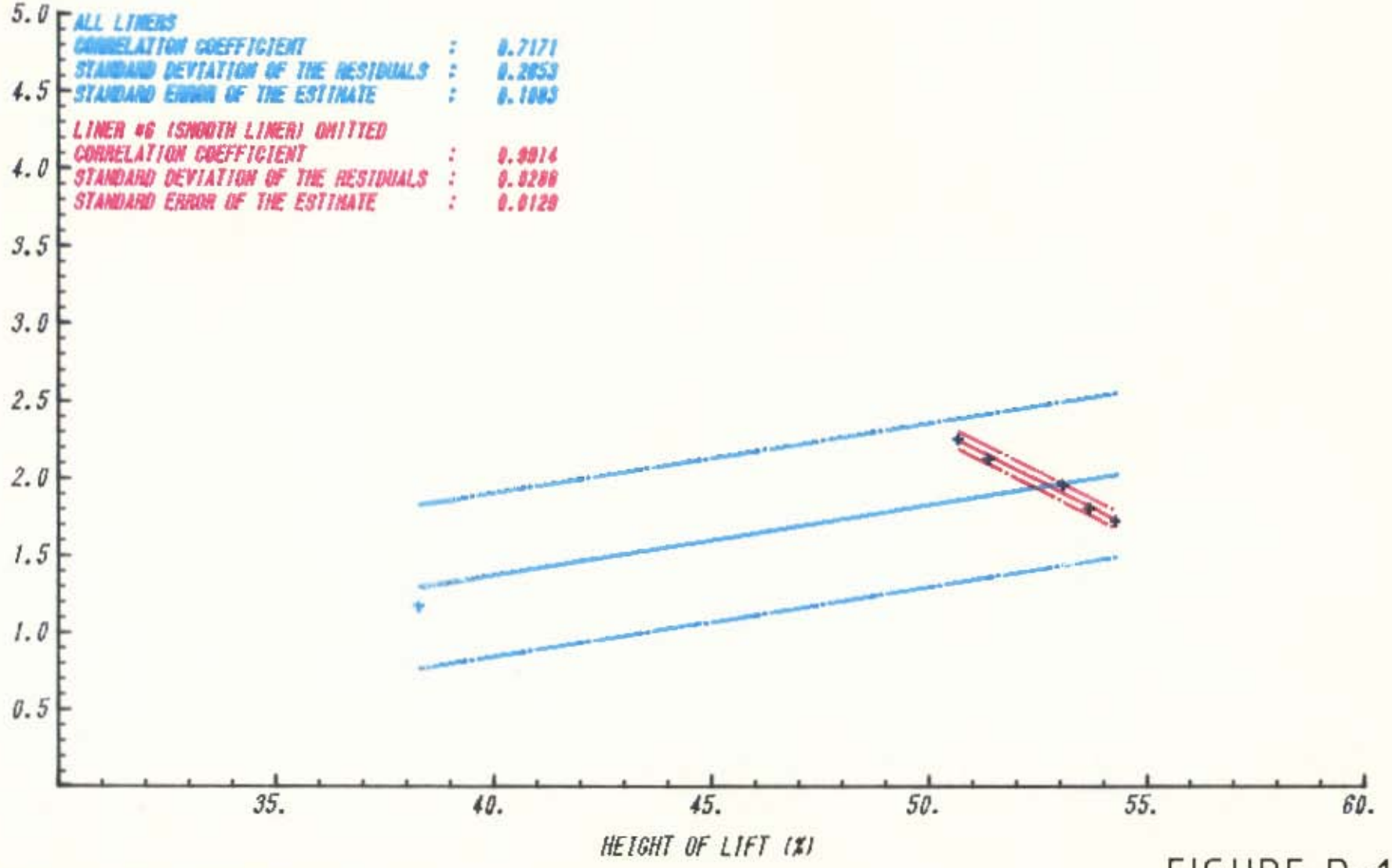

THE SPREAD : TWO STANDARD DEVIATIONS

FIGURE D-1

SPEED : 65 % CHARGE VOLUME : 15 %

TOTAL AGITATED AREA (cm2) - LINER WEAR RATE (g/6h)

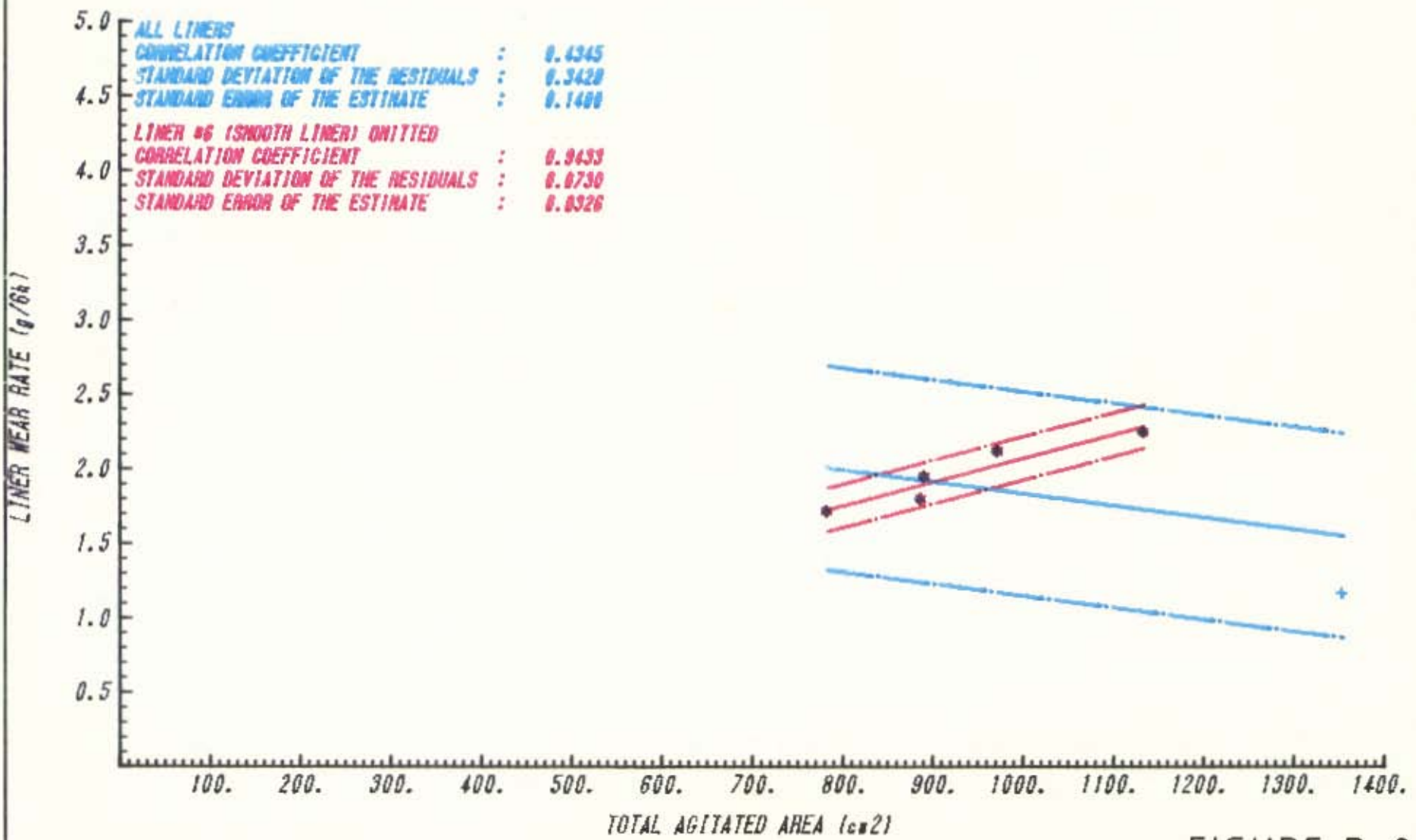

THE SPREAD : TWO STANDARD DEVIATIONS

FIGURE D-2

SPEED : 65 % CHARGE VOLUME : 15 %

IMPACT FORCE (N) - LINER WEAR RATE (g/6h)

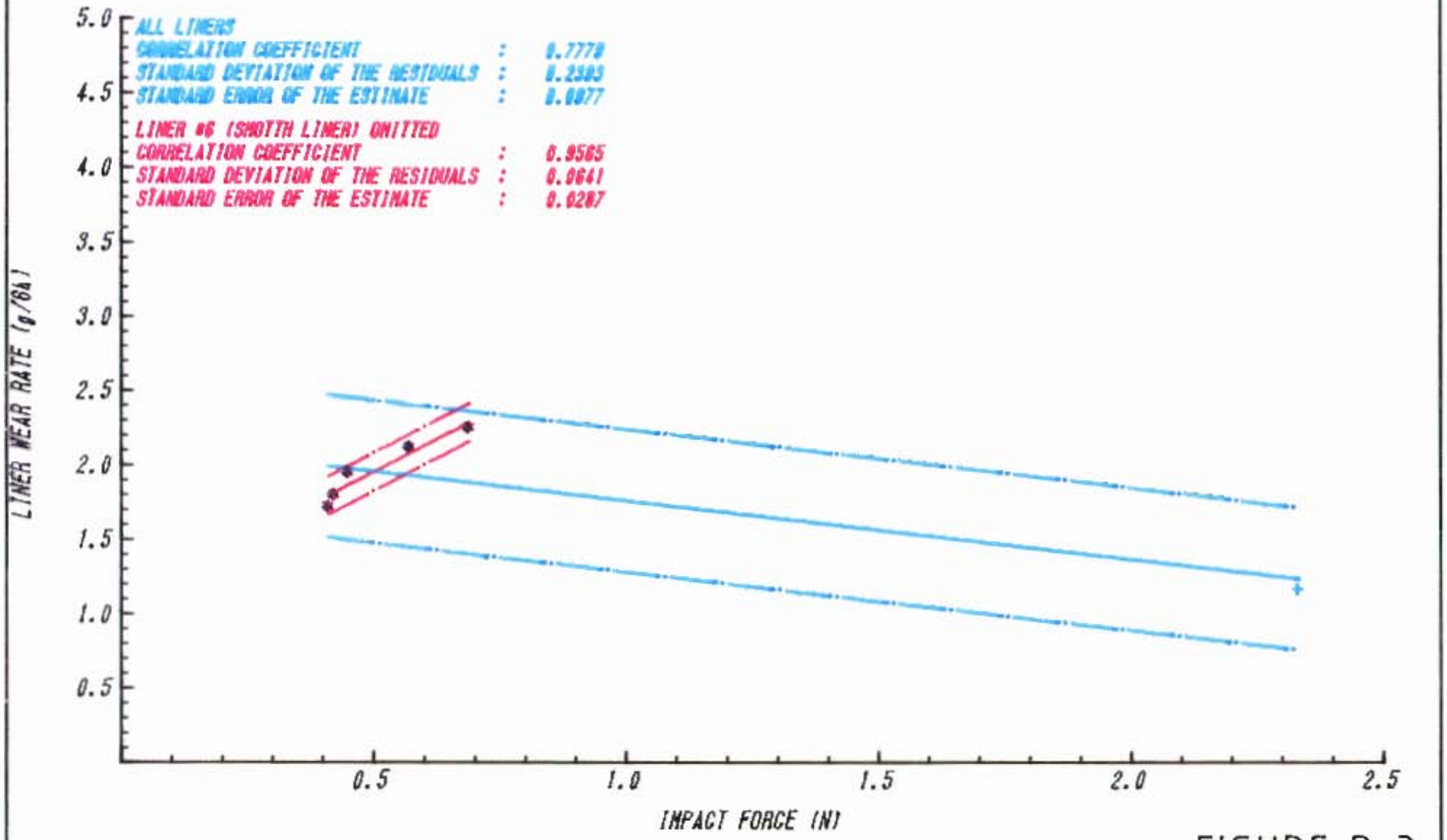

THE SPREAD : TWO STANDARD DEVIATIONS

FIGURE D-3

HEIGHT OF LIFT (%) vs. MILL SPEED (%) & CHARGE VOLUME (%)
'SKELETON'-PLOTS : DATA AS MEASURED

COLOUR CODE FOR : HEIGHT OF LIFT

57.00	-	60.00 (%)
54.00	-	57.00 (%)
51.00	-	54.00 (%)
48.00	-	51.00 (%)
45.00	-	48.00 (%)
42.00	-	45.00 (%)

ORDER OF LINERS :

LINER #4
LINER #5
LINER #3
LINER #1
LINER #2

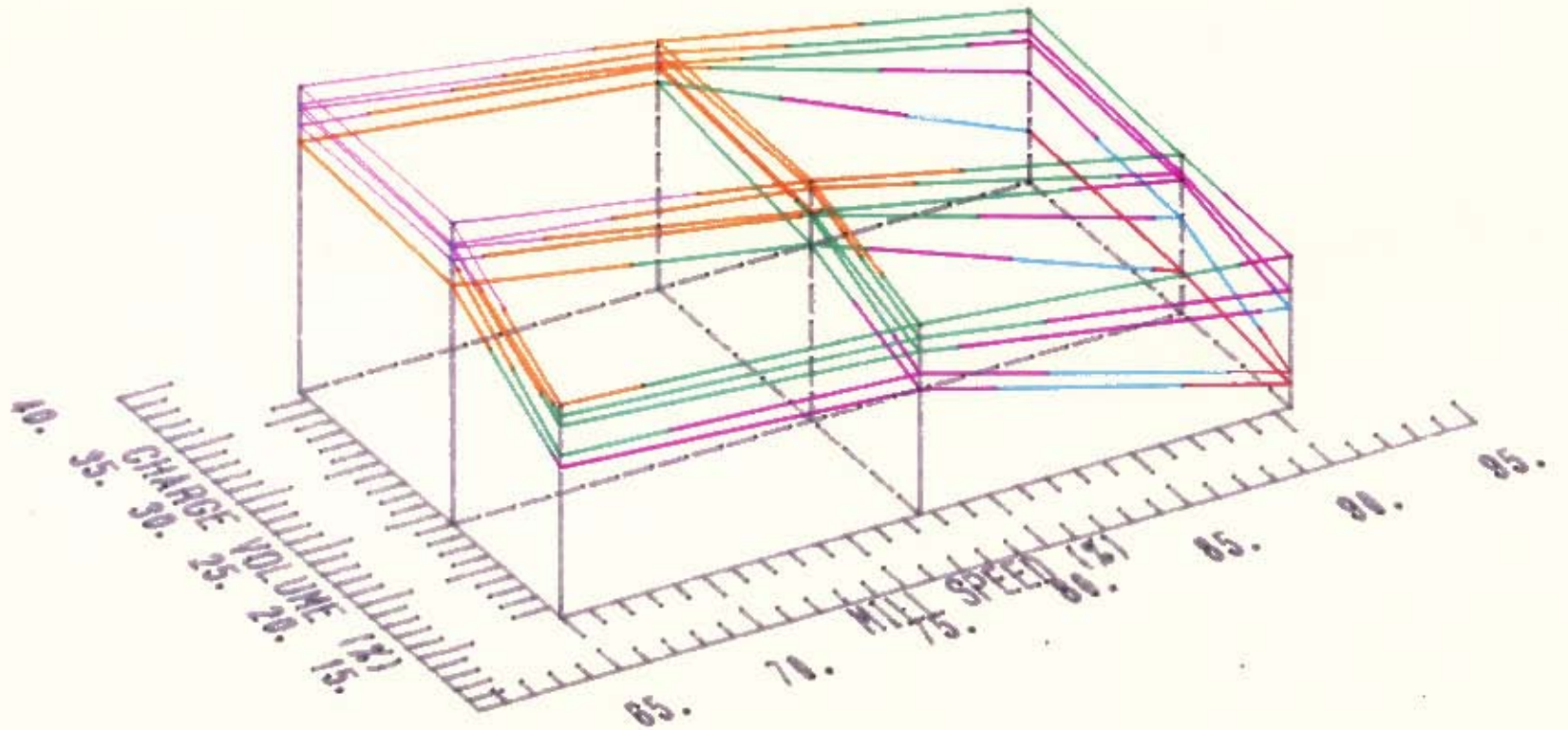

FIGURE D-4

IMPACT AREA (cm2) vs. MILL SPEED (%) & CHARGE VOLUME (%)
'SKELETON'-PLOTS : DATA AS MEASURED

COLOUR CODE FOR : IMPACT AREA

1200.00 - 1400.00 (cm2)
1000.00 - 1200.00 (cm2)
800.00 - 1000.00 (cm2)
600.00 - 800.00 (cm2)
400.00 - 600.00 (cm2)
200.00 - 400.00 (cm2)
0.00 - 200.00 (cm2)

ORDER OF LINERS :

LINER #2
LINER #1
LINER #3
LINER #5
LINER #4

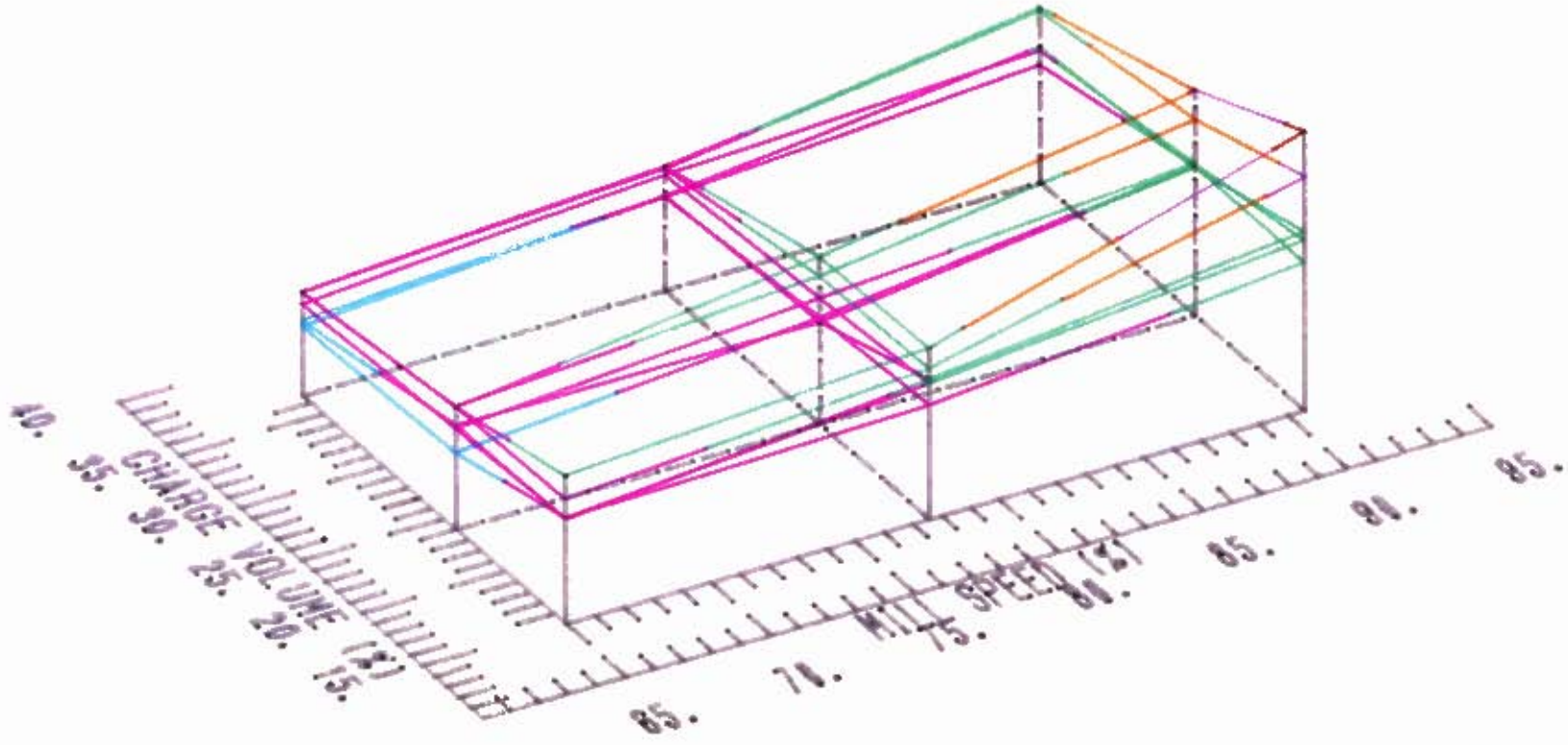

FIGURE D-5

IMPACT FORCE (N) vs. MILL SPEED (%) & CHARGE VOLUME (%)
'SKELETON'-PLOTS : DATA AS MEASURED

COLOUR CODE FOR : IMPACT FORCE

1.20	-	1.40 (N)
1.00	-	1.20 (N)
0.80	-	1.00 (N)
0.60	-	0.80 (N)
0.40	-	0.60 (N)
0.20	-	0.40 (N)
0.00	-	0.20 (N)

ORDER OF LINERS :

LINER #2
LINER #1
LINER #3
LINER #5
LINER #4

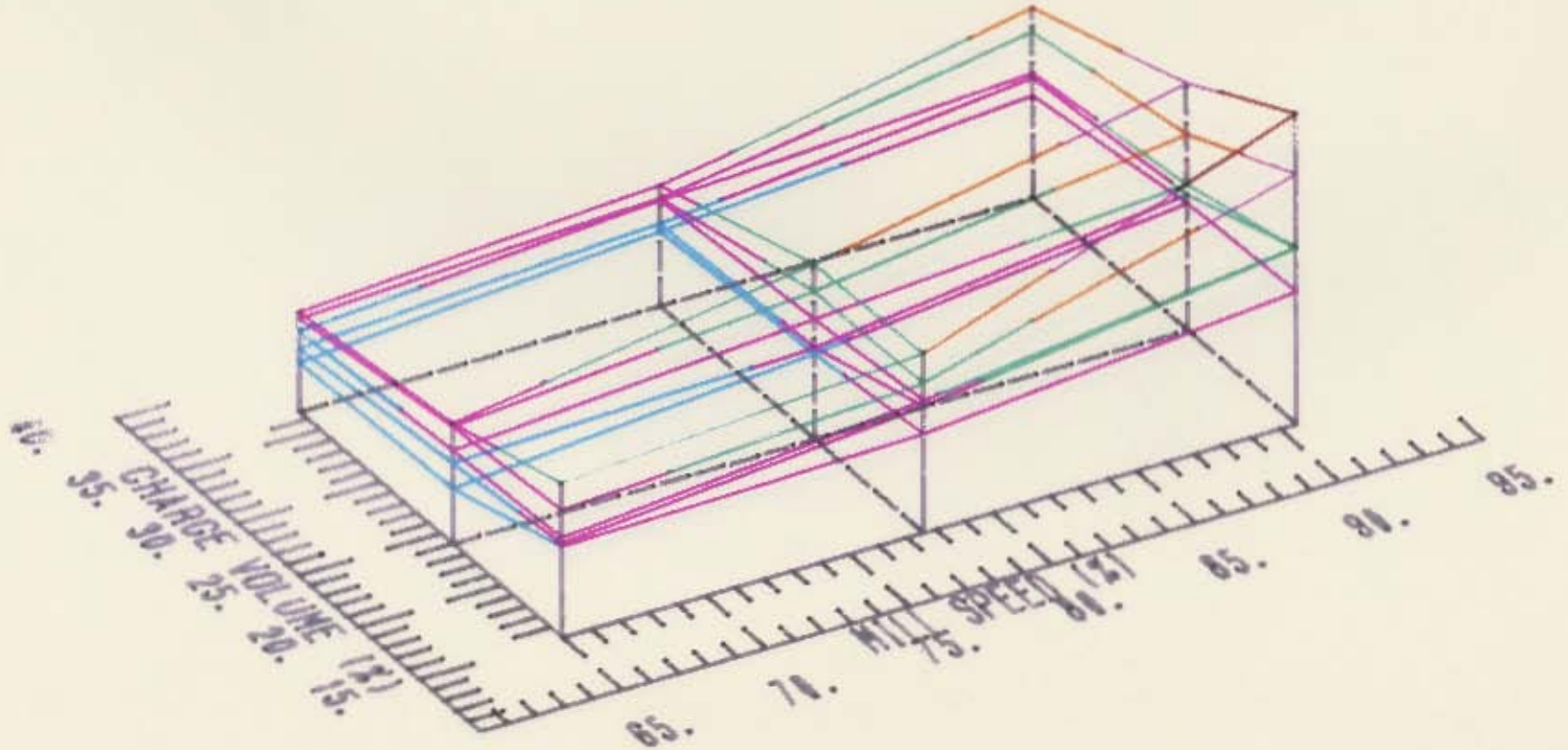

FIGURE D-6

IMPACT FORCE - RADIAL COMPONENT (N) vs. MILL SPEED (%) & CHARGE VOLUME (%)
'SKELETON'-PLOTS : DATA AS MEASURED

COLOUR CODE FOR : IMPACT FORCE - RADIAL COMPONENT

1.20	-	1.40	(N)
1.00	-	1.20	(N)
0.80	-	1.00	(N)
0.60	-	0.80	(N)
0.40	-	0.60	(N)
0.20	-	0.40	(N)
0.00	-	0.20	(N)

ORDER OF LINERS :

LINER #2
LINER #1
LINER #3
LINER #5
LINER #4

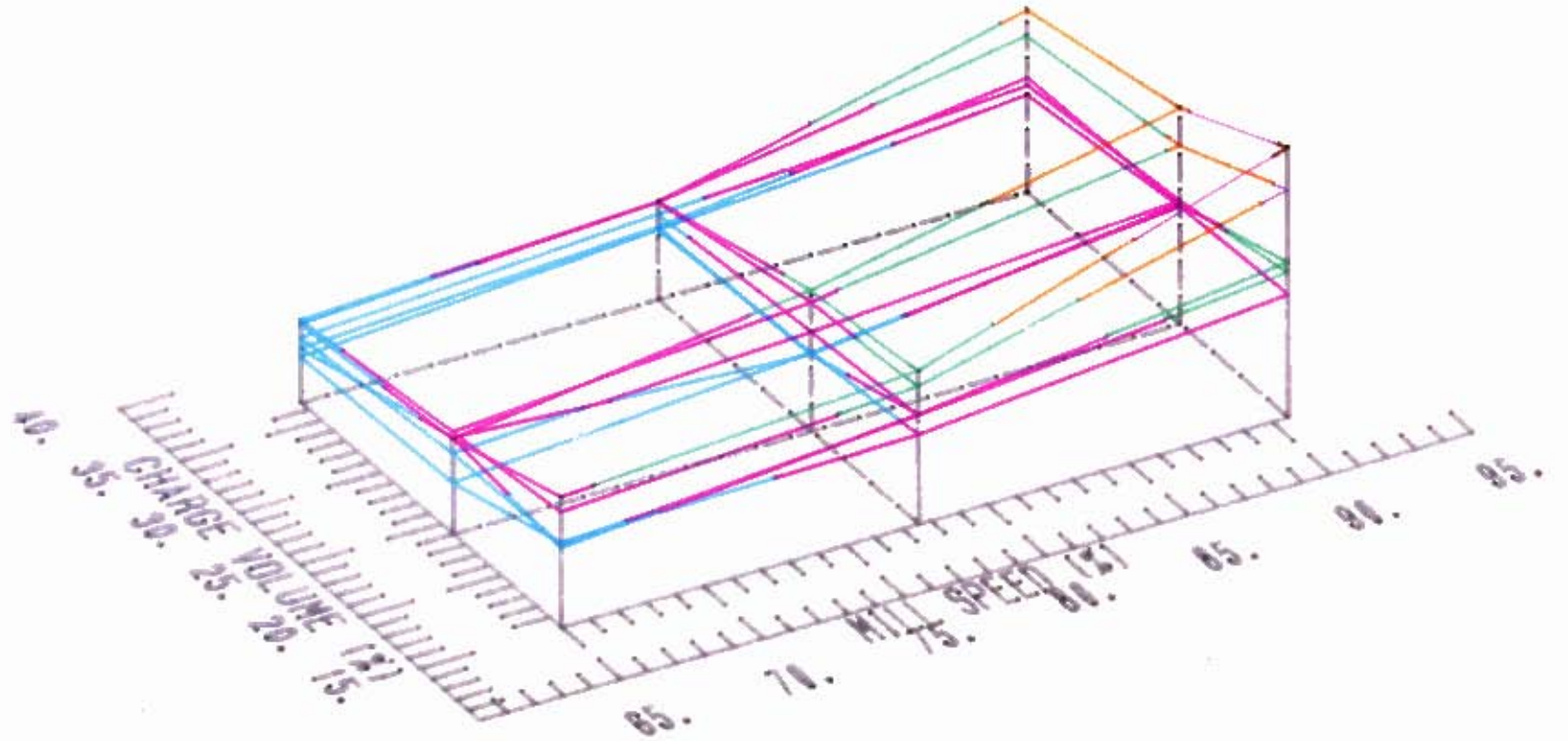

FIGURE D-7

LINER WEAR (g/6h) vs. MILL SPEED (%) & CHARGE VOLUME (%)

COLOUR CODE FOR : LINER WEAR

4.00 - 5.00 (g/6h)
3.00 - 4.00 (g/6h)
2.00 - 3.00 (g/6h)
1.00 - 2.00 (g/6h)
0.00 - 1.00 (g/6h)

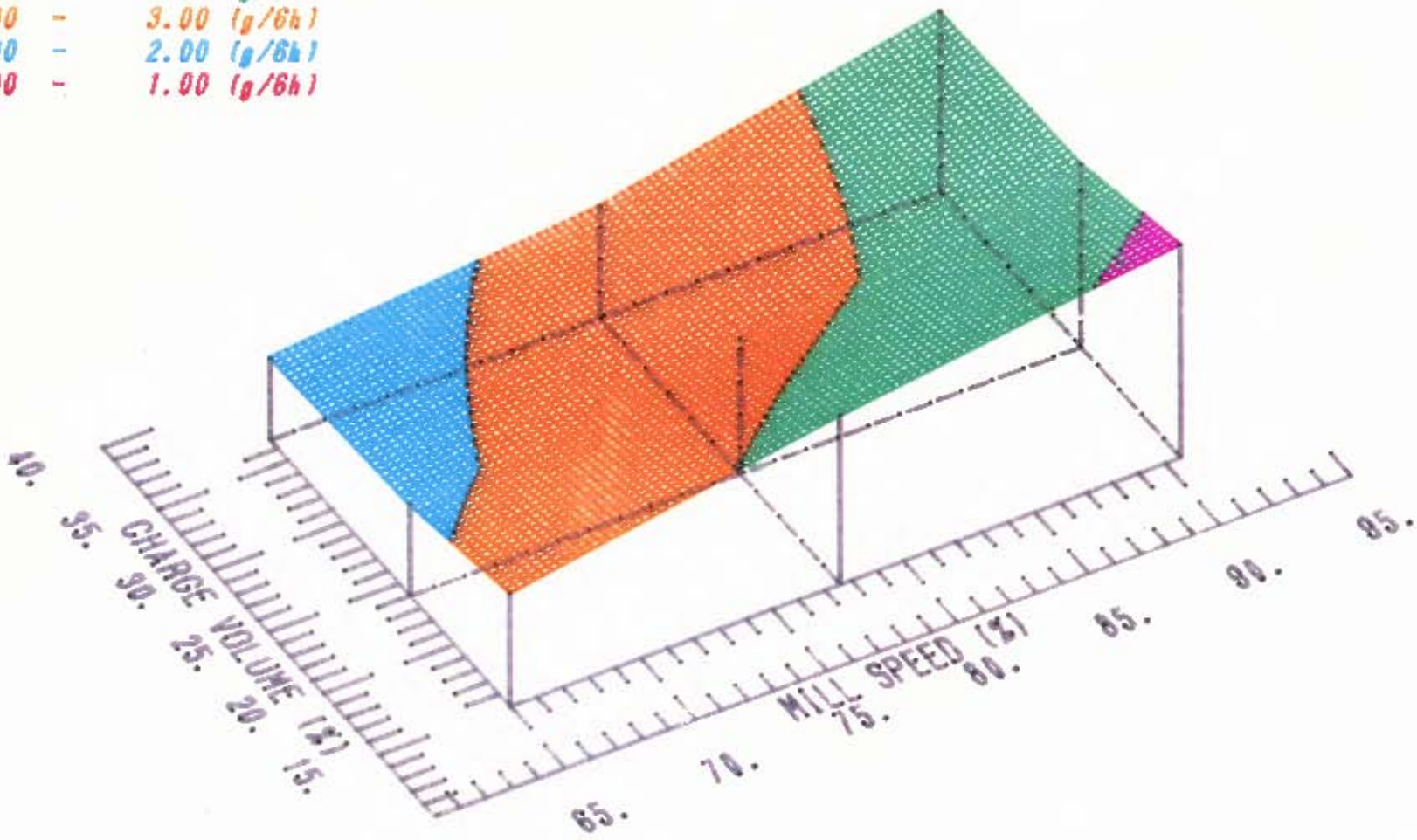

LINER #2

FIGURE D-13

LINER WEAR (g/6h) vs. MILL SPEED (%) & CHARGE VOLUME (%)

COLOUR CODE FOR : LINER WEAR

4.00 - 5.00 (g/6h)
3.00 - 4.00 (g/6h)
2.00 - 3.00 (g/6h)
1.00 - 2.00 (g/6h)
0.00 - 1.00 (g/6h)

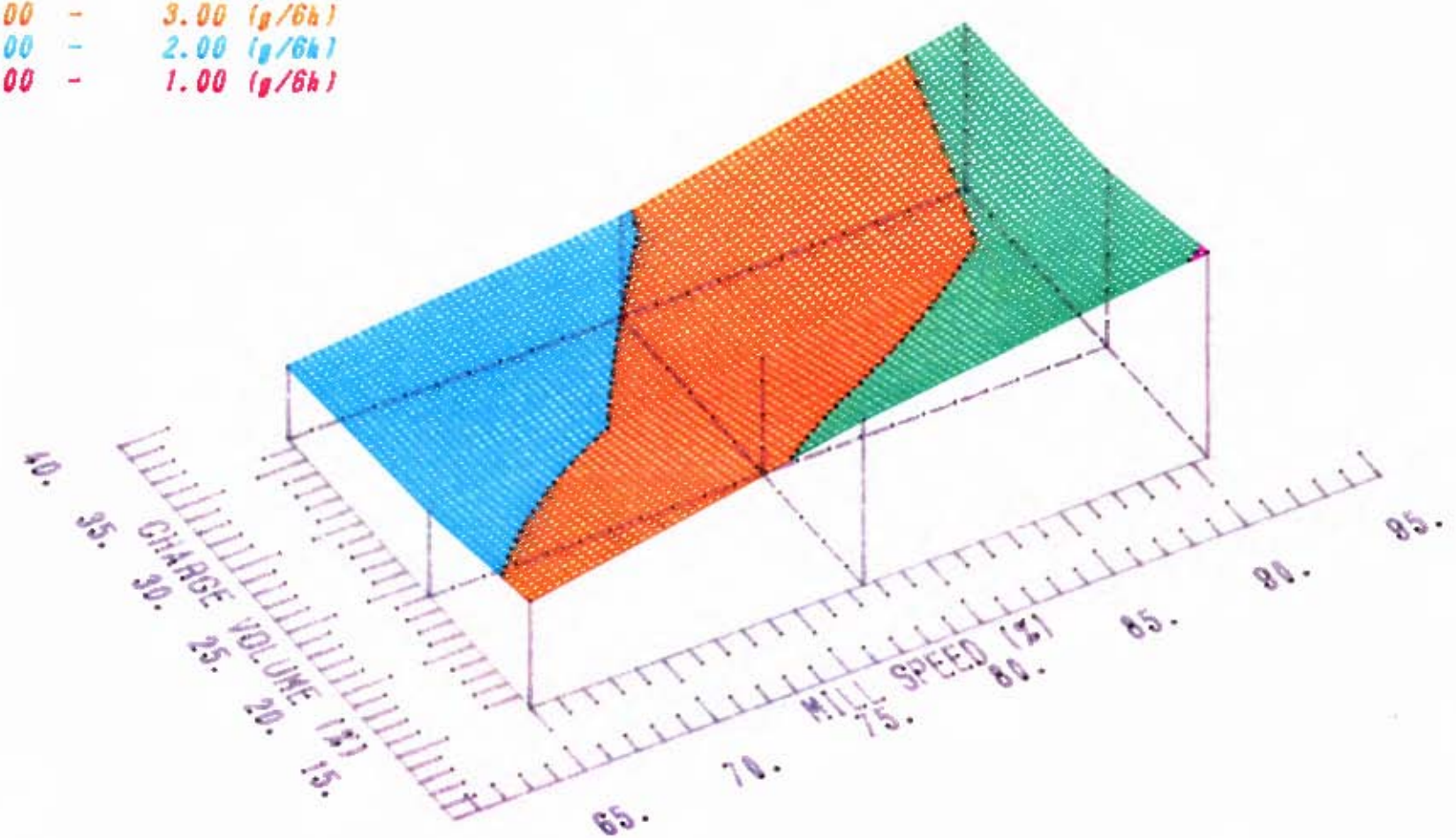

LINER #1

FIGURE D-12

LINER WEAR (g/6h) vs. MILL SPEED (%) & CHARGE VOLUME (%)

COLOUR CODE FOR : LINER WEAR

4.00 - 5.00 (g/6h)
3.00 - 4.00 (g/6h)
2.00 - 3.00 (g/6h)
1.00 - 2.00 (g/6h)
0.00 - 1.00 (g/6h)

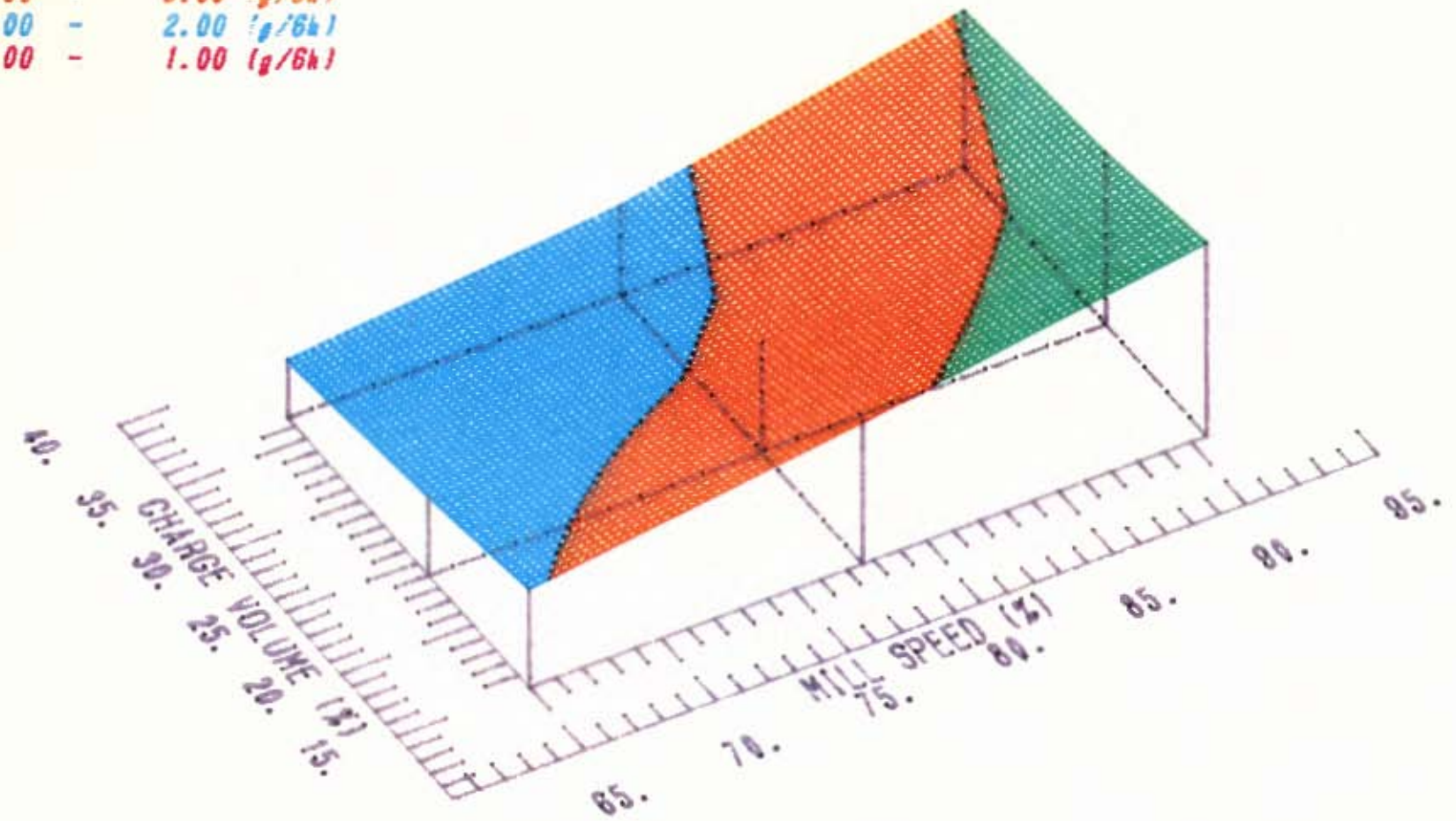

LINER #3

FIGURE D-11

LINER WEAR (g/6h) vs. MILL SPEED (%) & CHARGE VOLUME (%)

COLOUR CODE FOR : LINER WEAR

4.00 - 5.00 (g/6h)
3.00 - 4.00 (g/6h)
2.00 - 3.00 (g/6h)
1.00 - 2.00 (g/6h)
0.00 - 1.00 (g/6h)

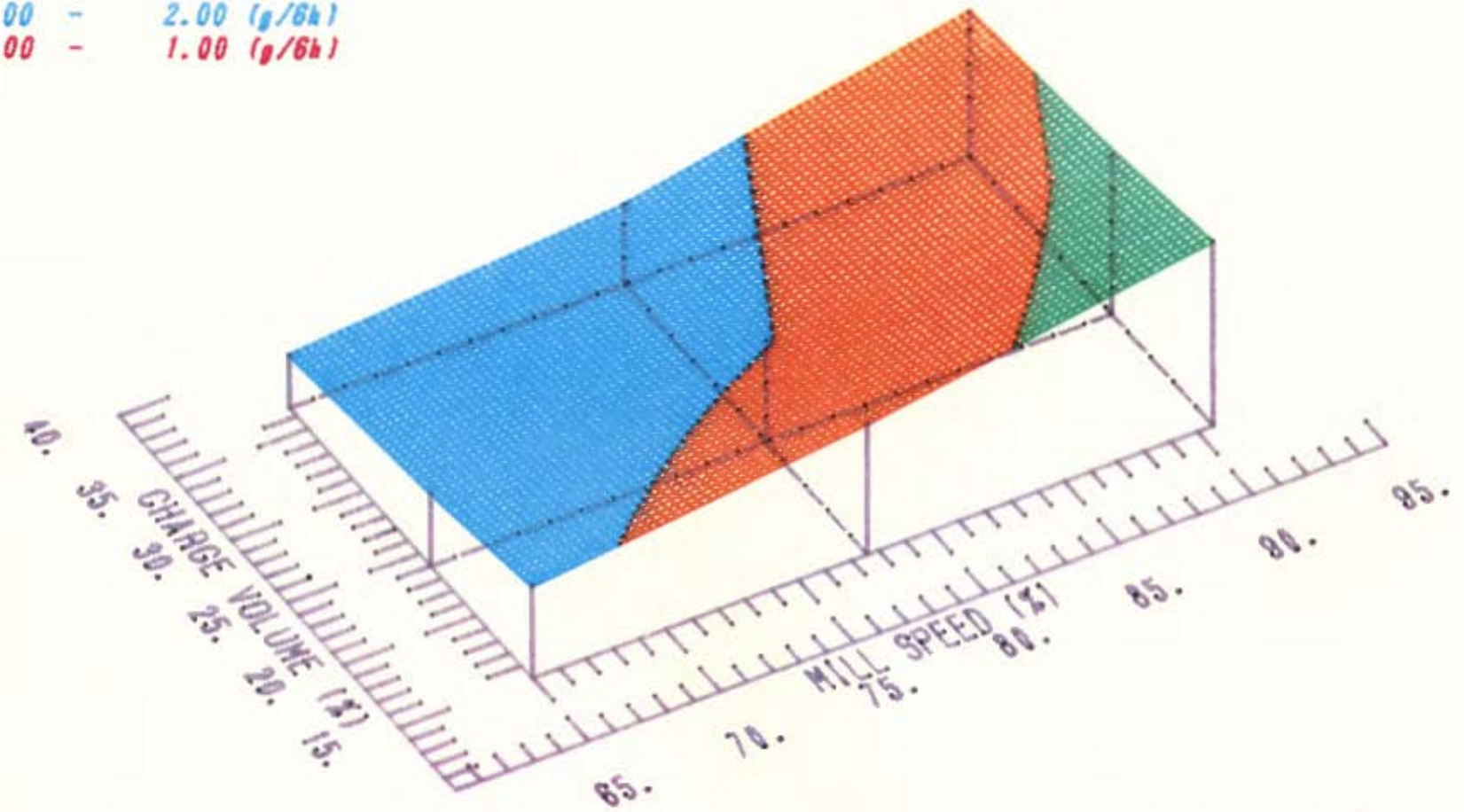

LINER #5

FIGURE D-10

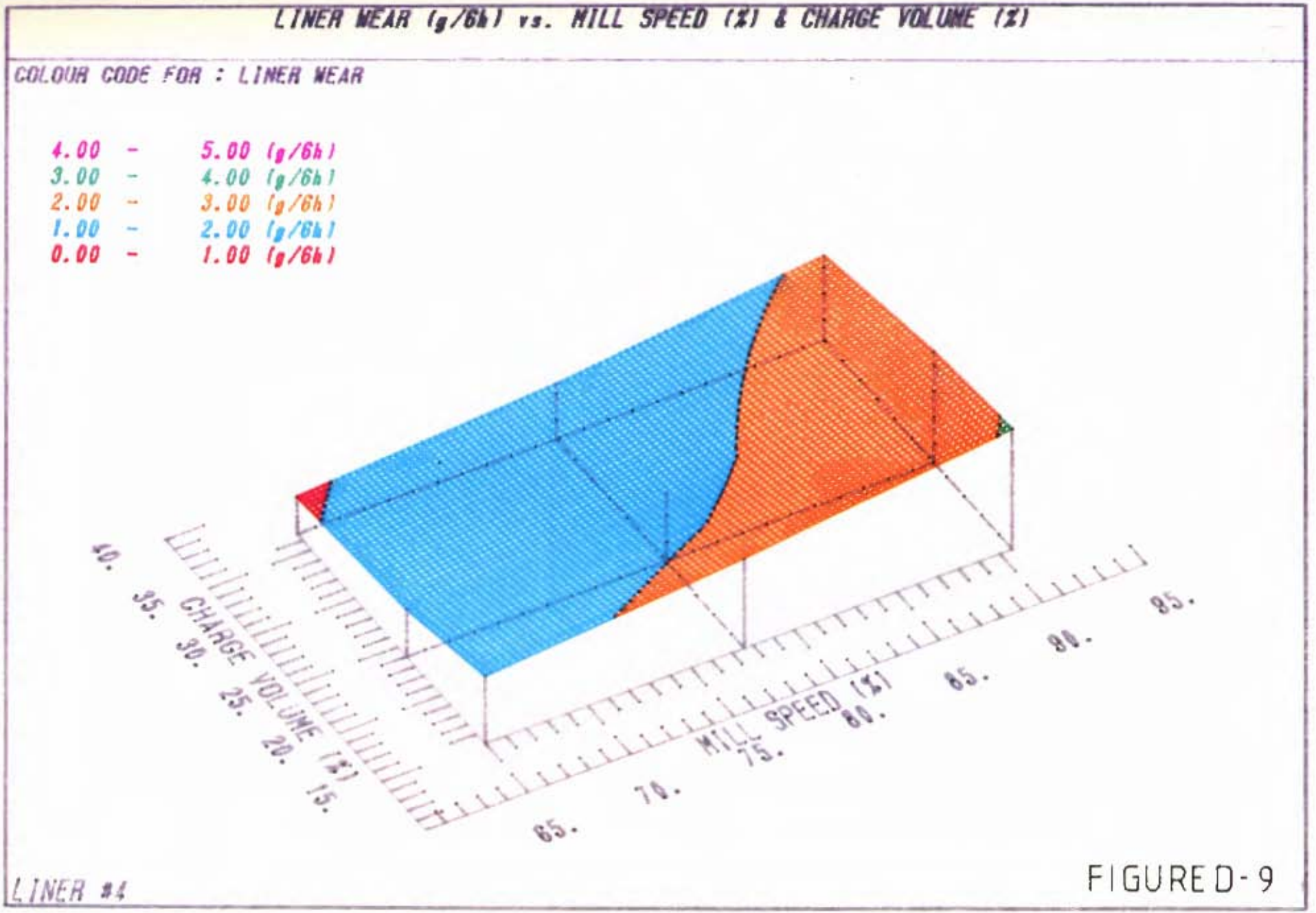
LINER WEAR (g/6h) vs. MILL SPEED (%) & CHARGE VOLUME (%)
COLOUR CODE FOR : LINER WEAR
4.00 - 5.00 (g/6h)
3.00 - 4.00 (g/6h)
2.00 - 3.00 (g/6h)
1.00 - 2.00 (g/6h)
0.00 - 1.00 (g/6h)
CHARGE VOLUME (%)
40.
35.
30.
25.
20.
15.
MILL SPEED (%)
65.
70.
75.
80.
85.
90.
LINER #4

FIGURE D-9

LINER WEAR (g/6h) vs. MILL SPEED (%) & CHARGE VOLUME (%)

COLOUR CODE FOR : LINER WEAR

4.00 - 5.00 (g/6h)
3.00 - 4.00 (g/6h)
2.00 - 3.00 (g/6h)
1.00 - 2.00 (g/6h)
0.00 - 1.00 (g/6h)

ORDER OF LINERS :

LINER #2
LINER #1
LINER #3
LINER #5
LINER #4

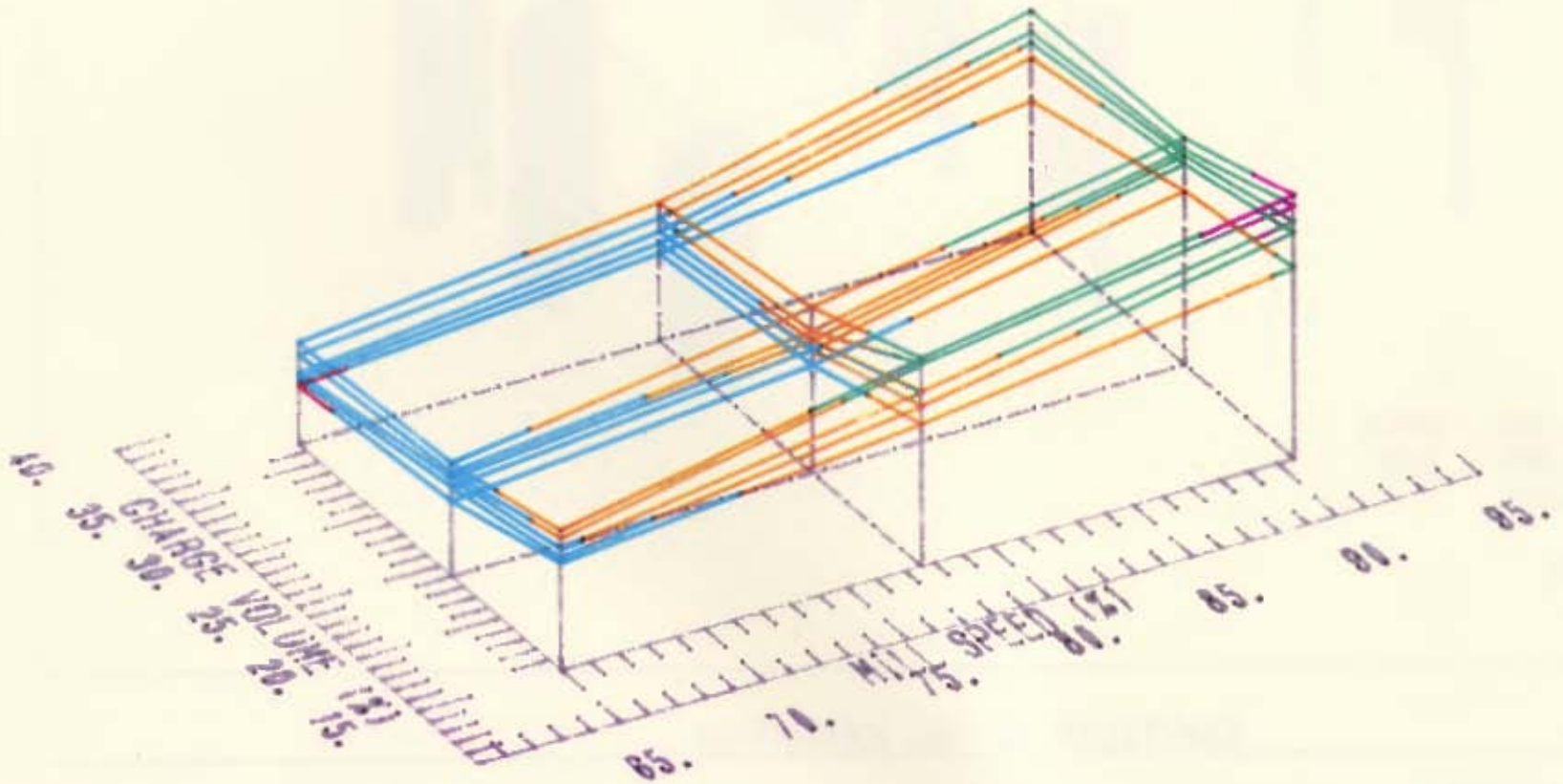

FIGURE D-8

COMPARISON OF THE 'COVARIATES'

NORMALIZED WEAR RATE
NORMALIZED LIFE
NORMALIZED IMPACT AREA
NORMALIZED IMPACT FORCE - TOTAL
NORMALIZED IMPACT FORCE - RADIAL

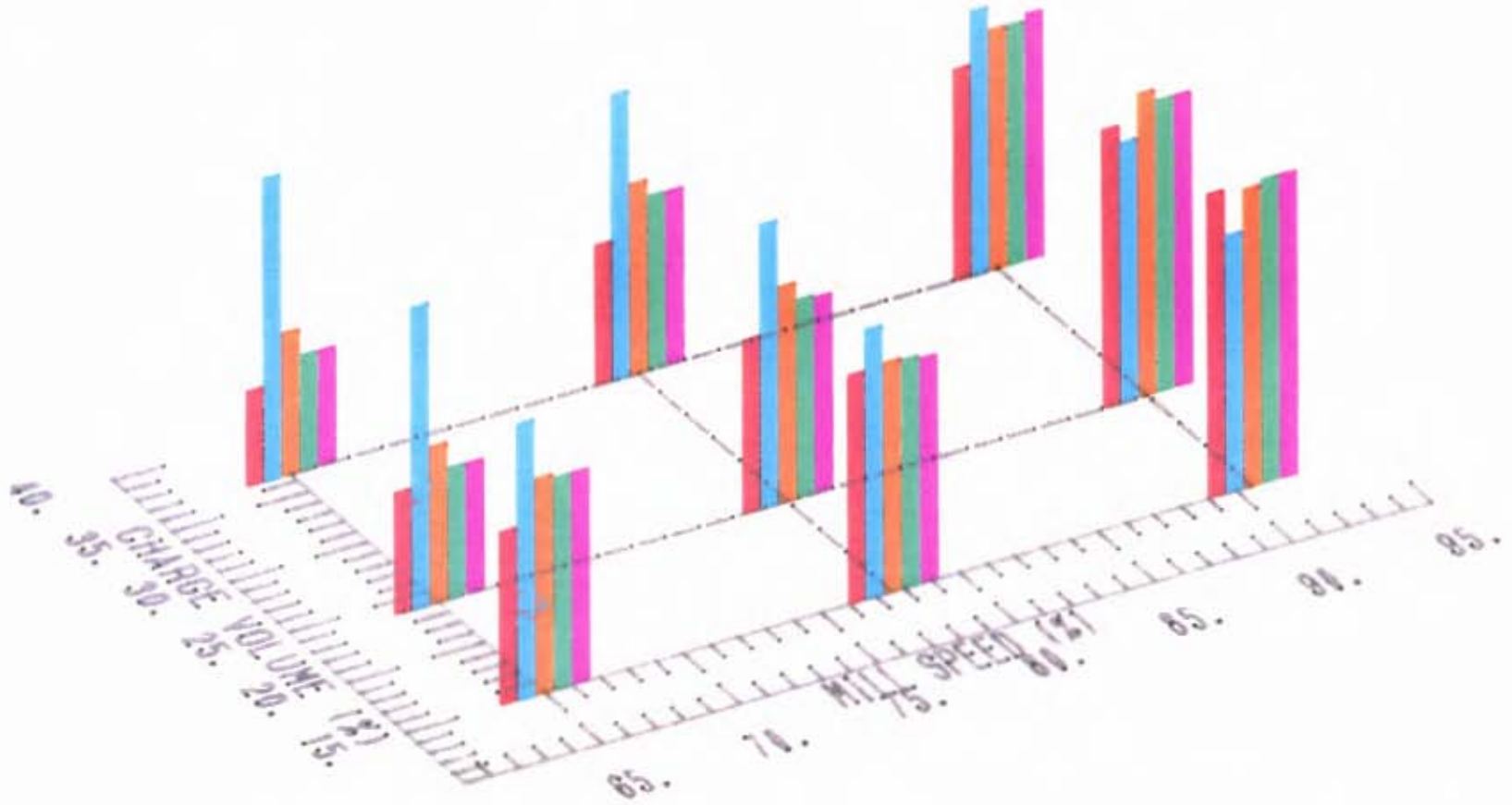

LINER #4

FIGURE D-14

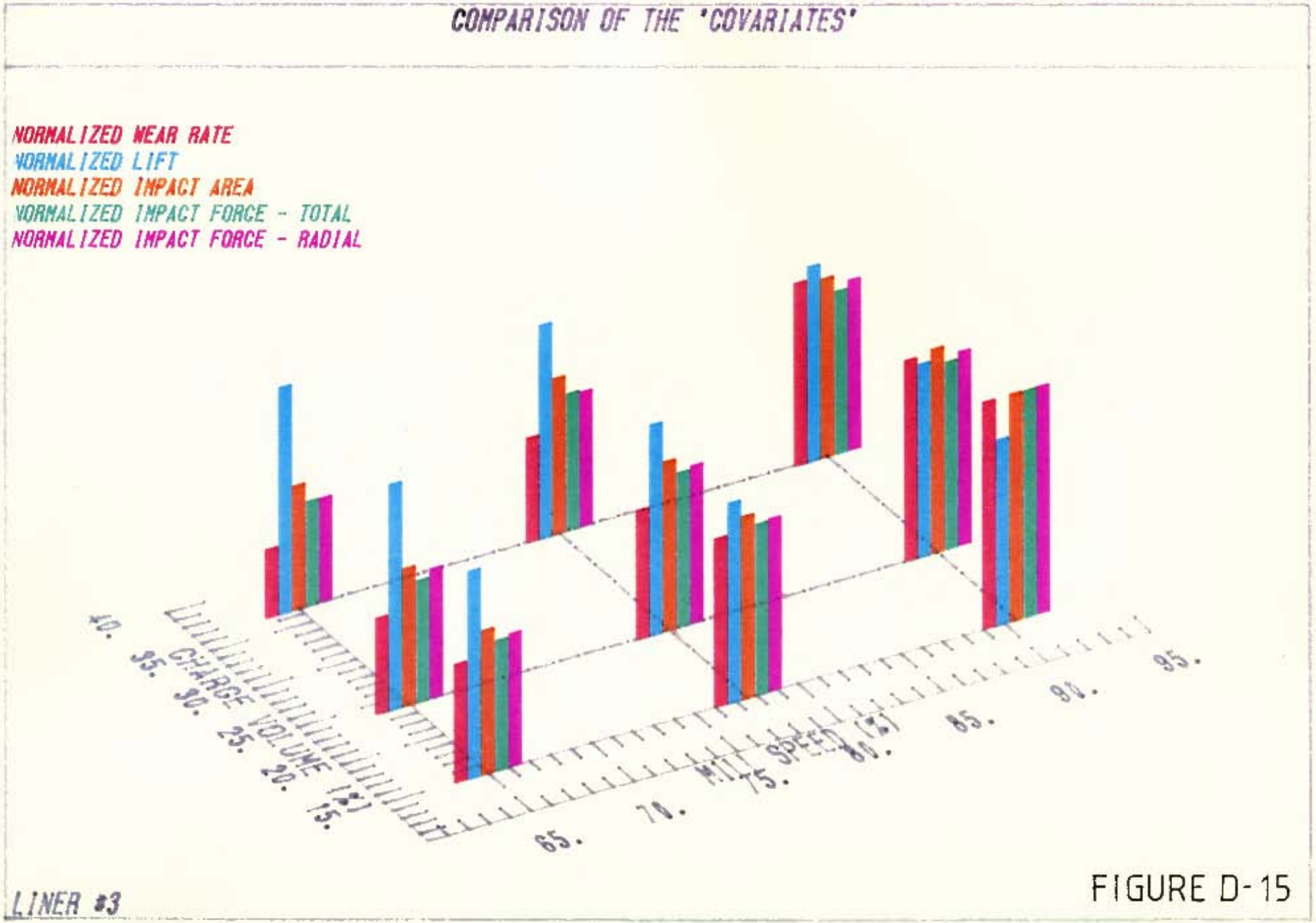
COMPARISON OF THE 'COVARIATES'
NORMALIZED WEAR RATE
NORMALIZED LIFT
NORMALIZED IMPACT AREA
NORMALIZED IMPACT FORCE - TOTAL
NORMALIZED IMPACT FORCE - RADIAL
CHARGE VOLUME (%)
10.
15.
20.
25.
30.
35.
MILL SPEED (%)
65.
70.
75.
80.
85.
90.
95.
LINER #3

FIGURE D-15

COMPARISON OF THE 'COVARIATES'

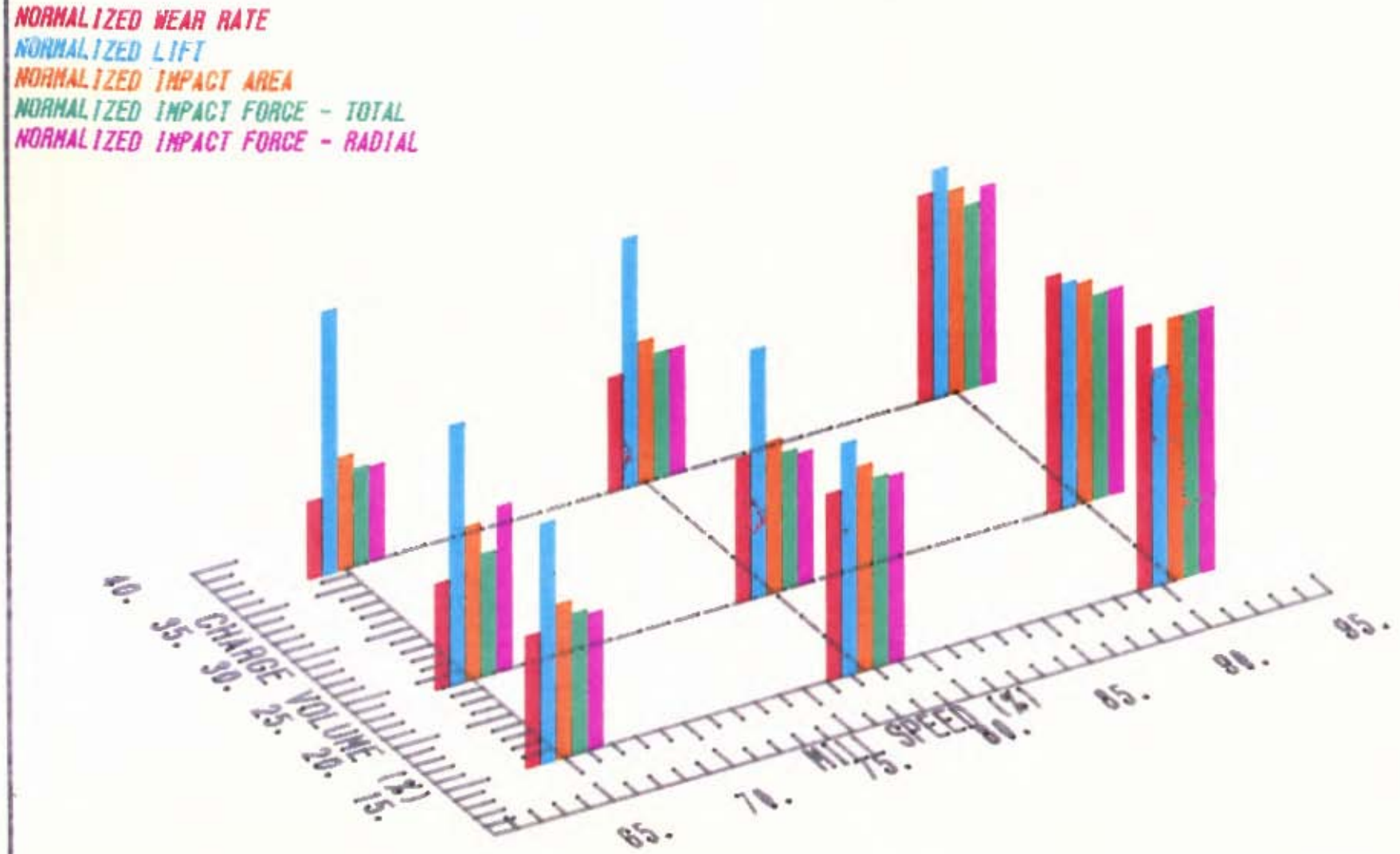

LINER #5

FIGURE D-16

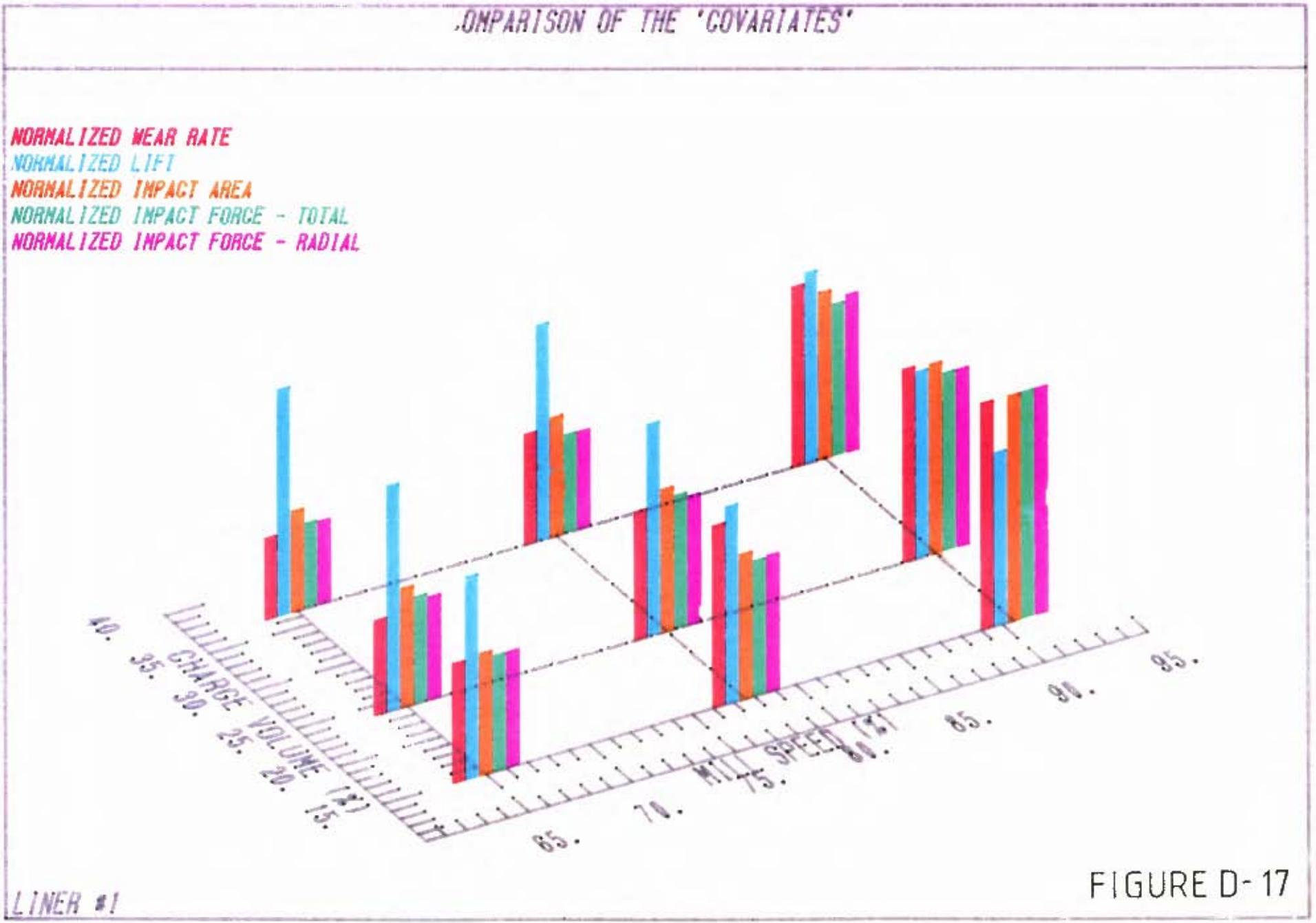
COMPARISON OF THE 'COVARIATES'
NORMALIZED WEAR RATE
NORMALIZED LIFT
NORMALIZED IMPACT AREA
NORMALIZED IMPACT FORCE - TOTAL
NORMALIZED IMPACT FORCE - RADIAL
CHARGE VOLUME (%)
40.
35.
30.
25.
20.
15.
MILL SPEED (%)
65.
70.
75.
80.
85.
90.
95.
LINER #1

FIGURE D-17

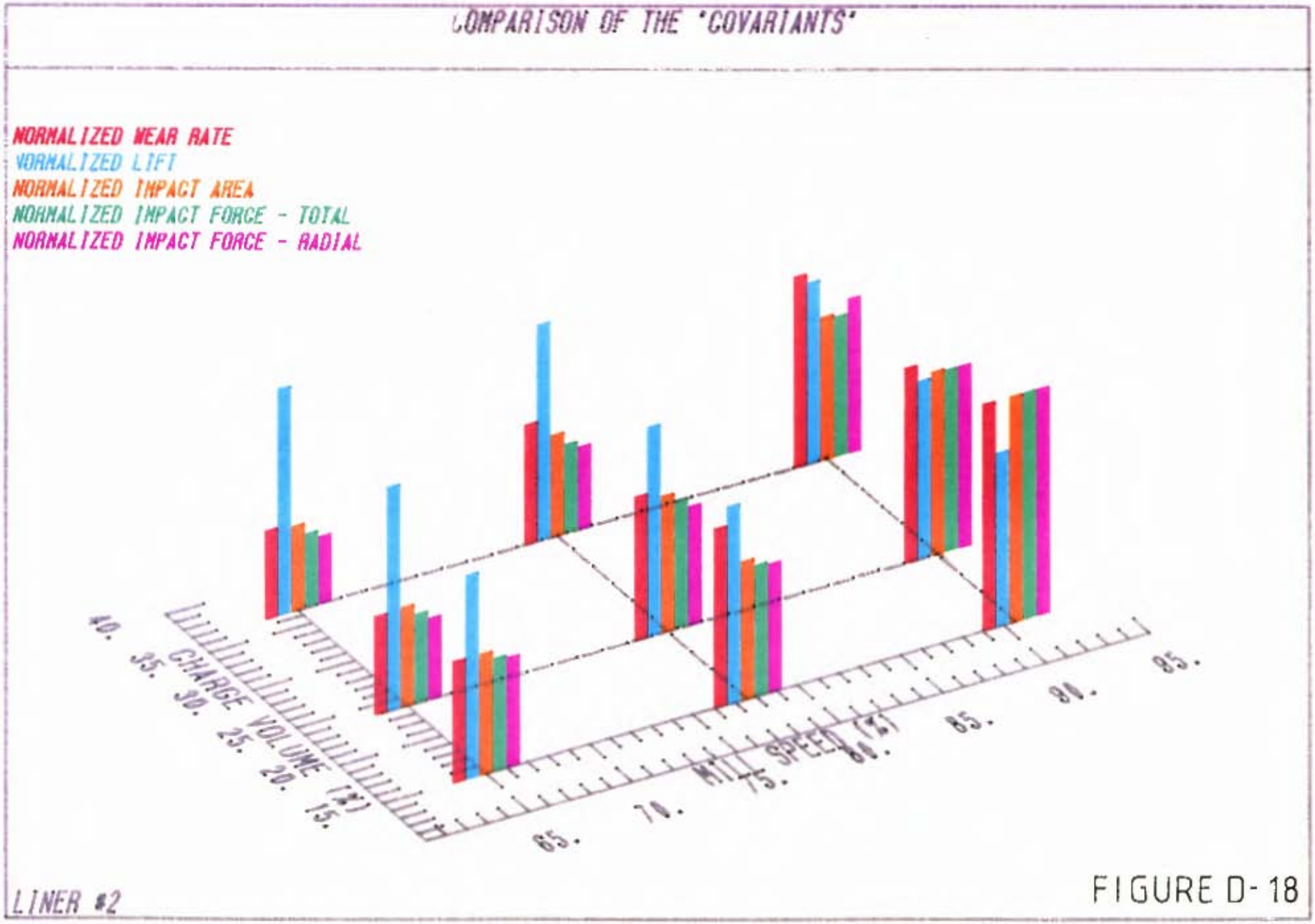
COMPARISON OF THE 'COVARIANTS'
NORMALIZED WEAR RATE
NORMALIZED LIFT
NORMALIZED IMPACT AREA
NORMALIZED IMPACT FORCE - TOTAL
NORMALIZED IMPACT FORCE - RADIAL
CHARGE VOLUME (%)
40.
35.
30.
25.
20.
15.
MILL SPEED (%)
65.
70.
75.
80.
85.
LINER #2

FIGURE D-18

SEPARATION AREA (cm2) vs. MILL SPEED (%) & CHARGE VOLUME (%)

COLOUR CODE FOR : SEPARATION AREA

400.00 - 500.00 (cm2)
300.00 - 400.00 (cm2)
200.00 - 300.00 (cm2)
100.00 - 200.00 (cm2)
0.00 - 100.00 (cm2)

ORDER OF LINERS :

LINER #5
LINER #3
LINER #1
LINER #4
LINER #2

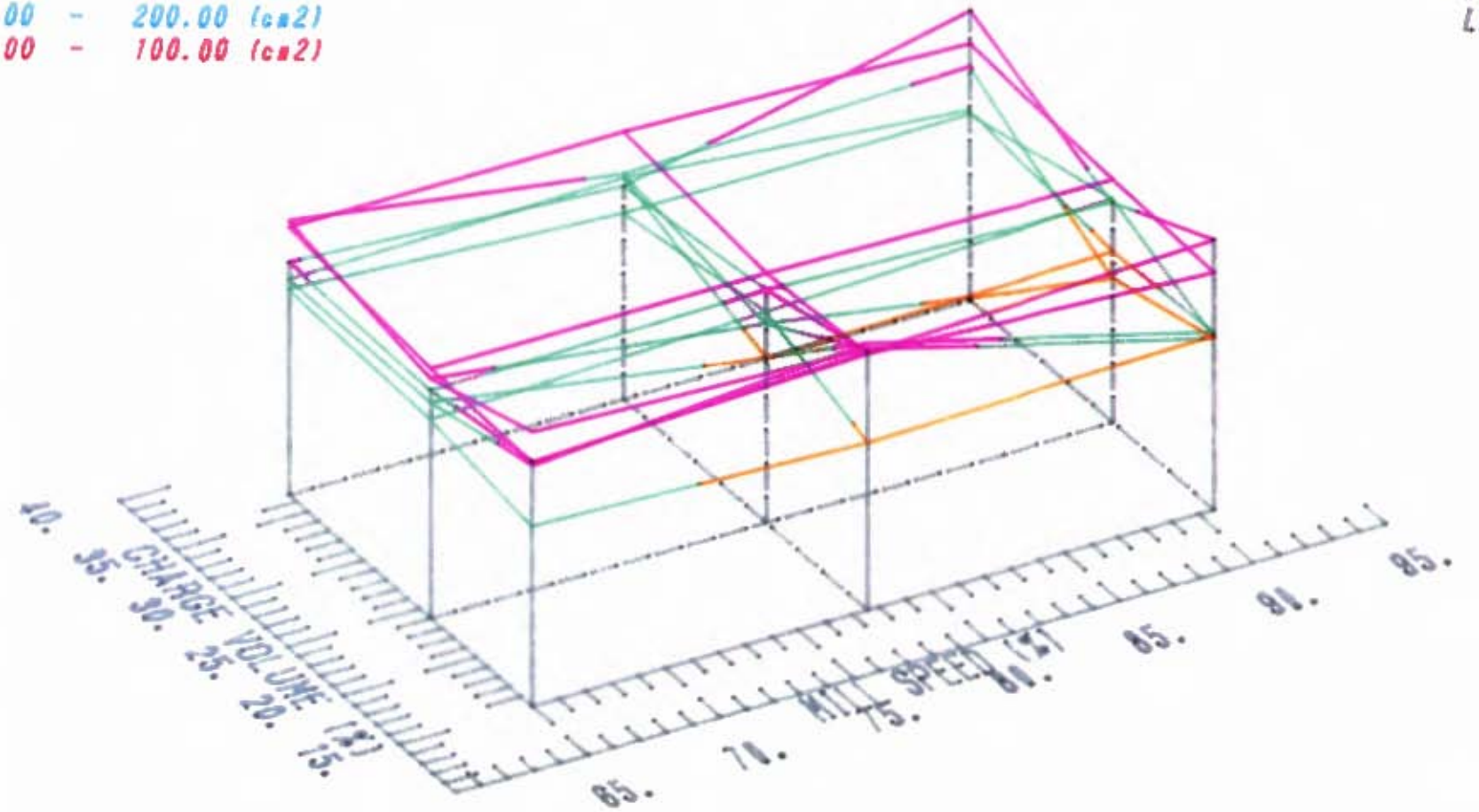

FIGURE D-19

LINER WEAR (g/6h) vs. ROUGHNESS COEFFICIENT & MILL SPEED (%)

COLOUR CODE FOR : LINER WEAR

4.00 - 5.00 (g/6h)
3.00 - 4.00 (g/6h)
2.00 - 3.00 (g/6h)
1.00 - 2.00 (g/6h)
0.00 - 1.00 (g/6h)

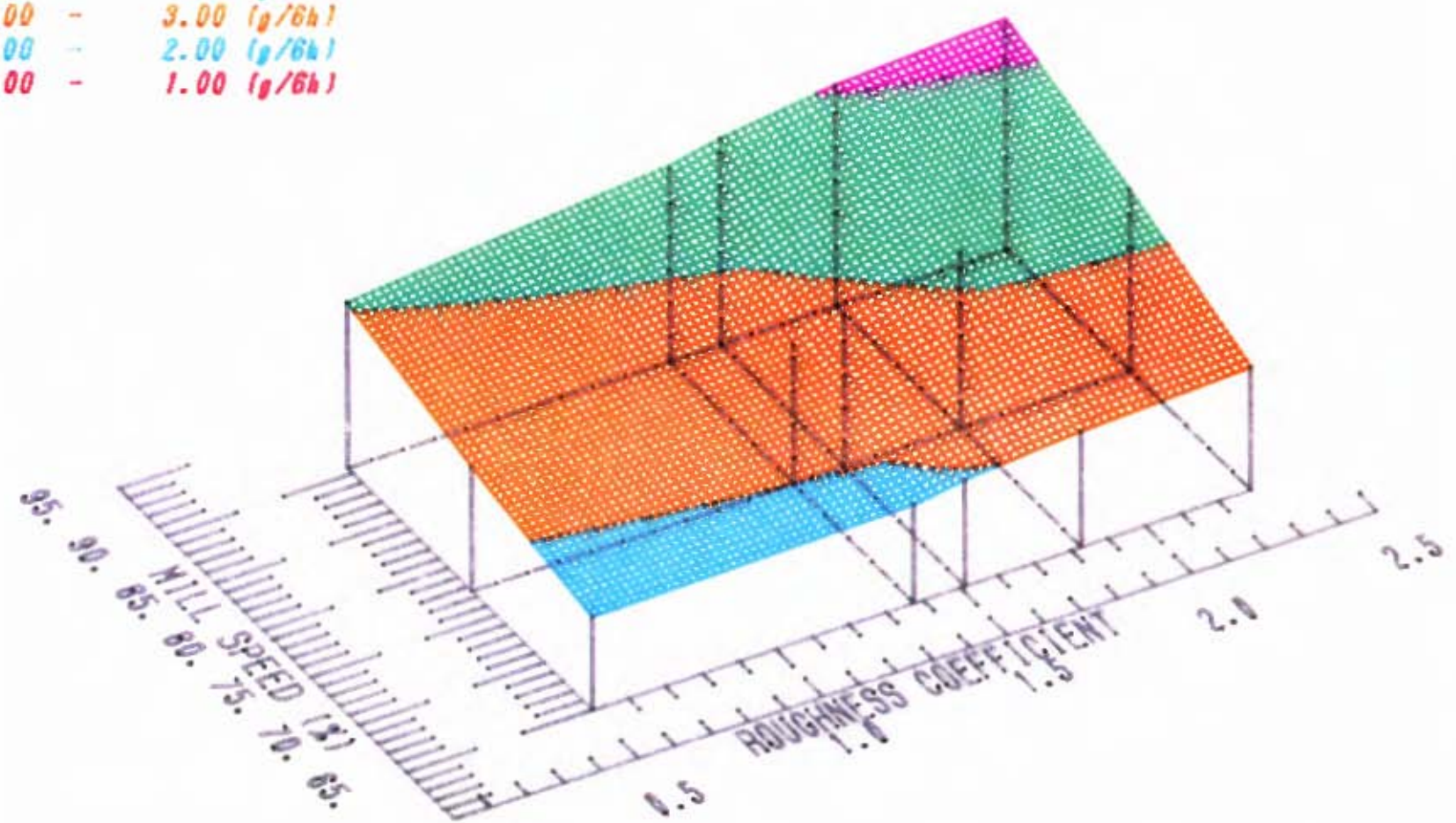

CHARGE VOLUME : 15 %

FIGURE E-1

LINER WEAR (g/6h) vs. ROUGHNESS COEFFICIENT & MILL SPEED (%)

COLOUR CODE FOR : LINER WEAR

4.00 - 5.00 (g/6h)
3.00 - 4.00 (g/6h)
2.00 - 3.00 (g/6h)
1.00 - 2.00 (g/6h)
0.00 - 1.00 (g/6h)

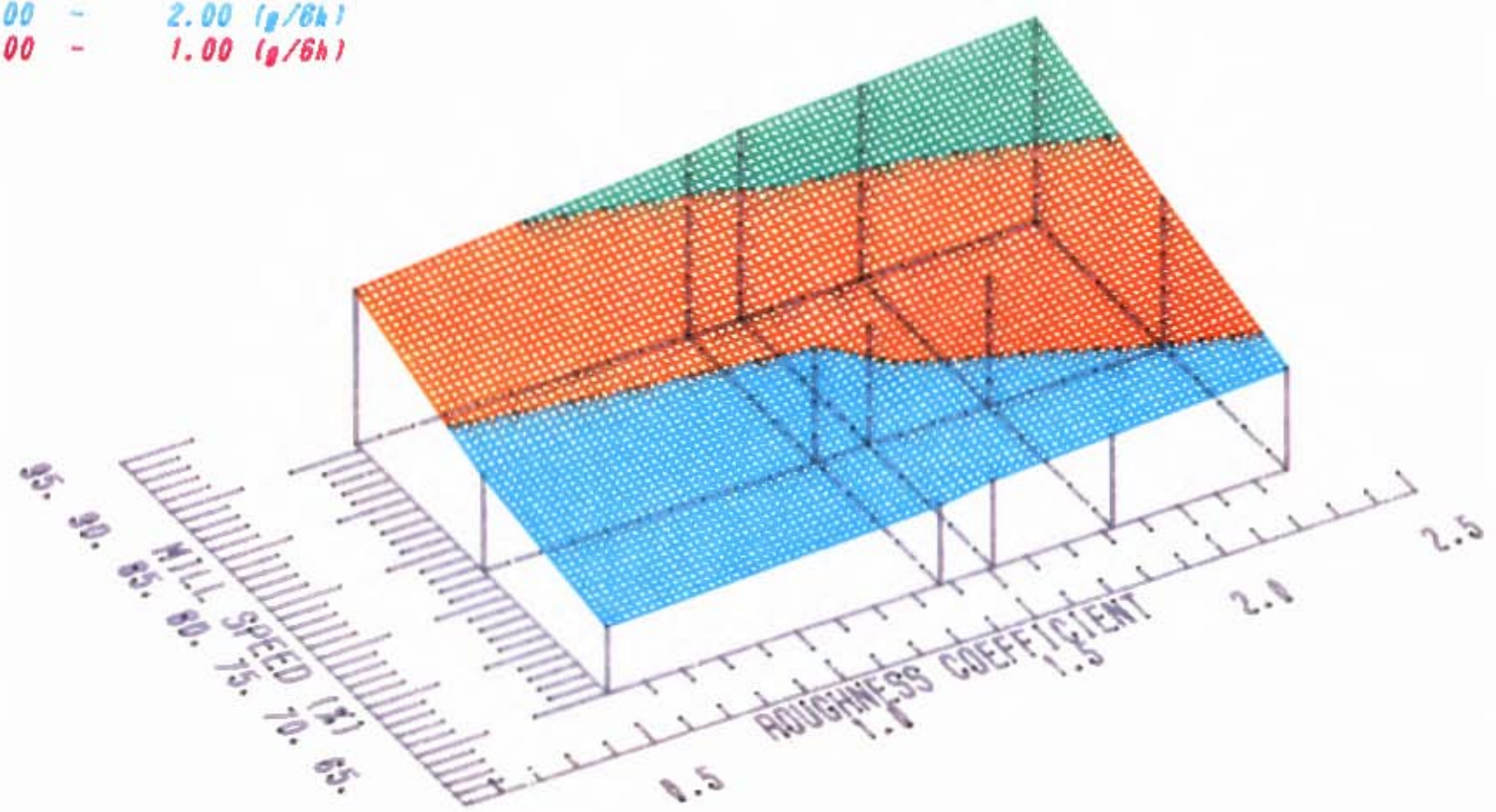

CHARGE VOLUME : 24 %

FIGURE E-2

LINER WEAR (g/6h) vs. ROUGHNESS COEFFICIENT & MILL SPEED (%)

COLOUR CODE FOR : LINER WEAR

4.00 - 5.00 (g/6h)
3.00 - 4.00 (g/6h)
2.00 - 3.00 (g/6h)
1.00 - 2.00 (g/6h)
0.00 - 1.00 (g/6h)

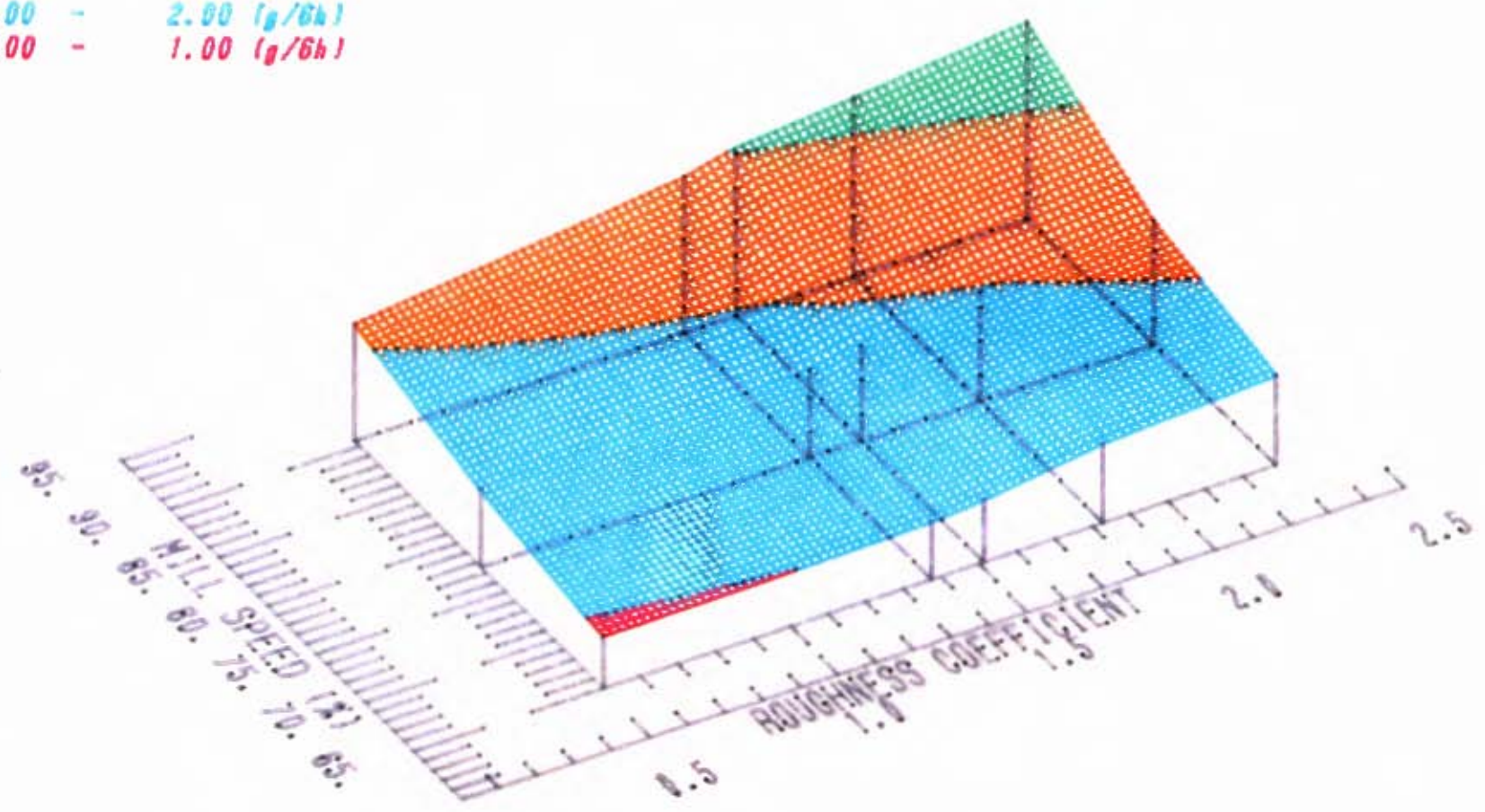

CHARGE VOLUME : 36.7%

FIGURE E-3

LINER WEAR (g/6h) vs. ROUGHNESS COEFFICIENT & CHARGE VOLUME (%)

COLOUR CODE FOR : LINER WEAR

4.00 - 5.00 (g/6h)
3.00 - 4.00 (g/6h)
2.00 - 3.00 (g/6h)
1.00 - 2.00 (g/6h)
0.00 - 1.00 (g/6h)

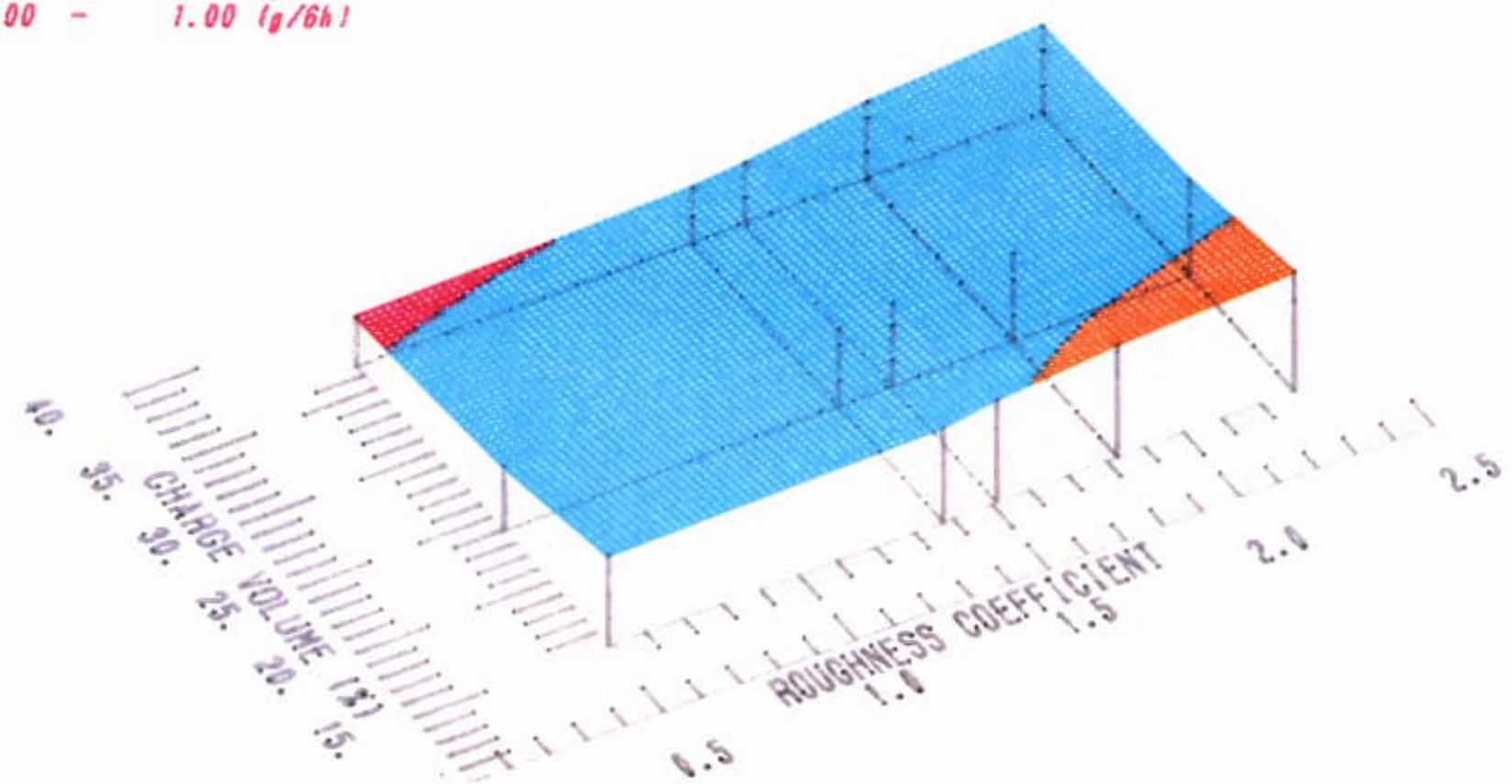

MILL SPEED : 65 (%)

FIGURE E- 4

LINER WEAR (g/6h) vs. ROUGHNESS COEFFICIENT & CHARGE VOLUME (%)

COLOUR CODE FOR : LINER WEAR

4.00 - 5.00 (g/6h)
3.00 - 4.00 (g/6h)
2.00 - 3.00 (g/6h)
1.00 - 2.00 (g/6h)
0.00 - 1.00 (g/6h)

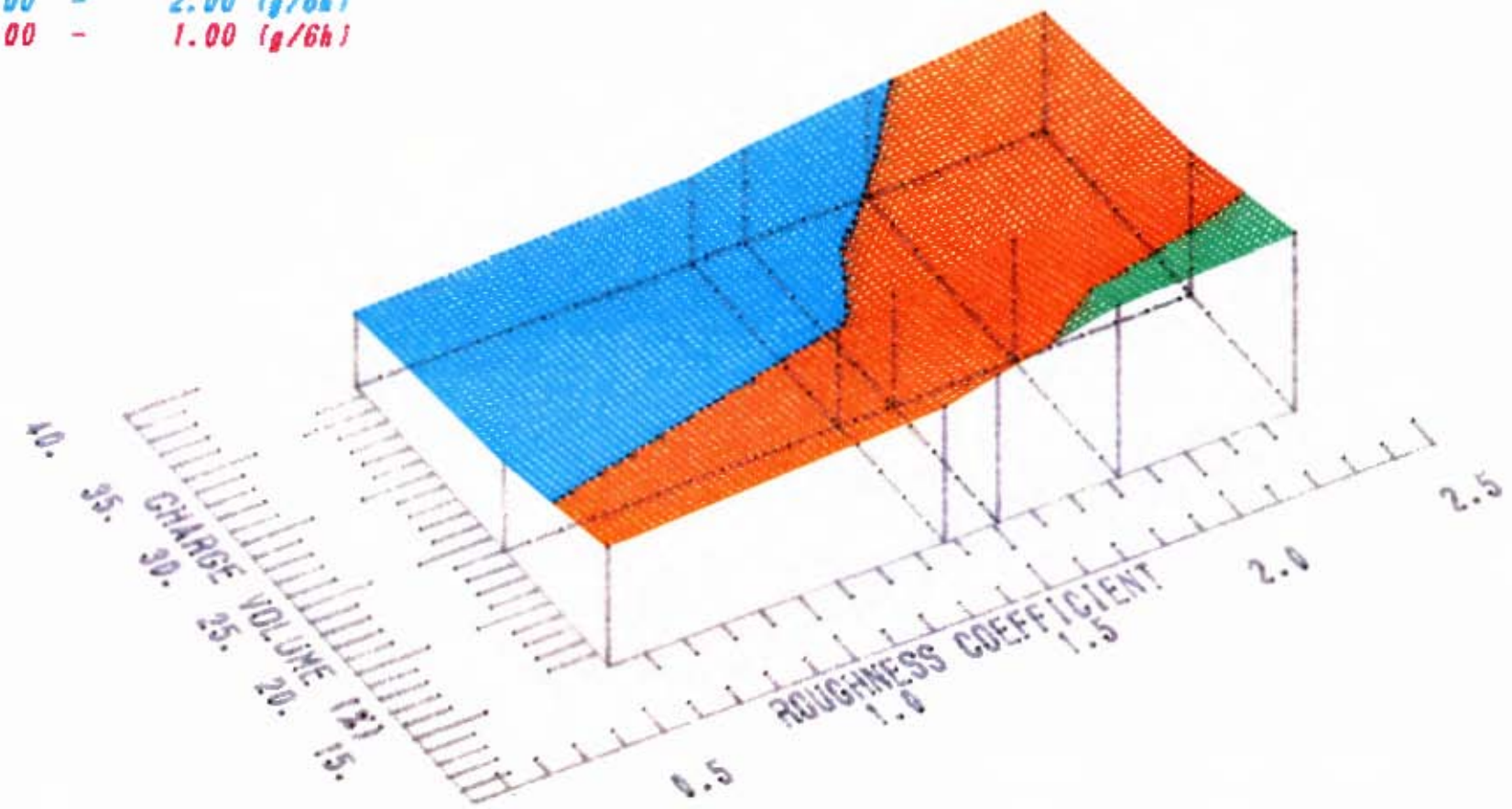

MILL SPEED : 77.6(%)

FIGURE E-5

LINER WEAR (g/6k) vs. ROUGHNESS COEFFICIENT & CHARGE VOLUME (%)

COLOUR CODE FOR : LINER WEAR

4.00 - 5.00 (g/6k)
3.00 - 4.00 (g/6k)
2.00 - 3.00 (g/6k)
1.00 - 2.00 (g/6k)
0.00 - 1.00 (g/6k)

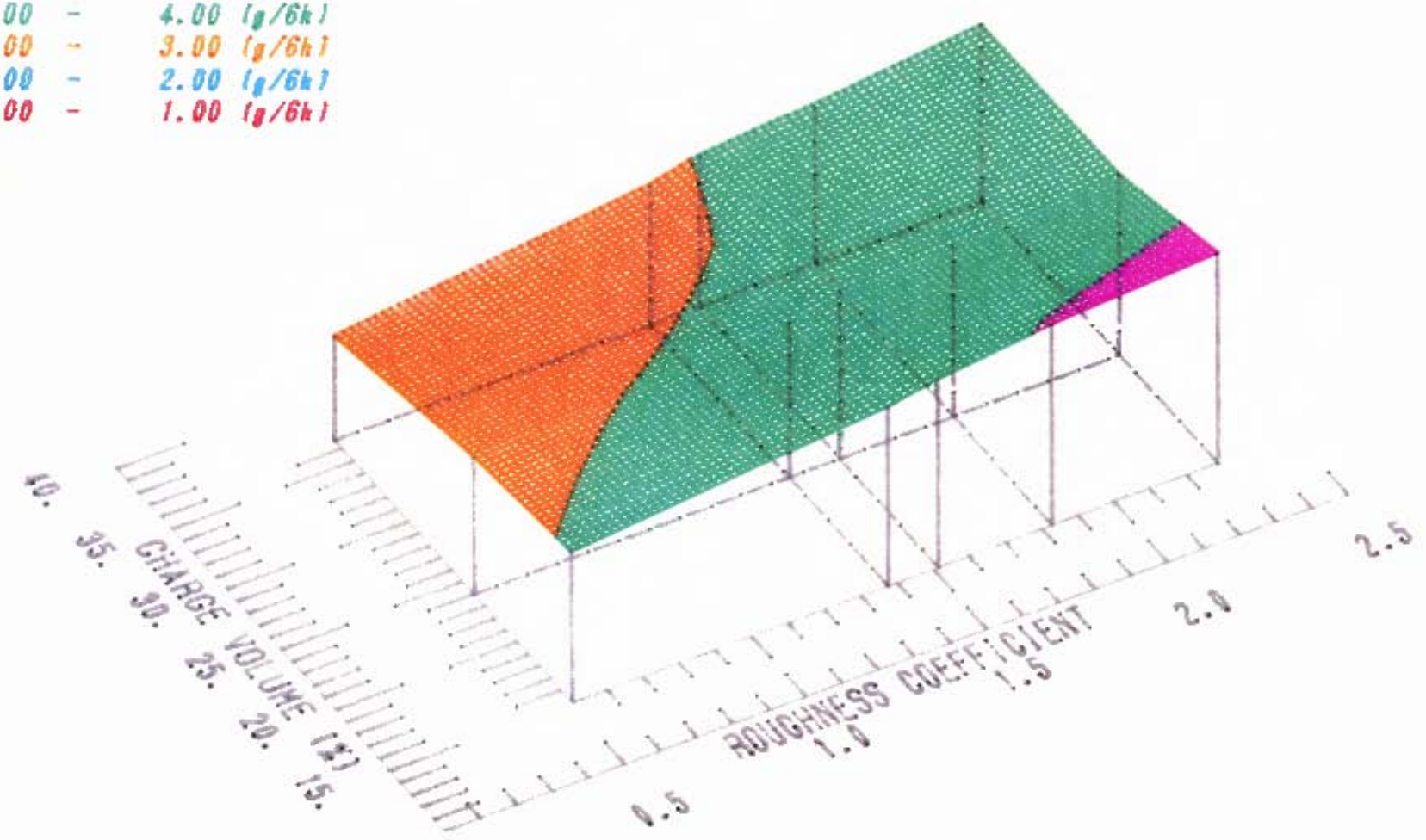

MILL SPEED : 90.6(%)

FIGURE E-6

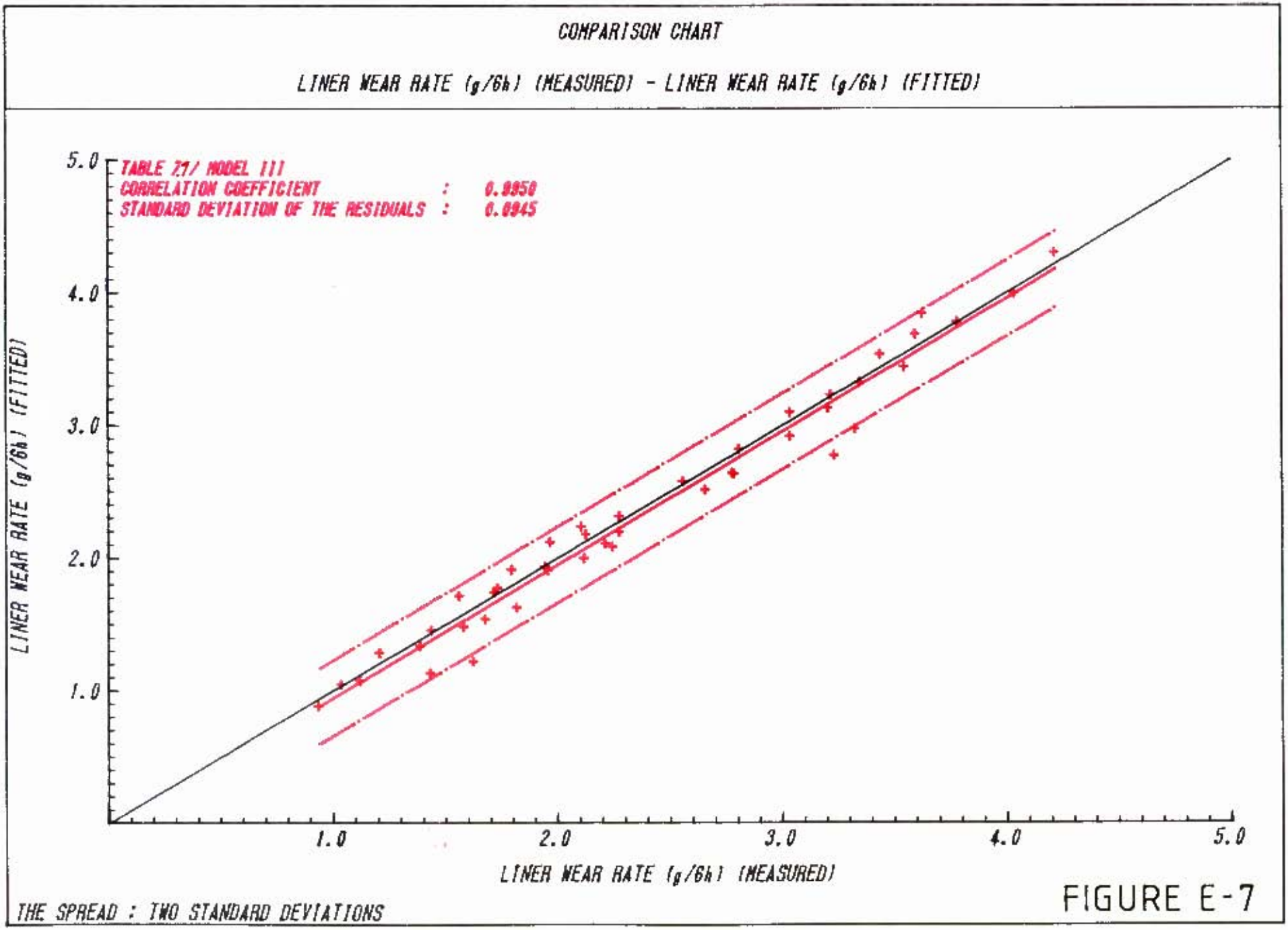
COMPARISON CHART
LINER WEAR RATE (g/6h) (MEASURED) - LINER WEAR RATE (g/6h) (FITTED)
TABLE 7/ MODEL III
CORRELATION COEFFICIENT : 0.9850
STANDARD DEVIATION OF THE RESIDUALS : 0.0945
LINER WEAR RATE (g/6h) (FITTED)
LINER WEAR RATE (g/6h) (MEASURED)
5.0
4.0
3.0
2.0
1.0
THE SPREAD : TWO STANDARD DEVIATIONS

FIGURE E-7

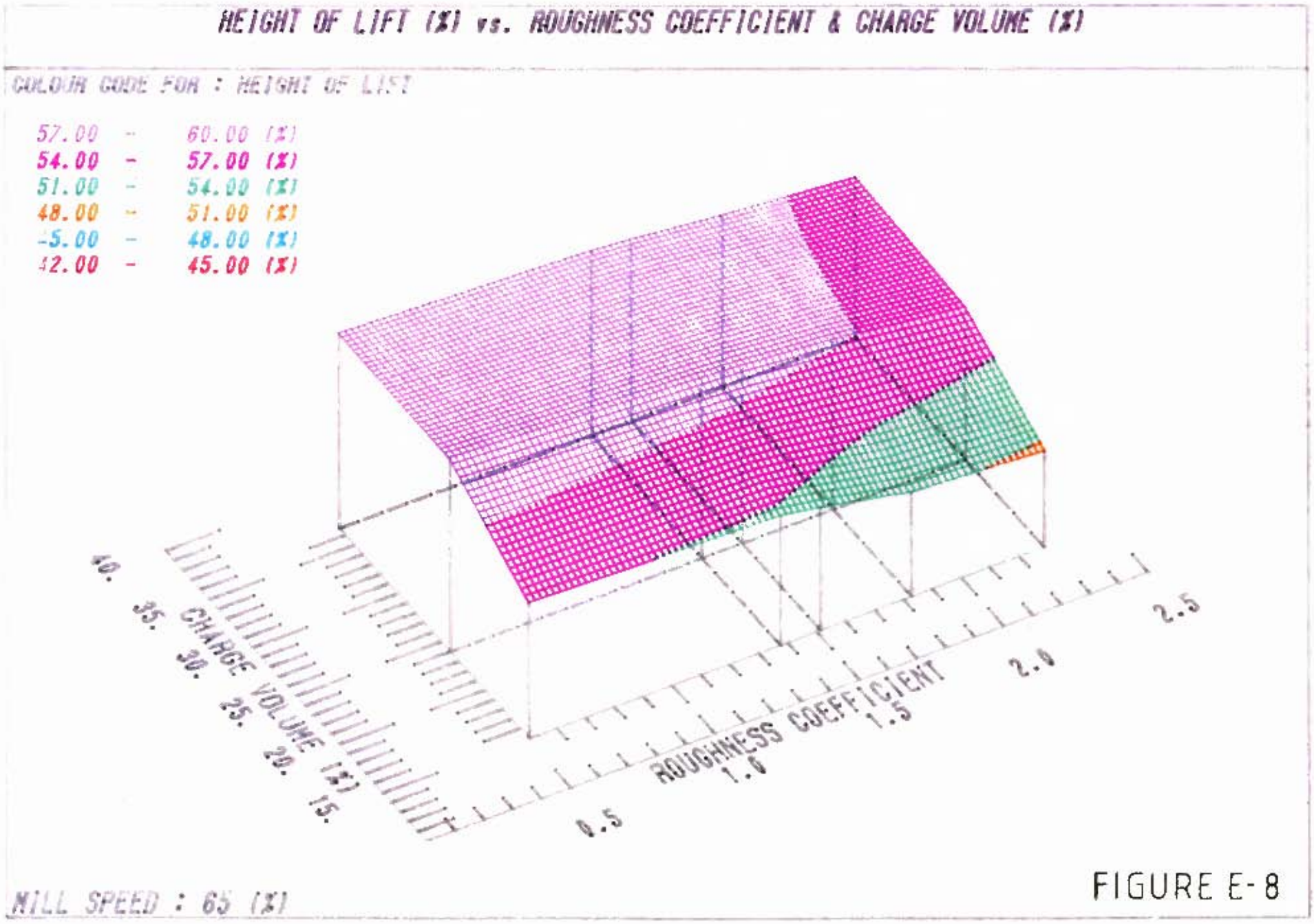
HEIGHT OF LIFT (%) vs. ROUGHNESS COEFFICIENT & CHARGE VOLUME (%)
COLOUR CODE FOR : HEIGHT OF LIFT
57.00 - 60.00 (%)
54.00 - 57.00 (%)
51.00 - 54.00 (%)
48.00 - 51.00 (%)
-5.00 - 48.00 (%)
42.00 - 45.00 (%)
CHARGE VOLUME (%)
40.
35.
30.
25.
20.
15.
ROUGHNESS COEFFICIENT
0.5
1.0
1.5
2.0
2.5
MILL SPEED : 65 (%)

FIGURE E-8

HEIGHT OF LIFT (%) vs. ROUGHNESS COEFFICIENT & CHARGE VOLUME (%)

COLOUR CODE FOR : HEIGHT OF LIFT

57.00 - 60.00 (%)
54.00 - 57.00 (%)
51.00 - 54.00 (%)
48.00 - 51.00 (%)
45.00 - 48.00 (%)
42.00 - 45.00 (%)

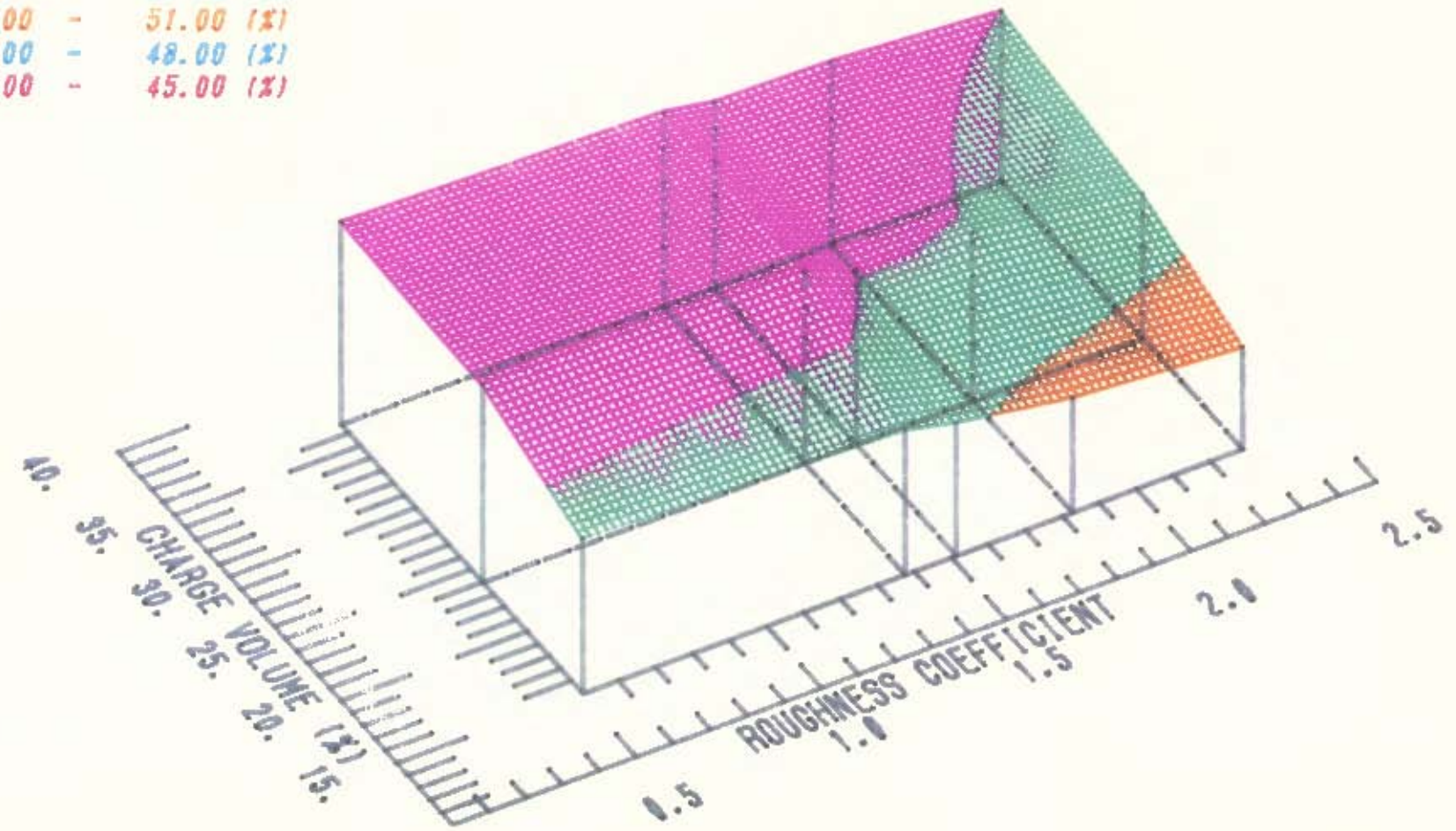

MILL SPEED : 77.6(%)

FIGURE E-9

HEIGHT OF LIFT (%) vs. ROUGHNESS COEFFICIENT & CHARGE VOLUME (%)

COLOUR CODE FOR : HEIGHT OF LIFT

57.00	-	60.00 (%)
54.00	-	57.00 (%)
51.00	-	54.00 (%)
48.00	-	51.00 (%)
45.00	-	48.00 (%)
42.00	-	45.00 (%)

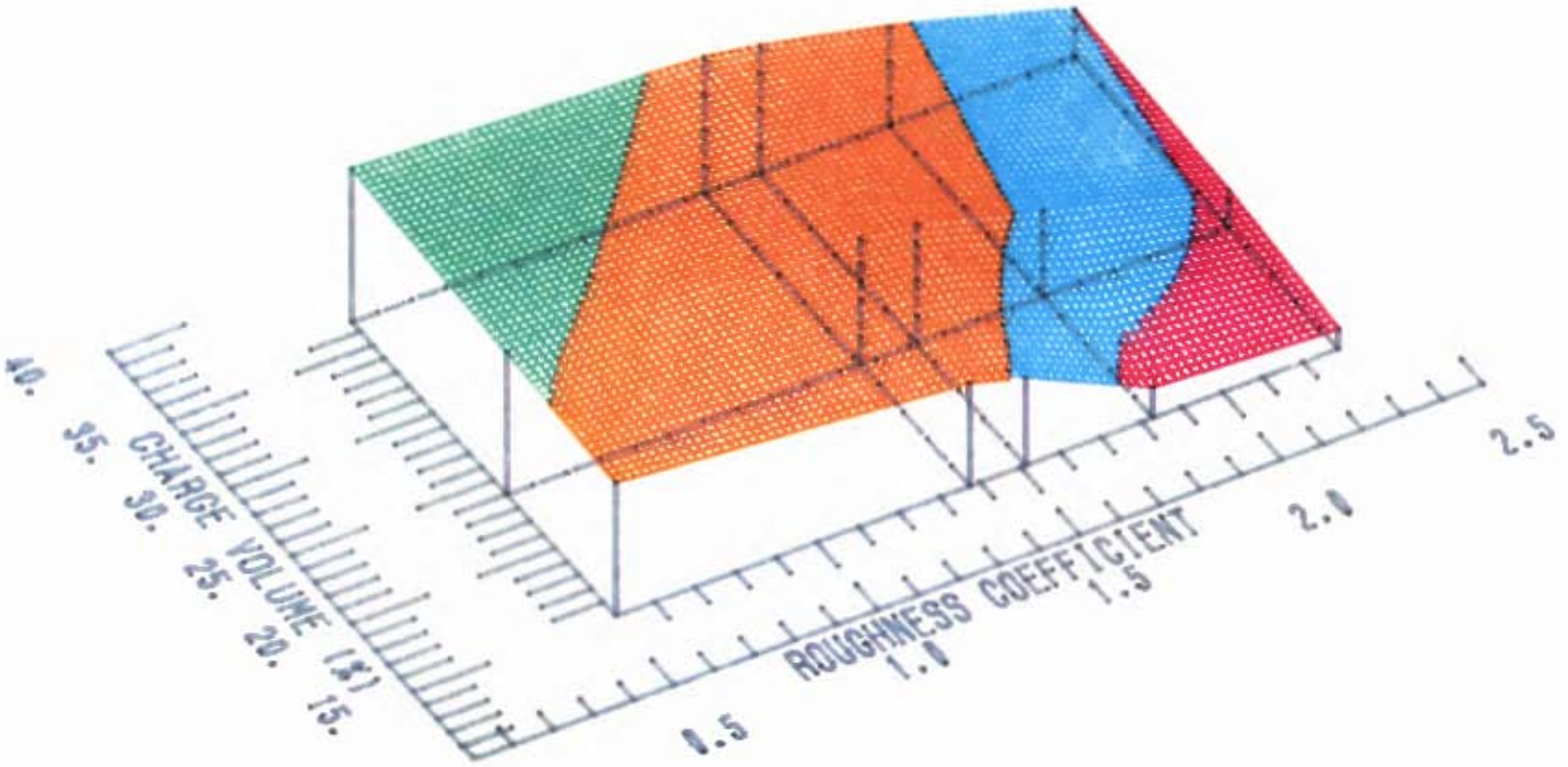

MILL SPEED : 90.6(%)

FIGURE E-10

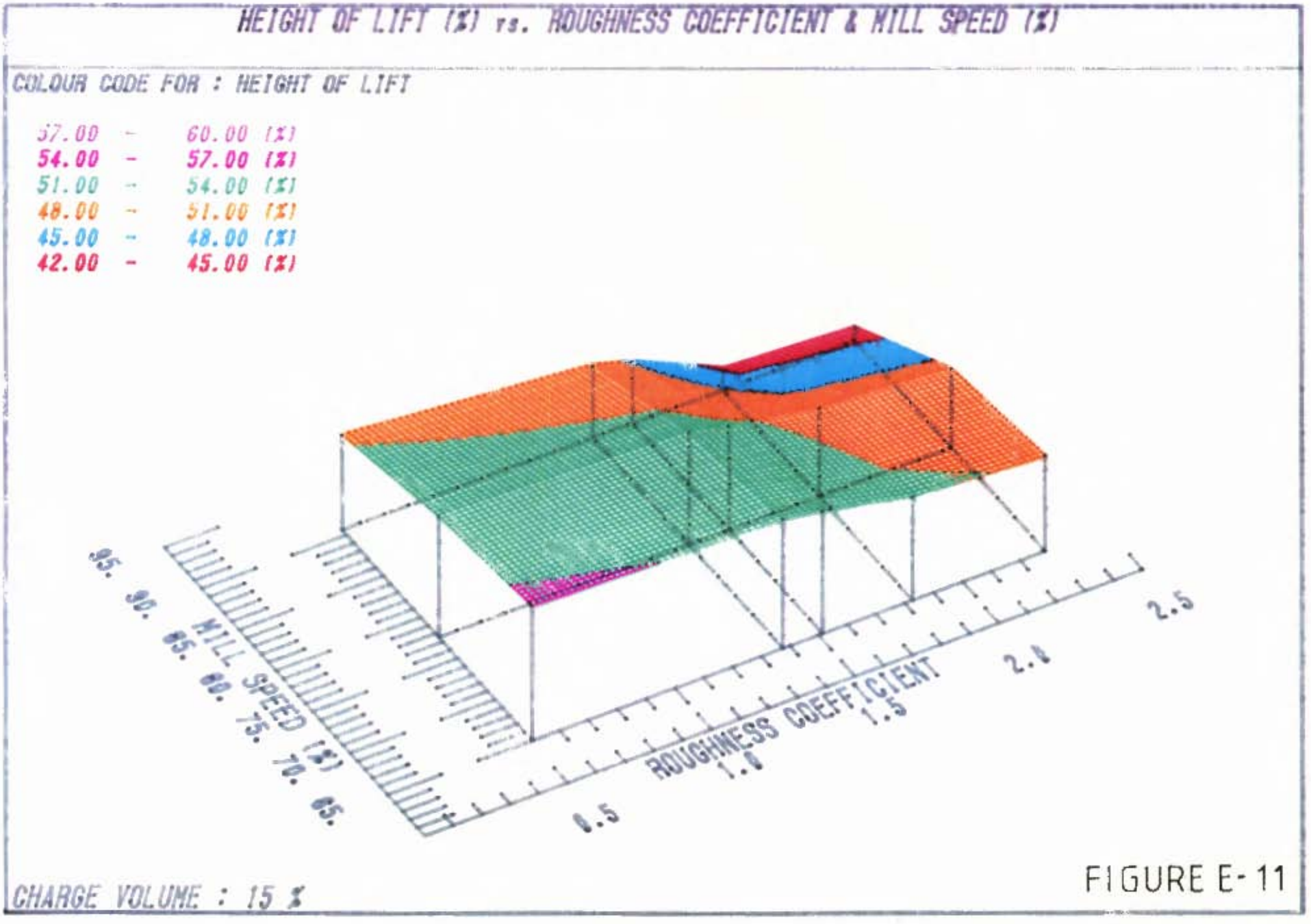
HEIGHT OF LIFT (%) vs. ROUGHNESS COEFFICIENT & MILL SPEED (%)
COLOUR CODE FOR : HEIGHT OF LIFT
57.00 - 60.00 (%)
54.00 - 57.00 (%)
51.00 - 54.00 (%)
48.00 - 51.00 (%)
45.00 - 48.00 (%)
42.00 - 45.00 (%)
95. 90. 85. 80. 75. 70. 65.
MILL SPEED (%)
0.5 1.0 1.5 2.0 2.5
ROUGHNESS COEFFICIENT
CHARGE VOLUME : 15 %

FIGURE E-11

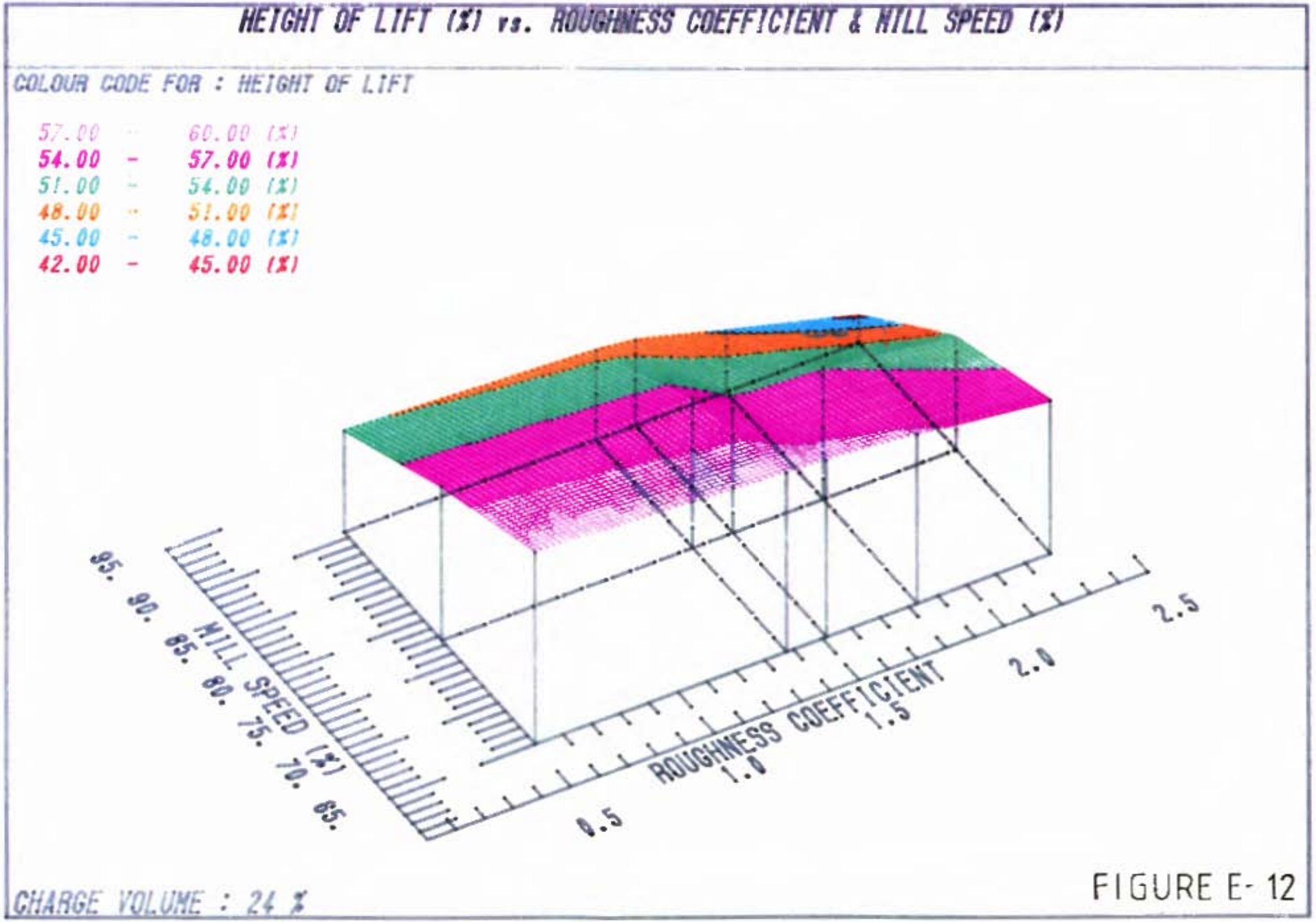
HEIGHT OF LIFT (%) vs. ROUGHNESS COEFFICIENT & MILL SPEED (%)
COLOUR CODE FOR : HEIGHT OF LIFT
57.00 - 60.00 (%)
54.00 - 57.00 (%)
51.00 - 54.00 (%)
48.00 - 51.00 (%)
45.00 - 48.00 (%)
42.00 - 45.00 (%)
MILL SPEED (%)
95.
90.
85.
80.
75.
70.
65.
ROUGHNESS COEFFICIENT
0.5
1.0
1.5
2.0
2.5
CHARGE VOLUME : 24 %

FIGURE E- 12

FIGURE F-1 : LINER 4 - BALLS CONFIGURATION FOR N_{10} = 78% and J = 24%

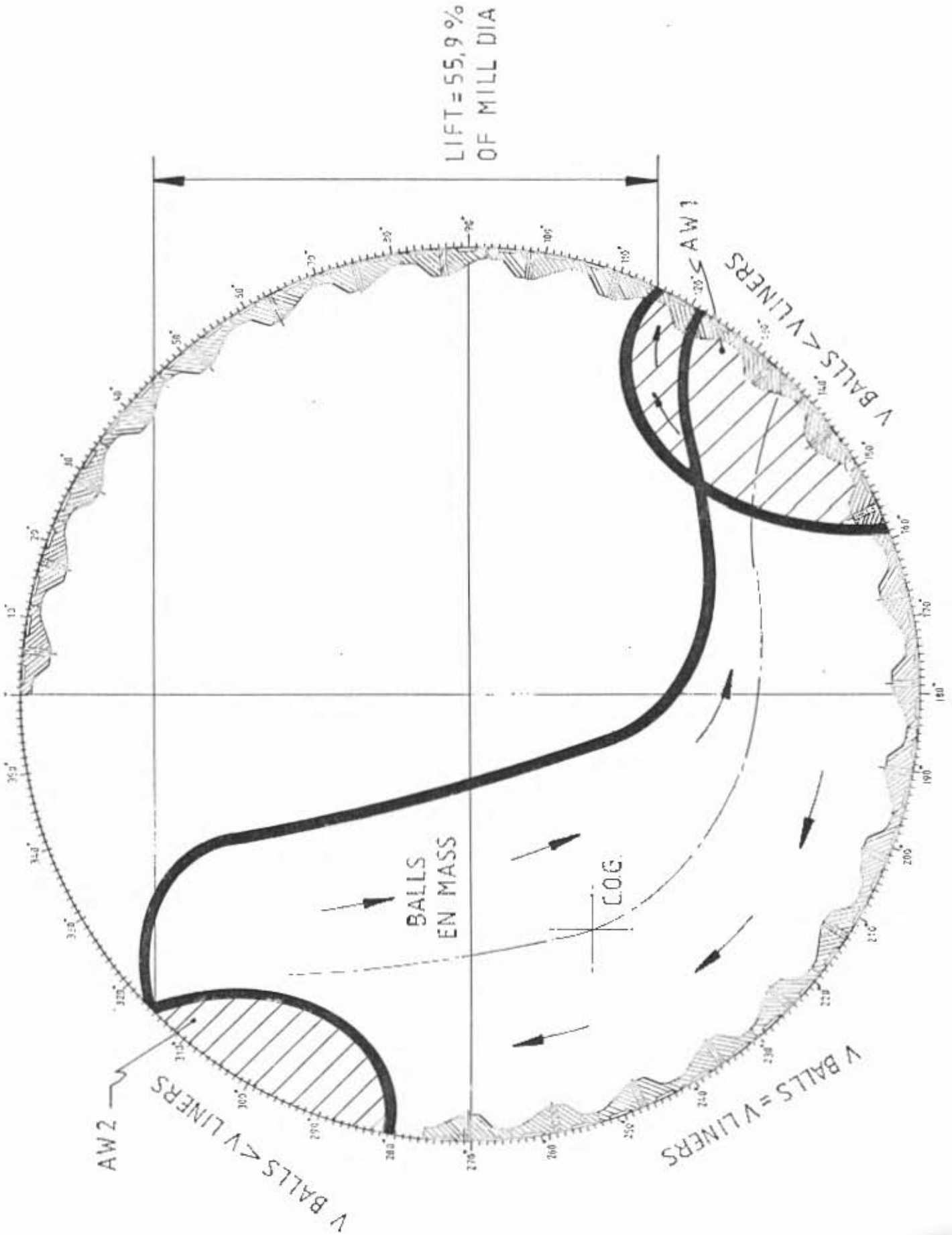

FIGURE F-2 : LINER 5 - BALLS CONFIGURATION FOR N_{cr} = 78% and J = 24%

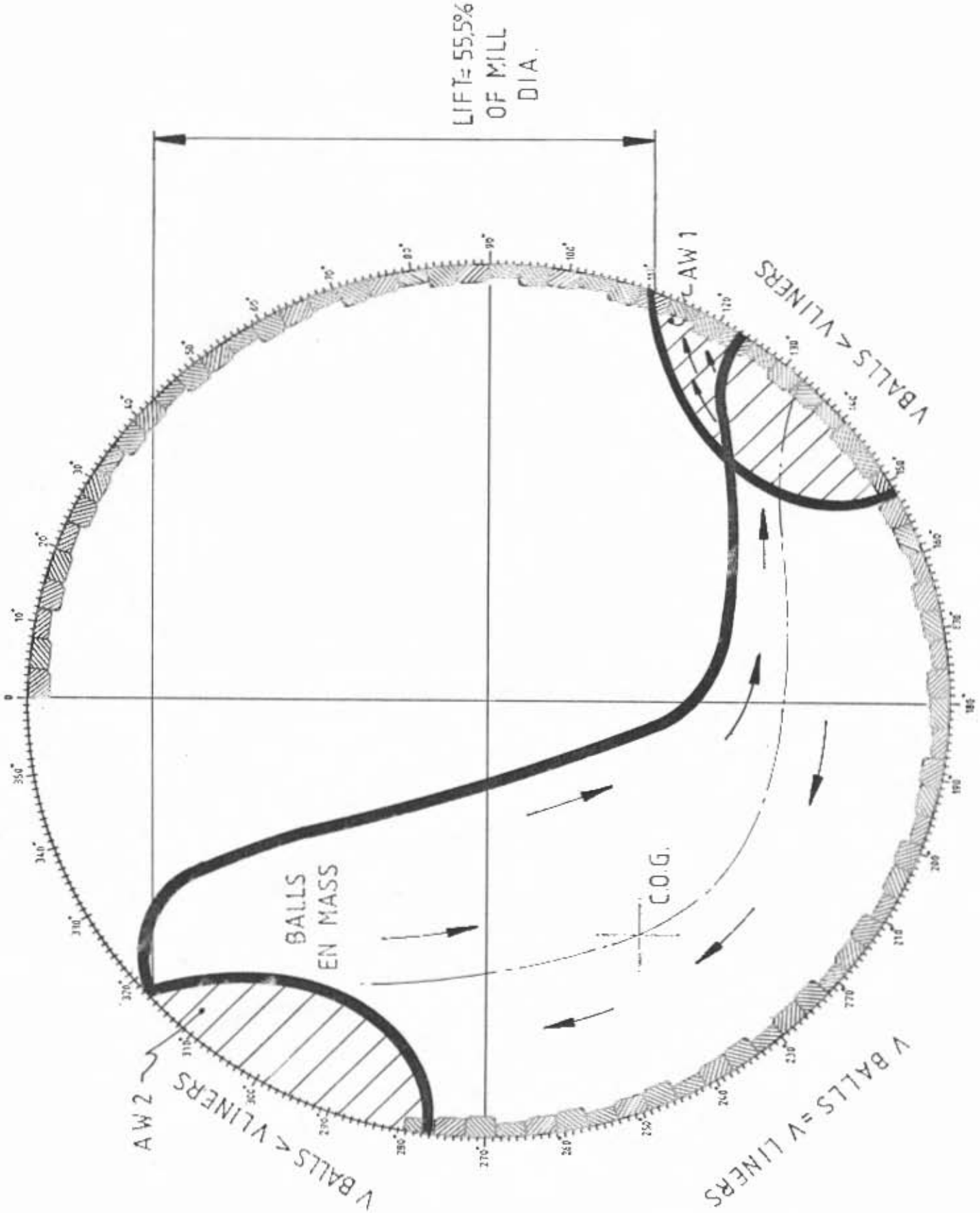

FIGURE F-4 : LINER 1 - BALLS CONFIGURATION FOR N_B = 78% and J = 24%

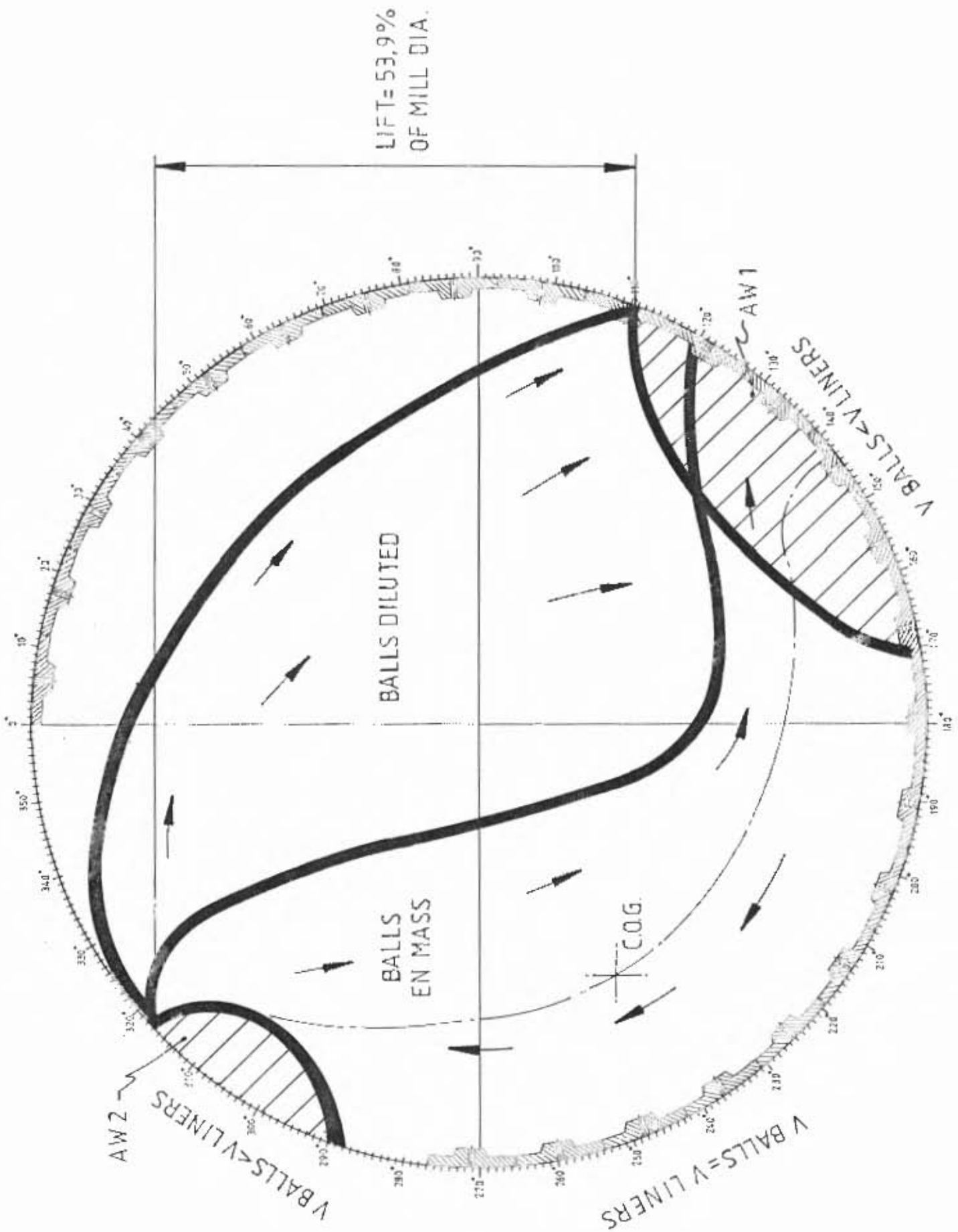

FIGURE F-5 : LINER 2 - BALLS CONFIGURATION FOR N_{cr} = 78% and J = 24%

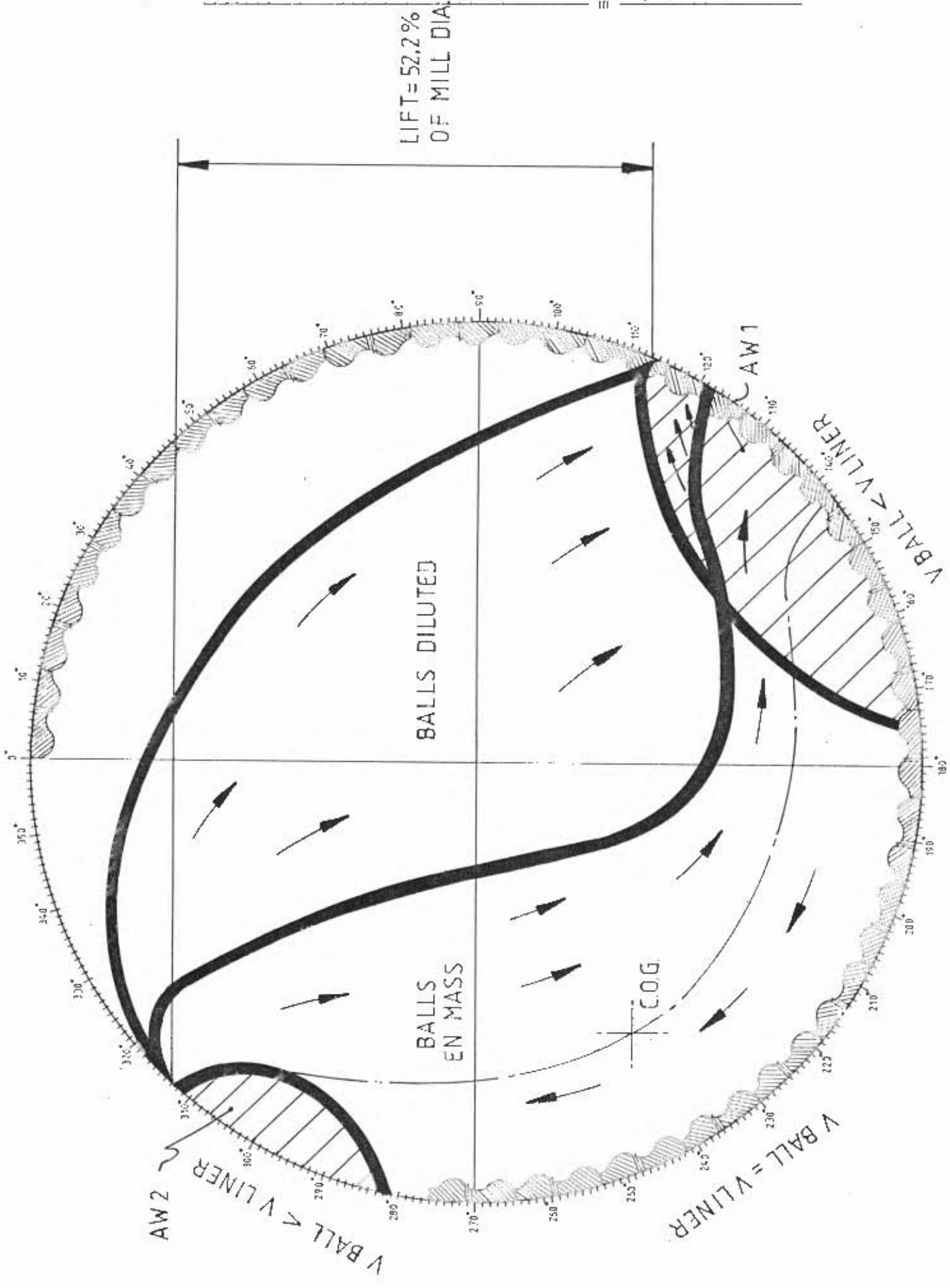

LISTING OF COMPUTER PROGRAM FOR NUMERICAL SOLUTION OF EQUATIONS IN CHAPTER 4.2.1

```
DECLARE SUB ARTAN (X!, Y!, ANG!)
     'PROGRAM NAME : SKORU0
     'SINGLE BALL IN A SMOOTH DRUM.
     INPUT "DRUM RADIUS (meter) : ", R
     INPUT "ANGULAR VELOCITY OF DRUM (% Crit) : ", OMD0
     OMD0 = .42305 * OMD0 / (2 * R) ^ .5
     PI = 3.14159
     OMD0 = 2 * PI * OMD0 / 60
     INPUT "STATIONARY AND MOVING FRICTION FACTORS : ", FMU0, FMUS
     INPUT "INITIAL VALUE OF BALL POSITION ANGLE (deg.) : ", FI0
     FI0 = 2 * PI * FI0 / 360
     INPUT "INITIAL ANGULAR VELOCITY OF BALL (% drum velocity) : ", BAV
     OM0 = .01 * BAV * OMD0
     DOM0 = -(OMD0 - OM0)
     INPUT "THE TIME INTERVAL (SUGGEST .01 sec.) : ", DELT0
     G = 9.8066
     ACRAD0 = R * OM0 ^ 2 - G * SIN(FI0)
     SCREEN 1
     VIEW (0, 0)-(319, 199), , 7
     WIN = 1.1 * 2 * R
     RAT = 319 / 199
     X2 = .5 * RAT * WIN
     X1 = -X2
     Y2 = .5 * WIN
     Y1 = -Y2
     WINDOW (X1, Y1)-(X2, Y2)
     PSET (1.02 * R, 0), 7
     DANG = 2 * PI / 360
     FOR I = 1 TO 360
     XI = I
     XC0 = 1.02 * R * COS(XI * DANG)
     YSI = 1.02 * R * SIN(XI * DANG)
     LINE -(XC0, YSI), 7
     NEXT I
START: '
     X = ABS(FMU0 * (R * OMD0 ^ 2 - G * SIN(FI0))) - ABS(G * COS(FI0))
     IF DOM0 = 0 AND X > 0 THEN
     DELT = DELT0
     DOM1 = 0
     OM1 = OMD0
     GOTO FINEX
     END IF
     DELDOM = -DELT0 * ((G / R) * COS(FI0) + FMUS * SGN(DOM0) * (OM0 ^ 2 - (G / R) * SIN(FI0)))
     IF DOM0 <> 0 AND DOM0 * (DOM0 + DELDOM) <= 0 THEN
     DELT = DELT0 * DOM0 / DELDOM
     DOM1 = 0
     OM1 = OMD0
     ELSE
     DELT = DELT0
     DOM1 = DOM0 + DELDOM
     OM1 = OMD0 + DOM1
     END IF
FINEX: '
     TIM1 = TIM0 + DELT
     FI1 = FI0 + .5 * (OM0 + OM1) * DELT
     ACRAD1 = R * OM1 ^ 2 - G * SIN(FI1)
     IF ACRAD0 * ACRAD1 < 0 THEN
     TIMSEP = (ACRAD0 * TIM1 - ACRAD1 * TIM0) / (ACRAD0 - ACRAD1)
     RATIO = (TIMSEP - TIM0) / (TIM1 - TIM0)
     TIM1 = TIMSEP
```

```
DOM1 = DOM0 + RATIO * (DOM1 - DOM0)
OM1 = OMD0 + DOM1
FI1 = FI0 + .5 * (OM0 + OM1) * (TIMSEP - TIM0)
END IF
FI1P = FI1 * 360 / (2 * PI)
IN = CINT(FI1P / 360)
XIN = IN
IF FI1P > 360 THEN FI1P = FI1P - 360 * XIN
X0 = .96 * R * COS(FI1)
Y0 = .98 * R * SIN(FI1)
LINE (0, 0)-(R, 0), 7
LINE (0, 0)-(-R, 0), 7
LINE (0, 0)-(0, -R), 7
LINE (0, 0)-(0, R), 7
FIRAD = OMD0 * TIM1
RADX = R * COS(FIRAD)
RADY = R * SIN(FIRAD)
LINE (0, 0)-(RADX, RADY), 1
   LINE (0, 0)-(RADX, RADY), 0
   IF DOM1 <> 0 THEN
   FOR K = 1 TO 5
   CIRCLE (X0, Y0), .01 * R, 1
   NEXT K
   CIRCLE (X0, Y0), .01 * R, 0
   END IF
IF ACRAD0 * ACRAD1 > 0 THEN
TIM0 = TIM1
DOM0 = DOM1
OM0 = OM1
FI0 = FI1
ACRAD0 = ACRAD1
GOTO START
END IF
FIS = FI1
OMSEP = OM1
XSEP = R * COS(FIS)
YSEP = R * SIN(FIS)
TFLIT = 4 * OMSEP * XSEP / G
XIMP = XSEP - 4 * XSEP * YSEP * OMSEP ^ 2 / G
YIMP = YSEP - 4 * (XSEP * OMSEP) ^ 2 / G
CALL ARTAN(XIMP, YIMP, FIMP)
TIMP = TIM1 + TFLIT
OMIMP = OMSEP * (YSEP * SIN(FIMP) - 3 * XSEP * COS(FIMP)) / R
DOMIMP = -(OMD0 - OMIMP)
FIMPX = FIMP * 360 / (2 * PI)
ING = CINT(FIMPX / 360)
XING = ING
IF FIMPX >= 360 THEN FIMPX = FIMPX - 360 * XING
 PRINT TIMP; FIMPX; DOMIMP; OMIMP
TIM0 = TIMP
FI0 = FIMP
DOM0 = DOMIMP
OM0 = OMIMP
GOTO START
END

SUB ARTAN (X, Y, ANG) STATIC
PI = 3.14159
IF X = 0 AND Y > 0 THEN ANG = PI / 2
IF X = 0 AND Y < 0 THEN ANG = 3 * PI / 2
```

```
ARGU = ABS(X / Y)
IF X > 0 AND Y > 0 THEN ANG = ATN(ARGU)
IF X > 0 AND Y < 0 THEN ANG = 2 * PI - ATN(ARGU)
IF X < 0 AND Y > 0 THEN ANG = PI - ATN(ARGU)
IF X < 0 AND Y < 0 THEN ANG = PI + ATN(ARGU)
END SUB
```